Drug binding to mammalian serum albumins

Mateusz Piotr Czub

Radom, Poland

B.S., Jagiellonian University, 2015

M.S., Jagiellonian University, 2017

A Dissertation Presented to the Graduate Faculty of the University of Virginia in Candidacy for the Degree of Doctor of Philosophy

Interdisciplinary Program in Biophysics

University of Virginia

December 2020

Abstract

Serum albumin (SA) is the most abundant protein in mammalian blood plasma. SA is primarily responsible for the transport of drugs, hormones, fatty acids, metals, and various other metabolites in the blood. More than 900 FDA-approved drugs are known to bind to plasma proteins, mainly albumin, but prior to this study complexes of SA with only 29 FDA-approved drugs have been structurally characterized. In this thesis, I present several structures of human serum albumin (complexes with ketoprofen, JMS-053, myristic acid) and equine serum albumin (complexes with ibuprofen, ketoprofen, etodolac, nabumetone, 6-MNA, testosterone, progesterone, dexamethasone, hydrocortisone, warfarin, tolbutamide, haloperidol, ampicillin, GHK(Cu), and glucose). I also present the binding constant of testosterone to equine and human albumins determined by two different methods (tryptophan fluorescence quenching and ultrafast affinity extraction). Previously, ibuprofen, warfarin, and ketoprofen complexes with other SAs were crystallized, and I discuss similarities and differences in their binding to SAs from different species. The analysis of all known albumin drug-binding sites shows that various drugs share common binding sites, which can lead to drug-drug displacement or other unwanted and dangerous effects during drug co-administration in patients. To better describe the location of drug-binding sites in albumin, I distinguish ten drug sites and propose a novel nomenclature based on the previously characterized sites. I also discuss the effect of non-enzymatic glycosylation (glycation) of albumin and drug competition with fatty acids on drug's binding to albumin and its free blood concentration, which is

especially important for drugs with a narrow therapeutic index. Information about the location of drug-binding sites contributes to a better understanding of the drug-drug displacement phenomena and the effect of metabolic disorders on drug transport. The results suggest that in some cases, physicians should consider altered drug doses that are needed to achieve desired therapeutic effects and avoid toxicity in relevant groups of patients.

Acknowledgments

I would like to thank my mentor Prof. Wladek Minor for years of continuous support and advice. I admire his dedication to science and express my gratitude for the great opportunity to work in his laboratory.

I wish to thank my committee members, Prof. Robert Nakamoto, Prof. Edward Egelman, and Prof. John Lazo for their advice and guidance.

Many thanks to my colleagues in the Minor Lab, both past and present, for the help in solving various problems. Especially Dr. Ivan Shabalin, Dr. Przemyslaw Porebski, and Dr. David Cooper for valuable discussions.

I would like to thank Dr. Karolina Majorek and Dr. Katarzyna Handing for collecting preliminary data for the albumin project, which helped to provide a context for my work. I also thank Prof. David Hage and his group for performing the UAE and zonal elution experiments, beamline scientists from the Advanced Photon Source for their assistance in data collection, and Dr. Adam Boulton for critical reading of this thesis.

I would like to acknowledge the contribution of undergraduate students, Barat Venkataramany and Ethan Steen, who helped me with the crystallization of SA complexes with some compounds and various other tasks.

I am grateful that I was entrusted to contribute to an already established project within the lab. Interactions with Minor lab collaborators (Prof. Misty Kuhn, Prof. Maks Chruszcz, Prof. Andrzej Joachimiak, and others) provided a foundation for the project, which permitted me to rapidly contribute to cutting-edge structural biology.

I would like to thank Dr. Heping Zheng, Dr. Marek Grabowski, Dr. Tomasz Osinski, Piotr Sroka, and Marcin Cymborowski for the creation of computing tools and unique computational environment. Without this environment, such fast progress would not be possible.

I would like to acknowledge the Robert R. Wagner Fellowship for their support.

I express a deep sense of gratitude to my parents for their endless love and encouragement.

Finally, I would like to thank my lovely wife, Justyna, for her love, help, and support that allowed me to carry on through many trying times in the completion of my degree.

Summary of research

The Ph.D. thesis is written on the basis of the following publications of which I am an author and uses their fragments:

- **Czub, M. P**.; Venkataramany, B. S.; Majorek, K. A.; Handing, K. B.; Porebski, P. J.; Beeram, S. R.; Suh, K.; Woolfork, A. G.; Hage, D. S.; Shabalin, I. G.; Minor, W. Testosterone Meets Albumin - the Molecular Mechanism of Sex Hormone Transport by Serum Albumins. *Chem. Sci*. 2019, 10 (6), 1607–1618.
- **Czub, M. P**.; Handing, K. B.; Venkataramany, B. S.; Cooper, D. R.; Shabalin, I. G.; Minor, W. Albumin-Based Transport of Nonsteroidal Anti-Inflammatory Drugs in Mammalian Blood Plasma. *J. Med. Chem*. 2020, 63 (13), 6847–6862.
- **Czub, M. P**.; Boulton, A. M.; Rastelli, E. J.; Tasker, N. R.; Maskrey, T. S.; Blanco, I. K.; McQueeney, K. E.; Bushweller, J. H.; Minor, W.; Wipf, P.; Sharlow, E. R.; Lazo, J. S. Structure of the Complex of an Iminopyridinedione PTP4A3 Phosphatase Inhibitor with Human Serum Albumin. *Mol. Pharmacol.* 2020, MOLPHARM-AR-2020-000131; DOI: 10.1124/molpharm.120.000131.
- Shabalin, I. G.; **Czub, M. P**.; Majorek, K. A.; Brzezinski, D.; Grabowski, M.; Cooper, D. R.; Panasiuk, M.; Chruszcz, M.; Minor, W. Molecular Determinants of Vascular Transport of Dexamethasone in COVID-19 Therapy. *IUCrJ* 2020, 7 (6).

Additional articles co-authored during the Ph.D. studies:

- Niedzialkowska, E.; Mrugała, B.; Rugor, A.; **Czub, M. P**.; Skotnicka, A.; Cotelesage, J. J. H.; George, G. N.; Szaleniec, M.; Minor, W.; Lewiński, K. Optimization of Overexpression of a Chaperone Protein of Steroid C25 Dehydrogenase for Biochemical and Biophysical Characterization. *Protein Expr. Purif*. 2017, 134, 47–62.

- **Czub, M. P.**; Zhang, B.; Chiarelli, M. P.; Majorek, K. A.; Joe, L.; Porebski, P. J.; Revilla, A.; Wu, W.; Becker, D. P.; Minor, W.; Kuhn, M. L. A Gcn5-Related N -Acetyltransferase (GNAT) Capable of Acetylating Polymyxin B and Colistin Antibiotics in Vitro. *Biochemistry* 2018, 57 (51), 7011–7020.
- Cooper D. R.; Grabowski M.; Zimmerman M. D.; Porebski P. J.; Shabalin I.G.; Woinska M.; Domagalski M. J.; Zheng H.; Sroka P.; Cymborowski M.; **Czub M. P**.; Niedzialkowska E.; Venkataramany B. S.; Osinski T.; Fratczak Z.; Bajor J.; Gonera J.; MacLean E.; Wojciechowska K.; Wajerowicz W.; Chruszcz M.; Minor W. State-of-the-art data management: improving the reproducibility, consistency, and traceability of structural biology and in vitro biochemical experiments, *Structural Genomics: General Applications, Methods in Molecular Biology*, C.-P. B. Yiu, Yu Wai Chen, Ed. (Springer, 2020), DOI: 10.1007/978-1-0716-0892-0_13, manuscript in press.

Manuscripts in preparation:

- **Czub M. P.**; Shabalin I. G.; Minor W. Albumin-based transport of ketoprofen in mammalian blood plasma.
- Baumgartner J.; Sifna T.; **Czub M. P**.; Majorek K.; Anonick M.; Arolli X.; Variot C.; Ballicora M.; Minor W.; Becker D. P.; Kuhn M. L. Evidence that some Gcn5-related N-acetyltransferases (GNATs) can play ping-pong too.

List of abbreviations

BSA – Bovine Serum Albumin

BLI – Biolayer Interferometry

CSA – Caprine Serum Albumin

ESA – Equine Serum Albumin

DS – Drug Site

FA – Fatty Acid binding site

FDA - Food and Drug Administration

GHK - Glycyl-l-Histidyl-l-Lysine peptide

HSA – Human Serum Albumin

ITC – Isothermal Titration Calorimetry

kDa – Kilodalton

LSA – Leporine Serum Albumin

MSA – Murine Serum Albumin

NSAID – Nonsteroidal Anti-Inflammatory Drug

OSA – Ovine Serum Albumin

PDB – Protein Data Bank

PEG - Polyethylene Glycol

PPB – Plasma Protein Binding

RMSD - Root-Mean-Square Deviation

SA – Serum Albumin

SPR – Surface Plasmon Resonance

TFQ – Tryptophan Fluorescence Quenching

Table of Contents

1. Introduction

1.1. Albumin structure and function

Serum albumin (SA) is the major plasma protein that constitutes up to 55% of total plasma proteins. Human serum albumin (HSA) consists of 585 amino acids and has a molecular weight of 66.5 kilodaltons (kDa).[1] Its typical blood concentration is in a range of 3.5-5.0 g/dL (average 600 µM).[2] HSA is synthesized in the liver, by polysomes bound to the endoplasmic reticulum of hepatocytes, at a daily rate of about 10-15 grams in healthy adults.[3,4] The initial form of albumin (preproalbumin) contains proalbumin with an additional N-terminal peptide (signal peptide, 18 amino acids), which is removed before the protein leaves the endoplasmic reticulum as proalbumin. The next cleavage, which removes six amino acids from the N-terminus, occurs in the Golgi vesicles and creates the mature form of albumin.[5] The synthesis of SA can be stimulated by hormones (e. g., insulin, cortisol) and inhibited by pro-inflammatory substances (e. g., interleukin-6).[4] Insufficient food intake and multiple disease states may also negatively affect the synthesis rate of SA.[6,7]

SA is a valuable marker for various pathological conditions.[8] An unusually low concentration of SA in the blood is often associated with an increased risk of mortality in many diseases, including various cancers, and cardiovascular diseases. [8–10] Recently, low SA level has been recognized as a risk factor in COVID-19.[11] The analysis of clinical data from Wuhan showed that each 1 g/L increase in the albumin level of the patient was associated with a 50% increased odds of surviving COVID-19.[12]

Thanks to its high concentration, SA acts as the major facilitator of vascular drug transport.[13–15] SA also transports hormones, metal ions, and common metabolites such as fatty acids and sugars. It also serves as the main determinant of plasma osmotic pressure by virtue of its high concentration and is a vital free radical scavenger.[1,8,16–20] During its month-long circulation in the bloodstream, SA makes nearly 15,000 trips around the body and travels through the lymphatic system 28 times, enabling the continuity of transport.[1,3,16] Together with SA's ability to bind diverse compounds, this circulation facilitates the deep-tissue delivery of therapeutic agents.[21] Because of its role as the major protein responsible for plasma protein binding (PPB), a molecule's affinity to SA plays a crucial role in drug candidate optimization.[13,15,22]

The extensive binding capacity of SA is the result of its highly flexible structure, high concentration in blood, and the presence of several binding sites that are able to accommodate a variety of small molecules. Crystal structures of mammalian SAs show three homologous domains: I (residues 1–195 in HSA), II (196–383), and III (384–585); each domain contains two subdomains (A and B) composed of 6 and 4 alpha-helices, respectively (**Figure 1.1**). The overall structure of SA is stabilized by 17 disulfide bridges. This structural arrangement results in multiple, mostly hydrophobic, binding cavities located between the domains, subdomains, and helices. In addition, the arrangement of helices and loops in SA confers some degree of interdomain flexibility that results from the binding of certain ligands.[1]

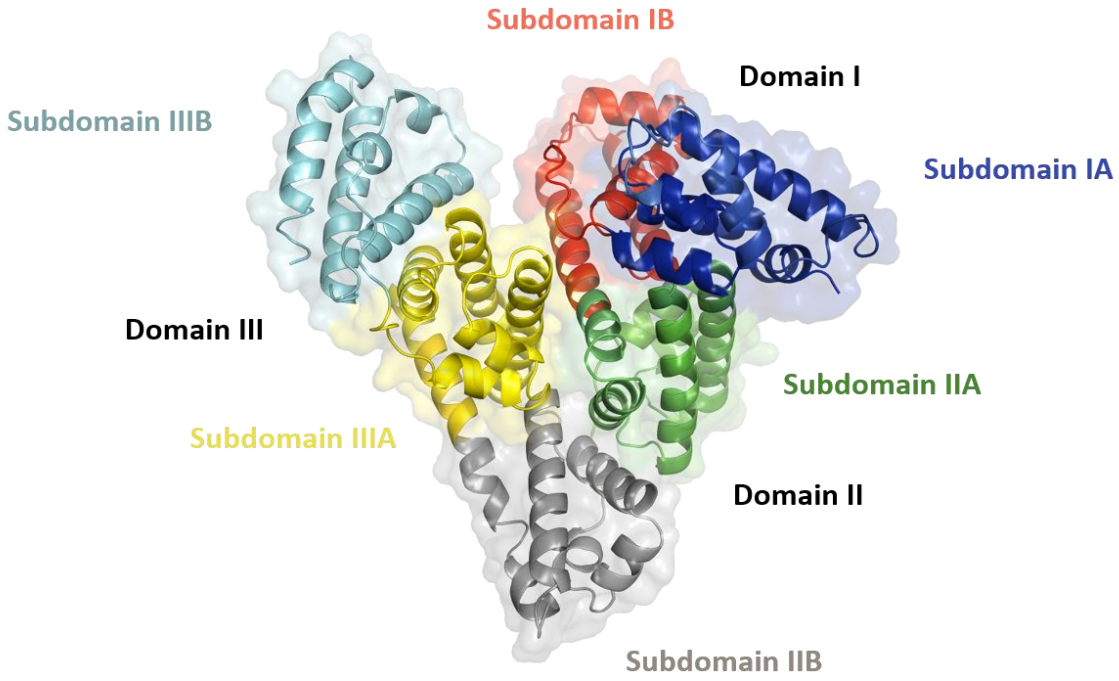

Figure 1.1. The overall structure of serum albumin. Domains are labeled with Roman numerals (I, II, III) and subdomains with letters (e.g., IA), with each subdomain shown in a different color.

Albumin's unique properties had led to its broad applications in medicine and have been leveraged since the 1940s, when fractionation of human serum plasma was first described,[23] and albumin was applied in the treatment of cirrhosis of the liver.[24,25,26] At that time, the only source of HSA was donated human blood, which is associated with the risk of transmitting pathogenic viruses and requires special handling (e.g., pasteurization during purification) to be safe for a recipient.[27] Nowadays, gene manipulation techniques have enabled large quantities of recombinant human albumin to be produced in various organisms such as *E. coli* bacteria,[28] *P. pastoris* yeasts,[29]

transgenic rice seeds,[30] and transgenic cattle,[31] without any health concerns related to its clinical use. Recombinant albumin has replaced plasma-derived albumin in many clinical applications, namely as a component of MMR2 vaccines[32] or as a component of an artificial human[33] or animal blood.[34] Production of recombinant albumin also provides an opportunity to modify HSA's properties, particularly in ligand binding and transport, by introducing mutations in selected regions to improve or change its current applications. For instance, a single deletion at the N-terminus (Asp1) is used in the production of hypoallergenic albumin.[35,36]

Albumin's great ligand-binding capacity is used in the blood dialysis systems for the treatment of liver failure. Healthy humans are able to maintain a proper concentration of small molecules in the blood and cleanse metabolites, but patients with liver failure suffer from toxin accumulation in the body and face life-threatening complications. One possible treatment for patients with liver failure is blood detoxification with a liver support system, such as a Single-Pass Albumin Dialysis system[37] (SPAD) or Molecular Adsorbent Recirculating System (MARS).[38] In both of these systems, a patient's blood is dialyzed against an albumin dialysate solution (recombinant HSA), allowing toxins in the blood to pass the membrane pores, bind to albumin, and be removed from the patient's body.[39]

1.1.1. Genetic variability of HSA

HSA is encoded by a single copy gene, *Alb,* that is located on the long arm of chromosome 4 near the centromere at position q11–22.[8] Over 70 genetic variants of its mature version have been studied and reported in the literature.[8,40–44] Moreover, the single nucleotide polymorphism database (dbSNP), which contains genomic data for hundreds of thousands of individuals, reports 452 missense variants (single point mutations in amino acid sequence) of HSA.[45] Single amino acid substitutions may affect HSA's ligand-binding properties, but the effects of these variants on human health are sparsely studied. Some of these variants are reported to have significant effects on HSA binding properties. For example, in individuals with Arg218 mutated to histidine, proline, or serine or Arg222 changed to isoleucine, HSA binding of thyroxine (a thyroid hormone) is significantly increased, and extremely high concentrations of total thyroxine (up to 15-fold increases) are observed,[46,47] resulting in familial dysalbuminemic hyperthyroxinemia, also known as FDH.[48] These mutations change the size of the binding site, reduce the steric restrictions, and allow thyroxine to bind with higher affinity. The frequency of occurrence of this condition depends on the race and origin. The estimated prevalence in Caucasians is 0.01%, while in people of Hispanic origin is 1.0–1.8%.[49,50] Some other HSA mutations were shown to result in altered binding of endogenous ligands, such as fatty acids,[51–53] bilirubin,[40] prostaglandins,[41] progesterone,[42] and testosterone.[41] However, the effect of natural genetic variations in HSA on the binding of most drugs has not been studied. The elucidation of the location of binding sites on HSA for the most-used drugs could identify drugs that might be affected by mutations in these sites.

1.1.2. Glycation of albumin

Nonenzymatic glycosylation (glycation), which occurs during SA's long circulation time, is an important phenomenon that may affect the binding of various ligands to SA and alter their free blood concentration. According to the American Diabetes Association, blood sugar levels in healthy people measured after an overnight fast should be in the range 70-100 mg/dL (3.9-5.5 mM) and two hours after the start of a meal less than 140 mg/dL (7.8 mM). For people with diabetes the targeted ranges are 80 to 130 mg/dL (4.4-7.2 mM) and less than 180 mg/dL (10 mM), respectively.[54] It is estimated that more than 50% of individuals older than 45 years of age taking a prescription drug have abnormally elevated levels of glycated hemoglobin, indicating high glycation of serum albumin.[55] Depending on the method, it is estimated that between 0.6-16% of the HSA in a healthy human is glycated. In diabetic patients, these values are 2-5 times higher than normal values for a given reporting method.[56–58] HSA has multiple lysine and arginine residues that are known to undergo glycation (**Figure 1.2**),[56,58–60] which can alter albumin binding affinity to drugs.[58,61–63] For example, the binding of warfarin, an anticoagulant, and (*R*)-cetirizine, a common antihistamine, has been shown to be affected by glycation.[56–58,64,65] The process of glycation starts from the reaction of reducing sugar (typically D-glucose) with sidechains of protein's lysine (amino group) or arginine (guanidino group) and forms a Schiff base.[58] This reaction is reversible and can be followed by the formation of a stable Amadori product (**Figure 1.3**). Glucose adducts can exist in both open-chain or cyclic form. SA was reported to catalyze the ring-opening reaction of glucose.[66] These reactions are

typically described as early-stage glycation and can be followed by further oxidation, dehydration, and cross-linking steps leading to the formation of reactive dicarbonyl compounds (e.g., glyoxal) that form advanced glycation end-products with protein residues.[58]

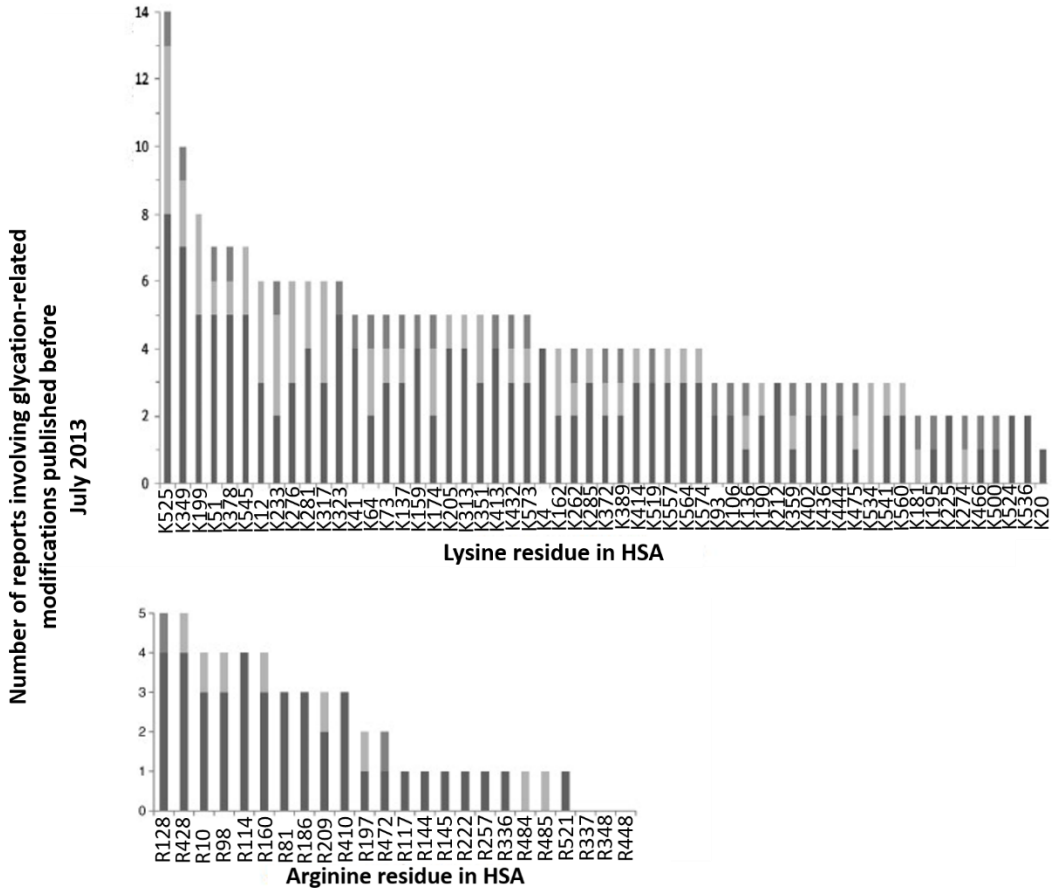

Figure 1.2. Residues in HSA that have been identified to undergo glycation-related modifications. The number of reports that have involved *in vitro* samples is shown in dark grey, light gray is associated with *in vivo* samples, and intermediate gray with plasma that was spiked with glucose and incubated under *in vitro* conditions. Figure adapted from Anguizola et al.[58]

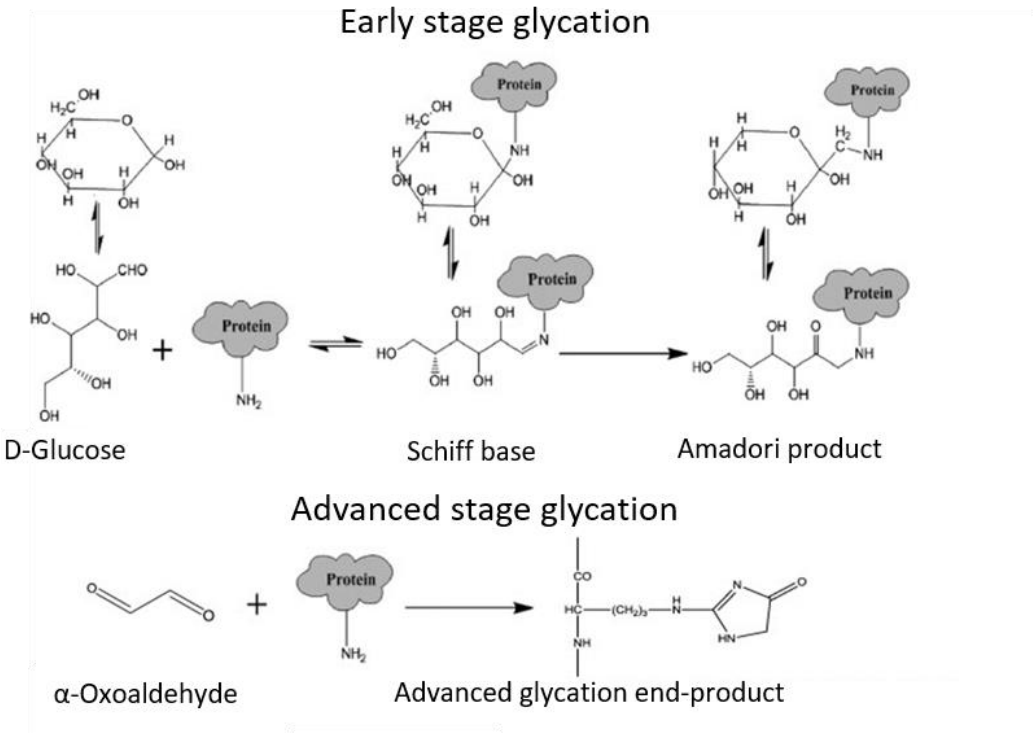

Figure 1.3. Products of early and advanced stage glycation. Figure adapted from Anguizola et al.[58]

Glycation of SA is typically studied using mass spectrometry,[58] but structural methods have also been employed to investigate sugar binding to SA. Wang et al. determined the crystal structures of HSA complexes with glucose and fructose (PDB IDs: 4IW2 and 4IW1, respectively) and reported that two molecules of glucose or fructose can bind to drug site 1 (Sudlow site I) at the same time.[66] In both cases, they found one molecule of sugar bound in the cyclic form and the other one in linear form. Based on the interactions between sugar molecules and protein residues observed in these structures (e.g., the covalent bond between glucose and Lys195), they hypothesized that Lys195 and Lys199 play a crucial role in the mechanism of sugar ring-opening by SA. Moreover, their

structures showed that the glycated Lys195 forms additional hydrogen bonds with surrounding residues and thus blocks the access to one of the major drug-binding sites in SA.[66] These findings clearly demonstrate the need for studies of SA glycation at the molecular level, which will help to understand why glycated SA binds some drugs stronger (e.g., cetirizine[64]) and other drugs weaker (e.g., acetohexamide[67]) as compared to the non-glycated form.

1.1.3. Albumin sequence variability across mammalian species

Serum albumin is very well conserved across mammals, with a typical sequence identity between HSA and SA from other species on the level of 70%. For instance, pairwise sequence identity for HSA/ESA and HSA/BSA is 76.1% and 75.6%, respectively (**Figure 1.4**). The secondary structure of SA is also conserved in mammals (**Figure 1.5**).[68] Due to that, the affinity of compounds for plasma proteins is typically expected to be similar across species. However, some compounds show significantly different interspecies PPB, greater than an order of magnitude.[69–73] For example, 70% of cefotetan (an antibiotic) is free in rat plasma, but only 9% of this drug is free in human plasma; 88% of valproate (an anticonvulsant) is free in mouse plasma, but only 5.2% of this drug is free in human plasma.[69] The reasons that lead to interspecies differences in PPB are not yet fully understood but may be explained in part by the differences in the amino acid sequences of the corresponding albumins. Plasma binding of drugs with significantly different interspecies PPB is highly correlated with the binding to SA, which is the major drug-binding component.[69] SA binding differences can be caused by differences in the

amino acid residues forming the drug-binding sites in different SAs or even by differences in the location of the preferred binding site(s) for a particular drug. A molecular understanding of what leads to these differences is crucial for biomedical researchers to predict human pharmacokinetic and pharmacodynamic relationships based on studies in animal models.

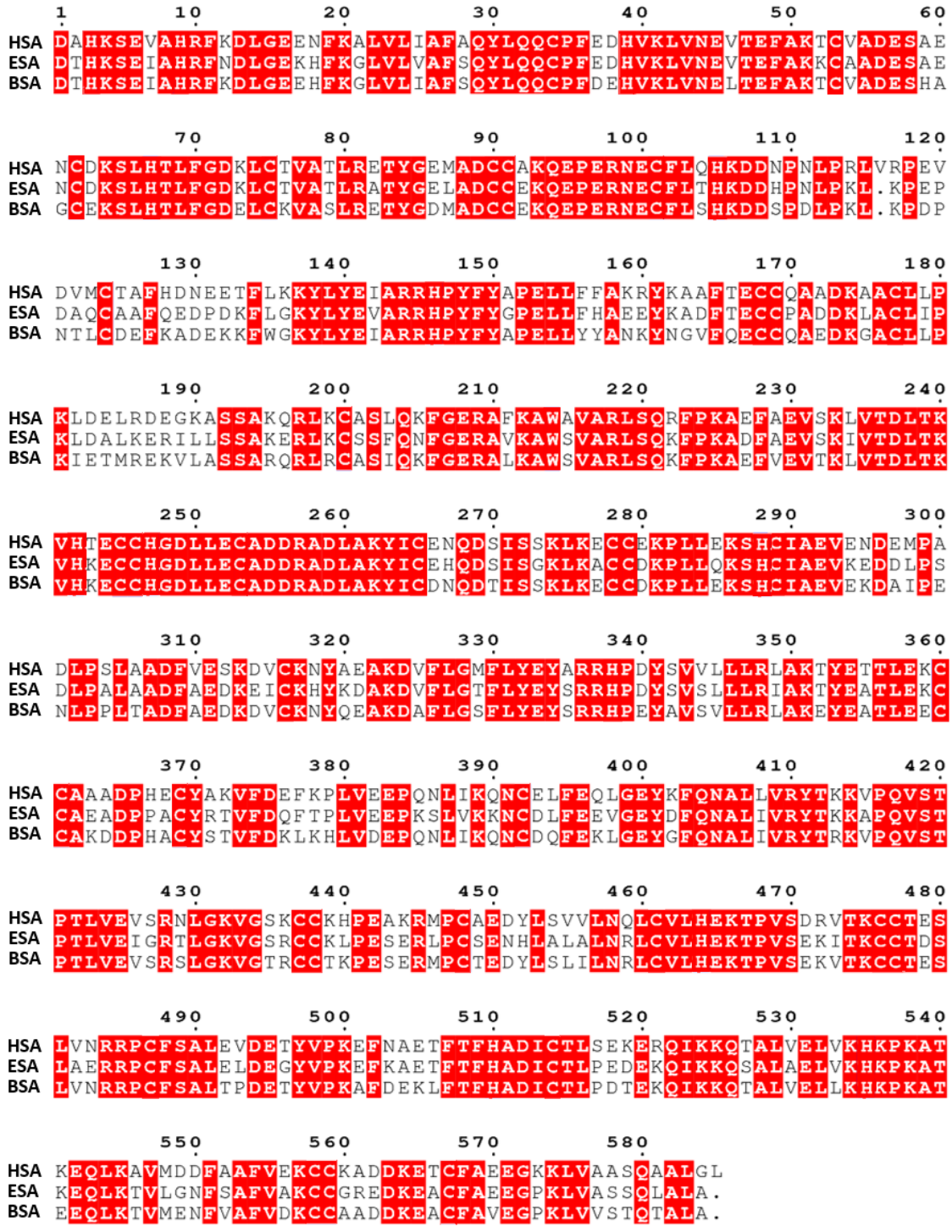

Figure 1.4. Alignment of HSA, ESA, and BSA sequences. Identical residues are highlighted in red.

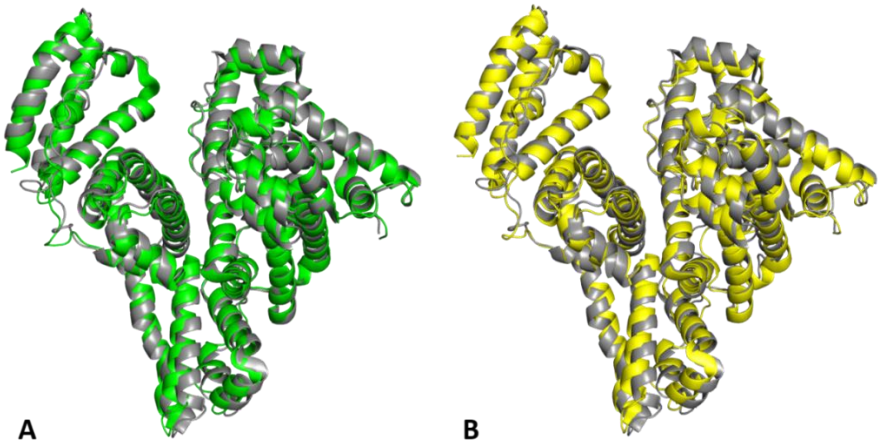

Figure 1.5. A) Superposition of the ligand-free HSA structure (PDB ID: 4K2C; shown as a grey cartoon) with the ligand-free ESA structure (PDB ID: 3V08; green cartoon); RMSD calculated between the aligned Cα atoms: 1.7 Å. B) Superposition of the ligand-free HSA structure (PDB ID: 4K2C; shown as a grey cartoon) with the ligand-free BSA structure (PDB ID: 3V03; yellow cartoon) ; RMSD calculated between the aligned Cα atoms: 1.7 Å.

1.2. Albumin drug-binding properties

Until recently, drug sites 1 and 2 (Sudlow sites I and II) were generally expected to bind most drugs.[15,68,74–78] Recent structural studies of HSA and other mammalian SAs have revealed several additional drug sites in this molecule (**Figure 1.6**).[79,80] In this study, albumin binding sites are described using a novel nomenclature, based on the site numbers used previously by other scientists,[79] and extended to include sites 7, 8, 9, and 10. With a variety of binding sites, SA has the impressive capability to bind various, often structurally different classes of drugs such as anticancer agents, anticoagulants, antihistamines, anesthetics, anthelmintic agents, antiretrovirals, benzodiazepines,

steroid- and amino acid-derived hormones, contrast media, and NSAIDs.[1,81,82] More than 900 FDA-approved drugs were reported to bind significantly to plasma proteins, mostly SA.[14] As a result of these interactions, the biodistribution, and bioavailability of many drugs are dictated by binding to SA.[83] In mammalian circulation, drugs are bound to SA, bound to other transport proteins (e.g., lipoproteins and globulins), or unbound.[15] The PPB of a drug is a reversible and rapid equilibrium process. According to the free drug theory, only unbound drugs can enter tissues and exert their pharmacological effects.[15,78] By virtue of its high blood concentration and high binding capacity, SA is one of the major factors that determine the free plasma concentration of many drugs, thereby modulating their therapeutic effects. Thus, drugs with higher affinities for SA may require higher dosages to achieve and maintain a desired therapeutic effect.[81] In drug development, an overly high affinity of a lead compound to SA and other plasma proteins results in insufficient free drug concentrations, influencing the lead optimization process.[78,84] SA also provides a reservoir for drugs as they are removed from the blood by various processes, which prolongs the duration of the therapeutic action. Furthermore, SA plays an important role in the therapeutic efficiency of some drugs by decreasing the formation of drug aggregates.[81] Consequently, the efficacy and toxicology of a drug are often impacted by the extent of its PPB, which significantly influences the pharmacokinetic and pharmacodynamic properties of a drug.[13,15] These factors make drug binding to SA an essential parameter for a drug's efficacy and safety that is investigated in drug development programs.[13,15]

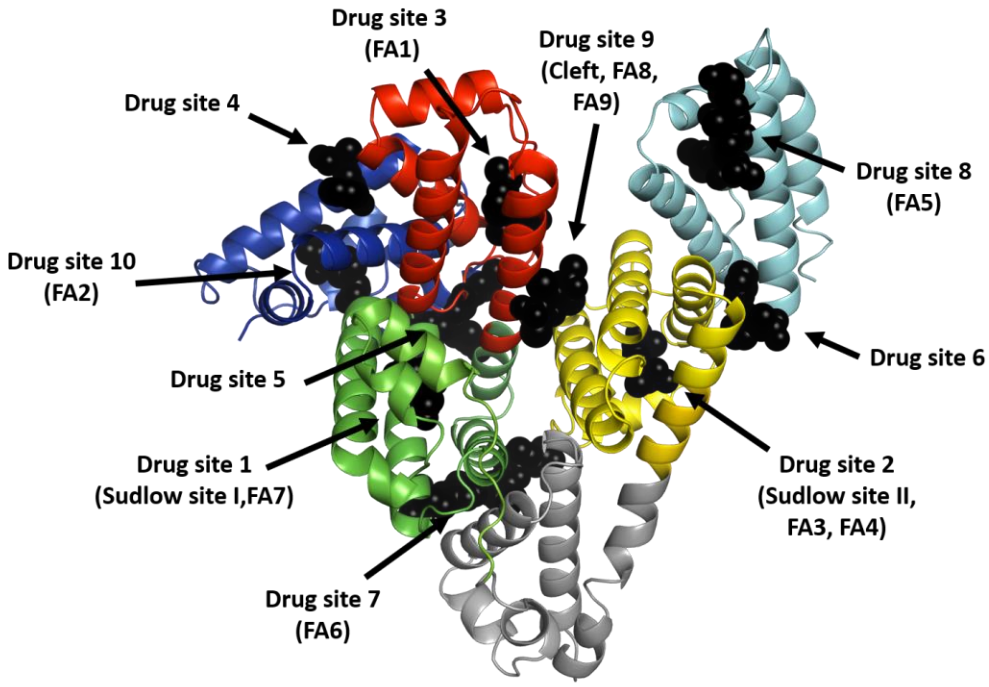

Figure 1.6. Drug-binding sites on SA. Atoms of all ligands at a particular site are shown as black spheres. Site numbers are according to Handing et al.[79] with sites 7, 8, 9, and 10 added. Alternative names of sites are listed in parentheses. FA stands for the fatty acid binding site.

1.2.1. Drug-drug displacement

When SA binds multiple drugs in circulation, a drug may be displaced by another strong-binding drug administered at a high concentration.[85–88] Drug-drug displacement usually occurs due to direct competition for a particular binding site but may also happen due to allosteric effects that change the affinity of one drug upon the binding of another.[13,15,89] This phenomenon likely occurs in a substantial number of individuals who take multiple drugs at the same time. According to the Centers for Disease Control, 72%

of people taking any prescription drug take more than one drug at the same time (3.7 drugs on average).[55] One of the most commonly taken drugs are nonsteroidal anti-inflammatory drugs (NSAIDs). Roughly 72 million people in the U.S. take NSAIDs at least three times a week for more than three months per year, often in conjunction with other drugs.[55] Gastrointestinal bleeding is a notable example of a detrimental drug-drug displacement effect that occurs when warfarin, an anticoagulant, is displaced from SA when co-administered with NSAIDs.[76,90,91] Some other drugs that have been shown to be displaced by NSAIDs include methotrexate (an immunosuppressant) and valproate (an anticonvulsant), and the displacement of small molecules such as SA-bound toxins have been shown to lead to adverse physiological effects (e.g., uremia).[15,92] However, the way in which SA binds commonly co-administered drugs has not been thoroughly investigated on a structural basis, precluding the molecular understanding of how commonly used drugs compete for binding to SA.

Many of albumin binding sites were reported to bind endogenous compound as well. For instance, fatty acids bind to at least nine different sites in HSA that often overlap with drug sites (e.g., drug site 2 can bind two molecules of fatty acid at the same time; see **Figure 1.6**). It is estimated that 99% of non-esterified fatty acids circulating in the human body are bound to HSA,[93,94] which mediates their solubilization and transport in the body. Fatty acids were shown to diminish the binding of some drugs to HSA due to their high load on HSA, e.g., the intravenous anesthetic thiamylal.[95] Typically, 0.5-2 moles of fatty acids are bound per mole of HSA, but in states of cardiovascular disease or

diabetes, these ratios can be as high as 6:1, which might significantly affect the binding and transport of many drugs.[93,96]

1.2.2. Albumin drug-binding studies

Interactions of serum albumin with small molecules are often very difficult to characterize due to multiple binding sites of albumin and non-specific character of binding (mostly hydrophobic interactions). Over the years, various methods using different approaches and phenomena have been used for albumin binding studies. Historically, one of the first of these methods was equilibrium dialysis, used since the 1940s.[97] This method uses dialysis to measure the ratio between the free fraction of a ligand (e.g., drug) in the solution and the fraction of ligand that is bound to the protein of interest at equilibrium.[98] At the beginning of the experiment, solutions containing protein and ligands are separated by a membrane. The membrane allows small molecules (ligands) to pass through and interact with the protein but retains proteins and their complexes. Equilibrium dialysis has been used to characterize the interactions of numerous drugs with plasma proteins, including albumin,[99–102] and is still considered as the gold standard method to measure unbound drug plasma concentration.[103] Another technique based on the measurements of protein-bound and free drug fractions used for albumin drug binding studies is ultrafast affinity extraction. In this method, albumin mixed with the drug of interest is injected onto a column containing immobilized albumin.[104] Based on the amount of free drug fraction eluted from the column and elution time, the binding affinity

can be calculated. Ultrafast affinity extraction combined with other chromatographic techniques (e.g., zonal elution) has also found an application in competition studies and can be used to investigate drug binding to glycated albumin.[105–107] The great advantage of these techniques include factors such as they can be used to study interactions of most ligands with albumin, their sensitivity typically depends on other methods used for the measurements of free drug fraction in the solution (e.g., spectrophotometric methods, radioimmunoassays), and that they only have a small number of limitation. However, all of these techniques provide only global affinity for albumin and does not allow the determination of the number of binding sites and cannot distinguish between them.

Other biophysical methods, such as surface plasmon resonance (SPR), isothermal titration calorimetry (ITC), or tryptophan fluorescence quenching (TFQ), can be used for further characterization of albumin interactions with small molecules as well. However, they often have many limitations. SPR has been shown to be a good technique for high-throughput measurements of drug binding to human serum albumin.[108] It requires immobilization of the protein on a sensor (metal film) that has contact with the solution containing the ligand of interest during the experiment.[109] In this technique, the phenomenon of surface plasmon resonance is used to monitor protein-ligand interactions. The changes of the refractive index caused by protein interactions with a ligand can be displayed as a sensorgram and used for calculations of the rates of association and dissociation (k_{on} and k_{off}, respectively), and the association constant (K_a). The same information can be obtained from biolayer interferometry (BLI), which uses a very similar setup and monitor protein interactions with small molecules by measuring

the interference of white light reflected from the protein immobilized on the sensor and from an internal reference layer.[110] Both of these techniques are label-free but require immobilizing the protein onto the sensor surface, which depending on the used method, may block access to some of the binding sites. Another technique often used for albumin-drug binding studies is TFQ.[79,111] In this method, changes in protein's intrinsic fluorescence (tryptophan is the dominant intrinsic fluorophore) upon binding of a ligand are monitored and can be used to calculate the association constant. Tryptophan's fluorescence is known to be highly sensitive to the changes in its local environment.[112] However, quenching of tryptophan fluorescence can only occur if the distance between the tryptophan side-chain and a quencher is short (<15 Å).[113] Human serum albumin has only one tryptophan residue (Trp214), which is located close to drug site I (Sudlow site I). Due to that, the application of this method is limited only to ligands that bind to sites located close to Trp214.

Another technique commonly used for the characterization of protein interactions with small molecules is ITC. ITC measures the heat released or absorbed during the interactions between two molecules (e.g., ligand binding to protein).[114] ITC experiment can provide broad characteristics of the molecular interactions by revealing the binding enthalpy (ΔH), entropy (ΔS), constant (K_a), and reaction stoichiometry (n). This technique is frequently used for studying albumin interactions with drugs.[115–117] However, its application may be limited for ligands that bind weakly to albumin and which binding is not associated with moderate thermal effects. Also, ITC experiments often require highly concentrated protein and ligand and are problematic for ligands insoluble in water.

1.2.3. Structures of albumin complexes with FDA-approved drugs

SA is a protein of interest for researchers in many biomedical disciplines, but especially so for structural biologists, who provide a basis for understanding mechanisms underlying albumin-based transport of drugs and metabolites in the blood. At the time of writing, 157 structures of SA from various organisms have been deposited in the Protein Data Bank (PDB); the majority of these structures are of human (111) and equine (25) serum albumin, but structures of bovine (6), leporine (5), caprine (4), ovine (4), canine (1), and feline (1) serum albumins have also been reported. All of the SA structures available in the PDB have been determined using X-ray crystallography. Most of these structures are SA complexes with various ligands such as drugs or metabolites. However, despite the high number of determined structures, SA complexes with only 29 FDA-approved drugs have been structurally characterized before this study (**Table 1.1**). Most of the drugs were crystallized with SA from only one species (typically HSA). Only five drugs were complexed with SA from two or more species: diclofenac (HSA and ESA), ibuprofen (HSA, ESA), ketoprofen (LSA, BSA), naproxen (HSA, ESA, BSA, and LSA) and suprofen (ESA, LSA). The determination of structures of drug complexes with SA from various species allows us to study differences in drug transport by model organisms at the molecular level and provides an additional evaluation of the usefulness of these model organisms. However, not only changes in albumin sequence between species or modifications of binding sites architecture affects its binding properties. The presence of metabolites (e.g., fatty acids, sugars) or various small molecules being a part of the crystallization solution (e.g., PEGs) in the SA's binding sites may also alter albumin interactions with drugs. Nevertheless,

these effects have not been well-studied. For instance, the effect of fatty acids on drug binding by SA has been studied using structural methods (their complexes with HSA in the presence and absence of fatty acids are available in the PDB) only for five drugs: warfarin, thyroxine, azapropazone, phenylbutazone, and oxyphenbutazone. Similarly, the effects of sugar binding to SA remains understudied at the molecular level.

Table 1.1. List of all structures of SA complexes with FDA-approved drugs reported to the PDB prior to this study.

Ligand name	Drug's trade name	Drug's classification	DrugBank ID	PDB ID / Organism
Halothane	Fluothane	Anesthetic	DB01159	1E7B,[118] 1E7C[118] / Human
Lidocaine	Xylocaine	Anesthetic	DB00281	3JQZ[119] / Human
Propofol	Diprivan	Anesthetic	DB00818	1E7A[118] / Human
Fusidic acid	Fucidin	Antibiotic	DB02703	2VUF[120] / Human
Bicalutamide	Casodex	Anti-cancer drug	DB01128	4LA0[80] / Human
Etoposide	Etopophos	Anti-cancer drug	DB00773	4LB9[80] / Human
Teniposide	Vumon	Anti-cancer drug	DB00444	4L9Q[80] / Human
Warfarin	Coumadin	Anticoagulant	DB00682	2BXD,[81] 1H9Z,[121] 1HA2[121] / Human
Aripiprazole	Abilify	Antipsychotic	DB01238	6A7P[122] / Human
Amantadine	Gocovri	Antiviral drug	DB00915	3UIV[123] / Human
Diazepam	Valium	Drug for anxiety disorders treatment	DB00829	2BXF[81] / Human
Zidovudine	Retrovir	Antiretroviral drug	DB00495	3B9L,[124] 3B9M[124] / Human
Idarubicin	Idamycin	Drug for leukemia treatment	DB01177	4LB2[80] / Human
Phenylbutyric acid	Ammonaps	Drug for urea cycle disorders treatment	DB06819	5YOQ[125] / Human
Cetirizine	Zyrtec	Histamine antagonist	DB00341	5DQF[79] / Horse
Aspirin	Bayer® Aspirin	Non-steroidal anti-inflammatory drug	DB00945	3B9M,[124] 2I30,[126] 2I2Z[126] / Human
Azapropazone	Rheumox	Non-steroidal anti-inflammatory drug	DB07402	2BXI,[81] 2BX8,[81] 2BXK[81] / Human
Diclofenac	Cambia	Non-steroidal anti-inflammatory drug	DB00586	4Z69[127] / Human 4ZBQ,[128] 4ZBR,[128] 5DBY[128] / Horse
Diflunisal	Dolobid	Non-steroidal anti-inflammatory drug	DB00861	2BXE[81] / Human
Ibuprofen	Advil	Non-steroidal anti-inflammatory drug	DB01050	2BXG[81] / Human, 6OCI[115] / Horse
Indomethacin	Indocin	Non-steroidal anti-inflammatory drug	DB00328	2BXK,[81] 2BXM,[81] 2BXQ[81] / Human
Ketoprofen	Orudis	Non-steroidal anti-inflammatory drug	DB01009	6QS9[129] / Bovine 6OCK[115] / Leporine
Naproxen	Aleve	Non-steroidal anti-inflammatory drug	DB00788	2VDB[130] / Human, 4ZBR,[128] 5DBY[128] / Horse 4OR0[131] / Bovine 4PO0[131] / Leporine
Oxyphenbutazone	Withdrawn	Non-steroidal anti-inflammatory drug	DB03585	2BXB,[81] 2BXO[81] / Human
Phenylbutazone	Butazolidine	Non-steroidal anti-inflammatory drug	DB00812	2BXC,[81] 2BXP,[81] 2BXQ[81] / Human
Sulfasalazine	Azulfidine	Non-steroidal anti-inflammatory drug	DB00795	6R7S[132] / Human
Suprofen	Withdrawn	Non-steroidal anti-inflammatory drug	DB00870	6OCJ[115] / Horse 6OCL[115] / Leporine
Iodipamide	Sinografin	Radiographic contrast media	DB04711	2BXN[81] / Human
Levothyroxine	Eltroxin	Thyroid hormone	DB00451	1HK1,[87] 1HK2,[87] 1HK3,[87] 1HK4,[87] 1HK5[87] / Human

1.3. Characteristics of drugs and drug candidates whose binding to SA is investigated in this study

1.3.1. Steroids

Steroids are a class of compounds with a characteristic structure consisting of four-fused-rings (steroid core structure). The class of steroids consists of compounds that are naturally present in the human organism and often act as hormones (e.g., androgens), but also includes synthetically made medications (corticosteroids), widely used in the treatment of inflammation and allergy.[133] In this study, I investigated albumin interactions with two sex steroid hormones (testosterone and progesterone) and two steroid medications (dexamethasone and hydrocortisone; **Figure 1.7**). Structures determined in this work show, for the first time, albumin interactions with steroids at the molecular level.

Testosterone is the primary male sex steroid hormone and is responsible for the development of primary and secondary sexual characteristics. Like other steroid hormones (e.g., progesterone), testosterone is synthesized from cholesterol and stimulates protein synthesis.[134] Upon puberty in males, the plasma concentration of testosterone rises to 17.3-24.3 nM.[2] Testosterone is 97.0-99.5% bound to SA or sex hormone-binding globulin (SHBG).[135] 53-55% of testosterone is bound to HSA, 43-45% is bound to SHBG, and the remaining fraction is free in the bloodstream.

Progesterone is one of the main female sex hormones. It plays an important role during the menstrual cycle and is crucial for the proper maintenance of pregnancy.[136] The

plasma concentration of progesterone varies in females from about 0.47 nM to more than 4.7 nM, and during pregnancy rises to almost 500 nM.[137] It is estimated that 96-99% of progesterone in the blood is bound to plasma proteins, primarily to HSA and transcortin, and the remaining fraction is unbound.[138]

Dexamethasone is a corticosteroid medication used to treat multiple conditions, including severe pneumonia, rheumatic problems, skin diseases, severe allergies, asthma, chronic obstructive lung disease, brain swelling, and many others.[139,140] Dexamethasone also exhibits anti-inflammatory activity and immunosuppressant effects. Recently, dexamethasone has been reported to lower mortality in patients with severe COVID-19.[141] About 77% of dexamethasone in the blood is bound to plasma proteins, mostly to serum albumin.[140]

Hydrocortisone (cortisol) is a corticosteroid used in the treatment of multiple conditions, such as inflammation, dermatitis, asthma, arthritis, and adrenal insufficiency.[142] The name hydrocortisone is typically used when the corticosteroid is used as a medication (synthetically prepared), while the name cortisol is associated with the steroid hormone. Cortisol is responsible for mediation of the stress response in humans, and in the presence of a threat, its levels surge.[143] Hydrocortisone in the blood is bound to plasma proteins in about 90%, mostly to albumin and transcortin.

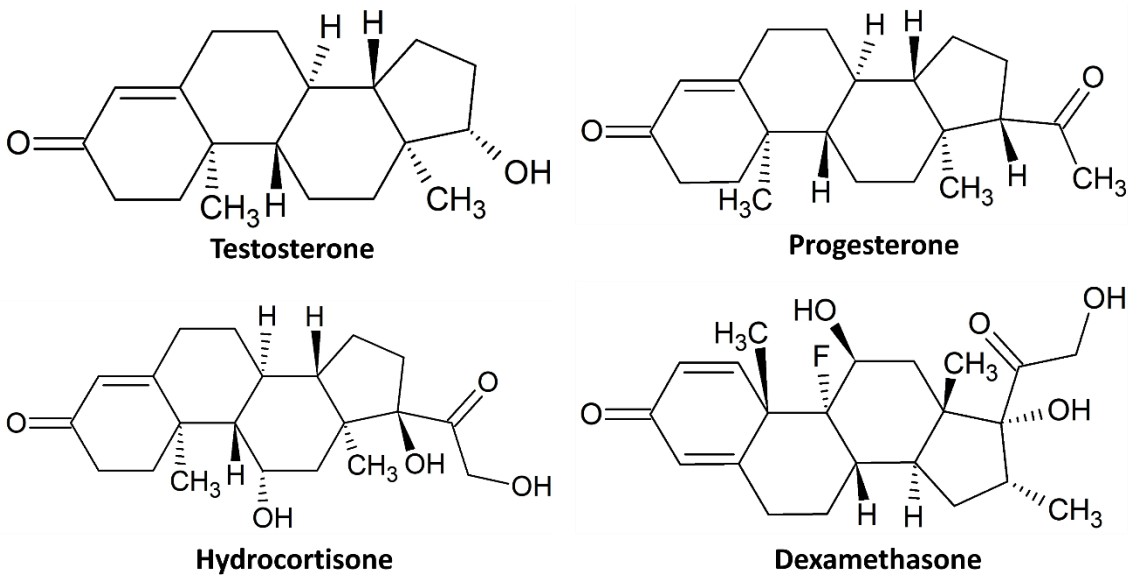

Figure 1.7. Structures of steroids used in this study.

1.3.2. Nonsteroidal anti-inflammatory drugs

Nonsteroidal anti-inflammatory drugs (NSAIDs) are non-opioid therapeutic agents used in the management of mild to moderate pain, fever, and inflammation. These represent some of the most widely used medicines in the world. It has been estimated that up to 30 million people in the United States use NSAIDs every day and that over 30 billion doses of NSAIDs are taken annually.[144–147] NSAIDs are not only used by humans, as domesticated animals are also treated with NSAIDs for inflammation and pain.[148–150] NSAIDs act via the inhibition of cyclooxygenase enzymes (COX), thereby inhibiting prostaglandin and thromboxane biosynthesis and reducing the inflammatory response and blood clotting.[151,152]

NSAIDs are typically used in medicine as racemic mixtures and were used as such in this study (**Figure 1.8**). However, their ability to inhibit COX is typically confined to

enantiomers of the (*S*)-stereoconfiguration,[153] and (*R*)-enantiomers of those drugs either are inactive or exhibit a different activity. (*R*)-ibuprofen is not a COX inhibitor, but a significant fraction of it undergoes metabolic conversion to the (*S*)-enantiomer in the body.[154,155] A similar conversion of the (*R*)-enantiomer to the (*S*)-enantiomer is observed for (*R*)-ketoprofen, which is more analgesic than the (*S*)-enantiomer when acting alone.[156] For etodolac, (*R*)- to (*S)*-enantiomer conversion has not been observed *in vivo*;[157] (*S*)-etodolac shows anti-inflammatory effects, while (*R*)-etodolac exhibits gastroprotective effects.[158] NSAIDs are often administered orally and are generally well-absorbed in the gastrointestinal tract before subsequent delivery to the site of action by blood.[159] They can also be administered topically, intravenously, intramuscularly, and rectally, and all of these delivery methods are followed by delivery via blood. In the bloodstream, NSAIDs are highly bound to plasma proteins (NSAIDs described here are 99% bound), mainly to SA.[159] Their interactions with plasma proteins are widely studied, which reflects in a high number of the determined structures of SA-NSAID complexes (**Table 1.1**). In this study, I investigated interactions of serum albumin with the following NSAIDs: ibuprofen, ketoprofen, etodolac, nabumetone, and 6-methoxy-2-naphthylacetic acid (6-MNA), the active metabolite of nabumetone (**Figure 1.8**).

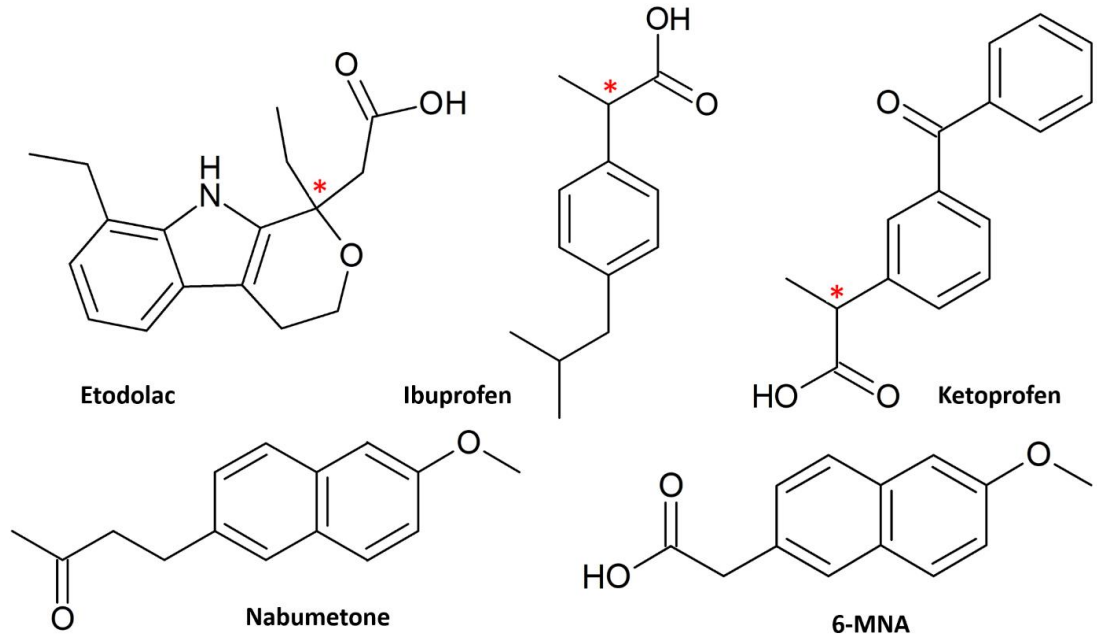

Figure 1.8. Structures of NSAIDs used in this study; chiral centers are labeled with an asterisk. All of the chiral compounds (etodolac, ibuprofen, and ketoprofen) are used in medicine as racemic mixtures and were used as such in this study.

1.3.3. Various other FDA-approved drugs

This chapter describes the properties of commonly used drugs that belong to different classes of drugs (antibiotics, antipsychotic drugs, etc.) and have distinct structures.

1.3.3.1. Warfarin

Warfarin is one of the most widely used anticoagulants, typically administered as a racemic mixture (**Figure 1.9**).[160] Both enantiomers of warfarin exhibit similar activity (inhibition of the vitamin K epoxide reductase complex 1), but it is estimated that the (*S*)-

enantiomer is three to five times more potent than the opposite enantiomer.[161] Warfarin is a drug with a narrow therapeutic index, and unexpected differences in its blood concentration may cause adverse drug reactions.[162] Moreover, warfarin is known to interact with many commonly prescribed drugs, which co-administered with warfarin may cause internal bleeding.[163] In the bloodstream, warfarin is primarily transported by albumin (99% bound).[160] Both enantiomers of warfarin have been reported to bind to drug site 1 in HSA.[81,121]

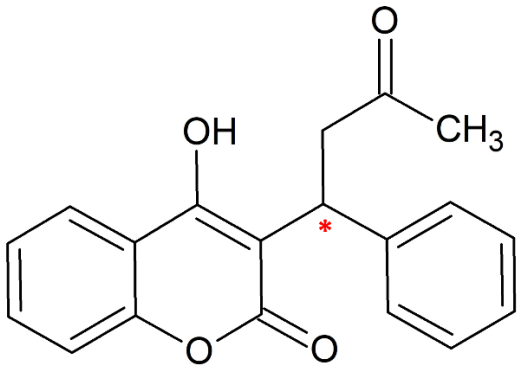

Figure 1.9. Structure of warfarin; chiral center is labeled with an asterisk. Warfarin is used in medicine as a racemic mixture and was used as such in this study.

1.3.3.2. Tolbutamide

Tolbutamide is a first-generation sulfonylurea used to lower glucose blood levels in patients with type 2 diabetes by stimulating the release of insulin from the pancreas (**Figure 1.10**).[164,165] In the bloodstream, tolbutamide is transported by plasma proteins (bound 98%), mostly SA.[166] Its binding to albumin has been studied using chromatographic methods,[167–169] which revealed that tolbutamide binds stronger (up to

1.4 times higher association equilibrium constant) to glycated albumin than to unmodified albumin. However, the location of tolbutamide binding sites in SA was not known prior to this study.

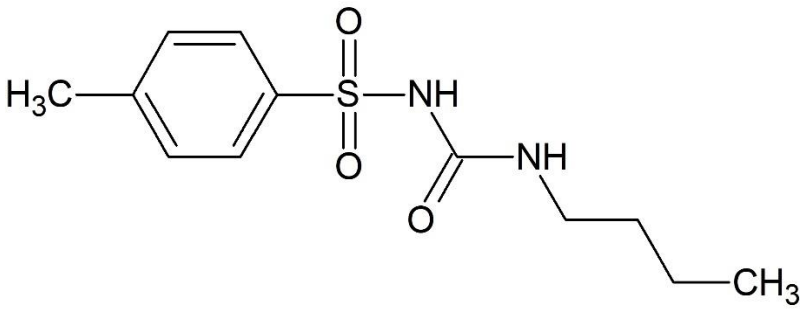

Figure 1.10. Structure of tolbutamide.

1.3.3.3. Haloperidol

Haloperidol is one of the most commonly prescribed antipsychotic drugs used in the treatment of schizophrenia and delirium (**Figure 1.11**).[170,171] Haloperidol blocks postsynaptic dopamine (D2) receptors leading to the elimination of dopamine neurotransmission, resulting in antidelusionary and antihallucinagenic effects.[172,173] It is estimated that about 90% of haloperidol in the blood is bound to plasma proteins (mostly to SA).[174] Haloperidol binding to albumin has been studied using spectroscopic and computational methods that suggested its binding to drug site 1.[175] However, prior to this study, structural methods have not been employed to test this hypothesis.

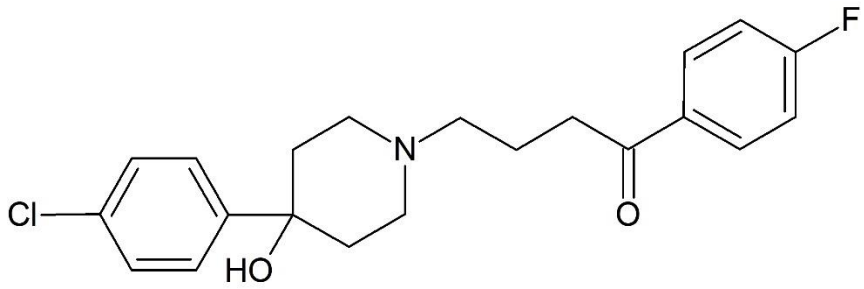

Figure 1.11. Structure of haloperidol.

1.3.3.4. Ampicillin

Ampicillin is an antibiotic used to treat various bacterial infections, such as bladder infections, pneumonia, bacterial meningitis, and gonorrhea.[176] Ampicillin is a member of β-lactam antibiotics (penicillin derivative; **Figure 1.12**) and works by inhibiting bacterial cell wall synthesis.[177] Its PPB has been characterized to be low (about 20%),[178–180] but at the same time, ampicillin has been reported to react with albumin and form covalent penicilloyl-protein conjugates.[181] Before this study, ampicillin binding to albumin has not been investigated at the molecular level.

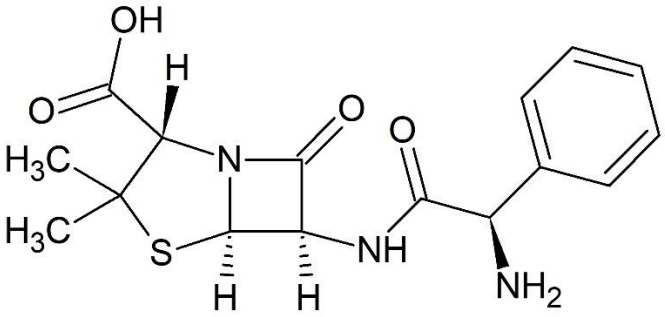

Figure 1.12. Structure of ampicillin.

1.3.4. Drug candidates

1.3.4.1. JMS-053

JMS-053 is a novel iminopyridinedione, recently shown to be a reversible, allosteric PTP4A3 phosphatase inhibitor (**Figure 1.13**).[182,183] PTP4A3 is overexpressed in many cancer diseases such as ovarian, liver, lung, breast, brain, stomach, and bladder cancer.[184,185] Potential application of JMS-053 in the treatment of ovarian and breast cancers is currently investigated.[182,183] Its mechanism of action has not been fully elucidated,[182] but it was reported that JMS-053 has a long plasma half-life ($t_{1/2}$ ~24 h) in mice, which suggests binding to plasma proteins.[186] JMS-053 binding to SA has been confirmed by ITC studies.[186]

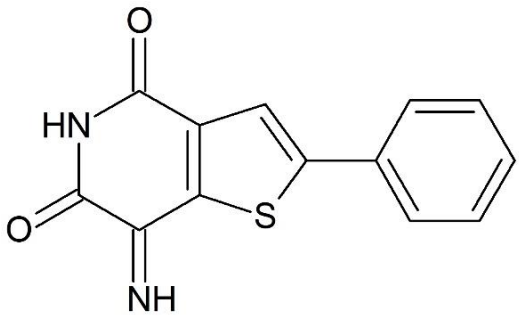

Figure 1.13. Structure of JMS-053.

1.3.4.2. GHK(Cu)

GHK peptide (glycyl-l-histidyl-l-lysine, also known as prezatide; **Figure 1.14**) naturally occurs in the human plasma and easily forms a complex with copper ions (GHK-Cu).[187,188] GHK(Cu) is known to accelerate wound healing and skin repair and exhibits

regenerative effects.[189] Thanks to these properties, GHK(Cu) is used as an ingredient in skin and hair cosmetics. The peptide is not registered as an FDA-approved drug, but its potential applications in the treatment of colon cancer and lung diseases are investigated.[187,188] GHK peptide is naturally present in human plasma, and its level declines with age, from about 100 nM at the age of 20 to 40 nM at the age of 60.[190] It was reported that GHK peptide interacts with albumin in physiological conditions,[189] but these interactions have not been studied at the molecular level.

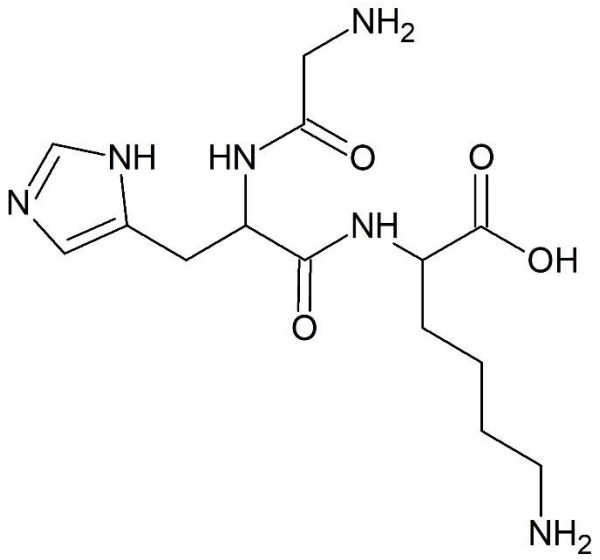

Figure 1.14. Structure of GHK peptide.

1.4. Rationale for the study

The ligand-binding properties of SA are affected by several factors, such as the presence of endogenous (e.g., metabolites) or exogenous (e.g., drugs) compounds in its binding sites or by alterations of its binding sites caused by covalent modifications (e.g., glycation). These effects are especially promoted in patients taking multiple drugs at the same time and those having elevated blood levels of metabolites, such as glucose and fatty acids (e.g., diabetics). The identification of cases in which alteration of SA binding capacity may affect the free fraction of the drug in the blood is crucial to ensure that the drug doses are appropriately adjusted to achieve the desired therapeutic effect and avoid unexpected toxicity.

The goal of this study is to further characterize albumin drug-binding sites and identify drugs whose binding to SA may be affected by elevated levels of glucose and fatty acids. In this work, I investigate the interactions of SA (HSA and ESA) with drugs and common metabolites using biophysical methods. ESA was used in most of these experiments because its crystallization is more reproducible than the crystallization of HSA and does not require using PEGs that may potentially occupy drug-binding sites (all known crystallization conditions of HSA require highly concentrated PEGs). Moreover, ESA has a very high identity and similarity when compared to HSA (76.1%/86.2%, respectively), which leads to the expectation of drug-binding sites being similar or identical in albumin from both species. The newly determined crystal structures of SA complexes with drugs provide information about the location of drug-binding sites,

contribute to our knowledge about the molecular determinants of binding, and may be a key element to understanding phenomena associated with drug co-administration, such as drug−drug displacement or drug co-binding. This study also provides the molecular details underlying the influence of abnormal levels of common metabolites on drug transport by SA.

2. Materials and methods

2.1. Materials

ESA was purchased from Equitech-Bio (#ESA62; ≥96% purity; Kerrville, TX, USA), HSA from Sigma-Aldrich (SA isolated from human serum #A8763, ≥99.0% purity; recombinant HSA expressed in *Pichia pastoris* #A7736; ≥90% purity; St. Louis, MO, USA), DMSO was purchased from Sigma-Aldrich (#276855; ≥99.9% purity; St. Louis, MO, USA), Trizma® base from Sigma-Aldrich (Tris; # T1503; ≥99.9% purity; St. Louis, MO, USA), ammonium sulfate from Sigma-Aldrich (#A4915; ≥99.0 % purity; St. Louis, MO, USA), lithium sulfate from Alfa Aesar (#A10410; 99% purity; Ward Hill, MA, USA), ampicillin from Sigma-Aldrich (#ROAMP; ≥95%; St. Louis, MO, USA), glucose from Sigma-Aldrich (#G5767; ≥95%; St. Louis, MO, USA), myristic acid from Sigma-Aldrich (#M3128, ≥99% purity St. Louis, MO, USA), testosterone from Sigma-Aldrich (#T1500; ≥98%; St. Louis, MO, USA), potassium phosphate monobasic from Sigma-Aldrich (#P5379; ≥99%; St. Louis, MO, USA), etodolac from Santa Cruz Biotechnology (#204747; ≥98% purity; Dallas, TX, USA), ibuprofen from Sigma-Aldrich (#I4883; ≥98% purity; St. Louis, MO, USA), ketoprofen from Santa Cruz Biotechnology (#205359; ≥99% purity; Dallas, TX, USA), sodium acetate from Sigma-Aldrich (#S2889; ≥99% purity; St. Louis, MO, USA), nabumetone from Sigma-Aldrich (#N6142; ≥99% purity; St. Louis, MO, USA), 6-MNA from Sigma-Aldrich (#CDS014591; ≥98% purity; St. Louis, MO, USA), warfarin from Sigma-Aldrich (#A2250; ≥98% purity; St. Louis, MO, USA), tolbutamide from Santa Cruz Biotechnology (#203298; ≥98% purity; Dallas, TX, USA), haloperidol from Sigma-Aldrich (#H1512; ≥95% purity; St. Louis, MO,

USA). The purity of all reagents mentioned above was reported by vendors. JMS-053 (7-imino-2-phenylthieno[3,2-c]pyridine-4,6(5H,7H)-dione) was synthesized by the group of Prof. Peter Wipf from the University of Pittsburgh.[191] GHK peptide was synthesized by the group of Prof. Wojciech Bal from the Institute of Biochemistry and Biophysics of the Polish Academy of Sciences.

2.2. Protein purification and crystallization

SA (ESA or HSA) was dissolved in a buffer containing 10-50 mM Tris (pH 7.4) and 50-150 mM NaCl. Size exclusion chromatography using a Superdex 200 column attached to an ÄKTA FPLC (GE Healthcare) was used to separate dimeric and monomeric fractions of SA. The purification buffer was the same as the buffer in which protein being purified was dissolved. The final protein purity was assessed by SDS-PAGE. The absorbance at 280 nm measured with a Nanodrop 2000 (Thermo Scientific) was used to estimate protein concentrations using the extinction coefficient ($\varepsilon_{280\text{-ESA}}$ = 27,400 M^{-1} cm^{-1}; $\varepsilon_{280\text{-HSA}}$ = 34,440 M^{-1} cm^{-1}) and molecular weight (MW_{ESA} = 65,700 Da; MW_{HSA} = 66,470 Da). Collected fractions of monomeric ESA were concentrated to 15-34 mg/mL (0.23-0.52 mM) and HSA to 100-162 mg/mL (1.5-2.44 mM) using an Amicon Ultra Centrifugal Filter (Millipore Sigma, #UFC903024) with a molecular weight cut-off (MWCO) of 30 kDa.

Crystallization of SA was performed in 15-well hanging drop plates (ESA; EasyXtal 15-Well Tools, Qiagen) set manually or in 96-well hanging drop plates (ESA and HSA; Swissci 3-Well Midi) that were set using a Mosquito crystallization robot (TTP Labtech,

Boston, MA). ESA crystals were obtained using three different crystallization conditions: A) 0.2 M lithium sulfate, 1.8-2.4 M ammonium sulfate, 0.1 M Tris buffer pH 7.4; B) 1.8 M ammonium dihydrogen citrate at pH 7.0; C) 1.6 M ammonium sulfate, 0.1 M Sodium acetate at pH 4.6. HSA was crystallized using a solution containing 50 mM potassium phosphate buffer at pH 7.0 and 24-28% PEG 3350. Ligands were added to the protein in different ways: etodolac, ketoprofen, nabumetone, tolbutamide, and 6-MNA were prepared as 100 mM solutions in pure DMSO and added to crystallization drops containing ESA crystals to reach a final drug concentration of 3 mM (ketoprofen, 6-MNA) or 10 mM (tolbutamide, nabumetone, etodolac), and then incubated for several hours before harvesting; ibuprofen, haloperidol, testosterone, progesterone, glucose and hydrocortisone powder was added directly to the crystallization drop containing crystals for 48 h before harvesting; dexamethasone powder was incubated with protein for 60 min at room temperature prior to the crystallization; JMS-053 powder was added to crystals of HSA that were cocrystallized with 5 mM myristic acid (dissolved in ethanol); ampicillin was dissolved in 50 mM Tris pH 7.4 and added to ESA crystals (final concentration 5 mM) several hours before harvesting; GHK peptide was dissolved in 50 mM Tris (5 mM ligand concentration), mixed with 2 molar excess of copper ions and incubated with ESA for several hours prior to crystallization. Warfarin and ketoprofen were prepared as 100 mM solutions in pure DMSO and mixed with the protein in ratio 9:1 (ESA and HSA, respectively) and incubated for several hours at 37 ^{o}C before the crystallization. ESA crystals were flash-cooled in liquid nitrogen using Paratone® N as a cryoprotectant (except for ESA-dexamethasone crystals when Paratone® N was mixed

with mineral oil in 1:1 ratio), while HSA crystals were flash-cooled without using any cryoprotectant (they were cryo-ready). ESA crystals typically grew in one week, but they often diffracted weakly, or the observed diffraction was anisotropic. The time of HSA crystallization with ligands varied from two weeks to several months. Furthermore, harvested HSA crystals diffracted weakly (resolution worse than 4 Å) in most cases. Due to all of that, the determination of a single SA structure required collecting data for a high number of crystals.

2.3. Structure determination

Diffraction data were collected at the 19-BM, 19-ID, 21-ID-F, 21-ID-G, and 23-ID-D beamlines at the Advanced Photon Source (Argonne National Laboratory), at a nominal temperature of 100 K.[192] The collected data were processed, integrated, and scaled with HKL-3000 using corrections for radiation decay and anisotropic diffraction.[193–195] Resolution cut-offs were chosen based on values of CC½ and <I>/<σ(I)>.[196] The structures were determined by molecular replacement (PDB ID: 3V08 was used as the template for ESA structures and PDB ID: 6HSC or PDB ID: 4K2C for HSA structures) and refined with hydrogen atoms in riding positions using HKL-3000 seamlessly integrated with REFMAC,[193,194] Fitmunk,[197] and programs from the CCP4 package.[198–200] Coot[201,202] was used for manual inspection and correction of the model. If ligands, whether from the crystallization conditions, intrinsic binding to SA, or addition during ligand soaking, could not be unambiguously assigned to positive regions of electron density, these regions were

modeled using unknown atoms or ions (UNX) or unknown ligand (UNL), in keeping with previously suggested guidelines.[203,204] The length of modeled fatty acids was based only on how many atoms were visible in the electron density, the actual fatty acid chains could be longer. A single mutation of Arg560Ala reported previously by Handing et al.[79] was observed in all ESA structures described in this study. The ACHESYM server was used for the standardized placement of the protein models in the unit cell.[205] The TLS Motion Determination server was used to determine TLS groups for use in structure refinement.[206] The TLS parameters were kept if confirmed by a significantly improved R_{free} and the Hamilton R-factor ratio test[207] as implemented in HKL-3000. All decisions made during structure refinement adhered to recently published, state-of-the-art guidelines.[203,208] All enantiomeric species used for soaking of SA crystals (ibuprofen, ketoprofen, etodolac, and warfarin) were used in a racemic mixture, which is the same as commercially available formulations of these drugs. In the structures of SA complexes with those drugs, both enantiomers were modeled, and the (*S*)- or (*R*)-enantiomers were chosen by careful evaluation of each candidate fit to the 2mFo-DFc, and mFo-DFc omit maps (calculated for 10 cycles of REFMAC refinement without the ligand), and each choice was supported by a comparison of fit to the after-refinement maps, the resulting B-factor values, and the interactions with the protein (hydrogen bonds, salt bridges, and the lack of clashes). Stereochemical restraints for ligands molecules used during the refinement were generated using Grade Web Server[209] or AceDRG[210] (included in the CCP4 suite). Both MOLPROBITY[211] and wwPDB validation servers[212] were used to validate the models. PyMOL (The PyMOL Molecular Graphics System, Version 1.5.0.3, Schrödinger, LLC) was

used to visualize protein structures. All experimental steps were tracked using LabDB.[213,214] Molstack, a rich internet application,[215,216] was used for interactive interpretation, and comparison of the models and their respective electron density maps. Diffraction images for all structures presented herein are available at the Integrated Resource for Reproducibility in Macromolecular Crystallography at http://proteindiffraction.org.[217,218] Atomic coordinates and structure factors for all structures were deposited in the Protein Data Bank with the following accession codes: 5V0V (ESA in complex with etodolac), 6MQD (ESA in complex with testosterone), 6U4X (ESA in complex with ibuprofen), 6U4R (ESA in complex with ketoprofen), 6CI6 (ESA in complex with nabumetone), 6U5A (ESA in complex with 6-MNA), 6WUW (HSA in complex with JMS-053), 6XK0 (ESA in complex with dexamethasone), and 7JWN (HSA in complex with ketoprofen).

2.4. Binding studies

2.4.1. Tryptophan fluorescence quenching

For TFQ measurements, the procedure described by Handing et al.[79] was employed. TFQ experiments were performed in the PBS buffer with pure DMSO added to a final concentration of 20%. The final concentrations of HSA and ESA were 2.3 μM. Testosterone was dissolved in 100% DMSO and diluted five-fold with the PBS buffer to the final DMSO concentration of 20%, which, therefore, remained constant throughout the TFQ experiment. The final testosterone concentration ranged from 1080 μM to 0.86

µM (achieved by serial dilutions). The intensity of tryptophan fluorescence was measured at 37°C by a Pherastar FS (BMG Labtech) device using an excitation wavelength of 280 nm and a 340 nm filter for the fluorescence detection. Sample solutions (100 µL in each well) were placed on UV-transparent, half-area 96-well plates (Corning®, One Riverfront Plaza, NY, Catalog# CLS3635). The gain value was set to 720 for HSA and 680 for ESA. The focal height was set to 6.7 mm. The measurement of albumin fluorescence intensity for each testosterone concentration consisted of three independent experimental repetitions, where each repetition was the average of 10 fluorescence measurements of the well. Fluorescence values for wells without protein were used for background corrections for each testosterone concentration. For K_d calculations, I used a simplified model of TFQ that assumes that the concentration of free ligand can be approximated by the concentration of added ligand when the protein concentration is significantly lower than that of the ligand (Eqn. 1).[219] I further applied corrections by multiplying the measured fluorescence by a correction factor G (Eqn. 2) proposed by Ehrenberg et al.[220] to compensate for the absorbance of testosterone at the excitation wavelength of 280 nm (internal filter effect). Obtained data were analyzed with OriginPro 2016 software using non-linear regression (Eqn. 3).

$$\frac{F_0 - F}{F_0 - F_C} = \frac{[L]}{K_d + [L]} \qquad \text{Eqn. (1)}$$

$$G = \frac{1 - e^{-A_p}}{1 - e^{-(A_p + A_l)}} * \frac{A_p + A_l}{A_p} \qquad \text{Eqn. (2)}$$

$$F = F_0(1 - f\frac{[L]}{K_d+[L]}) \qquad \text{Eqn. (3)}$$

In these equations, [L] is the ligand concentration, F is the corrected fluorescence intensity, F_0 is the fluorescence of protein in the absence of ligand, F_C is the fluorescence of protein complexed with a ligand, K_d is the dissociation constant, f is the efficiency of quenching ($f = F_0 - \frac{F_C}{F_0}$), G is the correction factor, A_p is protein absorbance at 280 nm, and A_l is ligand absorbance at 280 nm.

2.4.2. Ultrafast affinity extraction and zonal elution

The ultrafast affinity extraction (UAE) and zonal elution studies were performed by the group of Prof. David Hage from the University of Nebraska-Lincoln. UAE studies were carried out using a high-performance liquid chromatography (HPLC) system from Jasco that consisted of two PU-2080 pumps, a UV-2075 absorbance detector, a X-LC 3167CO column oven, an AS-2057 plus autosampler equipped with a 100 µL sample loop, and LC-Net software. This system also included Advantage PF six-port and ten-port valves from Rheodyne. A similar HPLC system and LC-Net were used in the zonal elution studies that also included a Jasco DC-2080 degasser and HV-2080-01 column selector. Jasco ChromNAV software (v 1.8.04) was used to control these systems, and the chromatograms were analyzed using PeakFit 4.12 (Jandel Scientific Software).

The microcolumns used for UAE and zonal elution studies contained HSA that was immobilized to Nucleosil Si-300 silica by the Schiff base method, as described previously.[221,222] A control support was prepared in the same manner but without the

addition of HSA during the immobilization step. The HSA silica and the control support were packed into 5.0 mm × 2.1 mm i.d. (for UAE) or 10.0 mm × 2.1 mm i.d. (for competition studies) stainless steel columns using a Prep 24 pump from ChromTech, according to a previous method.[222] The microcolumns were stored in 67 mM potassium phosphate buffer (pH 7.4) at 4°C when not in use. The UAE and competition studies were both carried out at a column temperature of 37°C and used 67 mM potassium phosphate buffer (pH 7.4) as the mobile phase. The procedure described by Zheng et al.,[221] based on the partitioning of testosterone between a hexane solution and a mutually insoluble layer of an aqueous phosphate buffer (i.e., hexane and the phosphate buffer did not dissolve to any significant extent in each other), was used in most cases for the preparation of aqueous solutions and samples of testosterone or testosterone plus SA for the UAE and zonal elution studies.

The injected standard and samples that were used for UAE contained 10 μM testosterone or 10 μM of testosterone mixed with 20 μM HSA or ESA in 67 mM potassium phosphate buffer (pH 7.4). Each sample or standard was incubated at 37°C for at least 30 minutes prior to injection. The injection volume was 2 μL, and the samples or standards were injected at flow rates of 0.5-3.0 mL/min in the studies with HSA and 0.25-2.0 mL/min in the studies with ESA. The elution of testosterone was monitored at 249 nm. The apparent free fraction of testosterone was determined by calculating the peak area ratio between the retained peak obtained for a testosterone standard and the retained peak for a sample containing the same total concentration of testosterone in the presence of a known concentration of HSA or ESA.[221]

The free fractions obtained by UAE at high flow rates (or short column residence times) were used to obtain the global affinity constant (nK_a', where n is the number of binding sites per protein) of testosterone with SA, as accomplished by using Eqn. (4).[221,222]

$$nK_a' = \frac{1 - F_{t0}}{F_{t0}([\mathrm{P}]_{tot} - [\mathrm{T}]_{tot} + [\mathrm{T}]_{tot} F_{t0})} \qquad \text{Eqn. (4)}$$

The terms $[\mathrm{T}]_{tot}$ and $[\mathrm{P}]_{tot}$ in Eqn. (4) represent the total concentrations of the testosterone and soluble SA in the injected sample, while F_{t0} is the original free fraction of testosterone in the sample at equilibrium. Data that were acquired at low-to-moderate flow rates by UAE were also analyzed by using Eqn. (5) to obtain F_{t0}, which was then utilized in Eqn. (4) to provide a second estimate of nK_a'.[221,223]

$$\ln \frac{1}{(1-F_t)} = k_d t - \ln(1 - F_{t0}) \qquad \text{Eqn. (5)}$$

In Eqn. (5), k_d is the dissociation rate constant for the testosterone-SA complex, and F_t is the apparent free fraction measured for testosterone when part of the complex is allowed to dissociate for time t in the microcolumn. A plot of $\ln[1/(1 - F_t)]$ versus t for this data should result in a linear relationship in which the intercept gives the value of F_{t0} and the slope provides k_d.[221]

The zonal elution studies were conducted by injecting 10-µL samples 3-4 times under each set of operating conditions. The testosterone samples contained a 20 µM concentration of the hormone and were prepared in the same solution that was used as the mobile phase. The elution of testosterone was monitored at 231 nm in these experiments. Samples containing 20 µM sodium nitrate, which was detected at 205 nm,

were prepared in the solution being employed as the mobile phase and injected to determine the void times for the column and system. The following mobile phases were used in the zonal elution studies: (1) 67 mM potassium phosphate buffer (pH 7.4); (2) 20 μM sodium citrate in 67 mM potassium phosphate buffer (pH 7.4); (3) 40 μM sodium citrate in 67 mM potassium phosphate buffer (pH 7.4); and (4) 20% (v/v) DMSO in 67 mM potassium phosphate buffer (pH 7.4). These zonal elution studies were carried out at 0.50-0.75 mL/min, with no significant changes being seen in the retention factors over this flow rate range. The retention or elution times of the peaks for testosterone or sodium nitrate were determined by using the progressive linear baseline subtraction mode of PeakFit 4.12 and an exponentially-modified Gaussian fit.

2.5. Sequence and structure analysis

The Dali server[224] was used for structure comparison and calculation of RMSD values between the aligned Cα atoms. Sequence alignments were performed using the UniProt server.[225] The geometry of copper complexes with albumin was checked using the CheckMyMetal server.[226]

3. Results

3.1. NSAID binding by serum albumin

3.1.1. Structures of ESA complexes with NSAIDs

All crystals of ESA grew in the $P6_1$ space group ($P6_1$ is the most common space group observed for ESA crystals) and contained one ESA molecule in the asymmetric unit (**Table 3.1**). The quality of electron density for all determined structures and built models can be inspected interactively at https://molstack.bioreproducibility.org/c/WFY4. The models are complete, except for the first two or three residues that were not located in the electron density maps of these structures. The determined structures revealed these NSAIDs bound in several binding sites, which are located in all three ESA domains (**Figure 3.1**). The electron density observed for NSAIDs in the determined structures is shown in **Figure 3.2** and all residues involved in the drug binding are listed in **Table 3.2**. The ESA-NSAID structures were compared to each other, and ligand-free ESA and HSA structures using the Dali server and RMSD values between the aligned Cα atoms are presented in **Table 3.3**. The ESA-NSAID structures presented in this report essentially have an identical fold to previously determined structures of ESA and show low RMSD values when compared to the ligand-free ESA and HSA structures, indicating similar structural morphology.

Table 3.1. Data collection, structure refinement, and structure quality statistics for ESA-NSAID structures. Values in parentheses are for the highest resolution shell. Ramachandran plot statistics are calculated by MolProbity. DS1-DS10 refer to drug-binding sites 1-10. The protein was crystallized by Dr. Katarzyna Handing, and X-ray data were collected by Dr. Katarzyna Handing and Dr. Ivan Shabalin.

Name	Etodolac	Ketoprofen	Ibuprofen	Nabumetone	6-MNA
PDB ID	5V0V	6U4R	6U4X	6CI6	6U5A
Diffraction images DOI	10.18430/M35V0V	10.18430/M36U4R	10.18430/M36U4X	10.18430/M36CI6	10.18430/M36U5A
Data collection statistics					
Crystallization conditions	0.2 M lithium sulfate, 1.8-2.4 M ammonium sulfate, 0.1 M Tris buffer pH 7.4				
SA source	ESA isolated from horse blood (Equitech-Bio #ESA62)				
SA concentration	34 mg/mL				
Additives	Etodolac was prepared as 100 mM solution in pure DMSO and added to crystallization drops containing ESA crystals to reach a final drug concentration of 10 mM	Ketoprofen was prepared as 100 mM solution in pure DMSO and added to crystallization drops containing ESA crystals to reach a final drug concentration of 3 mM	Ibuprofen powder was added directly to the crystallization drop containing crystals for 48 h before harvesting	Nabumetone was prepared as 100 mM solution in pure DMSO and added to crystallization drops containing ESA crystals to reach a final drug concentration of 10 mM	6-MNA was prepared as 100 mM solution in pure DMSO and added to crystallization drops containing ESA crystals to reach a final drug concentration of 3 mM
Resolution (Å)	50.00-2.45 (2.49-2.45)	50.00-2.45 (2.49-2.45)	50.00-2.25 (2.29-2.25)	50.00-2.80 (2.85-2.80)	50.00-2.65 (2.70-2.65)
Beamline	23-ID-D	21-ID-F	19-ID	23-ID-D	21-ID-F
Wavelength (Å)	0.979	0.979	0.979	0.979	0.979
Space group	$P6_1$	$P6_1$	$P6_1$	$P6_1$	$P6_1$
Unit-cell dimensions (Å)	a=b=94.2 c=141.8	a=b=95.5 c=141.7	a=b=95.2 c=141.9	a=b= 93.9 c=140.8	a=b=94.3 c=142.0
Protein chains in the ASU	1	1	1	1	1
Completeness (%)	99.9 (98.6)	99.9 (100.0)	99.7 (97.0)	100.0 (100.0)	100.0 (100.0)
Number of unique reflections	26311 (1304)	26761 (1340)	34270 (1661)	17321 (871)	20955 (1057)
Redundancy	4.0 (3.5)	7.7 (6.8)	10.7 (6.6)	5.1 (4.9)	7.6 (6.5)
<I>/<σ(I)>	14.0 (1.2)	17.3 (1.4)	21.8 (1.1)	14.1 (2.1)	18.9 (1.1)
CC ½	(0.75)	(0.66)	(0.68)	(0.82)	(0.50)
R_{merge}	0.088 (0.574)	0.119 (1.335)	0.113 (1.119)	0.115 (0.660)	0.113 (1.700)

R_{meas}	0.102 (0.629)	0.128 (1.445)	0.119(1.204)	0.129 (0.742)	0.121 (1.842)
Refinement statistics					
R_{work}/R_{free}	0.180/0.238	0.182/0.233	0.191/0.238	0.182/0.256	0.185/0.256
Bond lengths RMSD (Å)	0.007	0.002	0.002	0.007	0.003
Bond angles RMSD (°)	1.1	1.2	1.1	1.1	1.3
Mean B value (Å²)	65	48	44	64	55
Mean B value for ligands (Å²)	(*S*)-etodolac: 86.2 (DS1) 89.1 (DS7) (*R*)-etodolac: 85.7 (DS3) 78.3 (DS7)	(*S*)-ketoprofen: 64.1 (DS4) 69.5 (DS6) 36.4 (DS10)	(*S*)-ibuprofen: 49.1 (DS2) 79.4 (DS4)	Nabumetone: 65.7 (DS2) 85.3 (DS6)	6-MNA: 46.0 (DS2) 82.7 (DS6) 74.2 (DS7)
Number of protein atoms	4512	4578	4582	4524	4548
Mean B value for protein (Å²)	64	49	44	66	56
Number of water molecules	164	209	266	96	96
Mean B value for water molecules (Å²)	55	38	40	48	35
Clashscore	0.33	0.98	3.25	0.77	3.09
MolProbity score	0.62	0.81	1.12	0.74	1.10
Rotamer outliers (%)	0.00	0.20	0.40	0.00	0.20
Ramachandran outliers (%)	0.00	0.00	0.00	0.00	0.00
Ramachandran favored (%)	98.10	97.93	98.27	98.10	98.10

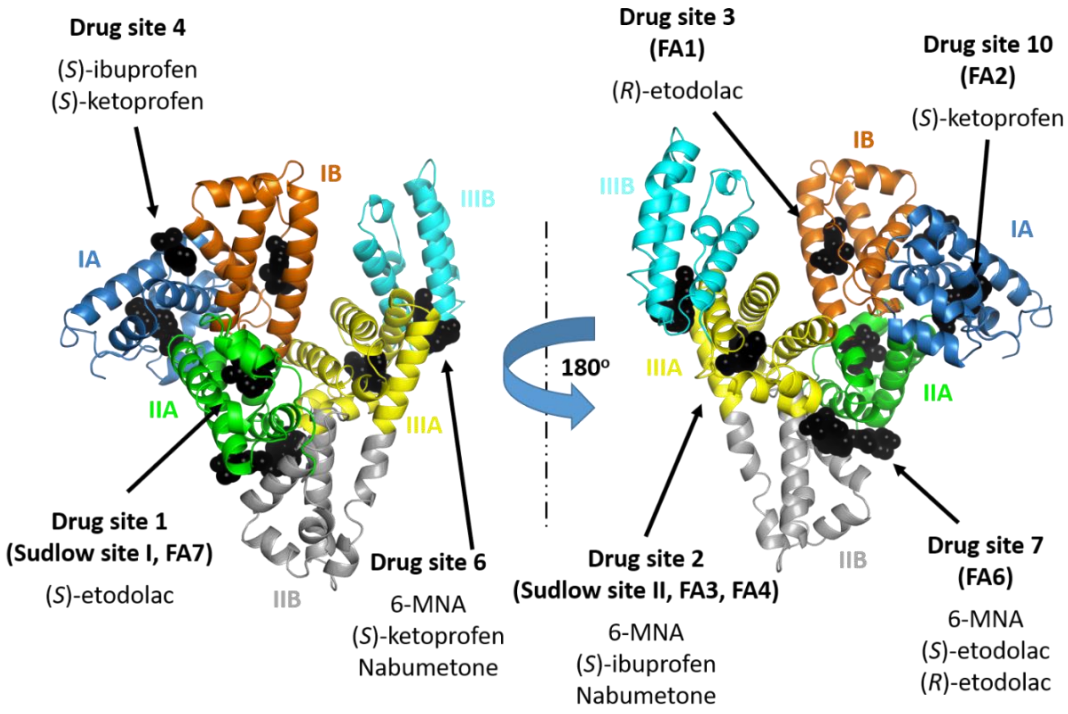

Figure 3.1. Location of the NSAID binding sites in ESA structures reported in this study (PDB ID: 5V0V, 6U4R, 6U4X, 6CI6, 6U5A). Molecules are shown with atoms as black spheres. Each site is labeled on only one panel. Domains are labeled with Roman numerals (I, II, III) and subdomains with letters (e.g., IA), with each subdomain shown in a different color; alternative names of the binding sites are in parentheses; FA stands for the fatty acid binding site.

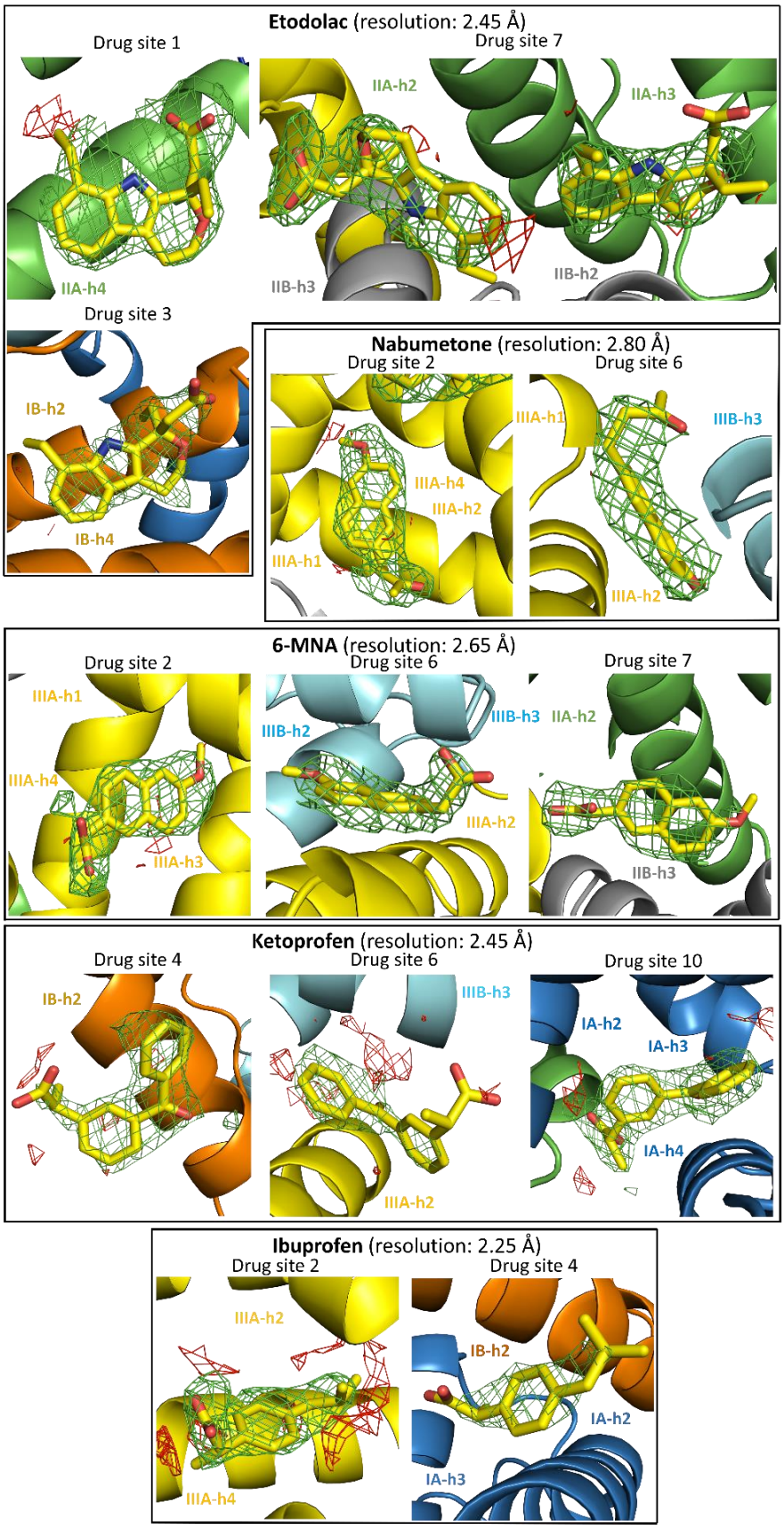
Etodolac (resolution: 2.45 Å)
Drug site 1
IIA-h4
Drug site 7
IIA-h2
IIA-h3
IIB-h3
IIB-h2
Drug site 3
IB-h2
IB-h4
Nabumetone (resolution: 2.80 Å)
Drug site 2
IIIA-h4
IIIA-h2
IIIA-h1
Drug site 6
IIIA-h1
IIIB-h3
IIIA-h2
6-MNA (resolution: 2.65 Å)
Drug site 2
IIIA-h1
IIIA-h4
IIIA-h3
Drug site 6
IIIB-h2
IIIB-h3
IIIA-h2
Drug site 7
IIA-h2
IIB-h3
Ketoprofen (resolution: 2.45 Å)
Drug site 4
IB-h2
Drug site 6
IIIB-h3
IIIA-h2
Drug site 10
IA-h2
IA-h3
IA-h4
Ibuprofen (resolution: 2.25 Å)
Drug site 2
IIIA-h2
IIIA-h4
Drug site 4
IB-h2
IA-h2
IA-h3

Figure 3.2. NSAIDs binding sites (PDB IDs: 5V0V, 6U4R, 6U4X, 6CI6, 6U5A) with an omit electron density map (mFo–DFc map, calculated after 10 refinement cycles without a drug, RMSD 2.5) presented in green and red (positive and negative contours). All NSAIDs are shown in stick representation with carbon atoms in yellow, oxygen atoms in red, and nitrogen atoms in blue. Helices are labeled with subdomain name and helix number. The electron density can be inspected interactively at https://molstack.bioreproducibility.org/c/WFY4 .

Table 3.2. Drug-binding sites, the residues that participate in binding the particular drug, and hydrophilic interactions involved in ESA-NSAIDs complexes reported in this study. An asterisk next to the drug name indicates that a small fraction of the opposite enantiomer may be present in this location.

DS	Subdomains	Drug	Residues	Salt bridges and hydrogen bonds
1	IIA and IIB	(*S*)-etodolac*	Tyr149, Glu152, Lys194, Glu195, Lys198, Trp213, Leu218, Lys221, Phe222, Ile233, Leu237, Val240, His241, Arg256, Leu259, Ala260, Ile263, Ser286, Ile289, Ala290, Glu291	(*S*)-etodolac's carboxylate group forms a salt bridge (with a hydrogen bond to NE atom) with the side-chain guanidine group of Arg256 and a hydrogen bond with the carboxylate group of Glu195 (OE2 atom). A water molecule acts as a hydrogen bond mediator between (*S*)-etodolac's nitrogen and a nitrogen atom (NE) of Arg256's side-chain
2	IIIA	(*S*)-ibuprofen	Leu386, Asn390, Leu406, Arg409, Tyr410, Lys413, Ala414, Val417, Leu422, Ile425, Leu429, Leu452, Leu456, Leu459, Ile472, Arg484, Phe487, Ser488, Leu490	(*S*)-ibuprofen's carboxylate group forms a salt bridge (with hydrogen bond to NH1 atom) with side-chain guanidine group of Arg409 and a hydrogen bond with Tyr410's hydroxyl group (OH)
		6-MNA	Leu386, Val387, Asn390, Cys391, Phe402, Leu406, Arg409, Tyr410, Lys413, Leu429, Val432, Gly433, Cys436, Cys437, Ser448, Leu452, Arg484, Ser488	6-MNA's carboxylate group forms a salt bridge with the side-chain guanidine group of Arg409 and hydrogen bonds with hydroxyl groups of Tyr410 (OH) and Ser488 (OG)

		Nabumetone	The same as for 6-MNA at DS2	Nabumetone's carbonyl group (atom O1) forms a hydrogen bond with the hydroxyl group of Tyr410 (atom OH)
3	IB	(*R*)-etodolac	Lys114, Leu115, Pro117, Gln122, Tyr137, Glu140, Val141, Arg144, His145, Tyr160, Leu181, Leu184, Lys185, Ile188, Ile189	(*R*)-etodolac's ring oxygen and carboxylate group form a bifurcated hydrogen bond with the side-chain nitrogen atom (NE2) of His145
4	IA and IB	(*S*)-ibuprofen*	Lys17, His18, Lys20, Gly21, Leu24, Asp131, Leu134, Gly135, Leu138, Leu154, Ala157, Glu158, Leu283	None
		(*S*)-ketoprofen	Lys17, Lys20, Gly21, Leu24, Phe36, Val40, Val43, Asn44, Asp129, Asp131, Lys132, Leu134, Gly135, Leu138	(*S*)-ketoprofen's carboxylate group forms a salt bridge (with a hydrogen bond) with Lys20's side-chain amino group (NZ atom)
6	IIIA and IIIB	(*S*)-ketoprofen	Leu393, Val397, Asp401, Asn404, Ala405, Val408, Leu528, Lys540, Glu541, Leu543, Lys544, Leu547	(*S*)-ketoprofen's carboxylate group forms a salt bridge with Lys540's side-chain amino group
		6-MNA	The same as for (*S*)-ketoprofen at DS6	6-MNA's carboxylate group forms a salt bridge (with a hydrogen bond) with the Lys540's side-chain amino group (NZ atom)
		Nabumetone	The same as for (*S*)-ketoprofen at DS6	The oxygen atom (O2') of nabumetone's methoxy functional group forms a hydrogen bond with Asn404's side-chain nitrogen atom (ND2)
7	IIA and IIB	(*R*)-etodolac	Phe205, Arg208, Ala209, Ala212, Asp323, Leu326, Gly327, Leu330, Leu346, Ala349, Lys350, Ser479, Leu480, Ala481, Glu482	(*R*)-etodolac's carboxylate group forms a salt bridge (with a hydrogen bond) with Lys350's side-chain amino group (NZ atom), a hydrogen bond with Ser479's backbone nitrogen (N), and a hydrogen bond with Ser479's side-chain oxygen (OG).
		(*S*)-etodolac*	Arg208, Lys211, Ala212, Val215, Phe227, Ser231, Thr235, Asp323, Gly327, Leu330	(*S*)-etodolac's carboxylate group forms a salt bridge (with a hydrogen bond) with Lys211's side-chain amino group (NZ atom)
		6-MNA	Arg208, Ala209, Ala212, Asp323, Leu326, Gly327, Leu330, Leu346, Ala349, Lys350, Ser479, Leu480, Ala481	6-MNA's carboxylate group forms a salt bridge with Lys350's side-chain amino group and hydrogen bonds with the hydroxyl group of Ser479 (OG) and with the backbone nitrogen atoms (N) of Leu480 and Ala481
10	IA	(*S*)-ketoprofen	Ile7, Phe19, Val23, Ala26, Phe27, Val46, Phe49, Leu66, His67, Leu69, Phe70, Lys73, Gly247, Asp248, Leu249, Leu250, Glu251	(*S*)-ketoprofen's carboxylate group forms hydrogen bonds with Glu251's side-chain and the backbone nitrogen atoms (N) of Leu249 and Leu250

Table 3.3. RMSD values [Å] between the aligned Cα atoms of ESA-NSAIDs complexes and ligand-free ESA and HSA molecules.

	Etodolac	Nabumetone	6-MNA	Ibuprofen	Ketoprofen	Ligand free ESA (3V08)	Ligand free ESA (5HOZ)*	Ligand free HSA (4K2C)
Etodolac	-	0.4	0.4	0.8	0.6	1.4	0.7	1.7
Nabumetone	0.4	-	0.3	0.8	0.6	1.4	0.8	1.7
6-MNA	0.4	0.3	-	0.8	0.7	1.3	0.5	1.6
Ibuprofen	0.8	0.8	0.8	-	0.8	1.5	1.0	1.8
Ketoprofen	0.6	0.6	0.7	0.8	-	1.5	1.0	1.9
Ligand-free ESA (3V08)	1.4	1.4	1.3	1.5	1.5	-	1.1	1.7
Ligand-free ESA (5HOZ)*	0.7	0.8	0.5	1.0	1.0	1.1	-	1.5
Ligand-free HSA (4K2C)	1.7	1.7	1.6	1.8	1.9	1.7	1.5	-

*Structure of ligand-free ESA (5HOZ) was obtained from similar conditions as structures presented in this chapter.

3.1.1.1. ESA complex with etodolac

Well-defined electron density indicates four etodolac molecules bound to the ESA molecule in drug sites 1, 3, and 7 (PDB ID: 5V0V; resolution 2.45 Å; **Figure 3.2**). Residues involved in etodolac binding to ESA, including details pertaining to salt bridges and hydrogen bonds, are listed in **Table 3.2**. The etodolac molecule bound to drug site 1 (also known as Sudlow site I) was modeled as (*S*)-etodolac, although the possibility of a small fraction of (*R*)-etodolac in the same position cannot be excluded. Drug site 1 is located between subdomains IIA and IIB and is formed by the helices of subdomain IIA and a seven-residue loop from subdomain IB. This site is predominantly hydrophobic in nature but contains hydrophilic residues as well; this mixed character allows for favorable hydrophobic interactions between drug molecules and amino acid residues as well as for

possible hydrogen bonds, van der Waals interactions, and charge-charge interactions (e.g., a salt bridge with a hydrogen bond between (*S*)-etodolac's carboxylate group and the side-chain guanidine group of Arg256 and a hydrogen bond with the carboxylate group of Glu195). The etodolac molecule bound at drug site 3 (also known as a major oncological drug-binding site)[80] was clearly identified as (*R*)-etodolac. Drug site 3 is located in subdomain IB, between α-helices IB-h2, IB-h3, and IB-h4 and a loop, and can be described as a hydrophobic groove with several amino acid residues having the possibility to form some hydrogen bonds (e.g., Gln122, Arg144, His145).[80] At this site, (*R*)-etodolac forms a bifurcated hydrogen bond with His145. Drug site 7 is located in domain II, between subdomains IIA (helices IIA-h2 and h3) and IIB (helices IIB-h2 and h3); this drug site is large and can be split into two subsites, each of which binds one enantiomer of etodolac. One was modeled as (*S*)-etodolac (a small fraction of (*R*)-etodolac might be present) and the other as (*R*)-etodolac. Most of the interactions in these subsites are hydrophobic in nature, but Arg208 forms a salt bridge with Asp323, which helps to close this cavity and is known to contribute to fatty acid binding. The (*R*)-etodolac molecule in drug site 7 is situated roughly 4 Å away from the (*S*)-etodolac molecule in the same site. Both (*R*)- and (*S*)-etodolac are surrounded mostly by hydrophobic residues that contribute to interactions with etodolac's rings. However, the carboxylate group of (*R*)-etodolac forms a salt bridge (with a hydrogen bond) with Lys350's side-chain amino group and hydrogen bonds with Ser479's backbone nitrogen and side-chain oxygen. The carboxylate group of (*S*)-etodolac forms a salt bridge (with a hydrogen bond) with Lys211's side-chain

amino group. In this structure, four Tris molecules and seven sulfate ions from the crystallization conditions were also observed.

3.1.1.2. ESA complex with nabumetone

In the crystal structure of ESA in complex with nabumetone (PDB ID: 6CI6; resolution 2.80 Å), the electron density clearly indicates the binding of two nabumetone molecules to drug sites 2 and 6 (**Figure 3.2**). Regions with the density that could not be unambiguously interpreted (observed in drug sites 3, 4, and 9) were modeled as unknown atoms or ions (UNX) and are likely due to a loosely bound drug, remnants of ESA purification from horse serum, or crystallization components. All of the residues involved in nabumetone binding to ESA are listed in **Table 3.2**. Nabumetone binds to drug site 2 (also known as Sudlow site II), which is located in subdomain IIIA and composed of six α-helices. Most of the interactions between the ligand and amino acid residues in this site are hydrophobic in nature (only one hydrogen bond between nabumetone's carbonyl group and the hydroxyl group of Tyr410 were observed). Nabumetone also binds to the predominantly hydrophobic drug site 6, which is situated in domain III, between subdomains IIIA (helices IIIA-h1 and h2) and IIIB (helix IIIB-h1). The electron density in this site is not as strong as that observed at drug site 2 in this structure but is still well-defined and supports the presence of a nabumetone molecule, which is stabilized by hydrophobic interactions and one hydrogen bond (between nabumetone's methoxy functional group and Asn404's side-chain nitrogen). The structure of ESA in complex with nabumetone also

contains several other small molecules: one Tris molecule, five sulfate ions, and one molecule of fatty acid, which was modeled as nonanoic acid.

3.1.1.3. ESA complex with 6-MNA

The active metabolite of nabumetone, 6-MNA, binds to drug sites 2, 6, and 7 in the ESA-6-MNA structure (PDB ID: 6U5A; resolution 2.65 Å; **Figure 3.2**). The 6-MNA molecule located in drug site 2 has the same orientation as the nabumetone molecule and is surrounded by the same residues (**Table 3.2**). The main difference between the binding mode of both molecules is that 6-MNA's carboxylate group forms a hydrogen bond not only with the hydroxyl group of Tyr410 but also with the hydroxyl group of Ser488 and forms a salt bridge with the side-chain guanidine group of Arg409. The 6-MNA molecule located in drug site 6 has its position and interactions with surrounding residues nearly identical (except for a hydrogen bond with Asn440 replaced by a salt bridge with Lys540) to those observed for the nabumetone molecule in the same site (PDB ID: 6CI6). The 6-MNA molecule bound to drug site 7 partially overlaps with the position of the (*R*)-etodolac molecule described in section 3.1.1.1 (PDB ID: 5V0V). The subsite of drug site 7 to which 6-MNA binds has a mixed character consisting of both hydrophobic and hydrophilic residues (**Table 3.2**). At this subsite, the 6-MNA molecule's carboxylate group forms a salt bridge with Lys350's side-chain amino group and hydrogen bonds with the hydroxyl group of Ser479 and with the backbone nitrogen atoms of Leu480 and Ala481.

Nabumetone was not observed to bind to site 7. The ESA-6-MNA structure also contains four sulfate ions, which were observed on the surface of the protein.

3.1.1.4. ESA complex with ketoprofen

Three molecules of ketoprofen were found to bind to ESA in drug sites 4, 6, and 10 (PDB ID: 6U4R; resolution 2.45 Å). All of them were modeled as (*S*)-ketoprofen (**Figure 3.2**); no (*R*)-ketoprofen molecules were located in this structure. Drug site 4 is located in domain I between α-helices IA-h2, IA-h3, IB-h2, and IB-h3. Most of the residues comprising this site contribute to hydrophobic interactions with the (*S*)-ketoprofen molecule; however, a salt bridge (with a hydrogen bond) between (*S*)-ketoprofen's carboxylate group and Lys20's side-chain amino group is observed (**Table 3.2**). Another (*S*)-ketoprofen molecule is bound at drug site 6 in the same mode as the molecule of nabumetone described in section 3.1.1.2 (PDB ID: 6CI6), although the electron density is weaker for this (*S*)-ketoprofen molecule. The aromatic rings of (*S*)-ketoprofen are placed in the hydrophobic cavity, while its carboxylate group is directed toward the protein-solvent interface and forms a salt bridge with Lys540's side-chain amino group. The electron density for the carboxylate and methyl groups is clearly weaker than for aromatic rings, which may suggest that this part of the drug is flexible and can rotate when bound at this site. The third (*S*)-ketoprofen molecule is bound to drug site 10. This site is located in subdomain IA, buried between α-helices h1, h2, h3, and h4 and overlaps with the previously characterized second fatty acid binding site (FA2). Ketoprofen is the second

FDA-approved drug known to bind in this site (the first being halothane). Though the (*S*)-ketoprofen molecule in this site is located in the hydrophobic cavity, its carboxylate group forms hydrogen bonds with Glu251's side-chain and the backbone nitrogen atoms of Leu249 and Leu250 (**Table 3.2**). The ESA-ketoprofen structure also contains three sulfate molecules, one molecule of fatty acid (modeled as nonanoic acid, bound at drug site 2), and two molecules modeled as unknown atoms or ions (UNX).

At drug site 1, weak electron density was observed and may suggest the binding of another (a fourth) ketoprofen molecule at this position, which was recently reported to be the only binding site for (*R*)-ketoprofen in BSA (PDB ID: 6QS9[129]). However, the positive region of electron density at drug site 1 in the ESA structure reported herein could not be unambiguously assigned to any particular enantiomer of ketoprofen (electron density for a part of the ligand is missing) and was modeled as an unknown ligand (UNL). Surprisingly, drug sites 4, 6, and 10 in the BSA-ketoprofen structure are unoccupied, which might be caused by different crystallization conditions (18% PEG MME 5000, 0.2 M ammonium chloride, 0.1 M MES pH 6.5), space group (*C*2), and lower ketoprofen concentration. (*S*)-ketoprofen was also recently reported to bind to drug sites 2 and 6 in LSA (PDB ID: 6OCK).[115] Both LSA and ESA bind (*S*)-ketoprofen at drug site 6, but the drug molecule bound at this site has a different conformation in each structure, likely due to different residues comprising the binding sites (pairwise sequence identity and similarity for ESA/LSA are 71.0% and 85.2%, respectively)[227] and different conformations of the proteins. The structure of the ESA-ketoprofen complex reported in this study was obtained from a solution containing 0.2 M lithium sulfate, 2.0 M ammonium sulfate, and

0.1 M Tris buffer at pH 7.4 ($P6_1$ space group), while the LSA-ketoprofen complex was crystallized from 8% PEG 400, 16% PEG 3350, 0.2 M ammonium acetate, and 0.1 M Tris buffer at pH 8.5 ($P2_12_12_1$ space group). Moreover, LSA was de-fatted before crystallization, and the ketoprofen molecule was shown to bind to LSA at drug site 2 (PDB ID: 6OCK), which is occupied by a fatty acid molecule in the structure reported herein (PDB ID: 6U4R).[115] Drug site 4 in the LSA structure is occupied by a molecule of polypropylene, and drug site 10 is unoccupied.

3.1.1.5. ESA complex with Ibuprofen

In the structure of ESA complexed with ibuprofen (PDB ID: 6U4X; resolution 2.25 Å), two molecules of (*S*)-ibuprofen were found to bind to drug sites 2 and 4 (**Figure 3.2**); no (*R*)-ibuprofen molecules were located in this structure. At drug site 2, the hydrophobic part of the (*S*)-ibuprofen molecule is bound inside the hydrophobic cavity, while (*S*)-ibuprofen's carboxylate group forms a salt bridge (with hydrogen bonds) with the guanidine moiety of Arg409's and a hydrogen bond with the hydroxyl group of Tyr410 (**Table 3.2**). Electron density observed for the (*S*)-ibuprofen molecule at drug site 4 is weaker than the density observed in drug site 2 but still clearly indicates drug binding, although the possibility of a small fraction of (*R*)-ibuprofen in the same position cannot be excluded. The (*S*)-ibuprofen molecule in drug site 4 partially overlaps with the position of the (*S*)-ketoprofen molecule from the structure described above (PDB ID: 6U4R, see 3.1.1.4) and is mostly stabilized by hydrophobic interactions with the surrounding amino

acid residues (**Table 3.2**). The weak density observed for (*S*)-ibuprofen's carboxylate group may suggest that this functional group is flexible. The ESA-ibuprofen structure also contains 10 sulfate ions and an unknown ligand (UNL). I believe that the unknown ligand is likely a sugar molecule, based on the shape of the observed density and its location, which is known to bind sugars in HSA (see PDB ID: 4IW2).[66] No sugars were added to ESA during purification or crystallization, so the presence of a sugar molecule in the structure is likely the result of its presence in the blood and binding to ESA under physiological conditions.

In a recently published structure of ESA in complex with ibuprofen (PDB ID: 6OCI), which was obtained from different crystallization conditions (75% Tacsimate at pH 6.0) but the same space group ($P6_1$), (*S*)-ibuprofen was found to bind to drug sites 2 and 7.[115] These two sites are known to bind (*S*)-ibuprofen in HSA (**Figure 3.3**). I compared this structure (PDB ID: 6OCI) with the structure reported in this thesis (PDB ID: 6U4X; crystallization conditions: 0.2 M lithium sulfate, 2.4 M ammonium sulfate, 0.1 M Tris buffer pH 7.4) and observed two different binding modes of (*S*)-ibuprofen at drug site 2 (**Figure 3.4**). In both structures, (*S*)-ibuprofen's carboxylate group occupies roughly the same position, while its hydrophobic parts are oriented in opposite directions. The only amino acid residue which has a different conformation in these structures is Tyr410. At drug site 4, where (*S*)-ibuprofen binds to ESA, Zielinski et al.[115] observed binding of succinic acid (a component of Tacsimate), which had potentially prevented the binding of ibuprofen at this site. At drug site 7, electron density for ibuprofen was not observed in the ESA structure reported herein.

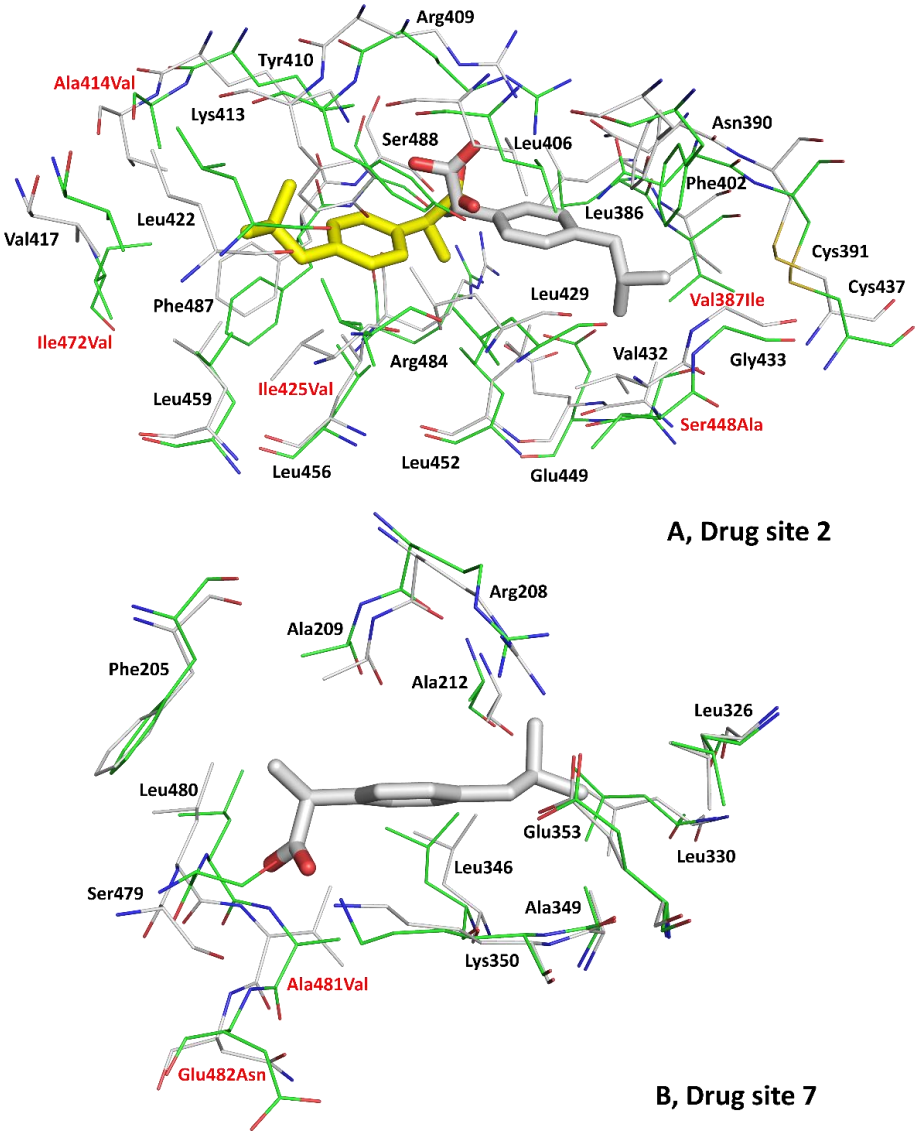

Figure 3.3. Comparison of ibuprofen binding in ESA (PDB ID: 6U4X) and HSA (PDB ID: 2BXG) in drug sites 2 and 7. Carbon atoms in ESA and HSA are shown in green and gray, respectively. Oxygen atoms are shown in red, nitrogen in blue; ibuprofen molecules are shown with carbon atoms in yellow (ESA structure) and in gray (HSA structure). Residue numbers correspond to positions in ESA; the naming scheme is as follows: residue from ESA, residue number, residue from HSA (if different). At drug site 4, electron density for

ibuprofen was observed only in the ESA structure (PDB ID: 6U4X); in the HSA-ibuprofen structure (PDB ID: 2BXG), drug site 4 in unoccupied.

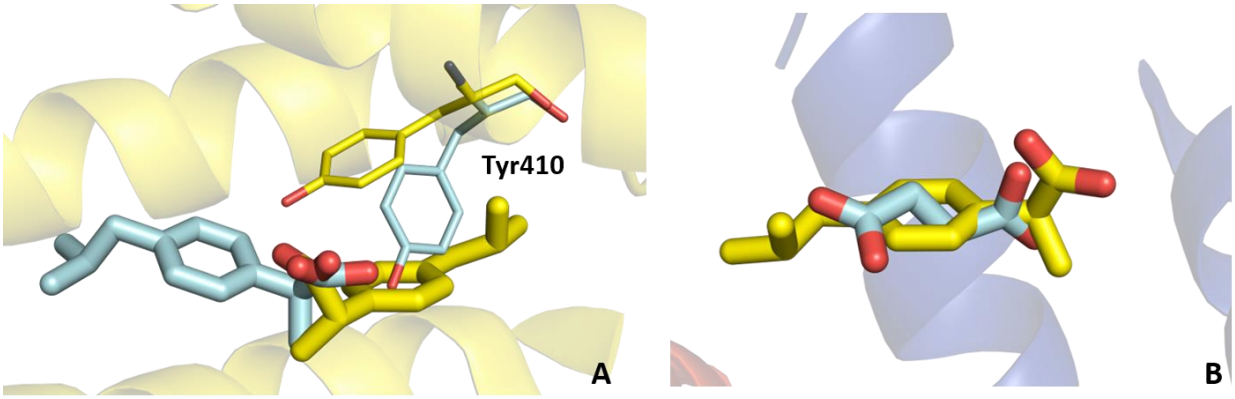

Figure 3.4. Superposition of the crystal structures of ESA complexes with ibuprofen obtained from different crystallization conditions. For ligands in yellow – ESA was crystallized with the crystallization conditions composed of 0.2 M lithium sulfate, 1.8-2.4 M ammonium sulfate, and 0.1 M Tris buffer pH 7.4 (PDB ID: 6U4X); for ligands in cyan - ESA was crystallized with the crystallization conditions composed of 75% Tacsimate at pH 6.0 (PDB ID: 6OCI). A) Drug site 2. Two different binding modes of ibuprofen and conformations of Tyr410. B) Drug site 4. Succinic acid (shown in cyan) binds at drug site 4 (PDB ID: 6OCI) and may prevent the binding of ibuprofen at this site, which was observed in the structure reported in this study (PDB ID: 6U4X). At drug site 7, electron density for ibuprofen was observed only in PDB ID: 6OCI ESA structure; in the ESA-ibuprofen structure reported in this thesis (PDB ID: 6U4X), drug site 7 is unoccupied.

3.1.2. Conservation of NSAIDs binding sites in ESA/HSA

Eighty-six percent of the residues involved in the binding of (*S*)-etodolac to drug site 1 (Sudlow site I, also known as FA7) in ESA are conserved in HSA (**Figure 3.5**). Eighteen residues are conserved (Tyr149, Glu152, Lys194, Lys198, Trp213, Leu218, Phe222, Leu237, Val240, His241, Arg256, Leu259, Ala260, Ile263, Ser286, Ile289, Ala290, Glu291), and three are different (Glu195Gln, Lys221Arg, Ile233Leu; naming scheme is as follows: residue from ESA, residue number, residue from HSA). Two of these differences involve the exchange of a hydrophilic residue for another hydrophilic residue, which causes a change in the overall charge of the cavity but does not directly affect observed interactions between the (*S*)-etodolac molecule and ESA. The third difference is hydrophobic-for-hydrophobic. Despite these small changes in drug site 1, the residues involved in the binding of (*S*)-etodolac exhibit no significant conformational differences when the ESA–etodolac complex is compared to structures of ligand-free ESA (PDB ID: 3V08) and HSA (PDB ID: 4K2C). Drug site 1 has been characterized for HSA, ESA, and BSA and has been previously shown to bind amantadine, aspirin/salicylic acid, azapropazone, diclofenac, diflunisal, etodolac, halothane, indomethacin, iodipamide, ketoprofen, naproxen, oxyphenbutazone, phenylbutazone, thyroxine, warfarin, and zidovudine. All of these compounds, excluding halothane and amantadine, contain at least one aromatic ring and are highly hydrophobic.

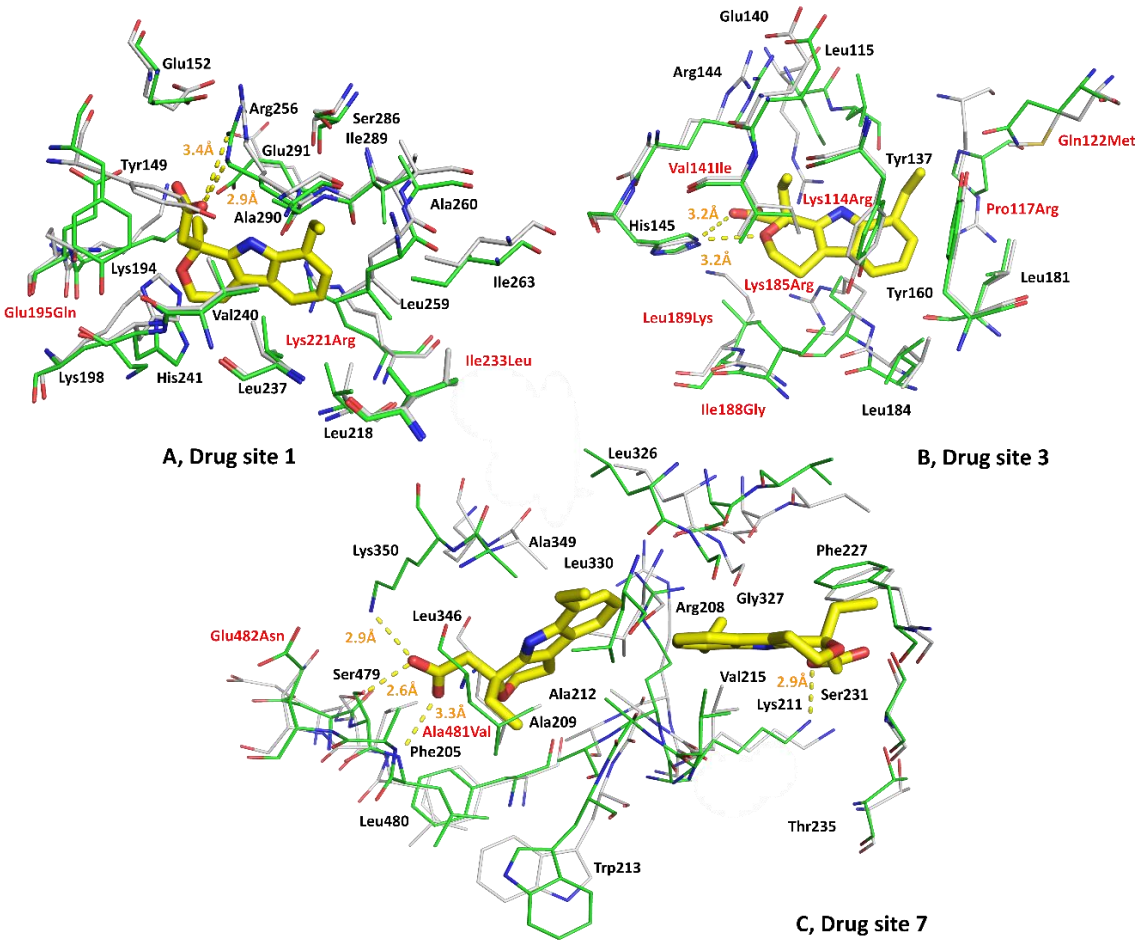

Figure 3.5. Comparison of residues involved in etodolac binding in ESA (PDB ID: 5V0V) and residues comprising the analogous sites in HSA (PDB ID: 4K2C). Carbon atoms in ESA and HSA are shown in green and gray, respectively. Oxygen atoms are shown in red, nitrogen in blue; etodolac molecules are shown with carbon atoms in yellow. Residue numbers correspond to positions in ESA; the naming scheme is as follows: residue from ESA, residue number, residue from HSA (if different). Models can be compared interactively at https://molstack.bioreproducibility.org/p/dupc/.

Drug site 2 (Sudlow site II, also known as FA3/FA4) of both HSA and ESA binds (*S*)-ibuprofen, but the binding mode is very different between species. In these structures,

(*S*)-ibuprofen's carboxylate group roughly occupies the same position and forms hydrogen bonds with Arg409 (Arg410 in HSA) and Tyr410 (Tyr 411); in HSA, there is also a third potential hydrogen bond with Lys414. However, the hydrophobic parts of the (*S*)-ibuprofen molecules are oriented in opposite directions. The whole binding site (consisting of residues involved in (*S*)-ibuprofen binding in either HSA or ESA) is 81% conserved between ESA and HSA; 22 residues are conserved (Leu386, Asn390, Cys391, Phe402, Leu406, Arg409, Tyr410, Lys413, Va417, Leu422, Leu429, Val432, Gly433, Cys437, Glu449, Leu452, Leu456, Leu459, Arg484, Phe487, Ser488, Leu490), and five are different (Val387Ile, Ala414Val, Ile425Val, Ser448Ala, Ile472Val). All of these modifications, excluding Ser448Ala, are hydrophobic-for-hydrophobic and do not cause any significant conformational changes in the structure of the binding site (**Figure 3.3**). Sixteen amino acid residues involved in the binding of nabumetone and its metabolite 6-MNA to drug site 2 in ESA are conserved in HSA (Leu386, Asn390, Cys391, Phe402, Leu406, Arg409, Tyr410, Lys413, Leu429, Val432, Gly433, Cys436, Cys437, Leu452, Arg484, Ser488), and two are altered (Val387Ile, Ser448Ala, **Figure 3.6**), resulting in 89% conservation of the residues comprising this site. The positions of nabumetone and 6-MNA in drug site 2 of ESA are nearly identical (**Figure 3.7**) and overlap with the position of the (*S*)-ibuprofen molecule in HSA; as a result of the high degree of amino acid residue conservation and overlapping positions of the three drug molecules, it can be expected that nabumetone, 6-MNA, and (*S*)-ibuprofen will mostly exhibit the same interactions with the residues comprising drug site 2 in HSA. Drug site 2 has been characterized in HSA, ESA, BSA, ovine SA (OSA), caprine SA (CSA), and LSA and has been shown to bind the following drugs:

aripiprazole, diazepam, diclofenac, diflunisal, halothane, ibuprofen, ketoprofen, nabumetone/6-MNA, naproxen, phenylbutyric acid, propofol, suprofen, and thyroxine. With the exception of halothane, all of these drugs are aromatic and predominantly hydrophobic. Drug site 2 also can bind two fatty acid molecules (e.g., myristic acid) at the same time and can be divided into two subsites known as FA3 and FA4 as a result.

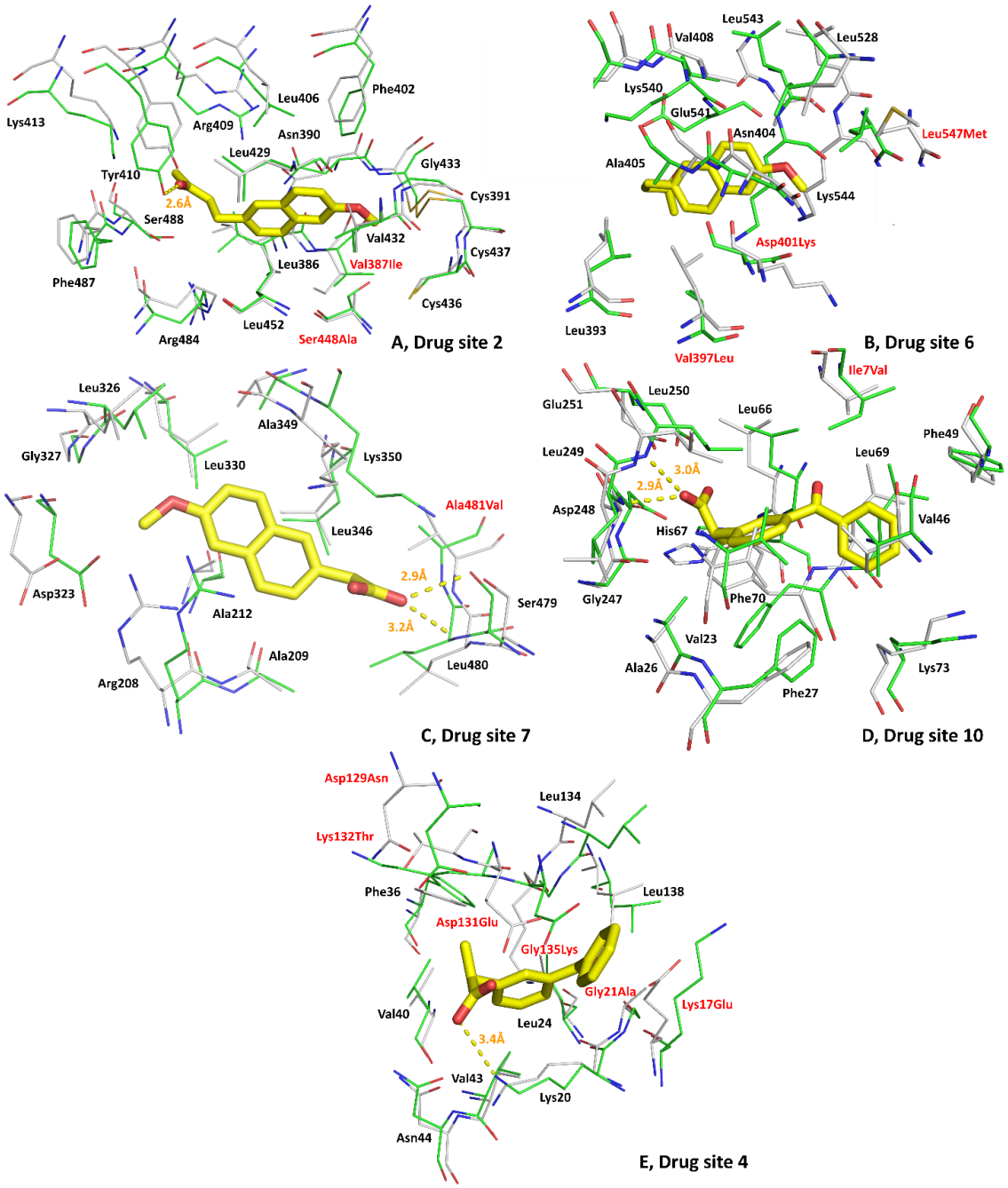

Figure 3.6. Superposition of NSAIDs binding sites in ESA and analogous sites in HSA (PDB ID: 4K2C). A-B) nabumetone (PDB ID: 6CI6); C) 6-MNA (PDB ID: 6U5A); D-E) ketoprofen (PDB ID: 6U4R). Carbon atoms in ESA and HSA are shown in green and gray, respectively. Oxygen atoms are shown in red, nitrogen in blue; NSAID molecules are shown with carbon atoms in yellow. Residue numbers correspond to positions in ESA; the naming scheme is

as follows: residue from ESA, residue number, residue from HSA (if different). Models can be compared interactively at https://molstack.bioreproducibility.org/p/dupc/ .

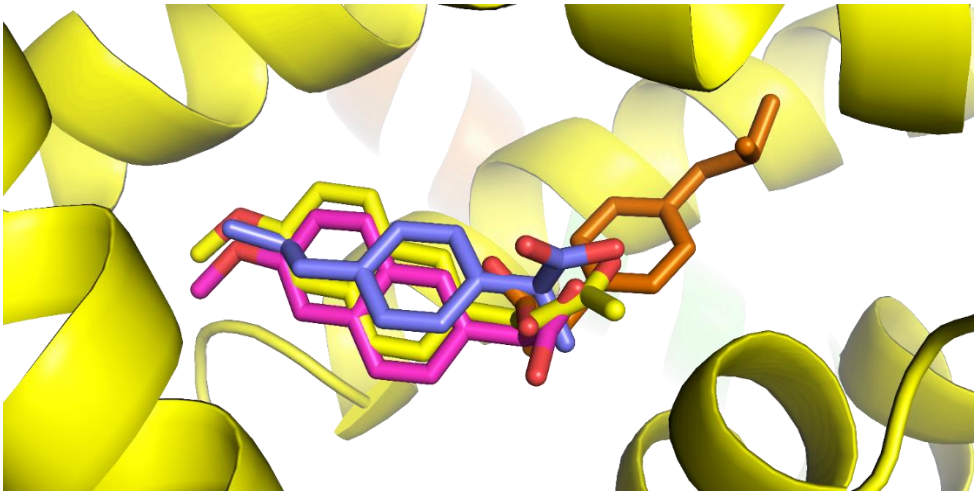

Figure 3.7. Drug site 2; superposition of ESA complexes with ibuprofen (PDB ID: 6U4X), nabumetone (PDB ID: 6CI6), and 6-MNA (PDB ID: 6U5A) and HSA complex with ibuprofen (PDB ID:2BXG). Orange – ibuprofen in ESA; yellow – nabumetone; magenta – 6-MNA; blue – ibuprofen in HSA.

Drug site 3 (also known as FA1 and the major oncological site) in ESA, which binds (*R*)-etodolac, significantly differs from the analogous site in HSA (53% of residues are conserved; see **Figure 3.5**). Eight of the amino acid residues comprising this site are conserved between ESA and HSA (Leu115, Tyr137, Glu140, Arg144, His145, Tyr160, Leu181, Leu184), and seven are different (Lys114Arg, Pro117Arg, Gln122Met, Val141Ile, Lys185Arg, Ile188Gly, Leu189Lys). Three of these differences (Pro117Arg, Gln122Met, Leu189Lys) significantly change the structure, character, and charge of one side of the

binding site. The rest of the differences involve exchanges of hydrophobic residues to other hydrophobic residues (Val141Ile, Ile188Gly) or hydrophilic to hydrophilic (Lys114Arg, Lys185Arg). Drug site 3 has been characterized in HSA, ESA, OSA, and CSA and has been reported to bind the following drugs: azapropazone, bicalutamide, diclofenac, etodolac, fusidic acid, idarubicin, indomethacin, lidocaine, naproxen, salicylic acid, teniposide, and zidovudine.

There is some variation in the set of residues involved in the binding of (*S*)-ketoprofen and (*S*)-ibuprofen in drug site 4 in ESA. Fifty-seven percent of the residues involved in (S)-ketoprofen binding at drug site 4 are conserved (eight residues are conserved: Lys20, Leu24, Phe36, Val40, Val43, Asn44, Leu134, Leu138; six are different: Lys17Glu, Gly21Ala, Asp129Asn, Asp131Glu, Lys132Thr, Gly135Lys; **Figure 3.6**). Some of the altered residues are involved only in hydrophobic interactions with the drug (aliphatic part of Lys17, Gly21), and their alterations should not affect drug binding. The Asp129Asn alteration will change the overall charge of the cavity and may change the orientation of (*S*)-ketoprofen's carboxylate group. Modification of Lys132 to Thr will cause a loss of the hydrophobic interactions between the aliphatic part of lysine and the drug but introduces a hydroxyl group that may be involved in a potential hydrogen bond with (*S*)-ketoprofen's carboxylate group (upon changes of (*S*)-ketoprofen's orientation). The loss of the hydrophobic interactions with Lys132 can be compensated by mutations, such as the introduction of an additional carbon atom through the Asp131Glu change. The most significant structural changes may be caused by steric effects resulting from the Gly135Lys modification, potentially preventing ligand binding. At the same time, residues involved

in binding (*S*)-ibuprofen, which partially overlaps with the location of (*S*)-ketoprofen, are only 54% conserved (seven residues are conserved: Lys20, Leu24, Leu134, Leu138, Leu154, Ala157, Leu283; six residues are altered: Lys17Glu, His18Asn, Gly21Ala, Asp131Glu, Gly135Lys, Glu158Lys). Most of these changes are of a hydrophilic residue for another hydrophilic residue or a hydrophobic residue for another hydrophobic residue, but they change the overall charge and size of the cavity. This binding site has been structurally characterized for ESA, OSA, and CSA, and five drugs have been reported to bind there: cetirizine, diclofenac, ibuprofen, ketoprofen, and testosterone.[79,105]

Three NSAIDs have been observed to bind to drug site 6 in ESA: nabumetone, 6-MNA, and (*S*)-ketoprofen. All three NSAIDs occupy roughly the same positions in this site. Drug site 6 is 75% conserved between ESA and HSA; nine amino acids are conserved (Leu393, Asn404, Ala405, Val408, Leu528, Lys540, Glu541, Leu543, Lys544), and three are altered (Val397Leu, Asp401Lys, Leu547Met; **Figure 3.6**). These alterations do not change the structure or character of the binding site significantly because they involve the exchange of one hydrophobic residue for another hydrophobic residue of a similar size (Val397Leu, Leu547Met) or involve amino acids that surround the drug molecules but are not involved in any direct interactions with them (Asp401Lys). Drug site 6 has been characterized for HSA, ESA, CSA, LSA, and OSA and has been reported to bind the following drugs: diclofenac, ketoprofen, nabumetone/6-MNA, naproxen, and oxyphenbutazone.

The location of the 6-MNA molecule in drug site 7 (also known as FA6) of ESA overlaps with that of the (*S*)-ibuprofen molecule in HSA, and the amino acids involved in

6-MNA binding are 92% conserved when the sequence of HSA is compared to ESA (twelve conserved residues: Arg208, Ala209, Ala212, Asp323, Leu326, Gly327, Leu330, Leu346, Ala349, Lys350, Ser479, Leu480; one altered residue: Ala481Val; **Figure 3.6**). Despite high sequence and secondary structure conservation, electron density for ibuprofen was not found at this binding site in ESA. The altered amino acid residue (Ala481Val) does not significantly change the character of the binding site because Ala481 is only involved in hydrophobic interactions with the drug. Both enantiomers of etodolac bind to drug site 7 as well; 18 amino acids comprising both etodolac subsites are conserved (Phe205, Arg208, Ala209, Lys211, Ala212, Val215, Phe227, Ser231, Thr235, Asp323, Leu326, Gly327, Leu330, Leu346, Ala349, Lys350, Ser479, Leu480), while two residues are altered (Ala481Val, Glu482Asn; 90% conservation; **Figure 3.5**). Glu482 is oriented away from the binding site, and its side-chain is not involved in (*R*)-etodolac binding. Ala481 is involved in hydrophobic interactions with the molecule of (*R*)-etodolac, but its modification to valine should not disrupt these interactions. Thus, the general structure and character of this binding site are conserved between ESA and HSA. Drug site 7 has been characterized for HSA, ESA, OSA, CSA, LSA, and BSA and has been shown to bind the following drugs: cetirizine, diclofenac, diflunisal, etodolac, halothane, ibuprofen, naproxen, testosterone, and 6-MNA.

The (*S*)-ketoprofen binding site (drug site 10, also known as FA2) is 94% conserved between ESA and HSA (16 are conserved: Phe19, Val23, Ala26, Phe27, Val46, Phe49, Leu66, His67, Leu69, Phe70, Lys73, Gly247, Asp248, Leu249, Leu250, Glu251; one residue is altered: Ile7Val; **Figure 3.6**). The structure of the binding site is conserved between ESA

and HSA, and the Ile7Val modification should not significantly affect the binding of (*S*)-ketoprofen because this residue is only involved in hydrophobic interactions with the drug. Drug site 10 was previously only known to exist in HSA and bind fatty acids and halothane (PDB ID: 1E7C).

3.1.3. Structure of HSA complex with ketoprofen

The HSA crystal (recombinant HSA expressed in *Pichia pastoris*) grew in the *C*2 space group (HSA typically crystallizes in *C*2 or *P*1 space groups) and contained one protein chain in the asymmetric unit (**Table 3.4**). According to the vendor, the construct has a single deletion of Asp from the N-terminus (Asp1) to create a hypoallergenic construct by eliminating the principal copper and nickel binding site of albumin.[36] The determined model of the HSA-ketoprofen complex (resolution 2.60 Å) is complete except for the first residue (Ala2), for which the electron density is not observed. The electron density revealed binding of one (*S*)-ketoprofen molecule to drug site 2, two (*S*)-ketoprofen molecules to drug site 3, and one (*R*)-ketoprofen molecule to drug site 9 (**Figure 3.8**, **Figure 3.9**). All three sites were previously reported to bind multiple FDA-approved drugs (**Figure 3.10**).[228] The structure also contains three molecules of fatty acids, modeled as myristic acid, bound to FA3 (which overlaps with drug site 2), drug site 5 (was not previously characterized as a fatty acid binding site), and FA5 (overlaps with drug site 8). Fatty acids were not added during crystallization and are most likely remnants from the purification. Free cysteine was added by the manufacturer to the protein during purification to block the solely free cysteine residue in HSA and prevent albumin

dimerization; based on the observed electron density, Cys34 forms a disulfide bond with another molecule of cysteine. The quality of electron density observed for ligands in the determined structure can be inspected interactively at https://molstack.bioreproducibility.org/project/view/VW8s7hb1Z9mnCLbg3NBU/. As a control, I have also determined a structure of HSA crystallized from the same crystallization conditions but not containing ketoprofen (data not shown). In the control structure, it was observed that all ketoprofen binding sites (drug sites 2, 3, and 9) remain unoccupied, Cys34 also forms a disulfide bond with another molecule of cysteine, and fatty acids bind to the same sites as in HSA-ketoprofen complex.

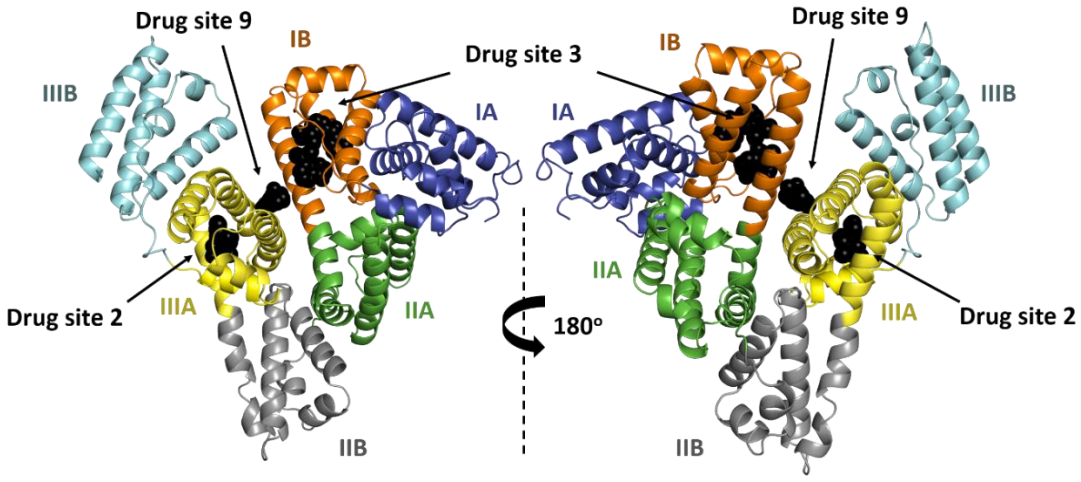

Figure 3.8. The overall structure of the HSA complex with ketoprofen. Albumin subdomains are shown each in a different color. Roman numerals (I, II, III) are associated with domains and letters (e. g., IB) with subdomains. Ketoprofen molecules are shown with atoms in black spheres.

Table 3.4. Data collection, structure refinement, and structure quality statistics for the HSA-ketoprofen structure. Values in parentheses are for the highest resolution shell. Ramachandran plot statistics are calculated by MolProbity. DS2, DS3, and DS9 refer to drug-binding sites 2, 3, and 9.

PDB ID	7JWN
Diffraction images DOI	10.18430/m37jwn
Crystallization conditions	50 mM potassium phosphate buffer at pH 7.0 and 24% PEG 3350
SA source	Recombinant HSA expressed in Pichia pastoris (Sigma # A7736)
SA concentration	162 mg/mL
Additives	Ketoprofen was prepared as 100 mM solution in pure DMSO and mixed with the protein in ratio 9:1 and incubated for several hours at 37 °C before the crystallization
Resolution (Å)	50.00-2.60
Beamline	(2.64-2.60)
Wavelength (Å)	0.979
Space group	C2
Unit-cell dimensions: a, b, c (Å)	170.5, 38.9, 98.5
Angles: α, β, γ (°)	90.0, 104.5, 90.0
Protein chains in the ASU	1
Completeness (%)	96.4 (88.5)
Number of unique reflections	18925 (851)
Redundancy	4.2 (3.5)
<I>/<σ(I)>	16.9 (1.3)
CC ½	(0.60)
R_{merge}	0.081 (0.803)
R_{work}/R_{free}	0.183 / 0.231
Bond lengths RMSD (Å)	0.002
Bond angles RMSD (°)	1.1
Mean B value (Å²)	52
Mean B value for ketoprofen molecules (Å²)	(*S*)-ketoprofen: 24.4 (DS2), 16.6 (DS3; sub-site A), 47.1 (DS3; sub-site B) (*R*)-ketoprofen: 72.1 (DS9)
Number of protein atoms	4646
Mean B value for protein (Å²)	53
Number of water molecules	192
Mean B value for water molecules (Å²)	36
Clashscore	1.27
MolProbity score	1.07
Rotamer outliers (%)	0.59
Ramachandran outliers (%)	0.0
Ramachandran favored (%)	96.23

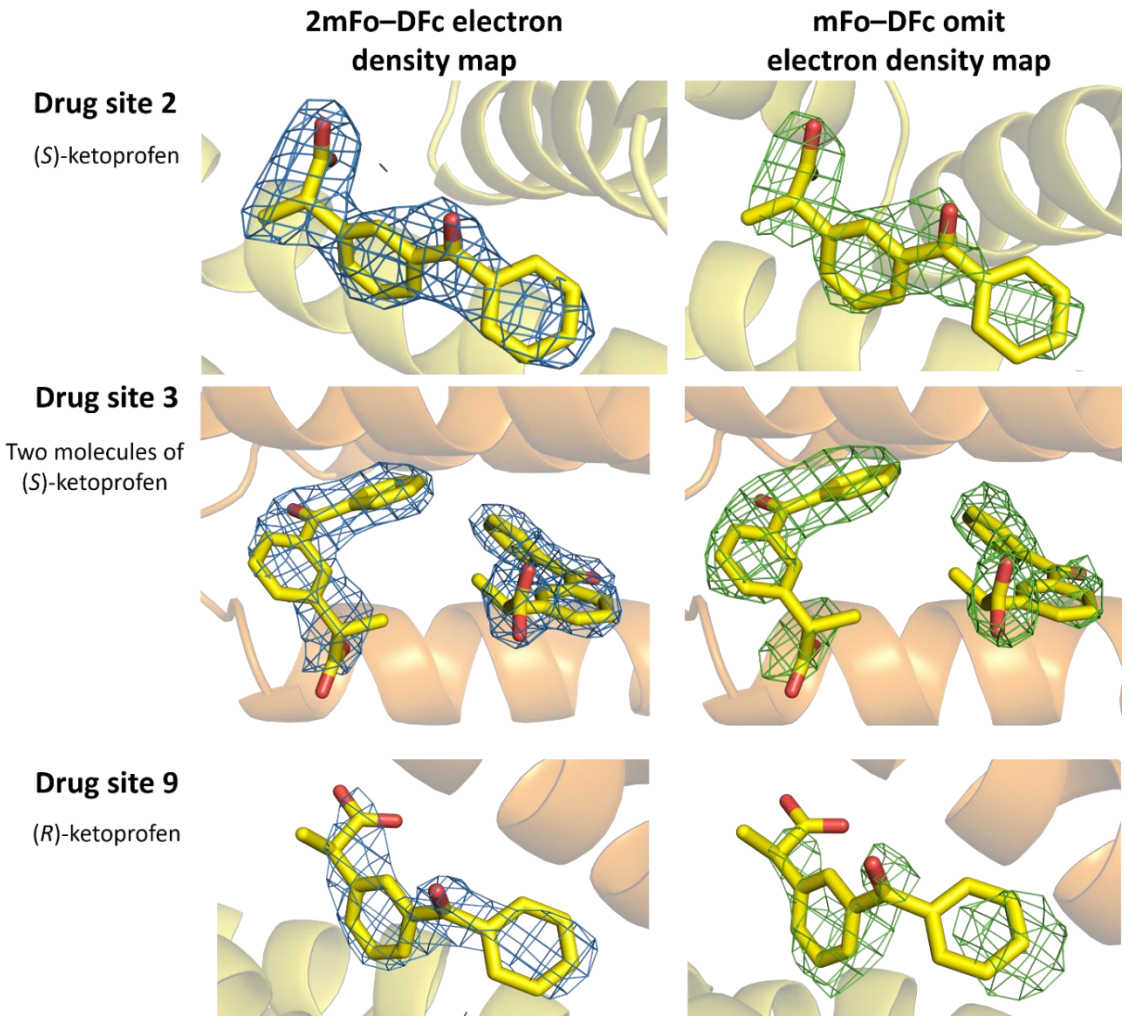

Figure 3.9. Ketoprofen binding sites in HSA (PDB ID: 7JWN) with 2mFo–DFc electron density map (RMSD 1.0) presented in blue and mFo–DFc omit electron density map (map calculated after 10 refinement cycles without a drug, RMSD 2.5) presented in green. Ketoprofen molecules are shown in stick representation with oxygen atoms in red and carbon atoms in yellow. The electron density can be inspected interactively at https://molstack.bioreproducibility.org/project/view/VW8s7hb1Z9mnCLbg3NBU/ .

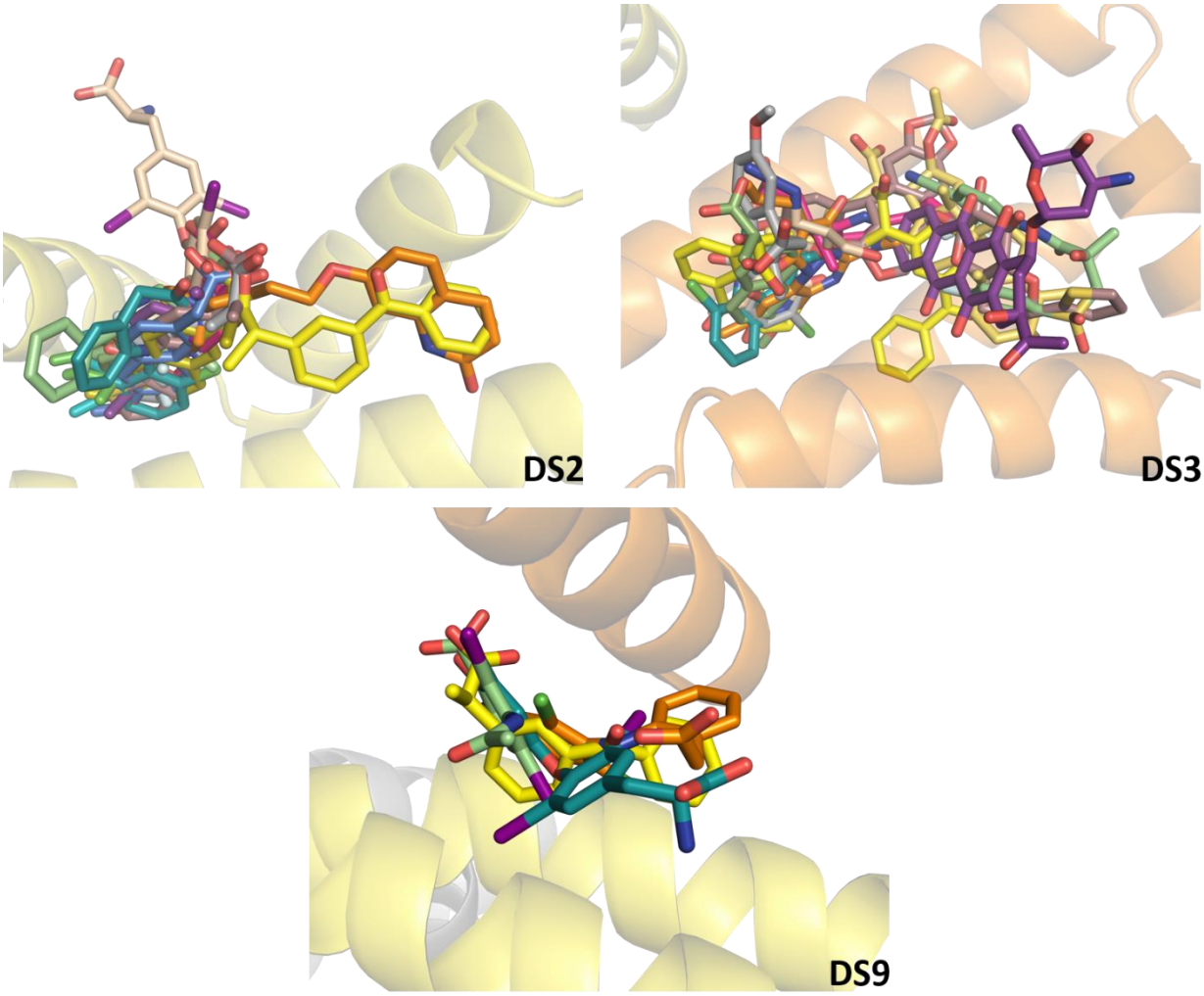

Figure 3.10. Superposition of the HSA-ketoprofen structure (PDB ID: 7JWN) and SA complexes with FDA-approved drugs known to bind to drug sites 2, 3 and 9. Ketoprofen molecules are shown with carbon atoms in yellow on all panels. Drug site 2: aripiprazole (PDB ID: 6A7P), diazepam (PDB ID: 2BXF), diclofenac (PDB ID: 4ZBQ), diflunisal (PDB ID: 2BXE), halothane (PDB ID: 1E7B), ibuprofen (PDB ID: 2BXG), ketoprofen (PDB ID: 6OCK), nabumetone (PDB ID: 6U5A), naproxen (PDB ID: 4ZBR), phenylbutyric acid (PDB ID: 5YOQ), propofol (PDB ID: 1E7A), suprofen (PDB ID: 6OCJ), thyroxine (PDB ID: 1HK1). Drug site 3: azapropazone (PDB ID: 2BXI), bicalutamide (PDB ID: 4LA0), diclofenac (PDB ID: 4Z69), etodolac (PDB ID: 5V0V), fusidic acid (PDB ID: 2VUF), idarubicin (PDB ID: 4LB2),

indomethacin (PDB ID: 2BXM), naproxen (PDB ID: 2VDB), salicylic acid (PDB ID: 3B9M), teniposide (PDB ID: 4L9Q), zidovudine (PDB ID: 3B9L). Drug site 9: diclofenac (PDB ID: 6HN0), iodipamine (PDB ID: 2BXN), thyroxine (PDB ID: 1HK4). DS stands for a drug site.

Drug site 2, also known as Sudlow site II and FA3/FA4, is one of the three major drug-binding sites in SA.[74,75,228] (*S*)-ketoprofen molecule at this site is stabilized by strong hydrophobic interactions with surrounding residues (mainly Tyr411, Val415, Val418, Leu423, Val426, Leu430, Leu453, Val456, Leu457, Leu460, Phe488) but also by hydrogen bonds between its carboxylate group and hydroxyl groups of Tyr411 and Ser489. Arg410 may also contribute by a remote charge-charge interaction with the carboxylate group. All of the residues involved in binding of (*S*)-ketoprofen to HSA at drug site 2 are listed in **Table 3.5**. The (*S*)-ketoprofen molecule bound to drug site 2 overlaps with the fatty acid previously reported to bind in FA4 (see PDB ID: 1BJ5),[96] and is located close to FA3, which is occupied by a molecule of myristic acid in the reported structure.

Drug site 3, called oncological drug site and FA1,[80] is also one of the three major drug-binding sites on SA.[74,75,228] This site has two (*S*)-ketoprofen molecules bound at the same time, and due to that, can be divided into two sub-sites. Sub-site A overlaps with previously characterized FA1[96] and has (*S*)-ketoprofen bound. (*S*)-ketoprofen at sub-site A is stabilized by strong hydrophobic interactions with residues forming a narrow binding pocket (mainly Leu115, Met123, Phe134, Tyr138, Leu139, Ile142, Leu154, Ala158, Tyr161, Phe165, and Leu182), by a salt bridge between its carboxylate group and Arg117's guanidine group, and a hydrogen bond of the carboxylate group with Tyr161's hydroxyl group (**Table 3.5**). Moreover, a remote charge-charge interaction of the carboxylate

group with Arg186 is likely an additional stabilizing factor. Sub-site B within drug site 3 harbors (*S*)-ketoprofen molecule surrounded by sparse hydrophobic residues, mainly Ile142, Phe149, Leu154, Phe157, Tyr161, and aliphatic part of Lys190's side-chain. At this sub-site, (*S*)-ketoprofen's carboxylate group forms a hydrogen bond with the His146's side-chain (NE2 atom) and a remote charge-charge interaction with Arg145. As compared to drug site 2 and the sub-site A, the sub-site B offers significantly smaller hydrophobicity (as can be seen by the significantly lower number of hydrophobic residues taking part in the interaction) and weaker hydrophilic interactions (no salt bridges and only one hydrogen bond), which may suggest weaker binding of (*S*)-ketoprofen. Indeed, the high values of B factors observed for this ligand (**Table 3.4**) may suggest its partial occupancy but may also be a result of its positional variability between HSA molecules in the crystal. Notably, the molecules of (*S*)-ketoprofen bound to the sub-sites of drug site 3 have their phenyl rings located within 4 Å of each other (**Figure 3.9**), suggesting that this hydrophobic interaction additionally stabilizes both (*S*)-ketoprofen molecules and may result in possible cooperativity in binding.

Drug site 9, which is located near FA8 and FA9, is a much less common drug-binding site on SA.[228] This site has the only (*R*)-ketoprofen molecule in the reported structure. The (*R*)-ketoprofen molecule is stabilized by some hydrophobic interactions (mainly Ala191, Ala194, Val433, Tyr452, Val455, Val456, and aliphatic parts of Lys190 and Lys432), a hydrogen bond formed by its carboxylate group with Tyr452's hydroxyl group, and a salt bridge between the carboxylate group and Lys436's amino group. The observed electron density is weaker than in other drug sites, and (*R*)-ketoprofen molecule has

relatively high B-factors, suggesting its partial occupancy or positional variability, which is also correlated with a significantly smaller hydrophobicity of this site that likely results in a lower affinity of this site.

Table 3.5. The residues that participate in binding of ketoprofen to HSA and hydrophilic interactions observed in ketoprofen binding sites.

Drug site	Subdomains	Drug	Residues	Salt bridges and hydrogen bonds
2	IIIA	(*S*)-ketoprofen	Arg410, Tyr411, Lys414 Val415, Val418, Leu423, Val426, Leu430, Leu453, Val456, Leu457, Leu460, Val473, Arg485, Phe488, Ser489, Leu491	(*S*)-ketoprofen's carboxylate group forms a hydrogen bond with hydroxyl groups of Tyr411 and Ser489 and a remote charge-charge interaction with Arg410
3, sub-site A	IB	(*S*)-ketoprofen	Leu115, Arg117, Met123, Phe134, Leu135, Tyr138, Leu139, Ile142, Leu154, Phe157, Ala158, Tyr161, Phe165, Leu182, Arg186	(*S*)-ketoprofen's carboxylate group forms a salt bridge with Arg117's guanidine group, a hydrogen bond with Tyr161's hydroxyl group, and a remote charge-charge interaction with Arg186
3, sub-site B		(*S*)-ketoprofen	Leu115, Ile142, Arg145, His146, Phe149, Leu154, Phe157, Tyr161, Leu185, Arg186, Gly189, Lys190, Ser193	(*S*)-ketoprofen's carboxylate group forms a hydrogen bond with His146's side-chain (NE2 atom) and a remote charge-charge interaction with Arg145
9	IB and IIIA	(*R*)-ketoprofen	Glu184, Asp187, Glu188, Lys190, Ala191, Ala194, Glu425, Asn429, Lys432, Val433, Lys436, Tyr452, Val455, Val456, Gln459	(*R*)-ketoprofen's carboxylate group forms a salt bridge with Lys436's amino group and a hydrogen bond with Tyr452's hydroxyl group

3.1.4. Comparison of ketoprofen binding sites in HSA and other mammalian SAs

The structure of the HSA complex with ketoprofen was compared to previously reported structures of ESA, BSA, and LSA complexes with ketoprofen, HSA complex with myristic acid, and ligand-free HSA (**Figure 3.11**). The determined HSA complex with ketoprofen has an almost identical fold to HSA complexed with myristic acid (PDB ID: 1BJ5). Calculated RMSD values are higher in the structural comparison of SA complexes with fatty acids and ligand-free SAs than in the comparison of SA complexes with ketoprofen and ligand-free SAs (**Table 3.6**). These results indicate that the presence of fatty acids alters the conformation of SA more significantly than the binding of ketoprofen. The conditions used for the crystallization of SA-ketoprofen complexes are presented in **Table 3.7**.

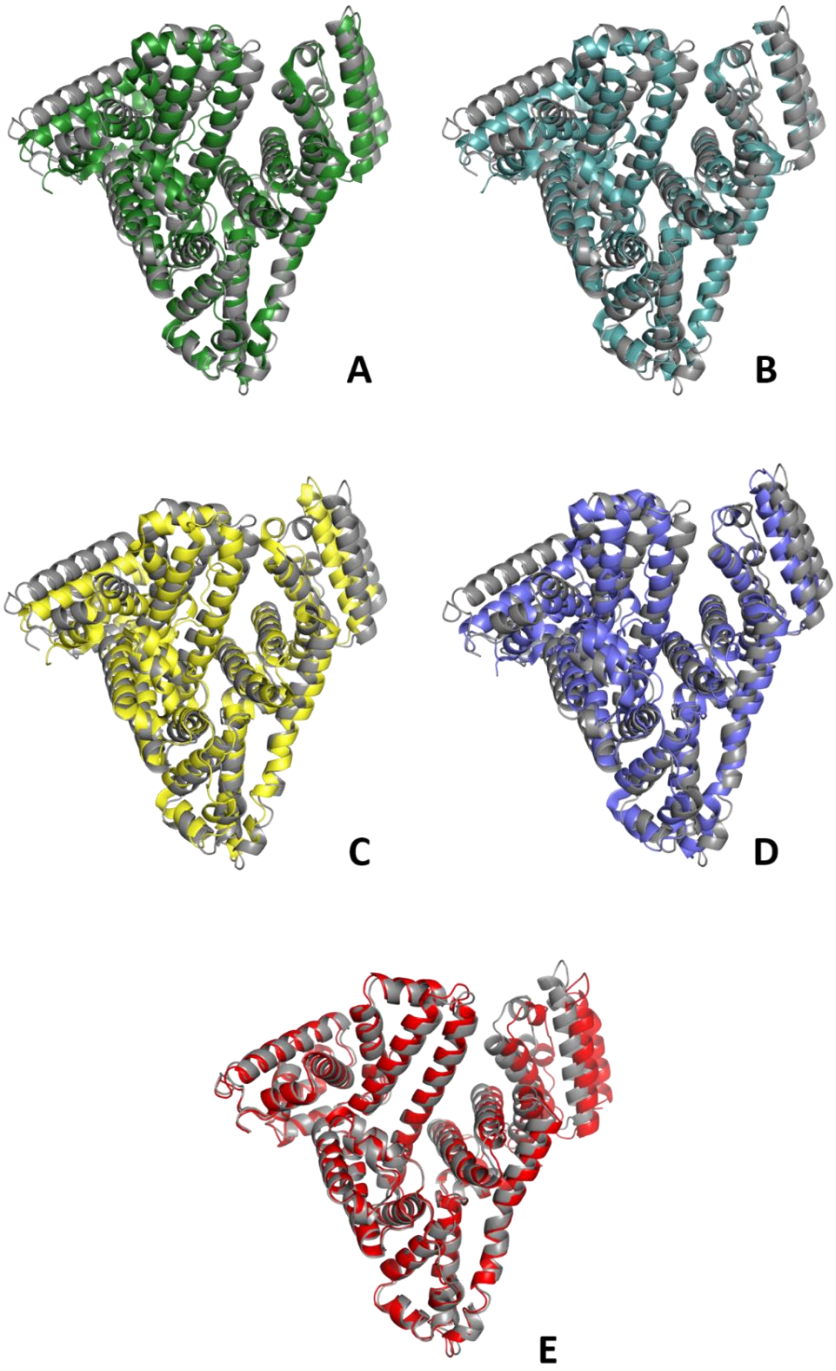

Figure 3.11. Superposition of structure of the HSA-ketoprofen complex (cartoon shown in gray; PDB ID: 7JWN) with the following complexes: A) ESA-ketoprofen (PDB ID: 6U4R); B) BSA-ketoprofen (PDB ID: 6QS9); C) LSA-ketoprofen (PDB ID: 6OCK); D) HSA-ligand free (PDB ID: 4K2C); E) HSA-myristic acid (PDB ID: 1BJ5).

Table 3.6. RMSD values [Å] between the aligned Cα atoms of SA-ketoprofen complexes, ligand-free SAs, and HSA complex with myristic acid.

-	HSA-ket (7JWN)	LSA- ket (6OCK)	BSA-ket (6QS9)	ESA-ket (6U4R)	BSA (3V03)	ESA (4F5T)	HSA (4K2C)	LSA (4F5V)	HSA-myr (1BJ5)
HSA-ket (7JWN)	-	4.5	4.0	3.7	4.5	3.6	3.9	4.6	1.5
LSA- ket (6OCK)	4.5	-	1.5	2.4	1.5	2.3	1.8	0.7	5.2
BSA- ket (6QS9)	4.0	1.5	-	1.7	0.5	1.7	1.6	1.7	4.8
ESA- ket (6U4R)	3.7	2.4	1.7	-	1.6	0.8	1.9	2.6	3.9
BSA (3V03)	4.5	1.5	0.5	1.6	-	1.7	1.6	1.7	4.9
ESA (4F5T)	3.6	2.3	1.7	0.8	1.7	-	1.8	2.5	3.9
HSA (4K2C)	3.9	1.8	1.6	1.9	1.6	1.8	-	1.9	4.2
LSA (4F5V)	4.6	0.7	1.7	2.6	1.7	2.5	1.9	-	5.2
HSA-myr (1BJ5)	1.5	5.2	4.8	3.9	4.9	3.9	4.2	5.2	-

Table 3.7. Conditions used for the crystallization of SA-ketoprofen complexes and the ligands observed in the common drug-binding sites. N/A – not available.

	HSA-ket (PDB ID: 7JWN)	**ESA-ket (PDB ID: 6U4R)**	**BSA-ket (PDB ID: 6QS9)**	**LSA-ket (PDB ID: 6OCK)**
Crystallization conditions	24% PEG 3350, 50 mM potassium phosphate buffer at pH 7.0	0.2 M lithium sulfate, 2.0 M ammonium sulfate, 0.1 M Tris buffer at pH 7.4	18% PEG MME 5000, 0.2M ammonium chloride, 0.1M MES buffer at pH 6.5	8% polypropylene glycol 400, 16% polyethylene glycol 3350, 0.2 M ammonium acetate, and 0.1 M Tris buffer at pH 8.0
SA source	Recombinant HSA expressed in *Pichia pastoris* (Sigma # A7736)	ESA isolated from horse blood (Equitech-Bio #ESA62)	BSA isolated from bovine blood (Sigma # N/A)	LSA isolated from leporine blood (Sigma # N/A) and defatted prior to the experiment
Protein concentration	Protein solution consisting of 162 mg/mL of HSA dissolved in a buffer containing 50 mM Tris (pH 7.5) and 20 mM NaCl was mixed with 100 mM ketoprofen in DMSO in ratio 9:1 (final ketoprofen concentration 10 mM). Aliquots of 0.2 µL of the protein solution were mixed with 0.2 µL aliquots of reservoir solution	1 µL of protein solution consisting of 34 mg/mL of ESA dissolved in a buffer containing 10 mM Tris (pH 7.5) and 150 mM NaCl was mixed with 1 µL aliquots of reservoir solution. ESA crystals were soaked with ketoprofen suspended in DMSO (3 mM final drug concentration)	Protein solution consisting of 10 mg/mL of BSA dissolved in a buffer containing 10 mM Tris (pH 7.5) and 150 mM NaCl was mixed with a reservoir solution. BSA was cocrystallized with 1.5 mM ketoprofen suspended in ethanol	Protein solution consisting of 67 mg/mL of LSA dissolved in a buffer containing 10 mM Tris (pH 7.4) and 100 mM NaCl was mixed with a reservoir solution. LSA was cocrystallized with 10 mM ketoprofen suspended in ethanol
DS1	-	UNL	(*R*)-ketoprofen	Acetate ion
DS2	(*S*)-ketoprofen; fatty acid	Fatty acid	-	(*S*)-ketoprofen
DS3	(*S*)-ketoprofen	-	-	PEG molecule
DS4	-	(*S*)-ketoprofen	-	Polymer with PDB code: 2J3
DS5	Fatty acid	-	-	-
DS6	-	(*S*)-ketoprofen	-	(*S*)-ketoprofen
DS7	-	-	-	Polymer with PDB code: POG
DS8	Fatty acid	-	-	-
DS9	(*R*)-ketoprofen	-	-	Acetate ion
DS10	-	(*S*)-ketoprofen	-	-

ESA (the pairwise sequence identity to HSA is 76.1%) has recently been reported to bind (*S*)-ketoprofen at drug sites 4, 6, and 10 (see 3.1.1.4, **Figure 3.12**).[228] These drug sites are unoccupied in the HSA structure reported herein. Conservation of residues comprising these drug sites in ESA and HSA has been described in section 3.1.1.6; drug site 4 significantly differs between ESA and HSA (57% conservation), drug site 6 is partially conserved (75% of residues is conserved), and drug site 10 is very well conserved between albumin from both species (94%). Therefore, the lack of (*S*)-ketoprofen in sites 4 and 6 may be attributed to these differences. But, among residues involved in binding of (*S*)-ketoprofen in ESA at drug site 10, all are the same in HSA except for Ile7, which is modified to Val. Moreover, Ile7 in ESA contributes only to hydrophobic interactions with the drug molecule, further suggesting conservation of the site and leading to the expectation that drug site 10 in HSA may bind (*S*)-ketoprofen as well. Drug site 2, where (*S*)-ketoprofen binds to HSA, is occupied by the molecule of fatty acid in the structure of the ESA-ketoprofen complex (PDB ID: 6U4R) and potentially prevent drug binding. Drug sites 3 and 9 remain unoccupied in the ESA-ketoprofen structure (PDB ID: 6U4R).

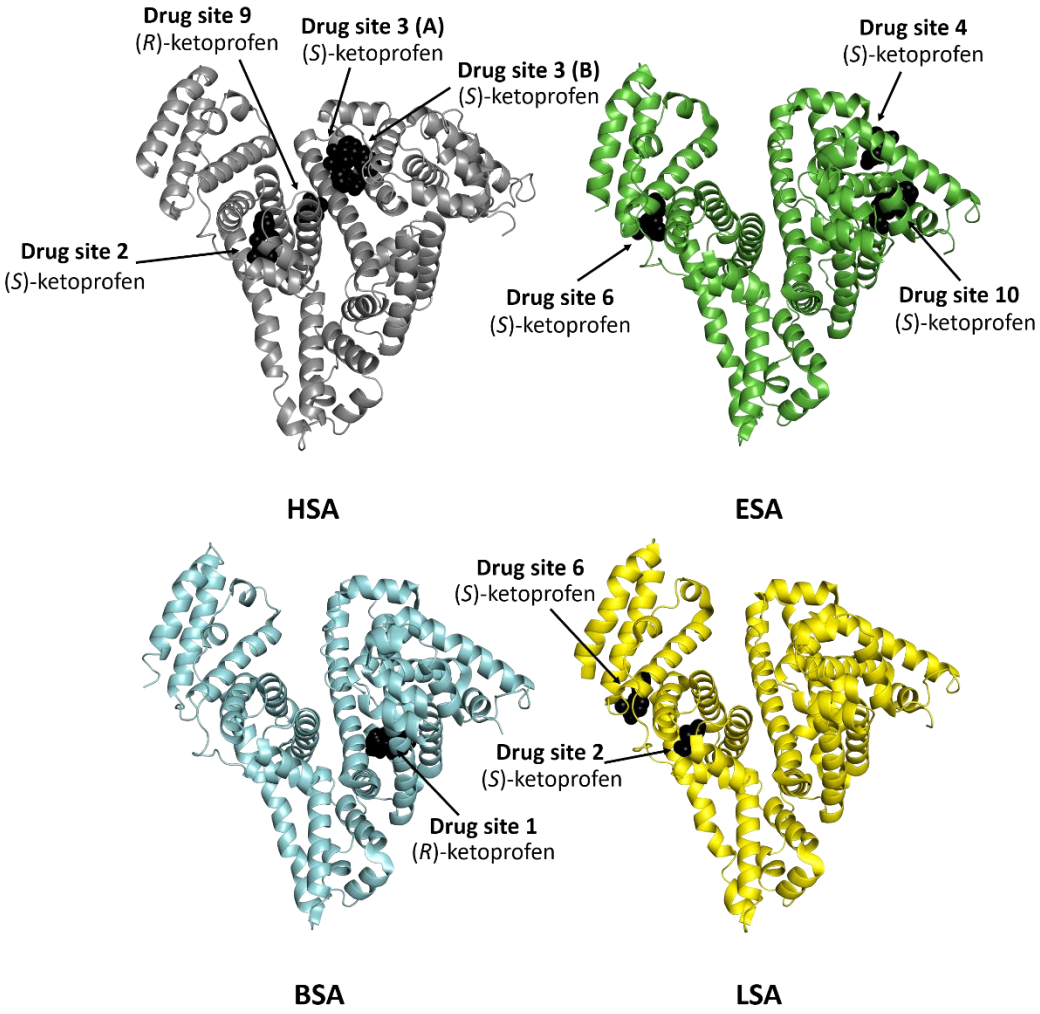

Figure 3.12. Ketoprofen binding sites in mammalian serum albumins. Structures of ketoprofen complexes with HSA (PDB ID: 7JWN), ESA (PDB ID: 6U4R), BSA (PDB ID: 6QS9), LSA (PDB ID: 6OCK).

Drug site 1 (Sudlow site I) has been reported as the only ketoprofen binding site in BSA (the pairwise sequence identity to HSA is 75.6%), and the drug molecule was modeled as (*R*)-enantiomer at this site (PDB ID: 6QS9, **Figure 3.12**).[129] Most of the residues involved in interactions with (*R*)-ketoprofen at drug site 1 are conserved between BSA and HSA (**Figure 3.13**), including Arg256 (Arg257 in HSA) and Tyr149 (Tyr150 in HSA) – the residues that form a salt bridge and a hydrogen bond with ketoprofen's carboxylate group, respectively. Only two residues are different, Arg198 (Lys199 in HSA) and Lys221 (Arg222). Moreover, they are involved only in hydrophobic interactions, and these changes should not affect the binding of ketoprofen to this site. However, despite the very high sequential conservation of drug site 1 between BSA and HSA (89%), this site remains unoccupied in the structure of the HSA-ketoprofen complex (PDB ID: 7JWN). Drug sites 2, 3, and 9 are free of ligands in the BSA-ketoprofen structure (PDB ID: 6QS9).

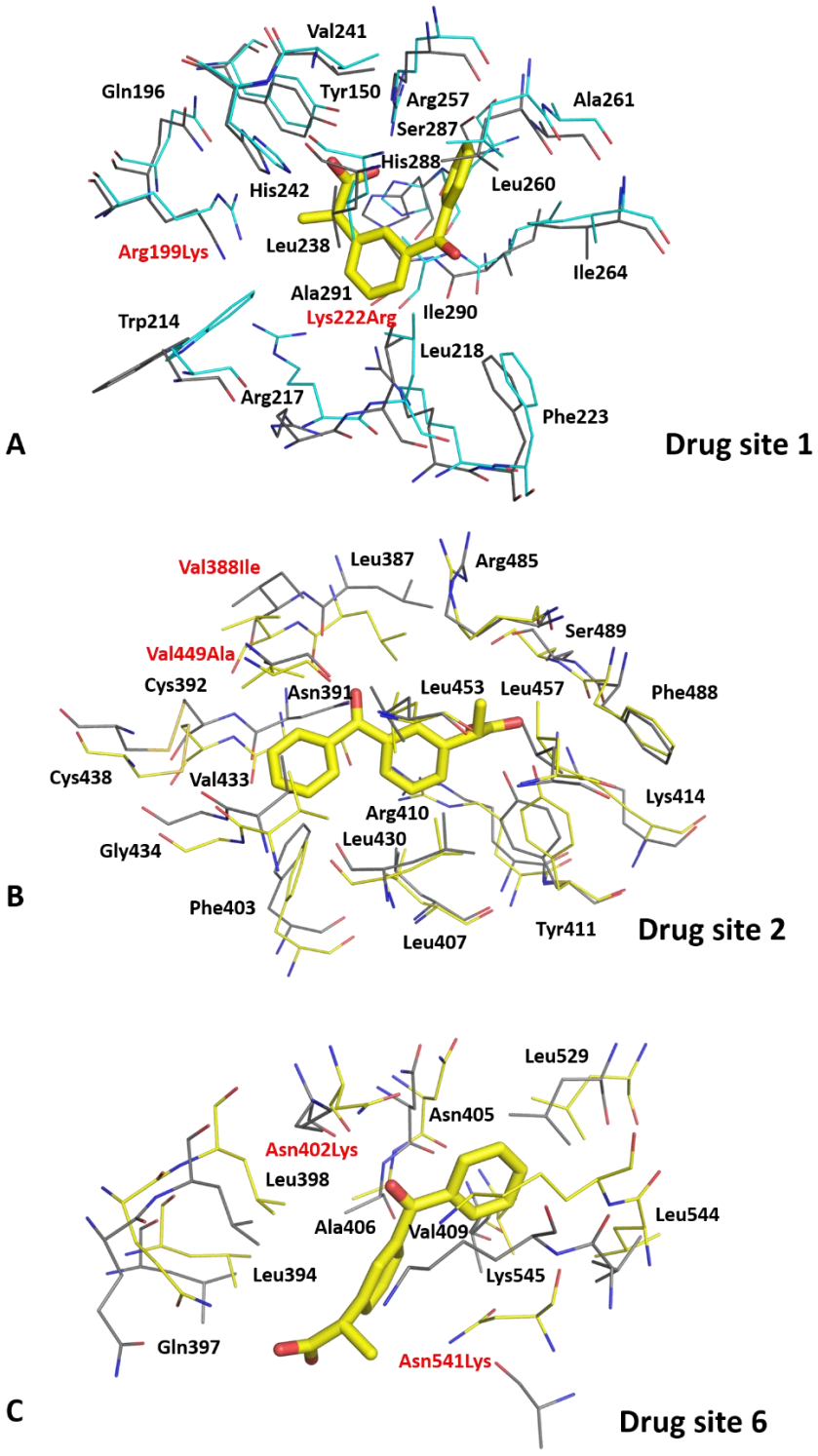

Figure 3.13. Superposition of ketoprofen binding sites in BSA (panel A, PDB ID: 6QS9) and LSA (panels B and C, PDB ID: 6OCK) with analogous sites in HSA (PDB ID: 4K2C). Carbon

atoms in BSA, LSA, and HSA are shown in cyan, yellow, and in gray, respectively. Residue numbers correspond to positions in HSA. Residues written in black are conserved between BSA or LSA and HSA, while those written in red differ. The naming scheme for differing residues is as follows: residue from BSA or LSA, residue number, residue from HSA.

LSA (the pairwise sequence identity to HSA is 73.4%) has been reported to bind (*S*)-ketoprofen to drug sites 2 and 6 (PDB ID: 6OCK, **Figure 3.12**).[115] Surprisingly, drug site 2 binds (*S*)-ketoprofen in both HSA and LSA, but the binding mode is different (**Figure 3.14**). At drug site 2 in LSA, (*S*)-ketoprofen molecule is stabilized by hydrophobic interactions with surrounding residues but also forms a salt bridge and a hydrogen bond between its carboxylate group and Lys414, and Tyr411, respectively. Most of the residues involved in these interactions are conserved (89%). Two residues that differ between LSA and HSA (Val388 is replaced by Ile and Val449 by Ala) do not change the character of the binding site (**Figure 3.13**). The drug's carboxylate group occupies roughly the same position in both structures (ketoprofen complexes with HSA and LSA), but its hydrophobic parts are oriented in opposite directions (**Figure 3.14**). Most likely, the presence of a fatty acid molecule at this site (FA3) in the HSA structure reported herein affects the conformation of (*S*)-ketoprofen. Previously, (*S*)-ibuprofen has been reported to bind to drug site 2 in HSA and ESA with two different binding modes that resemble those of (*S*)-ketoprofen (see **Figure 3.3**).[228] The other molecule of (*S*)-ketoprofen binds to drug site 6, where it is stabilized by hydrophobic interactions and by hydrogen bonds between its carboxylate group and Asn397's sidechain (NE2 atom) and between its carbonyl group

and sidechains of Asn402 (ND2 atom) and Lys545. This binding site is conserved in 82% between LSA and HSA. Two residues that are modified (Asn402 to Lys and Asn541 to Lys) change the overall charge in the cavity, and due to the bigger size of the side chain may affect the drug's conformation or even prevent its binding. Drug site 6 is unoccupied in the HSA-ketoprofen structure (PDB ID: 7JWN). In the LSA-ketoprofen structure (PDB ID: 6OCK), drug site 3 is occupied by a molecule of a polyethylene glycol, which may prevent drug binding to this site, and in drug site 9 is present acetate ion.

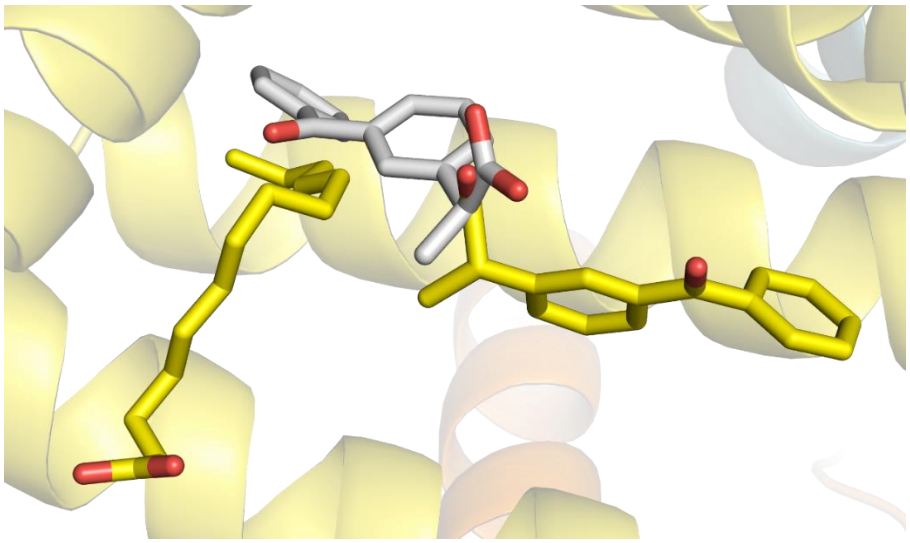

Figure 3.14. Comparison of (*S*)-ketoprofen binding to drug site 2 in HSA (PDB ID: 7JWN) and LSA (PDB ID: 6OCK). (*S*)-Ketoprofen molecule and molecule of a fatty acid bound to HSA are shown in stick representation with oxygen atoms in red and carbon atoms in yellow, while a molecule of (*S*)-ketoprofen bound to LSA is shown in stick representation with oxygen atoms in red and carbon atoms in gray.

3.2. Steroid binding by serum albumin

3.2.1. Structures of ESA complexes with steroids

All structures of the ESA-steroid complexes were determined in the $P6_1$ space group and contained one protein molecule in the asymmetric unit (**Table 3.8**). In the reported structures, the observed electron density indicates steroids bound to drug sites 4 and 7 (**Figure 3.15**). The first three residues are not modeled in each of these structures due to the lack of electron density. Overall, the structures of the ESA-steroid complexes are essentially identical to previously published structures of ESA. For instance, when the ESA-testosterone structure was compared to other proteins using the Dali server[229] the structure yielding the highest score was ESA complexed with diclofenac and naproxen (PDB ID: 5DBY).[128] RMSD between the aligned Cα atoms was 0.5 Å.

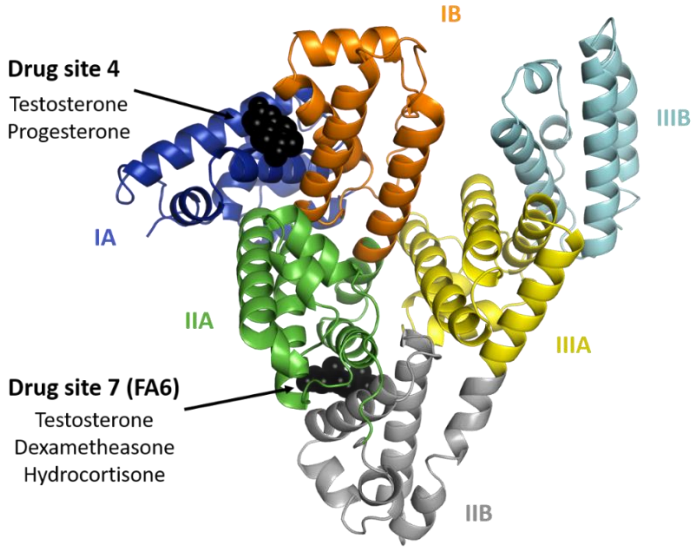

Figure 3.15. Location of the steroid binding sites in ESA structures reported in this study. Molecules are shown with atoms as black spheres. Domains are labeled with Roman

numerals (I, II, III) and subdomains with letters (e.g., IA), with each subdomain shown in a different color; FA stands for the fatty acid binding site.

Table 3.8. Data collection, structure refinement, and structure quality statistics for ESA-steroid structures. Values in parentheses are for the highest resolution shell. Ramachandran plot statistics are calculated by MolProbity. DS1-DS10 refer to drug-binding sites. Crystals of albumin complexes with testosterone and dexamethasone were produced and the X-ray data were collected by Dr. Karolina Majorek.

Name	Testosterone	Progesterone	Dexamethasone	Hydrocortisone
PDB ID	6MDQ	-	6XK0	-
Diffraction images DOI	10.18430/m36mdq	-	10.18430/m3.irrmc.5571	-
Data collection statistics				
Crystallization conditions	1.8 M ammonium dihydrogen citrate at pH 7.0	0.2 M lithium sulfate, 1.8-2.4 M ammonium sulfate, 0.1 M Tris buffer pH 7.4	1.8 M ammonium dihydrogen citrate at pH 7.0	1.6 M ammonium sulfate, 0.1 M Sodium acetate at pH 4.6
SA source	ESA isolated from horse blood (Equitech-Bio #ESA62)			
SA concentration	15 mg/mL	34 mg/mL	15 mg/mL	34 mg/mL
Additives	Testosterone powder was added directly to the crystallization drop containing crystals for 48 h before harvesting	Progesterone powder was added directly to the crystallization drop containing crystals for 48 h before harvesting	Dexamethasone powder was incubated with protein for 60 min at room temperature prior to the crystallization	Hydrocortisone powder was added directly to the crystallization drop containing crystals for 48 h before harvesting
Resolution (Å)	50.00-2.15 (2.19-2.15)	50.00-2.80 (2.85-2.80)	50.00-2.40 (2.44-2.40)	50.00-2.25 (2.29-2.25)
Beamline	21-ID-F	21-ID-F	21-ID-F	21-ID-F
Wavelength (Å)	0.979	0.979	0.979	0.979
Space group	$P6_1$	$P6_1$	$P6_1$	$P6_1$
Unit-cell dimensions (Å)	a=b=94.2 c=142.3	a=b=94.6 c=141.8	a=b=95.0 c=143.6	a=b=94.2 c=141.6
Protein chains in the ASU	1	1	1	1
Completeness (%)	99.7 (100.0)	99.3 (92.1)	99.8 (98.3)	100.0 (99.5)
Number of unique reflections	39 149 (1910)	17758 (813)	28870 (1412)	33420 (1680)
Redundancy	7.6 (6.8)	6.1 (3.8)	4.9 (3.5)	14.0 (8.6)
<I>/<σ(I)>	28 (2.0)	13.5 (1.0)	15.3 (1.3)	30.0 (1.2)
CC ½	(0.81)	0.56	(0.61)	0.65
R_{merge}	0.071 (1.027)	0.135 (1.070)	0.110 (1.053)	0.104 (1.375)

Refinement statistics				
R_{work}/R_{free}	0.183/0.226	0.189 / 0.250	0.203/0.249	0.184 / 0.232
Bond lengths RMSD (Å)	0.004	0.002	0.002	0.002
Bond angles RMSD (°)	0.8	1.2	1.1	1.2
Mean B value (Å²)	64	60	57	45
Mean B value for ligands (Å²)	134.7 (DS4), 103.3 (DS7)	97.7 (DS4)	90.5 (DS7)	44.4 (DS7)
Number of protein atoms	4501	4574	4589	4552
Mean B value for protein (Å²)	61	61	58	44
Number of water molecules	214	92	228	263
Mean B value for water molecules (Å²)	61	33	39	39
Clashscore	1.12	2.85	2.71	4.12
MolProbity score	0.82	1.19	1.25	1.36
Rotamer outliers (%)	0.00	0.00	0.60	0.00
Ramachandran outliers (%)	0.00	0.00	0.00	0.00
Ramachandran favored (%)	98.27	97.41	96.88	97.06

3.2.1.1. ESA complex with testosterone

In the ESA-testosterone crystal structure (PDB ID: 6MDQ; resolution 2.15 Å), well-defined electron density indicates two testosterone molecules bound to ESA (**Figure 3.15, Figure 3.16**). The first testosterone binds to drug site 7, which is located between the h2 helix of subdomain IIA and the h2 and h3 helices of subdomain IIB, 12.2 Å from the singular tryptophan residue of ESA (Trp213). Drug site 7 is predominantly composed of hydrophobic residues oriented inward with respect to the cavity, with hydrophobic interactions between the tetracyclic structure of testosterone and Ala212, Leu326, Gly327, Leu330, Leu346, and Ala349. The Arg208 residue is involved in a salt bridge with

Asp323, and its aliphatic portion also forms hydrophobic interactions with two of the three six-membered rings of testosterone. Drug site 7 contains several hydrophilic residues, which may also contribute to the binding of testosterone; a possible hydrogen bond exists between the hydroxyl group of the testosterone molecule and the carbonyl oxygen of the side-chain of Glu353.

The second testosterone molecule binds to drug site 4, which is located between subdomains IA and IB, 30.5 Å away from the tryptophan residue (**Figure 3.15**, **Figure 3.16**). The observed electron density in this site, while not as strong as that observed in drug site 7 (owing to the flexible nature of these subdomains, possible crystallographic disorder, or weaker ligand binding), is still well-defined and supports the presence of a testosterone molecule. Similar to drug site 7, drug site 4 is largely hydrophobic in character. The rings of the testosterone molecule are involved in hydrophobic interactions with Lys17, Lys20, Gly21, Asp131, Leu134, and Glu158. The hydroxyl group of testosterone forms a hydrogen bond with the carbonyl oxygen of the side-chain of Glu158. The hydrophilicity and hydrophobicity of testosterone binding sites are shown in **Figure 3.17** and **Figure 3.18**.

Due to the high concentration of citrate in the crystallization conditions (1.8 M), I considered the possibility of citrate molecules binding to drug sites 4 or 7 in place of testosterone. Overall, three citrate molecules are bound to ESA; two of them are located in the vicinity of the testosterone molecule bound to drug site 7. I attempted to place and refine citrate molecules in both drug site 4 and drug site 7, but they did not fit the observed electron density. This situation was observed for two other datasets collected

for the ESA-testosterone complex (data not shown). Moreover, the testosterone molecules form much more chemically reasonable interactions with the neighboring residues: the predominantly hydrophobic character of both drug site 4 and drug site 7 suggests that a highly charged citrate molecule is unlikely to bind in these sites. In addition, in other ESA structures that were determined from the same crystallization conditions but with different ligands (data not shown), the electron density was not observed in drug site 4 or drug site 7. These results are contrary to prior hypotheses, which were formulated solely from binding methods and stated that testosterone binds to Sudlow site I in subdomain IIA.[1,230]

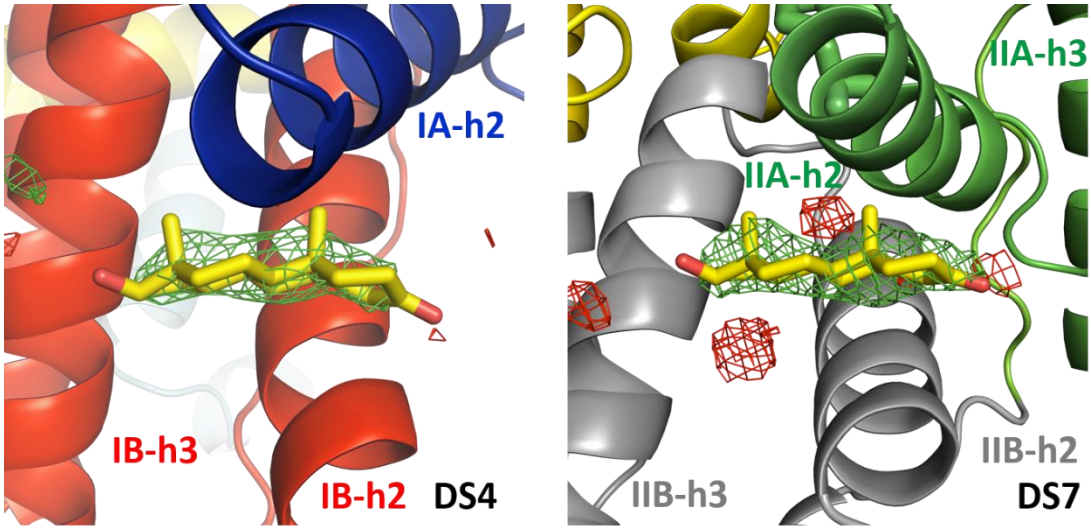

Figure 3.16. Testosterone binding sites with omit electron density map (mFo-DFc map, calculated after 10 refinement cycles without testosterone, RMSD 3.0) presented in green and red (positive and negative contours, respectively). Drug site 4 is located between subdomains IA and IB, while drug site 7 is surrounded by subdomains IIA and IIB. The

electron density can be inspected interactively at https://molstack.bioreproducibility.org/project/view/qfVhauem03OuCONzLXPz/ .

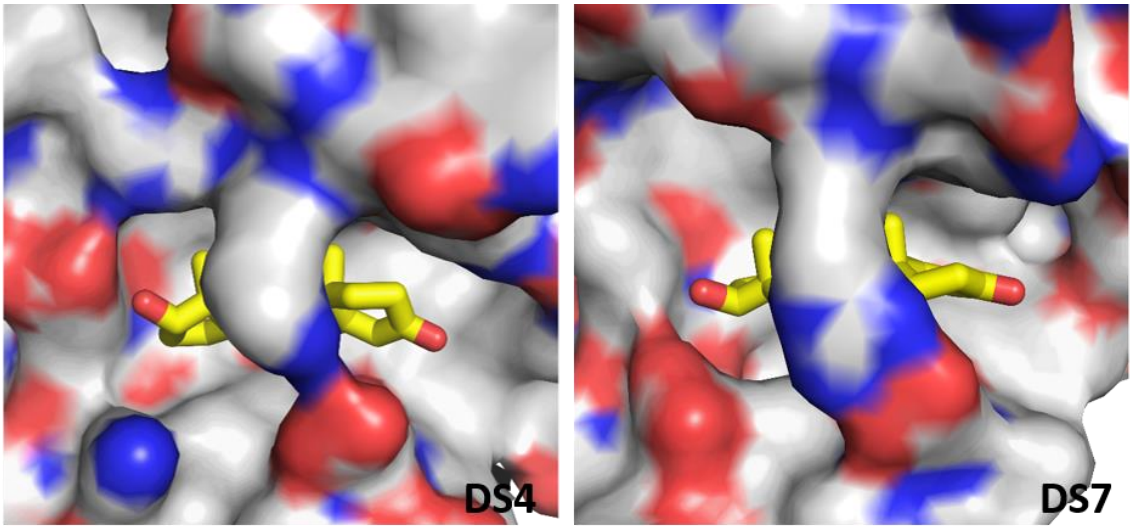

Figure 3.17. Hydrophobic nature of testosterone binding sites. The color of the protein surface indicates the contributions of the particular atoms to the surface. The color scheme is as follows: gray for carbon atoms, red for oxygen atoms, and blue for nitrogen atoms. Testosterone's carbon atoms are shown in yellow.

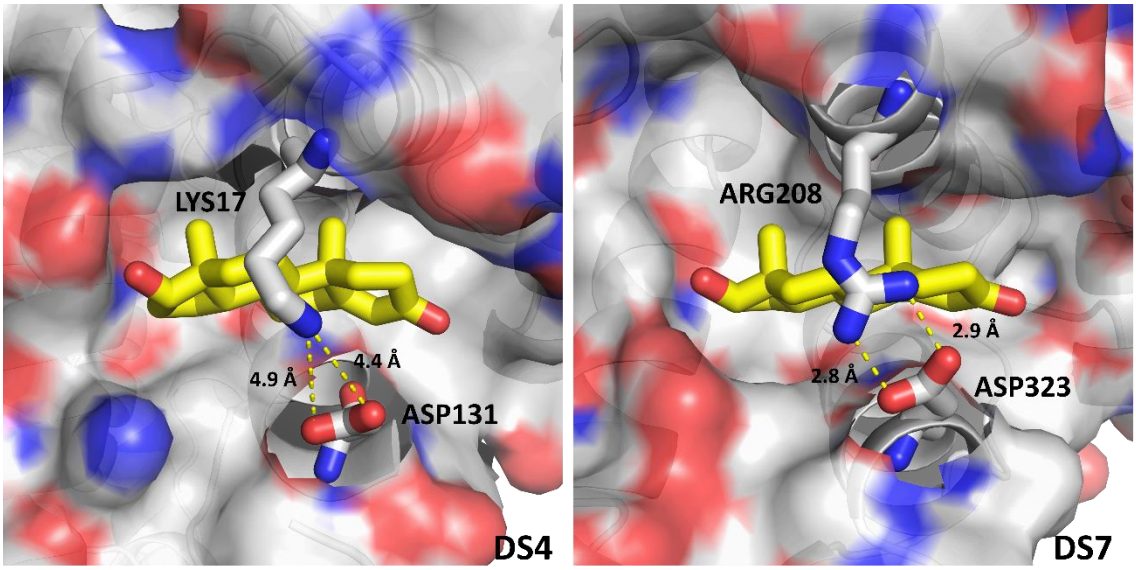

Figure 3.18. Testosterone binding sites are protected by electrostatic interactions between Lys17 and Asp131 in drug site 4 and Arg208 and Asp323 in drug site 7. The color of the protein surface indicates the character of the environment, and the color scheme is as follows: gray for carbon atoms in ESA, red for oxygen atoms, and blue for nitrogen atoms. Testosterone's carbon atoms are shown in yellow.

3.2.1.1.1. Tryptophan fluorescence quenching

To check whether testosterone binds with similar affinity to human and equine serum albumin, I employed tryptophan fluorescence quenching. TFQ binding studies performed at 37°C showed micromolar (ESA in PBS: K_d = 367 ± 69 µM; HSA in PBS: K_d = 363 ± 83 µM) values of K_d for both ESA and HSA with testosterone (**Figure 3.19**). ESA and HSA each contain a singular tryptophan residue located in the same spatial position (Trp213 in ESA, Trp214 in HSA). Trp213 is localized 12.2 Å from the testosterone molecule in drug site 7 and 30.5 Å from the testosterone molecule in drug site 4 in the ESA structure

(**Figure 3.20**), suggesting that the TFQ experiments may only represent the binding of testosterone to the closely located drug site 7. These studies were performed for the SA-testosterone complex in the presence of 20% DMSO to obtain testosterone concentrations high enough to saturate SA. At lower DMSO concentrations, the testosterone solution was unstable, and testosterone easily precipitated. However, a previous study with Raman spectroscopy suggested that SA in the presence of 20% DMSO may be partially unfolded.[231]

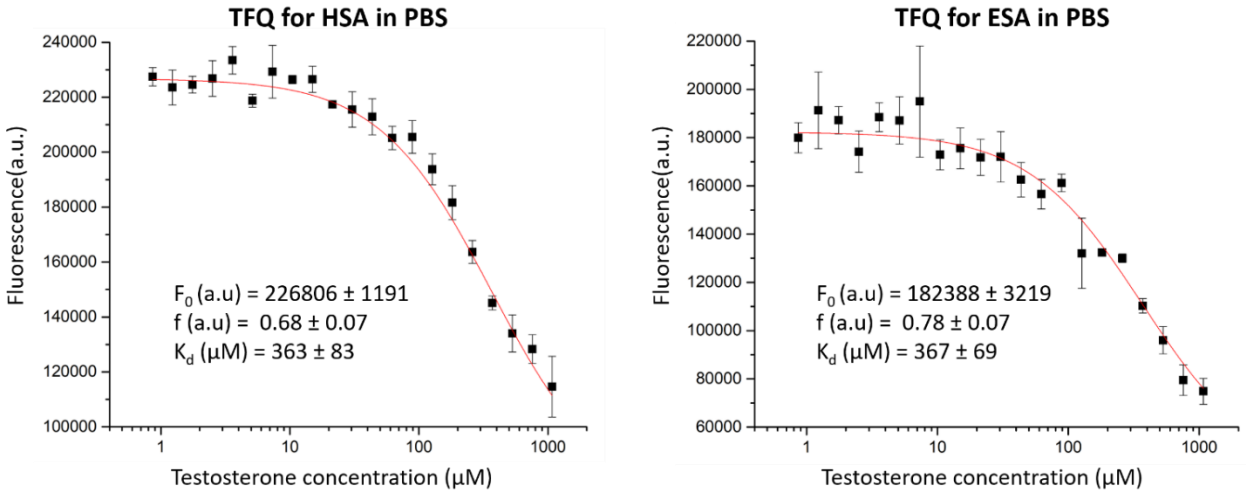

Figure 3.19. TFQ for HSA and ESA caused by testosterone. Standard deviation of fluorescence intensities is represented by error bars.

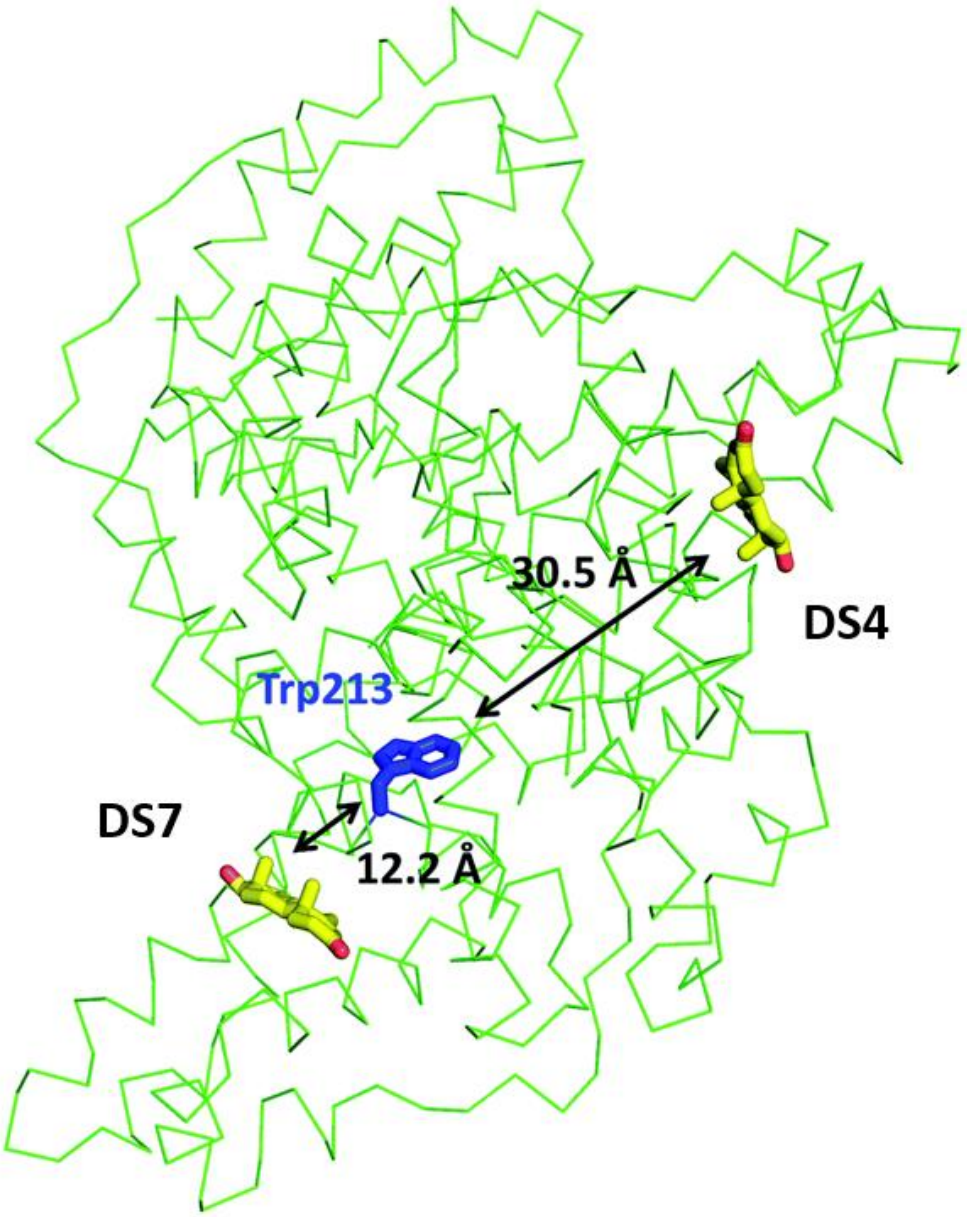

Figure 3.20. Testosterone binding sites and their distances from the tryptophan residue. Distances were calculated between the center of mass of tryptophan's indole ring center of mass and that of each testosterone molecule. The testosterone molecules (yellow) and the tryptophan's side-chain (blue) are shown in stick representation and labeled.

3.2.1.1.2. Ultrafast affinity extraction and zonal elution studies

The ultrafast affinity extraction and zonal elution studies described here were performed by the group of Prof. David Hage at the University of Nebraska-Lincoln.[105] The effect of varying the injection flow rate and column residence time on the apparent free fractions that were measured by the UAE for testosterone in the presence of ESA is shown in **Figure 3.21 (a)**. A consistent free fraction was obtained for mixtures of testosterone with ESA at an injection flow rate of at least 1.75 mL/min. The free fraction that was measured under these conditions was viewed as representing the state of the original sample at equilibrium. Using this method at 37°C in the presence of only phosphate buffer, the best estimate for nK_a' (pH 7.4) was 5.5 (± 0.5) × 10^4 M^{-1}, which corresponded to an overall equilibrium dissociation constant of 18 (± 2) μM for testosterone binding to ESA. This result was confirmed through the analysis of the same data by using Eqn. (5). The plot was made according to Eqn. (5), as shown in **Figure 3.21 (b)**, also gave a dissociation rate constant for ESA and testosterone of 0.59 (± 0.05) s^{-1}.

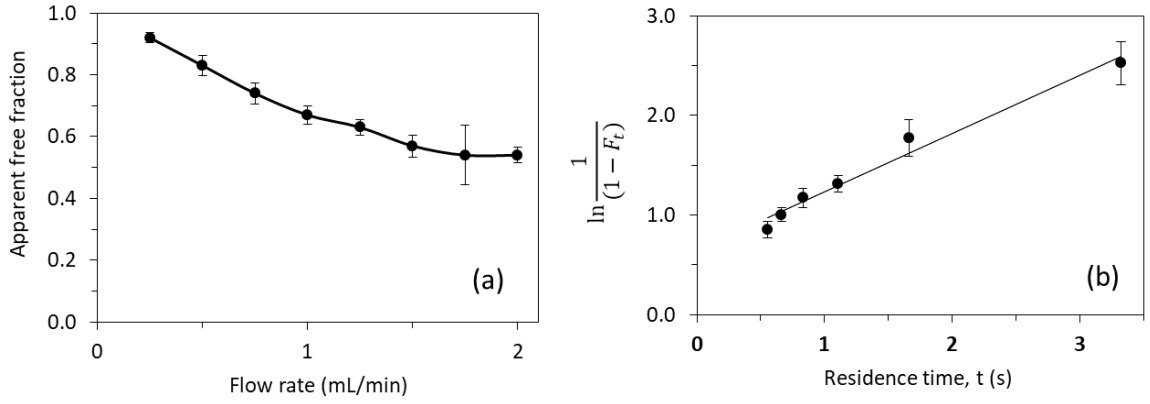

Figure 3.21 (a) Effect of flow rate on the measured free fraction of testosterone in the presence of ESA. (b) Analysis of the measured free fractions of testosterone/ESA mixtures based on Eqn. (5). The error bars represent a range of $\pm$ 1 S.D.

Prior experiments[221] in examining the interactions of testosterone with HSA by the same approach provided a similar value of 3.2-3.5 × 10^4 M^{-1} for nK_a', or an overall equilibrium dissociation constant of 28.6-31.3 µM, and a dissociation rate constant of 2.17-2.20 s^{-1}. These values for testosterone binding by HSA show good agreement with previous literature results obtained from the same system and through different techniques (e.g., equilibrium dialysis).[41,232,102]

Zonal elution studies were carried out on both an HSA column and a control column of the same size that contained the same support but no immobilized protein. The control column was used in this case to measure and correct for any non-specific binding by testosterone to the support. The retention factor for testosterone on both columns was determined in replicate, and the difference in retention between these two columns was used to determine the retention factor that could be attributed solely to testosterone's binding to HSA. The results of these studies are summarized in **Table 3.9**.

The addition of only 40 µM citrate to 67 mM potassium phosphate buffer (pH 7.4) resulted in a 51% decrease in the global affinity of testosterone for HSA. Testosterone concentration in adult male blood plasma ranges from 17.3-24.3 nM,[2] while the normal citrate concentration in human plasma is about 100–150 µM.[233] This suggests that in physiological conditions, citrate may affect the binding of testosterone to SA. The addition of 20% DMSO resulted in a 54% decrease in the global affinity. This effect shows that DMSO was at least partially responsible for the decreased binding affinity of testosterone for albumin measured in the TFQ experiments. Another reason for the decreased affinity observed in the TFQ experiments may be the possibility that TFQ only measures the binding of testosterone to drug site 7, which is much closer to the sole tryptophan residue. Therefore, the measured K_d from the TFQ experiment does not accurately reflect the cumulative affinity in physiological conditions. These results further show an advantage of UAE and zonal elution studies over TFQ in the use of much lower concentrations of testosterone (20 µM vs. 1080 µM), which allowed for the measurement of its binding affinity for albumin in the absence of organic solvents.

Table 3.9. Retention factors for testosterone on immobilized HSA and control columns in the presence of various mobile phases.

Mobile phase	Retention factor on HSA column[b]	Retention factor on control column[b]	Retention factor due to HSA[c]
67 mM phosphate buffer (KPB, pH 7.4)	26.6 (± 4.0)	4.4 (± 0.7)	22.2 (± 4.1)
KPB (pH 7.4) + 40 µM citrate	16.7 (± 0.9)	5.9 (± 0.1)	10.8 (± 1.1)
KPB (pH 7.4) + 20% DMSO	14.2 (± 1.2)	4.0 (± 0.3)	10.2 (± 1.2)

[a]All values in parentheses are a range of ± 1 S.D. (*n* = 3-4). [b]The retention factor (*k*) on the HSA column or control column was calculated by using the relationship $k = (t_R - t_M)/t_M$, where t_R is the retention time for testosterone on the column and t_M is the column void time (e.g., as measured by using sodium nitrate).[c]The retention factor for testosterone due to only HSA was found by calculating the difference between the retention factors that were measured on the HSA column and the control column.

3.2.1.2. ESA complex with progesterone

The structure of the ESA-progesterone complex was determined at 2.80 Å resolution (**Table 3.8**). The electron density indicates progesterone bound to drug site 4 (**Figure 3.22**). Progesterone bound to drug site 4 overlaps with the position of testosterone inside the same drug site, described in section 3.2.1., and is surrounded by the same residues as testosterone (residues found within 5 Å of progesterone molecule: Lys17, His18, Lys20, Gly21, Leu24, Phe36, Val40, Val43, Asp131, Leu134, Gly135, Leu138, Leu154, Ala157, Glu158, Lys161). However, due to different orientation and bigger structure, progesterone does not form any hydrogen bond and is stabilized only by hydrophobic interactions (testosterone at drug site 4 forms a hydrogen bond with Glu158).

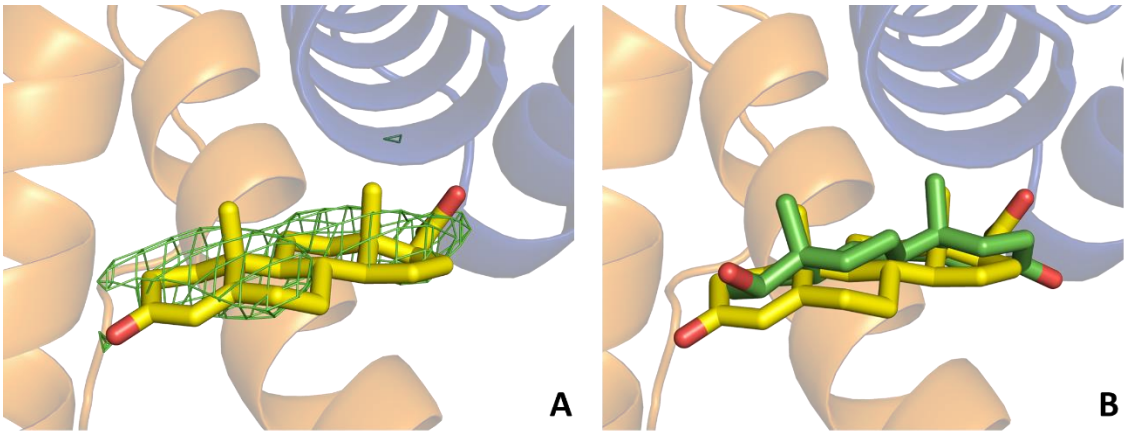

Figure 3.22. A) The electron density observed for progesterone in drug site 4 (mFo-DFc map, calculated after 10 refinement cycles without testosterone, RMSD 2.5) presented in green. B) Superposition of the ESA complexes with progesterone and testosterone. The progesterone molecule is shown with yellow carbon atoms and testosterone with green carbon atoms. The electron density can be inspected interactively at https://molstack.bioreproducibility.org/project/view/79OV3STtbo7hAa2Qnlkk/.

Drug site 7 remains unoccupied in the ESA-progesterone complex. The ESA-progesterone structure also contains an unknown ligand (UNL) bound to drug site 1 (**Figure 3.23**). The UNL is bound to a location known to bind sugars in HSA (see PDB ID: 4IW2) and overlapping with the position of UNL ligand in the ESA-ibuprofen structure (section 3.1.1.5). The shape of the observed density suggests that the unknown ligand is likely a sugar molecule but does not allow for unambiguous interpretation. Sugars were not added to albumin during the crystallization process and are most likely remnants of ESA purification from horse serum.

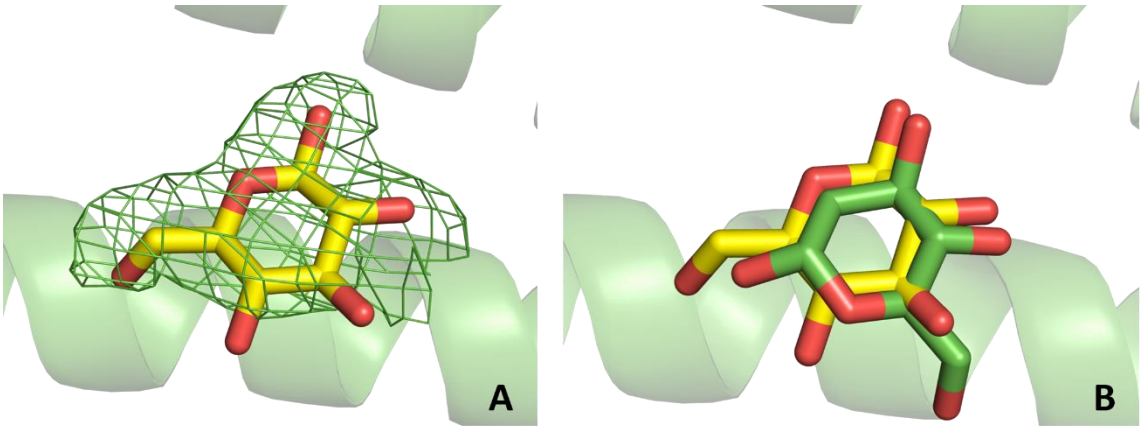

Figure 3.23. A) The electron density observed for an unknown ligand (modeled as glucose) in drug site 1 (mFo-DFc map, calculated after 10 refinement cycles without testosterone, $\sigma - 2.5$) presented in green. B) Superposition of the ESA-progesterone complex (glucose is shown with carbon atoms in yellow) and the HSA-glucose complex (PDB ID: 4IW2; glucose is shown with carbon atoms in green).

3.2.1.3. ESA complex with hydrocortisone

Well-ordered electron density indicates the hydrocortisone molecule bound to drug site 7 (structure resolution 2.25 Å, **Table 3.8**), which partially overlaps with the position of testosterone described in section 3.2.1 (**Figure 3.24**). Hydrocortisone is stabilized mostly by hydrophobic interactions (Ala212, Leu326, Gly327, Leu330, Leu346, Ala349, and aliphatic portions of Arg208, Asp323, and Lys350) but also forms two hydrogen bonds between its hydroxyl groups (O2 and 05 atoms) and Arg208's side-chain (NH1 and NH2 atoms). Hydrocortisone forms also a hydrogen bond (O2 atom) with a sulfate ion bound close to Arg208.

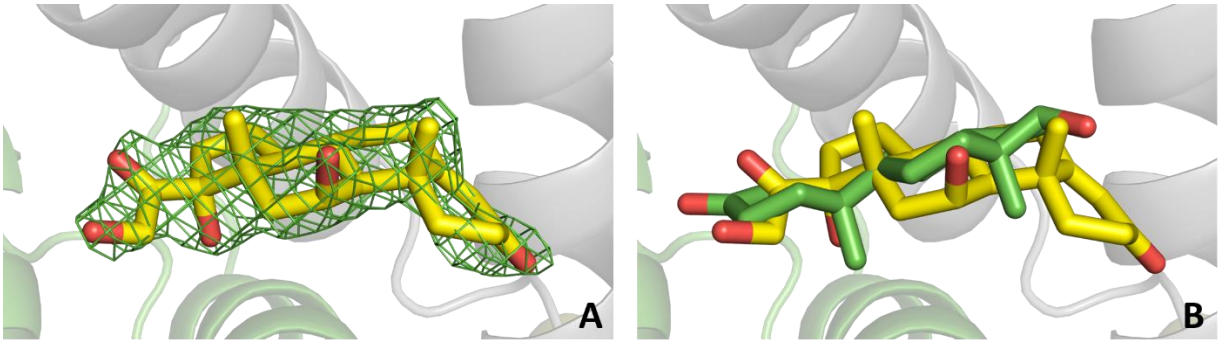

Figure 3.24. A) The electron density observed for hydrocortisone in drug site 7 (mFo-DFc map, calculated after 10 refinement cycles without testosterone, $\sigma - 2.5$) presented in green. B) Superposition of the ESA complexes with hydrocortisone and testosterone. Hydrocortisone molecule is shown with yellow carbon atoms and testosterone with green carbon atoms. The electron density can be inspected interactively at https://molstack.bioreproducibility.org/project/view/79OV3STtbo7hAa2Qnlkk/.

Positive regions of electron density were also observed at drug site 1 (location known to bind fructose in HSA, see PDB ID: 4IW1), drug site 4 (overlap with position of testosterone described in section 3.2.1), and between drug site 1 and drug site 9 (**Figure 3.25**). In all of these locations, the shape of the observed electron density suggests binding of sugar molecules (open-chain or cyclic form). However, sugars were not added to albumin during crystallization, and bound molecules cannot be unambiguously identified based only on the observed electron density. Glucose and fructose modeled in these sites do not fully explain the observed density; always, one hydroxyl group is out of density. Sugar bound to drug site 1 clearly forms a covalent bond with Lys221 (**Figure**

3.25). The analogous residue in HSA (Arg222) is known to undergo glycation. In the reported structure, the glycated lysine is modeled as an Amadori product, but it is possible that the observed electron density is a result of different glycation products (early or advanced stage glycation, **Figure 1.3**). Also, density observed for Lys221 suggests that this residue may not be glycated in a small fraction of albumin molecules and potentially has a different conformation (alternative conformation is not shown in **Figure 3.25**). The ESA-hydrocortisone structure also contains fatty acid (modeled as myristic acid; not added to albumin during crystallization) bound to drug site 2.

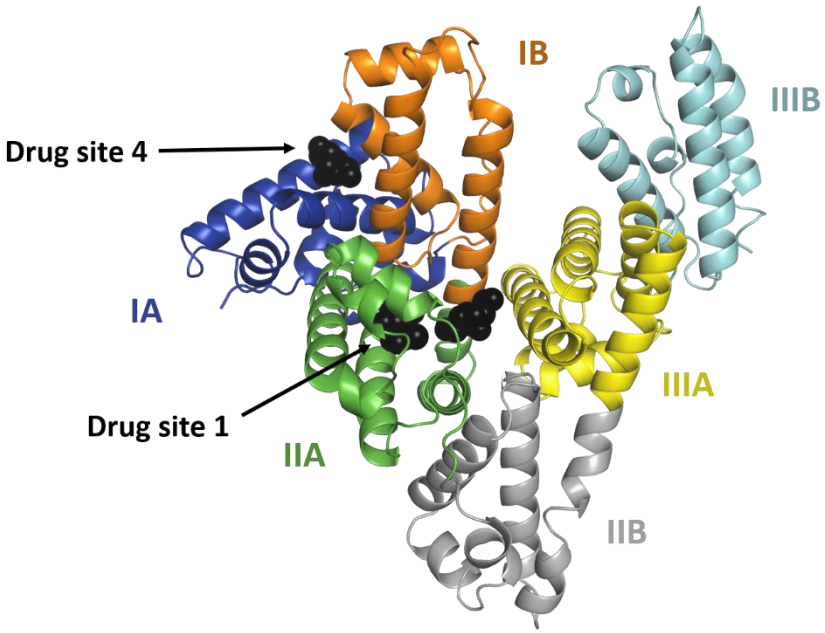

A

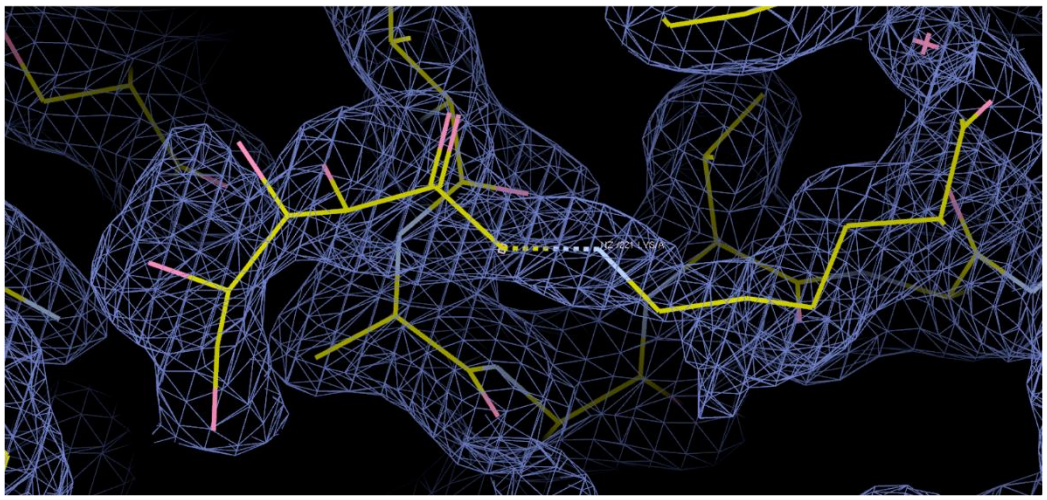

B

Figure 3.25. A) Location of potential sugar-binding sites in ESA observed in the structure of ESA-hydrocortisone. Molecules are shown with atoms as black spheres. B) Drug site 1; sugar molecule (modeled as fructose) is covalently bound to Lys221.

3.2.1.4. ESA complex with dexamethasone

The crystal structure of ESA in complex with dexamethasone was determined at 2.40 Å resolution (**Table 3.8**). The electron density maps are consistent with one dexamethasone molecule bound to drug site 7, which is located in domain II, between subdomains IIA and IIB (**Figure 3.26**). In addition to the dexamethasone, one citrate molecule and one fatty acid molecule were located in the structure. The citrate molecule is located inside the cleft between domains I and III, near drug site 9, at the same position as in ESA-testosterone complex; citrate was a major component of the crystallization cocktail. The fatty acid molecule, which was likely retained during purification of ESA from blood, is located in fatty acid site 8 (FA8). Very week electron density is also observed in drug site 4, which does not allow for any certainty in the interpretation. This density was accounted for by four UNX atoms.

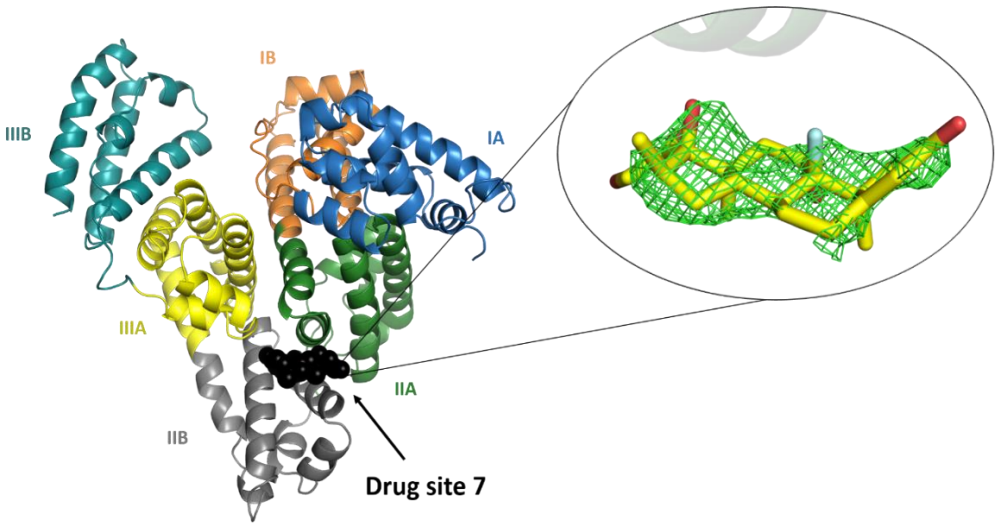

Figure 3.26. The overall structure of the ESA-dexamethasone complex. The electron density observed for dexamethasone in drug site 7 is shown as green mesh (mFo−DFc map, calculated after ten refinement cycles without the ligand, RMSD 2.5). Albumin subdomains are shown in different colors and labeled with Roman numerals and letters (e.g., IA). The dexamethasone molecule is shown in stick representation with carbon atoms in yellow, oxygen atoms in red and fluoride atom in cyan. The electron density, including the omit maps, and the model can be inspected interactively at https://molstack.bioreproducibility.org/project/view/gmvG1L8c66YgPpgqS0Zm/.

Fifteen residues are found within 5 Å of dexamethasone molecule: Arg208, Ala209, Lys211, Ala212, Val215, Asp323, Leu326, Gly327, Leu330, Leu346, Arg347, Ala349, Lys350, Glu353, and Ala481 (corresponds to Val482 in HSA). Side-chains of residues Ala212, Val215, Leu326, Leu330, Leu346, Ala349, and the hydrophobic part of Lys350 form a mostly hydrophobic surface at the inner side of the binding cavity, towards which the most hydrophobic part of dexamethasone molecule is oriented (**Figure 3.27**).

The cavity is partially separated from the solvent by a strong salt bridge between Arg208 and Asp323, which bridges the IIA and IIB subdomains. In addition to the hydrophobic interactions, the drug molecule is stabilized by two hydrogen bonds: O2 hydroxyl group with NH2 atom of Arg208 and O3 hydroxyl group with the main chain oxygen of Arg208. During the refinement, a different orientation of dexamethasone was tried as an alternative, in which the drug was rotated by 180° along the axis perpendicular to its rings. However, in the alternative orientation one of the four rings of dexamethasone was not covered by strong electron density, and the compound did not form any hydrogen bonds with the protein, clearly supporting the chosen conformation.

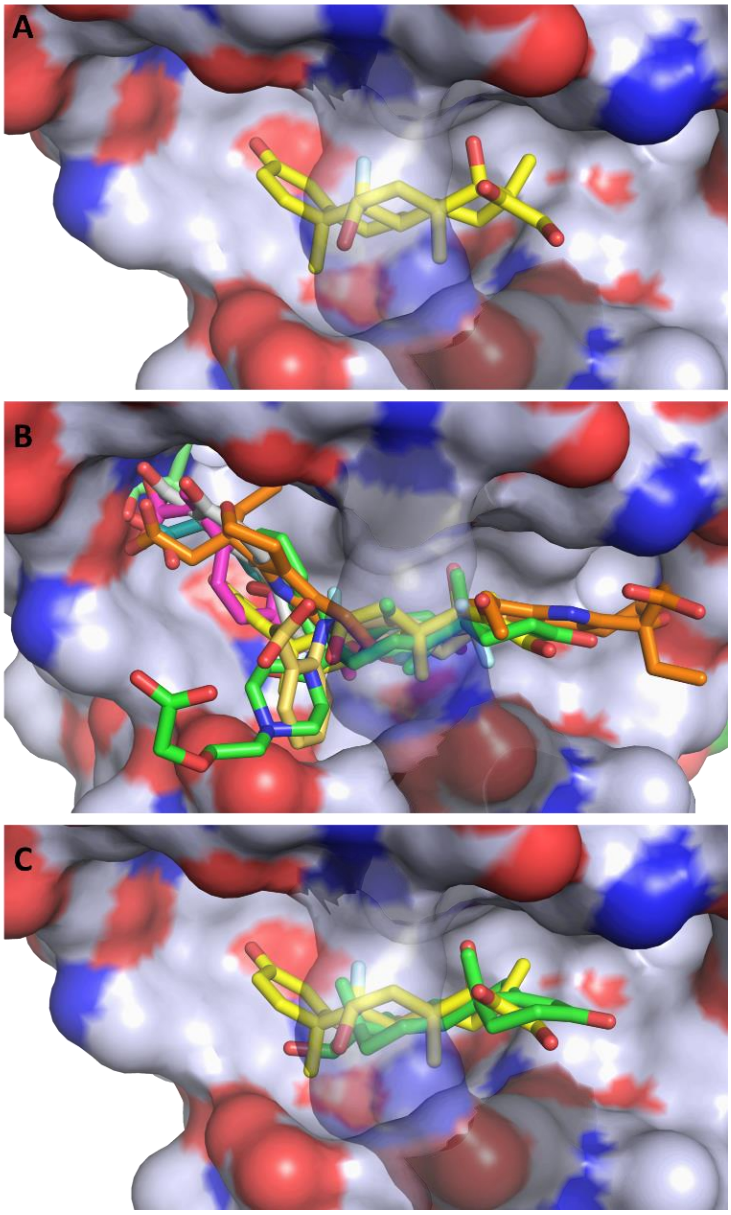

Figure 3.27. Hydrophobicity of drug site 7 and potential competition between dexamethasone and other drugs. (A) Dexamethasone bound to ESA. The color scheme for the protein surface is as follows: gray for the contribution from carbon atoms, red for oxygen atoms, and blue for nitrogen atoms. The link covering the cavity is formed by a salt bridge between Arg208 and Asp323 and is transparent on all panels for clarity. (B) Superposition of the serum albumin complexes with the FDA-approved drugs known to

bind to drug site 7: dexamethasone (PDB ID: 6XK0), ibuprofen (PDB ID: 2BXG), diflunisal (PDB ID: 2BXE), cetirizine (PDB ID: 5DQF), testosterone (PDB ID: 6MDQ), halothane (PDB ID: 1E7B), naproxen (PDB ID: 4ZBR), 6-MNA (PDB ID: 6U5A), diclofenac (PDB ID: 6HN0), and etodolac (PDB ID: 5V0V). (C) Superposition of the ESA-dexamethasone (PDB ID: 6XK0) and ESA-testosterone (PDB ID: 6MDQ) structures. Dexamethasone and testosterone largely overlap at drug site 7. Both steroids are shown in stick representation with oxygen atoms in red; dexamethasone is shown with carbon atoms in yellow and fluoride atom in cyan, while testosterone is shown with carbon atoms in green.

3.2.2. Conservation of steroid binding sites in ESA/HSA

The high sequence identity/similarity between HSA and ESA (76.1%/86.2%) and residue conservation in drug site 4 and drug site 7 allow us to expect similar binding properties of these sites in albumin from both species. A full alignment of the HSA and ESA sequences, with residues involved in testosterone binding (the only steroid that binds to both drug sites 4 and 7) marked, is shown in **Figure 3.28.** Testosterone bound to ESA at drug site 4 overlaps with location reported to bind progesterone (**Figure 3.22**), and at drug site 7 overlaps with location reported to bind hydrocortisone (**Figure 3.24**) and dexamethasone (**Figure 3.27**). The residues comprising drug site 7 in ESA (based on the testosterone binding: Arg208, Ala209, Lys211, Ala212, Val215, Phe227, Asp323, Val324, Leu326, Gly327, Leu330, Leu346, Ala349, Lys350, Glu353) are conserved in HSA (**Figure 3.29**). The salt bridge involving Arg208 in ESA is also observed in HSA (between Arg209 and Asp324) and contributes to the fatty acid binding.[234] Drug site 4 is less conserved

(retained residues are Glu16, Lys20, Leu24, Phe36, Val40, Val43, Asn44, Asp134, Leu138, Leu154, Ala157, Lys161, Leu283) and contains the following differences (written as ESA residue name, residue number, HSA residue name): Lys17Glu, His18Asn, Gly21Ala, Asp131Glu, Gly135Lys, and Glu158Lys. These differences, with the exception of Gly135Lys, involve the exchange of a hydrophilic residue for another hydrophilic residue (or hydrophobic for hydrophobic). Additionally, some of these changes result in the loss of hydrogen bonding capability or hydrophobic interactions, but other changes compensate for these effects (e.g., loss of H-bond in Glu158Lys, gain in Lys17Glu; loss of hydrophobic interactions in Lys17Glu, gain in Glu158Lys). However, despite these small changes in drug site 4, the residues involved in binding testosterone at the two binding sites exhibit no significant conformational differences when the ESA-testosterone complex is compared to structures of ligand-free ESA[68] (PDB ID: 3V08) and HSA[66] (PDB ID: 4K2C). Moreover, the hydrophobic character of the binding sites' environment in ESA and HSA is essentially the same (**Figure 3.30**). Therefore, the conservation of amino acid residues in drug sites 4 and 7, which leads to the essentially identical hydrophobic environments, suggests that testosterone may bind to HSA in the same sites as in ESA.

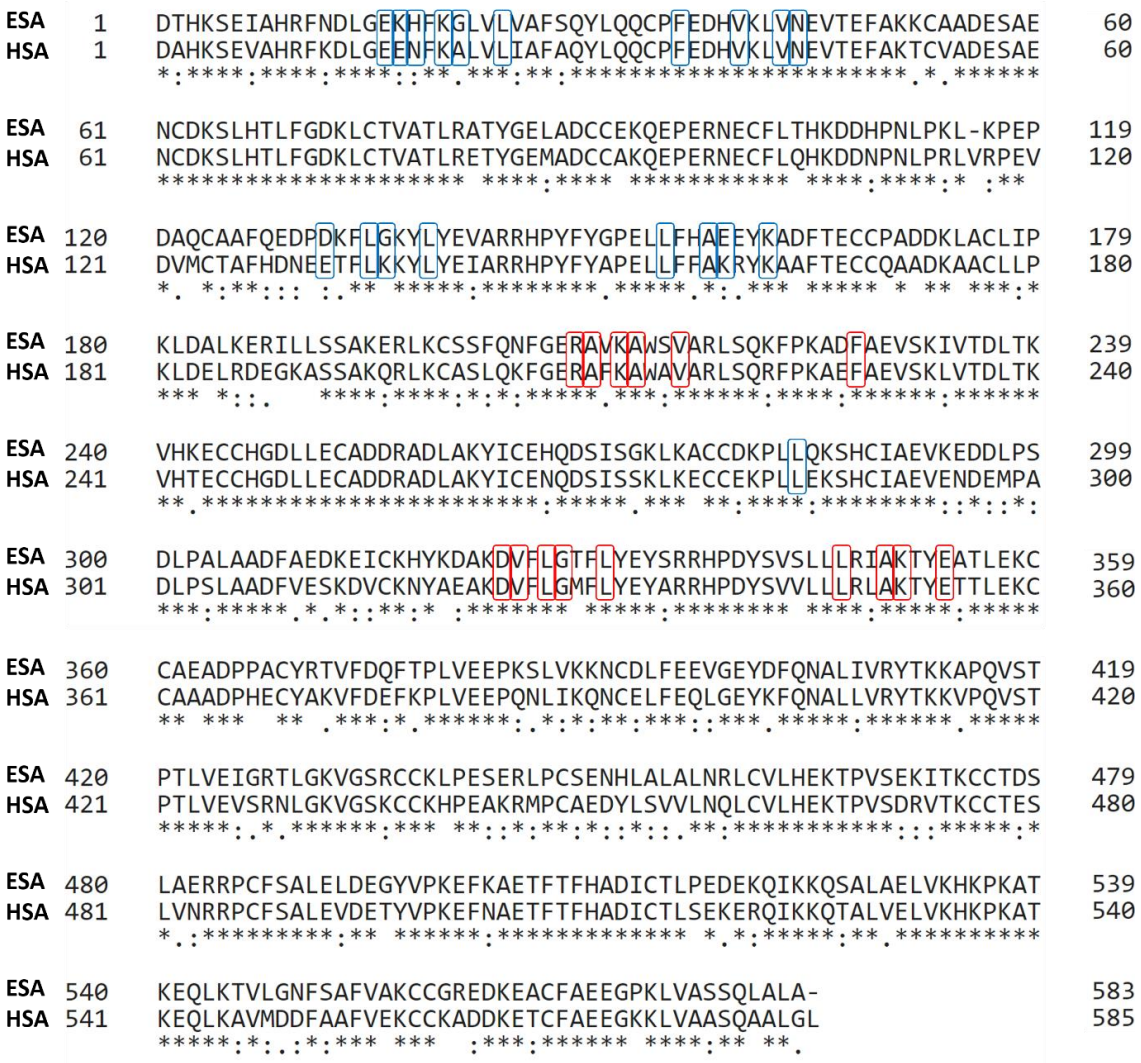

Figure 3.28. Alignment of ESA and HSA sequences. Residues involved in the binding of testosterone molecules in ESA (according to PISA server calculations) and analogous residues inferred for HSA are marked in red (drug site 7) and blue (drug site 4).

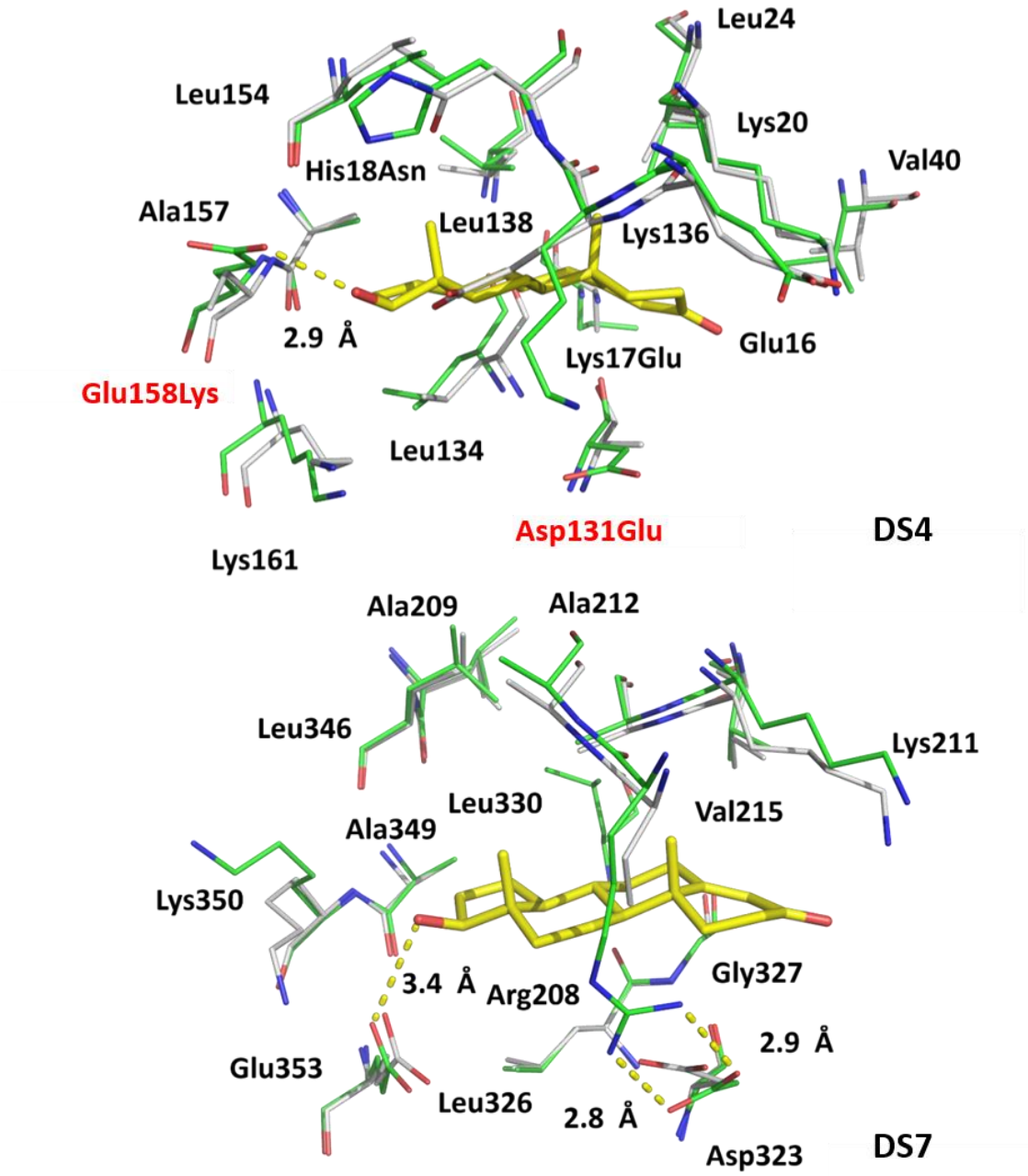

Figure 3.29. Superposition of testosterone binding sites in ESA (PDB ID: 6MDQ) and analogous sites in HSA (PDB ID: 4K2C). All residues are shown in stick representation. Carbon atoms in ESA and HSA are shown in green and gray, respectively, oxygen atoms are shown in red, nitrogen in blue; testosterone molecules are shown with carbon atoms

in yellow. Residue numbers correspond to positions in ESA; the naming scheme is as follows: residue from ESA, residue number, residue from HSA (if different).

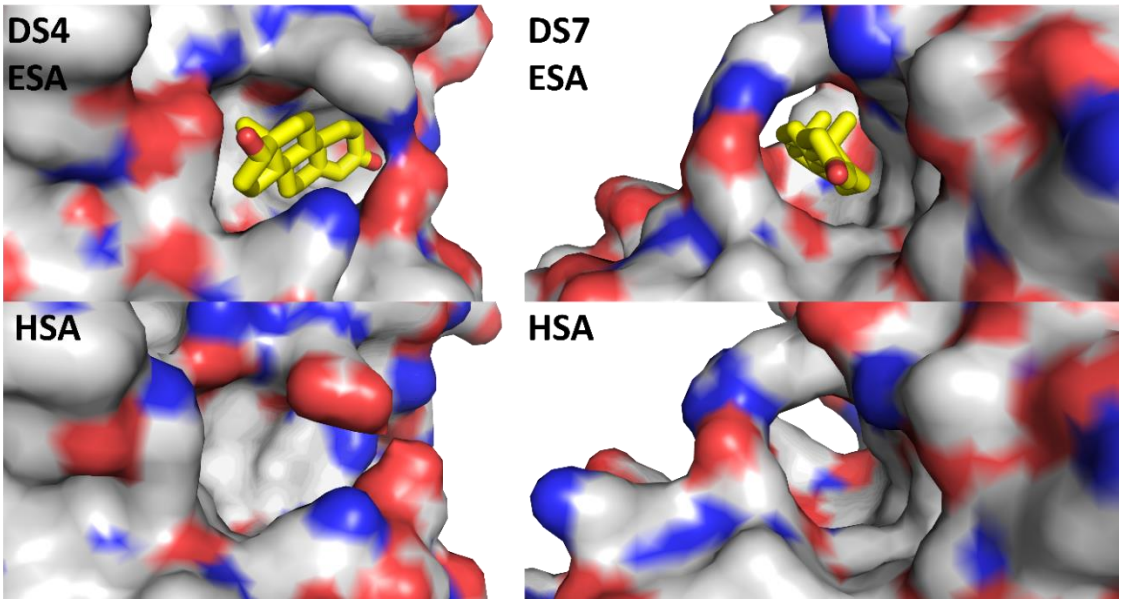

Figure 3.30. Comparison of the environment's character of drug site 4 (DS4) and drug site 7 (DS7) in ESA and HSA. The color of the protein surface indicates the character of the environment, and the color scheme is as follows: gray for carbon atoms in ESA and HSA, red for oxygen atoms, and blue for nitrogen atoms. Testosterone's carbon atoms are shown in yellow.

3.3. Binding of selected FDA-approved drugs by serum albumin

3.3.1. Structures of ESA complexes with various FDA-approved drugs

3.3.1.1. ESA complex with warfarin

In the crystal structure of the ESA-warfarin complex determined at 1.68 Å resolution (**Table 3.10**), well-defined electron density clearly indicates binding of (*R*)-warfarin to drug site 2 (**Figure 3.31**). The model is complete, except for the first two residues that were not located in the electron density map. One molecule of a fatty acid (modeled as octanoic acid; bound to FA4) and twenty residues are found within 5 Å from warfarin: Glu382, Pro383, Leu386, Val387, Asn390, Cys391, Phe402, Leu406, Arg409, Tyr410, Leu429, Val432, Gly433, Cys437, Leu445, Ser448, Glu449, Leu452, Arg484, Ser488. The molecule of (*R*)-warfarin is stabilized at this site mostly by hydrophobic interactions with surrounding residues but also forms two hydrogen bonds between its carbonyl group (O3 atom) and the hydroxyl group of Tyr410, and the carboxyl group of octanoic acid. The albumin structure also contains sugar molecules bound to drug site 1 and drug site 6. Thanks to the high resolution of the reported structure and well-ordered electron density observed for the sugar molecules, they were identified as glucose in the cyclic form (β-d-glucopyranose). Glucose bound to drug site 1 overlap with the location where warfarin was previously reported to bind to HSA ((*R*)-warfarin in PDB IDs: 1H9Z and 2BXD; (*S*)-warfarin in PDB ID: 1HA2; **Figure 3.32**). Sugars and fatty acids were not added to albumin during crystallization and are likely remnants of ESA purification from horse serum.

Drug site 2 is well conserved between ESA and HSA (see 3.1.2). Seventeen of the residues involved in the binding of (*R*)-warfarin in ESA are conserved in HSA, and three are different (Val387Ile, Leu445Met, and Ser448Ala). These modifications do not significantly change the character of the binding site. Drug site 2 remains unoccupied in one of the HSA-warfarin structures available in the PDB (PDB ID: 2BXD), while in the other two structures (PDB IDs: 1H9Z, 1HA2) is occupied by fatty acids that may prevent drug binding. Drug site 1, where warfarin binds to HSA, is also well conserved between ESA and HSA. Only three residues out of twenty involved in the binding of warfarin in HSA are different in ESA (conserved residues: Tyr150, Lys195, Lys199, Trp214, Arg218, Leu219, Phe223, Leu238, Val241, His242, Arg257, Leu260, Ala261, Ile264, Ile290, Ala291, Glu292; modified residues: Phe211Val, Ala215Ser, Arg222Lys). Two of these modifications involve exchanges of hydrophobic residue to another hydrophobic residue or hydrophilic to hydrophilic. In the HSA-warfarin complex, Arg222 forms a hydrogen bond with warfarin's carbonyl group (PDB ID: 2BXD), and Lys (Arg222Lys modification) likely would interact with warfarin in a similar manner. Ala215 contributes to hydrophobic interactions with warfarin, and its modification to Ser would decrease the hydrophobic character of the binding site but should not prevent drug binding. These observations suggest that warfarin likely can bind to both drug sites 1 and 2, depending on their availability.

Table 3.10. Data collection, structure refinement, and structure quality statistics for the ESA-warfarin structure. The crystallization of ESA was performed by undergraduate student Ethan Steen under my supervision. Values in parentheses are for the highest resolution shell. Ramachandran plot statistics are calculated by MolProbity.

PDB ID	-
Diffraction images DOI	-
Crystallization conditions	0.2 M lithium sulfate, 2.4 M ammonium sulfate, 0.1 M Tris buffer pH 7.4
SA source	ESA isolated from horse blood (Equitech-Bio #ESA62)
SA concentration	34 mg/mL
Additives	Warfarin was prepared as 100 mM solutions in pure DMSO and mixed with the protein in ratio 9:1 and incubated for several hours at 37 ^{o}C before the crystallization
Resolution (Å)	50.00-1.68 (1.71-1.68)
Beamline	21-ID-G
Wavelength (Å)	0.979
Space group	*P*61
Unit-cell dimensions: a, b, c (Å)	95.3, 95.3, 141.6
Angles: α, β, γ (^{o})	90.0, 90.0, 120.0
Protein chains in the ASU	1
Completeness (%)	100.0 (100.0)
Number of unique reflections	82531 (4100)
Redundancy	9.5 (9.3)
<I>/<σ(I)>	29.0 (1.2)
CC ½	(0.73)
R_{merge}	0.082 (2.307)
R_{work}/R_{free}	0.167 / 0.203
Bond lengths RMSD (Å)	0.006
Bond angles RMSD (°)	1.4
Mean B value (Å^2)	22
Mean B value for warfarin molecule (Å^2)	16.1
Number of protein atoms	4663
Mean B value for protein (Å^2)	32
Number of water molecules	695
Mean B value for water molecules (Å^2)	32
Clashscore	2.97
MolProbity score	1.14
Rotamer outliers (%)	0.98
Ramachandran outliers (%)	0.0
Ramachandran favored (%)	98.1

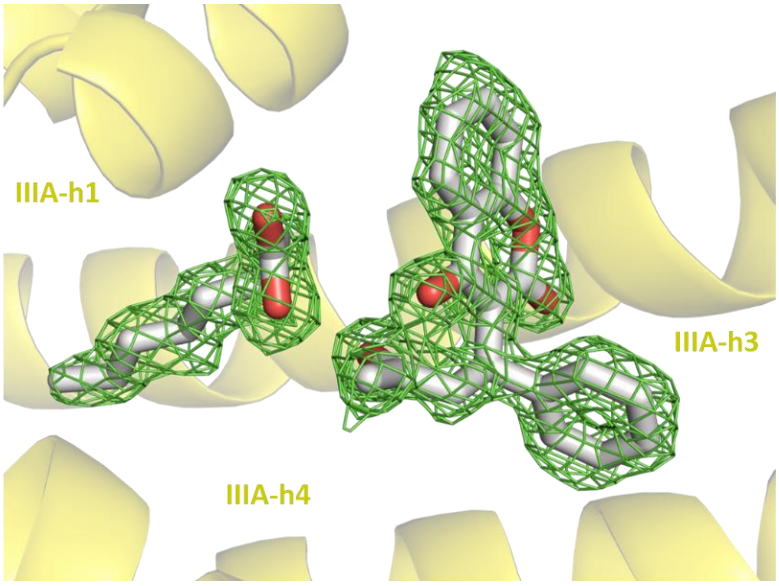

Figure 3.31. The electron density observed for (*R*)-warfarin and octanoic acid in drug site 2 is shown as green mesh (mFo−DFc map, calculated after ten refinement cycles without the ligand, RMSD 3.0). The warfarin and octanoic acid molecules are shown in stick representation with carbon atoms in gray and oxygen atoms in red. The electron density, including the omit maps, and the model can be inspected interactively at https://molstack.bioreproducibility.org/project/view/sCsITSQ5WCjvUjJEv2eP/.

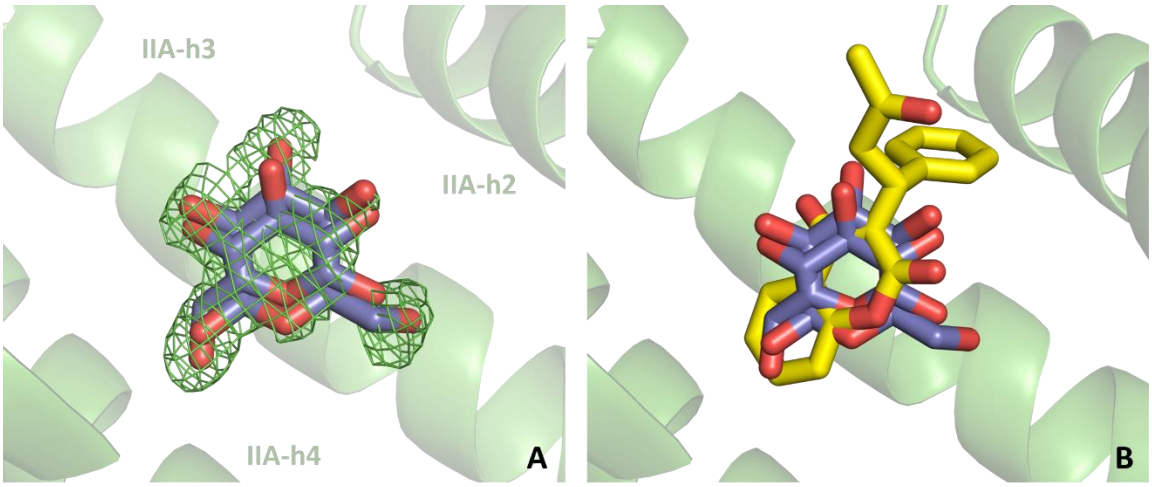

Figure 3.32. A) The electron density observed in the drug site 1 (mFo−DFc map, calculated after ten refinement cycles without the ligand, RMSD 3.0). A glucose molecule with two conformations (0.5 occupancies for each conformation) was modeled at this site. B) Superposition of the reported structure and HSA-warfarin complex (PDB ID: 2BXD). The glucose and warfarin molecules are shown in stick representation with oxygen atoms in red, and carbon atoms in violet (glucose) or yellow ((*R*)-warfarin).

3.3.1.2. ESA complex with tolbutamide

The structure of ESA-tolbutamide was determined at 2.02 Å resolution (**Table 3.11**) and revealed the binding of tolbutamide to drug sites 2, 4, 6, 9, and 10 (**Figure 3.33**). The positive regions of electron density also indicated binding of two sugar molecules to drug site 1 (location previously reported to bind glucose in HSA, see PDB ID: 4IW2). The model is complete except for the two first residues, which were not modeled due to the lack of electron density. ESA in the complex with tolbutamide has a fold almost identical to previously determined ESA structures.

Well-ordered electron density indicates tolbutamide binding to drug site 2 (**Figure 3.34**). At this site, tolbutamide is stabilized by three hydrogen bonds (with Ser488's hydroxyl group and side-chains of Asn390 and Arg409) and multiple hydrophobic interactions (e.g., its aromatic ring is placed between aromatic rings of Tyr410 and Phe487). Residues involved in tolbutamide binding are listed in **Table 3.12**. The tolbutamide molecule located in drug site 2 partially overlaps with the position of ketoprofen described in section 3.1.2 (PDB ID: 7JWN) and the position of ibuprofen described in section 3.1.1.5 (PDB ID: 6U4X). Drug site 2 is well conserved between ESA and HSA, and only two residues involved in tolbutamide binding in the reported structure are different in HSA (Ile425Val, Ser448Ala).

At drug site 4, tolbutamide's aromatic ring and aliphatic part are oriented to the hydrophobic cavity (hydrophobic interactions with Leu24, Phe36, Val40, Val43, aliphatic parts of Lys17 and Lys20) while its sulfonylurea group is exposed to the solvent. At this site, tolbutamide forms only one hydrogen bond with surrounding residues (with the amino group of Lys20; **Table 3.12**) and partially overlap with the position of ketoprofen and ibuprofen molecules described in sections 3.1.2 and 3.1.1.5, respectively (PDB IDs: 7JWN, 6U4X). Albumin sequence in this site is highly variable between ESA and HSA; different residues: Lys17Glu, Gly21Ala, Asp129Asn, Asp131Glu, Lys132Thr, Gly135Lys.

Tolbutamide molecule bound to drug site 6 is partially buried in the cavity (tolbutamide's aromatic ring is stabilized by hydrophobic interactions with Leu393, Ala405, and aliphatic parts of Lys540 and Lys544) and partially exposed to the solvent (tolbutamide's sulfonylurea group). Tolbutamide does not form any hydrogen bond at

this site, and its aliphatic part is placed on the protein surface, where is stabilized by hydrophobic interactions with aliphatic parts of Glu541, Lys 544, and Gln203. Gln203 is a part of another copy of albumin and interacts with tolbutamide (~4 Å distance) due to the crystal contacts. The electron density observed for the drug molecule at drug site 6 is weak (**Figure 3.34**); its binding to this site is likely possible only thanks to the crystal contacts and would not be observed in physiological conditions. Albumin typically occurs in monomeric form in solutions. Its dimerization in the blood is possible and has been observed in certain diseases; however, it was proved to be a result of a disulfide bridge formed between Cys34 from two albumin molecules rather than surface interactions.[235]

Binding of tolbutamide to drug site 9 is supported by well-ordered electron density (**Figure 3.34**). Drug site 9 has mixed character, and the tolbutamide molecule is stabilized by a hydrogen bond (between its carbonyl group and the side-chain guanidine group of Arg458's) and hydrophobic interactions (mainly with Leu190, Ile425, Val432, Leu459, and aliphatic part of Arg458; see **Table 3.12**). The tolbutamide molecule bound to drug site 9 partially overlaps with the position of the (*R*)-ketoprofen molecule described in section 3.1.2 (PDB ID: 7JWN). Nine of the residues involved in tolbutamide binding are conserved between ESA and HSA, and six are different (Leu190Ala, Ile425Val, Thr428Asn, His451Tyr, Leu454Val, Ala455Val).

Drug site 10 is one of the less common binding sites in albumin, previously reported to bind only ketoprofen (see 3.1.1.4) and halothane.[228] At this site, tolbutamide forms one hydrogen bond between its sulfonyl group and the carboxylate group of Glu251. Tolbutamide's aromatic ring is placed in the hydrophobic cavity formed by Ile 7,

Phe19, Phe27, Val46, Leu66, Leu69, Phe70, and Leu250, while its aliphatic part is stabilized by hydrophobic interactions with Tyr30, Phe70, Phe102, and Leu103. Residues involved in tolbutamide binding in ESA are well conserved in HSA; only one residue is different (Ile7Val).

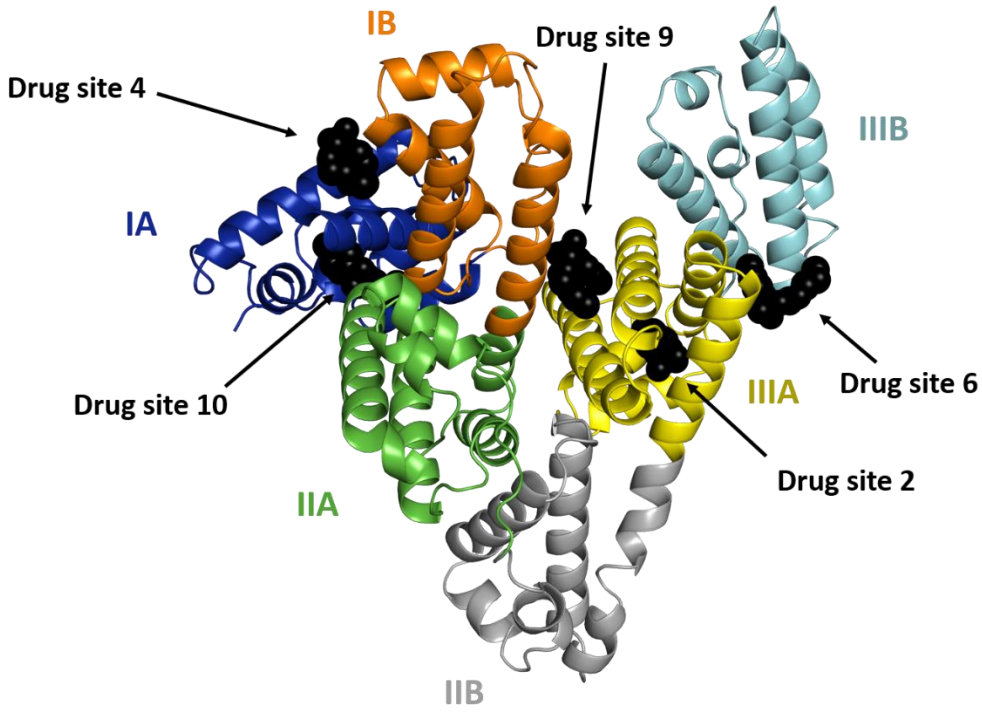

Figure 3.33. The overall structure of the ESA complex with tolbutamide. Albumin subdomains are shown each in a different color. Roman numerals (I, II, III) are associated with domains and letters (e. g., IB) with subdomains. Tolbutamide molecules are shown with atoms in black spheres.

Table 3.11. Data collection, structure refinement, and structure quality statistics for the ESA-tolbutamide structure. Values in parentheses are for the highest resolution shell. Ramachandran plot statistics are calculated by MolProbity. Crystallization of albumin and X-ray data collection were performed by Dr. Katarzyna Handing. DS2, DS4, DS6, DS9, and DS10 refer to drug-binding sites 2, 4, 6, 9, and 10.

PDB ID	-
Diffraction images DOI	-
Crystallization conditions	0.2 M lithium sulfate, 1.8-2.4 M ammonium sulfate, 0.1 M Tris buffer pH 7.4
SA source	ESA isolated from horse blood (Equitech-Bio #ESA62)
SA concentration	34 mg/mL
Additives	Tolbutamide was prepared as 100 mM solution in pure DMSO and added to crystallization drops containing ESA crystals to reach a final drug concentration of 10 mM
Resolution (Å)	50.00-2.02 (2.05-2.02)
Beamline	23-ID-D
Wavelength (Å)	0.979
Space group	*P*61
Unit-cell dimensions: a, b, c (Å)	95.0, 95.0, 141.7
Angles: α, β, γ (°)	90.0, 90.0, 120.0
Protein chains in the ASU	1
Completeness (%)	98.8 (84.7)
Number of unique reflections	46904 (2003)
Redundancy	6.6 (3.9)
<I>/<σ(I)>	18.4 (1.1)
CC ½	(0.55)
R_{merge}	0.102 (1.120)
R_{work}/R_{free}	0.190 / 0.233
Bond lengths RMSD (Å)	0.003
Bond angles RMSD (°)	1.2
Mean B value (Å²)	33
Mean B value for tolbutamide molecules (Å²)	53.1 (DS2), 72.0 (DS4), 55.5 (DS6), 61.5 (DS9), 47.8 (DS10)
Number of protein atoms	4566
Mean B value for protein (Å²)	35
Number of water molecules	240
Mean B value for water molecules (Å²)	37
Clashscore	1.64
MolProbity score	0.91
Rotamer outliers (%)	0.20
Ramachandran outliers (%)	0.0
Ramachandran favored (%)	98.27

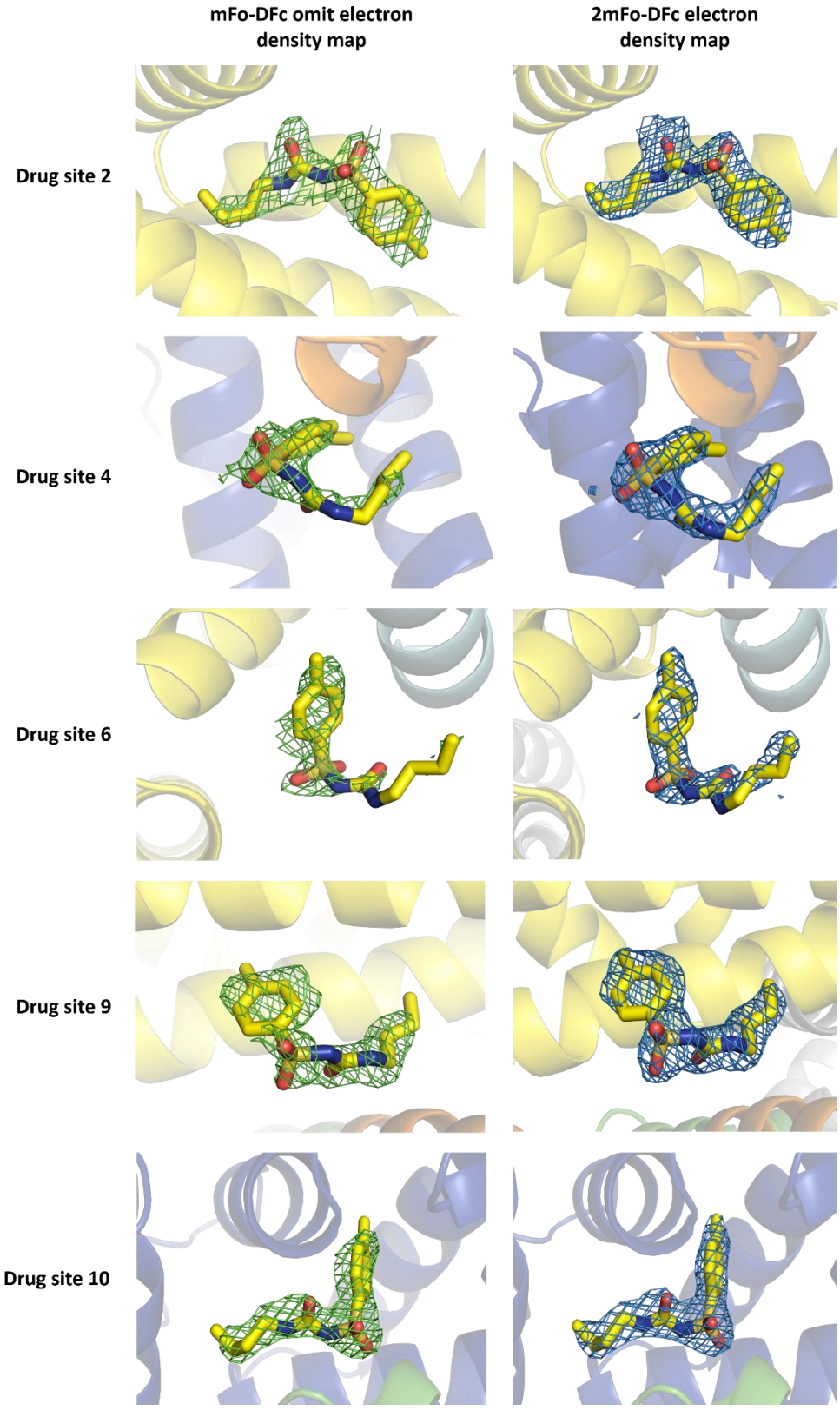
mFo-DFc omit electron density map
2mFo-DFc electron density map
Drug site 2
Drug site 4
Drug site 6
Drug site 9
Drug site 10

Figure 3.34. Tolbutamide binding sites in human serum albumin with mFo–DFc omit electron density map (map calculated after 10 refinement cycles without a drug, RMSD 2.5) presented in green and 2mFo–DFc electron density map (RMSD 1.0) presented in blue. Tolbutamide molecules are shown in stick representation with oxygen atoms in red, carbon atoms in yellow, sulfur atom in gold, and nitrogen atoms in blue. The electron density can be inspected interactively at https://molstack.bioreproducibility.org/project/view/pMu54I0XvMbx4hqG4Pcl/.

Table 3.12. The residues that participate in binding of tolbutamide to ESA and hydrophilic interactions observed in tolbutamide binding sites.

Drug site	Subdomains	Residues	Salt bridges and hydrogen bonds
2	IIIA	Phe402, Leu,406 Arg409, Tyr410, Lys413, Ile425, Leu429, Val432, Gly433, Cys437, Ser448, Leu452, Leu456, Leu459, Arg484, Phe487, Ser488,	Tolbutamide's sulfonyl group forms a hydrogen bond with Ser488's hydroxyl group; Tolbutamide's carbonyl group forms hydrogen bonds with Asn390's side-chain nitrogen atom (ND2) and Arg409's side-chain (NH2)
4	IA and IB	Lys17, Lys20, Gly21, Leu24, Phe36, Val40, Val43, Asn44, Asp129, Asp131, Lys132, Gly135, Leu138	Tolbutamide's carbonyl group forms a hydrogen bond with the amino group of Lys20 (NZ)
6	IIIA and IIIB	Leu393, Val397, Asp401, Asn404, Ala405, Val408, Lys540, Glu541, Gln542, Lys544, Thr545	-
9	IB and IIIA	Leu189, Leu190, Ala193, Thr421, Glu424, Ile425, Thr428, Leu429, Val432, His451, Leu454, Ala455, Arg458, Leu459, Leu462	Tolbutamide's carbonyl group forms a hydrogen bond with the side-chain guanidine group of Arg458's (NE)
10	IA	Ile7, Leu22, Val23, Ala26, Phe27, Tyr30, Val46, Leu66, His67, Leu69, Phe70, Asn99, Phe102, Leu103, His246, Gly247, Asp248, Leu249, Leu250, Glu251	Tolbutamide's sulfonyl group forms a hydrogen bond with the carboxylate group of Glu251 (OE1 atom)

3.3.1.3. ESA complex with haloperidol

The crystal structure of the ESA-haloperidol complex was determined at 2.05 Å resolution (**Table 3.13**). The model is complete, except for the first two residues that were not located in the electron density map. In the reported structure, well-defined electron density indicates the binding of haloperidol to drug site 2 (**Figure 3.35**). The drug molecule at this site is stabilized mostly by the hydrophobic interactions and forms one hydrogen bond between its hydroxyl group and the carbonyl group of Ser488 (mainchain). A part of the haloperidol molecule containing the fluorophenyl group is buried in the hydrophobic cavity (formed primarily by Leu386, Val387, Cys391, Phe402, Leu406, Val432, Cys436, Cys437, Leu452). The other part of haloperidol, containing the chlorophenyl group, is oriented towards the solvent (**Figure 3.36**). Haloperidol bound to this site partially overlaps with locations previously reported to bind warfarin and ibuprofen (**Figure 3.37**).

Twenty out of twenty-three residues found within 5 Å from haloperidol are conserved between ESA and HSA (conserved residues: Leu386, Asn390, Cys391, Phe402, Leu406, Arg409, Tyr410, Lys413, Leu429, Val432, Gly433, Cys436, Cys437, Leu452, Phe487, Ser488, Ala489, Leu490, Glu491, Lys540; different residues: Val387Ile, Lys389Gln, Ser448Ala). These changes in the sequence should not significantly affect the binding of haloperidol.

The structure also contains two unknown ligands bound to drug site 1. These are likely sugar molecules, based on the shape of the observed density and its location, which is known to bind sugars in HSA (see PDB ID: 4IW2). However, sugars were not added to

the protein during crystallization and most likely are remnants of albumin isolation from horse blood. Positive electron density was also observed in drug site 6 but could not be unambiguously interpreted and was accounted for by three UNX atoms.

Table 3.13. Data collection, structure refinement, and structure quality statistics for the ESA-haloperidol structure. Values in parentheses are for the highest resolution shell. Ramachandran plot statistics are calculated by MolProbity.

PDB ID	-
Diffraction images DOI	-
Crystallization conditions	0.2 M lithium sulfate, 2.1 M ammonium sulfate, 0.1 M Tris buffer pH 7.4
SA source	ESA isolated from horse blood (Equitech-Bio #ESA62)
SA concentration	34 mg/mL
Additives	Haloperidol powder was added directly to the crystallization drop containing crystals for 48 h before harvesting
Resolution (Å)	50.00-2.05 (2.09-2.05)
Beamline	19-ID
Wavelength (Å)	0.979
Space group	*P*61
Unit-cell dimensions: a, b, c (Å)	93.0, 93.0, 140.8
Angles: α, β, γ (°)	90.0, 90.0, 120.0
Protein chains in the ASU	1
Completeness (%)	99.8 (100.0)
Number of unique reflections	43996 (2196)
Redundancy	6.8 (5.8)
$\langle I \rangle / \langle \sigma(I) \rangle$	24.4 (1.6)
CC ½	(0.69)
R_{merge}	0.085 (1.724)
R_{work}/R_{free}	0.186 / 0.223
Bond lengths RMSD (Å)	0.002
Bond angles RMSD (°)	1.2
Mean B value (Å²)	37
Mean B value for haloperidol (Å²)	65.4
Number of protein atoms	4538
Mean B value for protein (Å²)	36
Number of water molecules	315
Mean B value for water molecules (Å²)	38
Clashscore	2.55
MolProbity score	1.23
Rotamer outliers (%)	0.41
Ramachandran outliers (%)	0.0
Ramachandran favored (%)	96.89

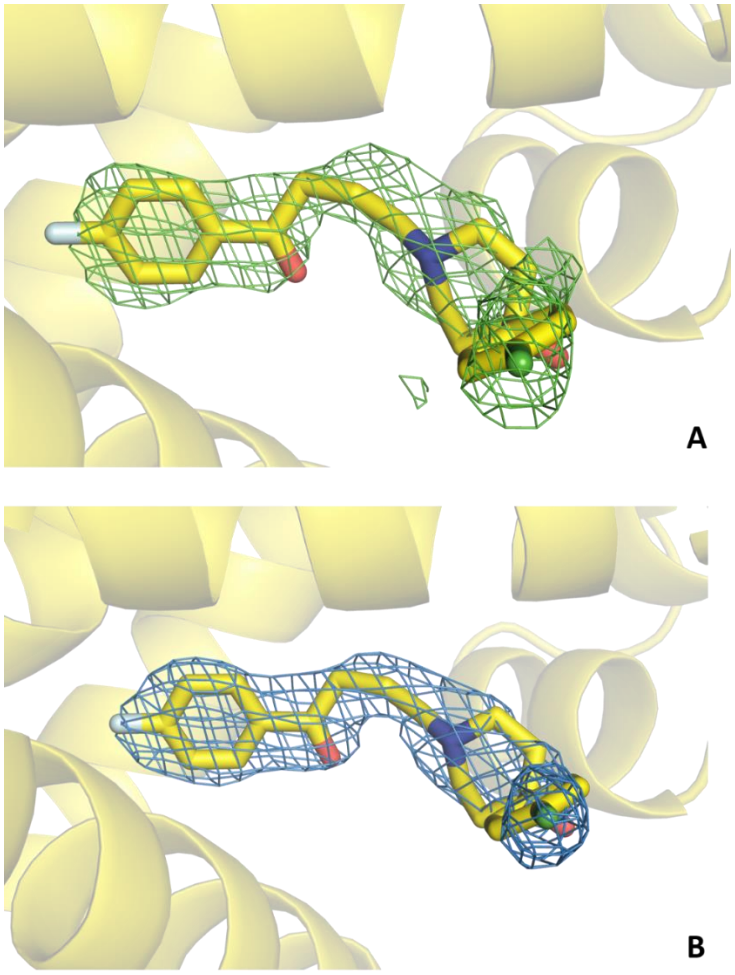

Figure 3.35. The electron density observed for haloperidol acid in drug site 2. Haloperidol molecule is shown in stick representation with carbon atoms in yellow, oxygen atoms in red, nitrogen atom in blue, chloride atom in green, and fluoride atom in gray. A) mFo−DFc omit electron density map calculated after ten refinement cycles without the ligand, RMSD 2.5. B) 2mFo−DFc electron density map, RMSD 1.0. The electron density, including the omit maps, and the model can be inspected interactively at https://molstack.bioreproducibility.org/project/view/qJGsEm9HgtaGYaoG0gsG/.

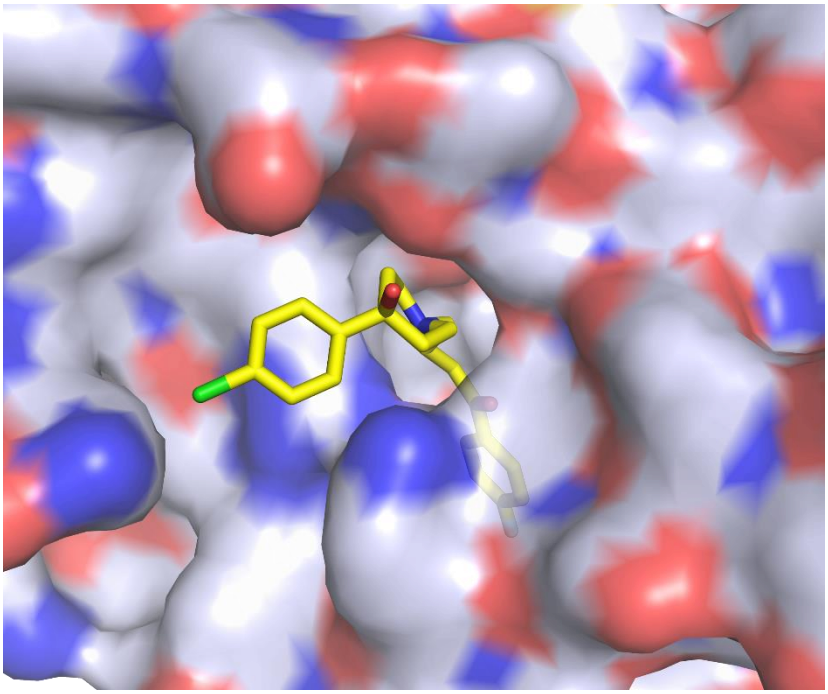

Figure 3.36. Haloperidol is partially buried in the hydrophobic cavity. Haloperidol molecule is shown in stick representation with carbon atoms in yellow, oxygen atoms in red, nitrogen atom in blue, chloride atom in green, and fluoride atom in gray. The color scheme for the protein surface is as follows: gray for the contribution from carbon atoms, red for oxygen atoms, and blue for nitrogen atoms.

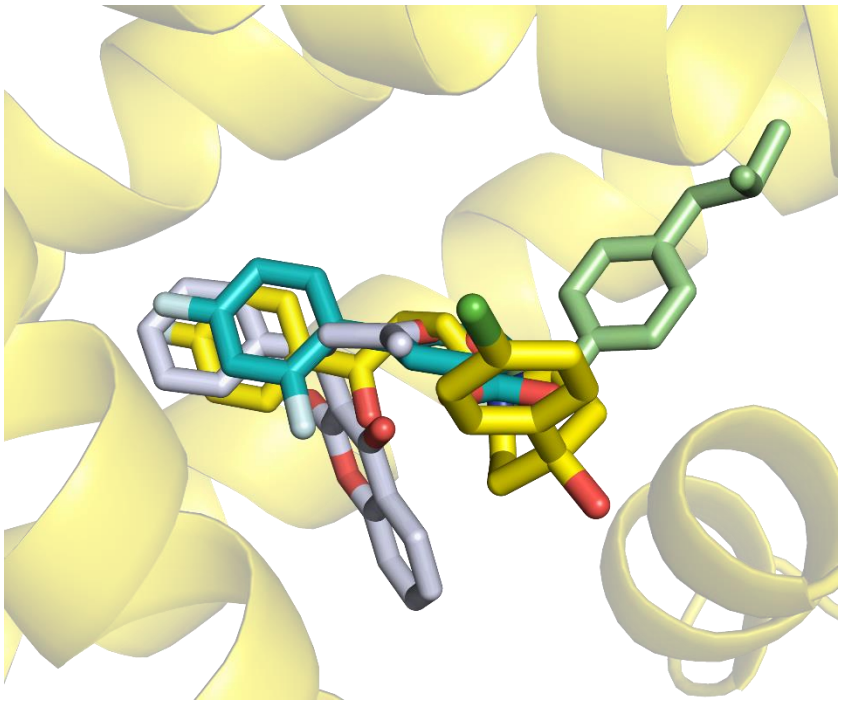

Figure 3.37. Superposition of SA complexes with haloperidol (carbon atoms shown in yellow), warfarin (see 3.3.1.1; gray), ibuprofen (see 3.1.1.5; PDB ID: 6U4X; green), and diflunisal (PDB ID: 2BXE; cyan). Oxygen atoms are shown in red, fluorine atoms in white, and chloride atom in green.

3.3.1.4. ESA complex with ampicillin

The structure of the ESA-ampicillin complex was determined at 2.80 Å resolution in $P6_1$ space group and contained one protein copy in the asymmetric unit (**Table 3.14**). The reported structure revealed ampicillin binding to drug site 3 and 7 (**Figure 3.38**) and contains two unknown ligands (UNL) bound to drug site 9 that could not be unambiguously identified. The protein model is complete, except for the first two residues that were not located in the electron density map.

The ampicillin molecule bound to drug site 3 forms hydrogen bonds between its carboxylate group and His145's side-chain nitrogen atom (NE2 atom), between its carbonyl group and Leu115's mainchain nitrogen atom, and between its nitrogen atoms (N1 and N2) and Leu115's mainchain carbonyl group. Ampicillin's phenyl group is stabilized by hydrophobic interactions with Pro117, Ile178, Leu181, and the aliphatic part of Lys185. Fifteen residues are found within the 5 Å from ampicillin molecule: Pro113, Lys114, Leu115, Lys116, Pro117, Glu140, Val141, Arg144, His145, Ile178, Leu181, Asp182, Lys185, Ile188, Leu189. This region is highly variable between ESA and HSA, and eight residues involved in the binding of ampicillin in ESA are different in HSA: Pro113Arg, Lys114Leu, Leu115Val, Lys116Arg, Val141Ile, Lys185Arg, Ile188Gly, Leu189Lys.

At drug site 7, the ampicillin molecule forms hydrogen bonds between its carboxylate group and the hydroxyl group of Ser479, and with mainchain nitrogen atoms of Leu480 and Ala481. Ampicillin's carbonyl and amino groups are oriented to the solvent, while its hydrophobic parts are oriented to the cavity and interact with Leu346, Ala349, Ala481, and aliphatic parts of Lys350. The carbonyl group being a part of ampicillin's β-lactam ring is out of density and has a very high B-factor value, which may suggest that the β-lactam ring is open as a result of the antibiotic degradation. Ampicillin is not very stable in solutions as water is able to hydrolyze the β-lactam ring.[236] Thirteen residues are located within 5 Å from ampicillin molecule bound to drug site 7: Phe205, Arg208, Ala209, Ala212, Leu346, Ala349, Lys350, Glu353, Asp478, Ser479, Leu480, Ala481, Glu482. Three of them are not conserved between ESA and HSA: Asp478Glu, Ala481Val, Glu482Asn.

Table 3.14. Data collection, structure refinement, and structure quality statistics for the ESA-ampicillin structure. Values in parentheses are for the highest resolution shell. Ramachandran plot statistics are calculated by MolProbity.

PDB ID	-
Diffraction images DOI	-
Crystallization conditions	0.2 M lithium sulfate, 1.9 M ammonium sulfate, 0.1 M Tris buffer pH 7.4
SA source	ESA isolated from horse blood (Equitech-Bio #ESA62)
SA concentration	34 mg/mL
Additives	Ampicillin was dissolved in 50 mM Tris pH 7.4 and added to ESA crystals (final concentration 5 mM) several hours before harvesting
Resolution (Å)	50.00-2.80 (2.85-2.80)
Beamline	19-ID
Wavelength (Å)	0.979
Space group	*P*61
Unit-cell dimensions: a, b, c (Å)	93.9, 93.9, 142.2
Angles: α, β, γ (°)	90.0, 90.0, 120.0
Protein chains in the ASU	1
Completeness (%)	99.3 (99.3)
Number of unique reflections	17653 (909)
Redundancy	8.2 (8.3)
<I>/<σ(I)>	13.8 (1.7)
CC ½	(0.52)
R_{merge}	0.176 (2.624)
R_{work}/R_{free}	0.199 / 0.240
Bond lengths RMSD (Å)	0.002
Bond angles RMSD (°)	1.2
Mean B value (Å²)	55
Mean B value for ampicillin (Å²)	95.0 (DS3); 72.8 (DS7)
Number of protein atoms	4507
Mean B value for protein (Å²)	55
Number of water molecules	65
Mean B value for water molecules (Å²)	36
Clashscore	1.56
MolProbity score	0.99
Rotamer outliers (%)	0.83
Ramachandran outliers (%)	0.0
Ramachandran favored (%)	97.58

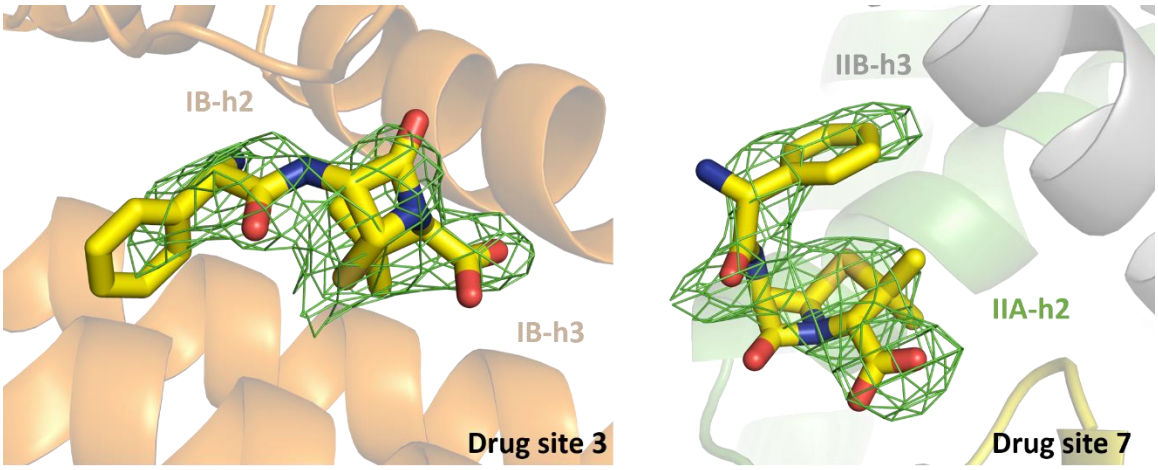

Figure 3.38. Ampicillin binding sites with an omit electron density map (mFo–DFc map, calculated after 10 refinement cycles without the ligand, RMSD 2.5) presented in green. The electron density can be inspected interactively at https://molstack.bioreproducibility.org/project/view/lsExEEAiWA9oQypphHvt/.

3.4. Binding of drug-candidates by serum albumin

3.4.1. Structure of HSA complex with JMS-053

In the crystal structure of the HSA-JMS-053 (resolution 2.20 Å), the electron density indicates binding of JMS-053 to drug site 3. To obtain this structure, HSA was co-crystallized with myristic acid, and the crystals were then soaked with JMS-053. Albumin crystals grew in the *P*1 space group and contained two HSA molecules in the asymmetric unit (**Table 3.15**), which were nearly identical. JMS-053 bound in both copies of the protein chain to drug site 3, which is located in subdomain IB (**Figure 3.39**). The electron density for JMS-053 at drug site 3 was observed in several structures determined from data collected for different albumin crystals soaked with the compound. The highest resolution data was selected for further consideration and PDB deposition. In the structures collected for albumin crystals obtained from the same crystallization condition but not soaked with JMS-053, the analogous position in drug site 3 remains unoccupied. The phenyl and thiophene portions of JMS-053 are well ordered in the reported structure (**Figure 3.39** and **Figure 3.40**) and stabilized by hydrophobic interactions with the following residues: Ile142, Phe149, Leu154, Phe157, Tyr161, and aliphatic parts of Arg186 and Lys190 side-chains. The pyridinedione moiety is oriented toward the solvent and appears to be less ordered and more flexible. Its carbonyl groups are engaged in hydrogen bonding with the side-chain nitrogen atoms of His146 and Lys190. Drug site 3 is known to be a fatty acid binding site. An elongated fragment of electron density observed in the vicinity of drug site 3 suggested the possible binding of a fatty acid close to the position

of JMS-053. However, the molecule of myristic acid modeled at this site clashes with the JMS-053 in chain A but not in chain B. To further explore other possibilities, the possibility of binding of a polyethylene glycol (PEG) molecule at this location (25% PEG 3350 was also in the crystallization cocktail) was examined. The PEG molecule modeled at this site does not cause clashes with the JMS-053 molecule, but based on the electron density alone, it is impossible to distinguish between fatty acid and PEG molecules. To avoid any misinterpretation, a PEG molecule was modeled in this location and labeled as an unknown ligand (UNL). Most of the crystallization conditions for HSA, including described in this study, contain highly concentrated PEGs that may affect proper identification of bound fatty acids. Nevertheless, in the determined structure, I modeled myristic and caprylic acids in several locations previously reported to bind fatty acids, such as FA2, FA3, FA4, FA5, and FA6.[96,237] The determined structure has essentially identical fold to the structure of HSA complexed with myristic acid (**Table 3.16**, **Figure 3.41**)

Table 3.15. Data collection, structure refinement, and structure quality statistics for the HSA-JMS-053 structure. Values in parentheses are for the highest resolution shell. Ramachandran plot statistics are calculated by MolProbity.

PDB ID	6WUW
Diffraction images DOI	10.18430/m3.irrmc.5549
Crystallization conditions	50 mM potassium phosphate buffer pH 7.0, 24-28% PEG 3350
SA source	HSA isolated from human blood (Sigma-Aldrich #A8763)
SA concentration	100 mg/mL
Additives	HSA was cocrystallized with 5 mM myristic acid (dissolved in 100% ethanol). JMS-053 powder was added to the crystallization drop containing crystals, which was then incubated for 48 h before harvesting
Resolution (Å)	50.00-2.20 (2.24-2.20)
Beamline	19-ID
Wavelength (Å)	0.979
Space group	*P*1
Unit-cell dimensions: a, b, c (Å)	38.4, 93.4, 94.9
Angles: α, β, γ (°)	74.6, 89.6, 80.4
Protein chains in the ASU	2
Completeness (%)	92.9 (91.0)
Number of unique reflections	59720 (2981)
Redundancy	2.6 (2.5)
<I>/<σ(I)>	18.5 (1.7)
CC ½	(0.61)
R_{merge}	0.051 (0.678)
R_{work}/R_{free}	0.192/0.247
Bond lengths RMSD (Å)	0.003
Bond angles RMSD (°)	1.1
Mean B value (Å²)	44
Mean B value for JMS-053 (Å²)	67
Number of protein atoms	9296
Mean B value for protein (Å²)	44
Number of water molecules	433
Mean B value for water molecules (Å²)	38
Clashscore	2.63
MolProbity score	1.05
Rotamer outliers (%)	0.88
Ramachandran outliers (%)	0.00
Ramachandran favored (%)	98.1

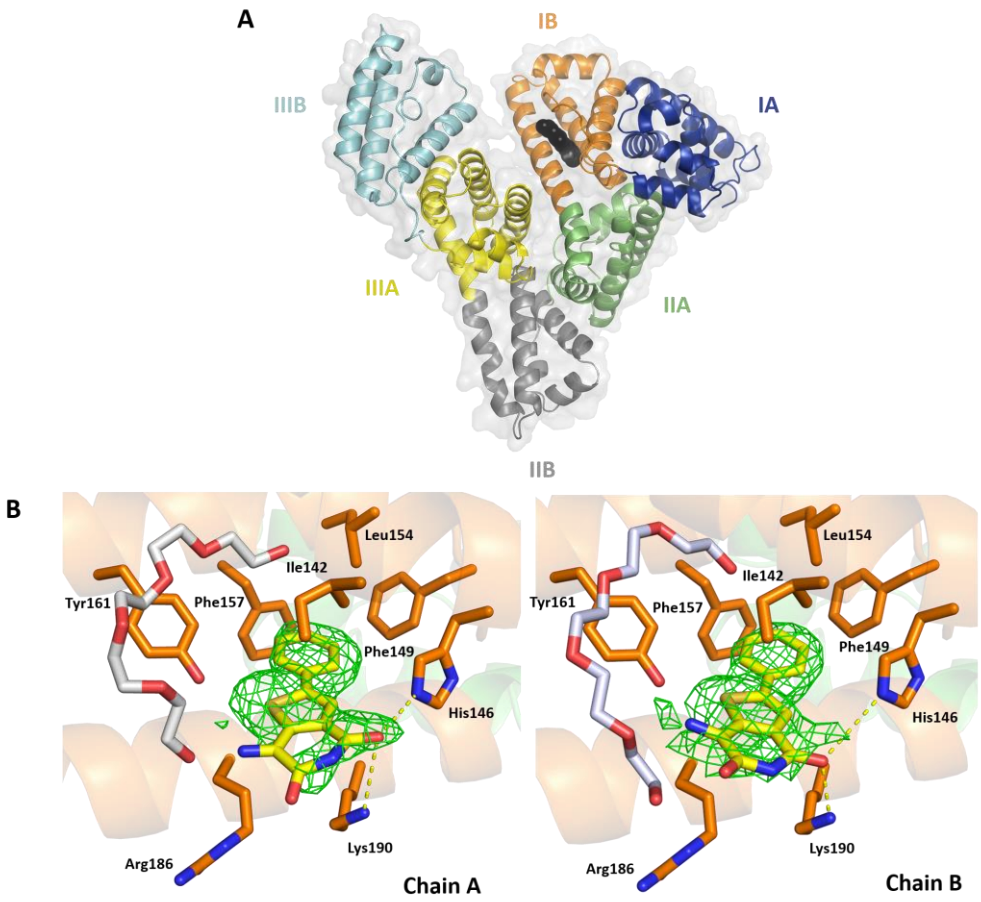

Figure 3.39. HSA domains and JMS-053 binding site. A) Domains are labeled with Roman numerals and subdomains with letters. Each subdomain is shown in a different color; JMS-053 at drug site 3 is shown with atoms as black spheres. B) JMS-053 binding site with omit electron density map (mFo–DFc map, calculated after 10 refinement cycles without the ligand, RMSD 2.5). Oxygen atoms are shown in red, nitrogen in blue, sulfur in gold; carbon atoms of JMS-053 are shown in yellow, PEG in gray and protein residues in orange. Gly189 is not shown. The electron density can be inspected interactively and in detail at the Molstack platform: https://molstack.bioreproducibility.org/project/view/gpt44gh1A2dDZOKWUqer/.

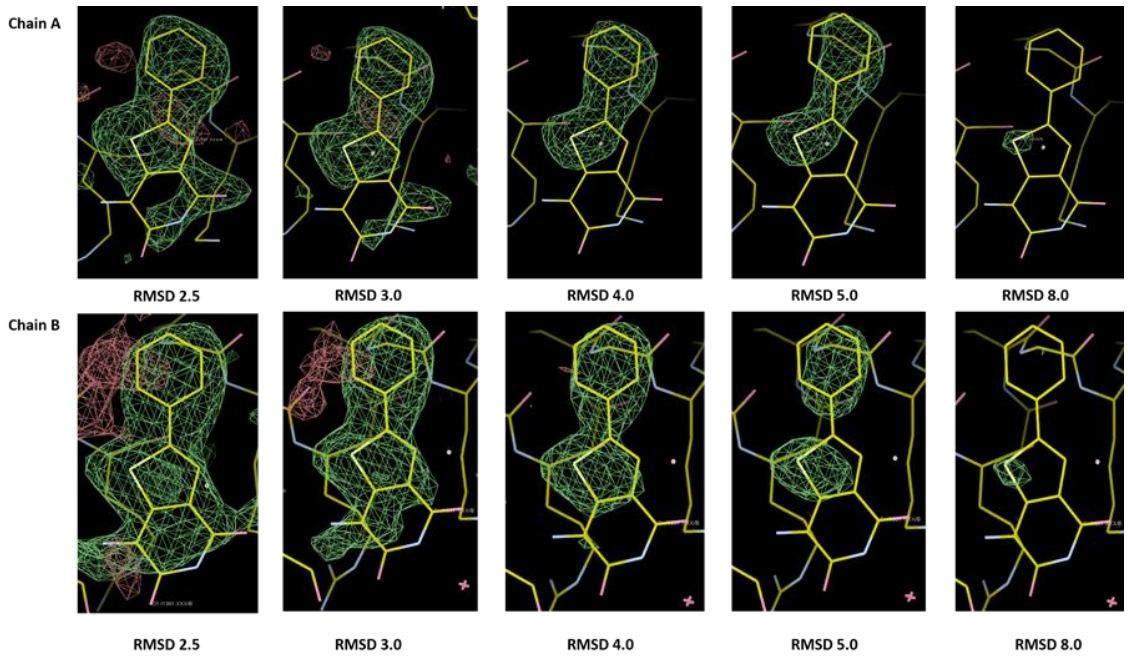

Figure 3.40. The omit electron density map (mFo−DFc map, calculated after 10 refinement cycles without JMS-053) at different contour levels. The strongest peak is observed for the sulfur atom (sulfur has more electrons than carbon, nitrogen, and oxygen) being a part of JMS-053.

Table 3.16. RMSD values [Å] between the aligned Cα atoms of the HSA complex with JMS-053, HSA complex with myristic acid, and ligand free HSA.

	HSA-JMS053 (PDB ID: 6WUW)	**HSA-myristic acid (PDB ID: 1BJ5)**	**HSA ligand-free (PDB ID: 4K2C)**
HSA-JMS053 (PDB ID: 6WUW)	-	0.7	4.1
HSA-myristic acid (PDB ID: 1BJ5)	0.7	-	4.2
HSA-ligand-free (PDB ID: 4K2C)	4.1	4.2	-

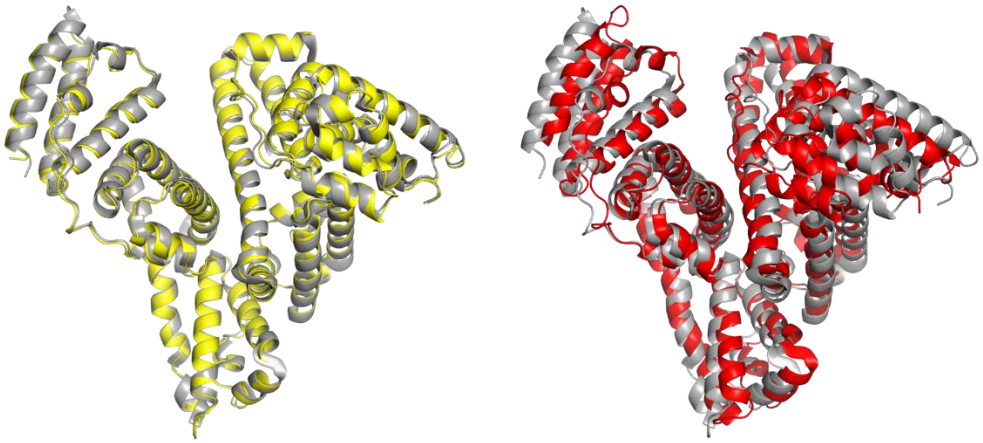

Figure 3.41. Superposition of the structure of HSA complex with JMS-053 determined in this study (cartoons are shown in grey, PDB ID: 6WUW) with structures of HSA complex with myristic acid (yellow, PDB ID: 1BJ5) and ligand free HSA (red, PDB ID: 4K2C).

JMS-053 binds to a hydrophobic groove on HSA formed by α-helices h7, h8, and h9 and an extended polypeptide domain, which is one of the most common drug-binding sites on HSA. The JMS-053 binding site is located in a region of albumin that varies among different species. Nonetheless, the three residues that create a hydrophobic hot spot at this site are conserved among HSA and albumin from two commonly used model organisms, BSA and MSA (murine serum albumin): Phe149, Leu154, and Tyr161. Moreover, His146, which interacts with JMS-053's carbonyl group, is also conserved (**Figure 3.39**, **Figure 3.42**). The four other contact residues retain the same amino acid characteristics: Ile142 is retained in BSA and modified to Val in MSA; Phe157 is replaced by Tyr in both MSA and BSA; and Arg186 is retained in BSA and exchanged for Lys in MSA (Arg186 contributes only to hydrophobic interactions with JMS-053). The exchange of Lys190 to Leu, which is observed in BSA and MSA, could potentially be a significant

change; however, it contributes mostly to hydrophobic interactions like Arg186. Thus, the observations with HSA will likely be applicable to model organisms (BSA and MSA) and may explain the prolonged in vivo half-life of JMS-053 observed in mice and differences in JMS-053 activity between *in vitro* experiments and experiments on cells, where FBS was present.[186]

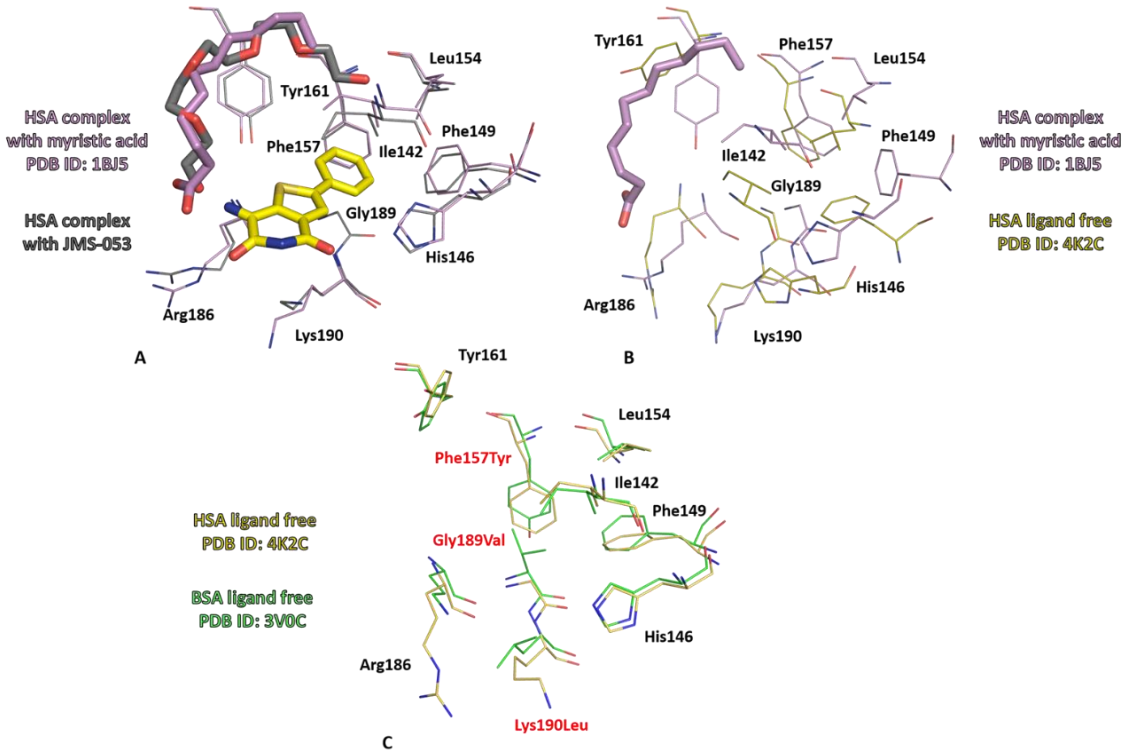

Figure 3.42. A) Superposition of crystal structures of HSA complexes with JMS-053 and with myristic acid (PDB ID: 1BJ5). Binding of JMS-053 to drug site 3 does not alter albumin's structure. B) Superposition of HSA complex with myristic acid (PDB ID: 1BJ5) and HSA ligand free (PDB ID: 4K2C). C) Superposition of crystal structures of ligand-free HSA (PDB ID: 4K2C) and BSA (PDB ID: 3V0C). Molecules of JMS-053, myristic acid, and PEG are shown in stick representation.

3.4.2. Structure of ESA complex with GHK(Cu)

The structure of the ESA complex with GHK(Cu) was determined at 2.85 Å resolution (**Table 3.17**) and revealed binding of GHK(Cu) complex to the albumin's surface, near His105 (subdomain IA, α-helix h6; see **Figure 3.43**). The protein model is complete, except for the two first residues that were not located in the electron density map. The structure also contains a copper ion bound between Asp311 and His317, and another copper ion interacting with His246. The binding of copper ions was indicated by a strong anomalous signal.

In the reported structure, GHK peptide primarily interacts with the Cu^{II} ion. The copper ion is penta-coordinated in a distorted square-planar pyramid, which agrees with the geometry observed in the previously determined crystal structure of the GHK(Cu) complex.[238] The Cu^{II} ion interacts with four nitrogen atoms (one from the protein: His105's side-chain nitrogen atom; three from the peptide: His's side-chain and mainchain nitrogen atoms and Gly's nitrogen atom) in equatorial positions and with an oxygen atom from a water molecule in the apical position (**Figure 3.43**). The amino group of peptide's lysine forms a hydrogen bond with the water molecule involved in the binding of the copper ion. The GHK(Cu) was modeled with 0.8 occupancy.

Table 3.17. Data collection, structure refinement, and structure quality statistics for the ESA-GHK(Cu) structure. Values in parentheses are for the highest resolution shell. Ramachandran plot statistics are calculated by MolProbity.

PDB ID	-
Diffraction images DOI	-
Crystallization conditions	0.2 M lithium sulfate, 2.2 M ammonium sulfate, 0.1 M Tris buffer pH 7.4
SA source	ESA isolated from horse blood (Equitech-Bio #ESA62)
SA concentration	34 mg/mL
Additives	GHK peptide was dissolved in 50 mM Tris (5 mM ligand concentration), mixed with 2 molar excess of copper ions and incubated with ESA for several hours prior to crystallization
Resolution (Å)	50.00-2.85 (2.90-2.85)
Beamline	19-BM
Wavelength (Å)	0.979
Space group	*P*1
Unit-cell dimensions: a, b, c (Å)	94.4, 94.4, 142.2
Angles: α, β, γ (°)	90, 90, 120
Protein chains in the ASU	1
Completeness (%)	99.9 (100.0)
Number of unique reflections	16607 (810)
Redundancy	7.8 (8.0)
<I>/<σ(I)>	13.3 (1.5)
CC ½	(0.70)
R_{merge}	0.178 (1.697)
R_{work}/R_{free}	0.192/0.260
Bond lengths RMSD (Å)	0.004
Bond angles RMSD (°)	0.8
Mean B value (Å²)	66
Mean B value for GHK peptide	77.8
Number of protein atoms	4533
Mean B value for protein (Å²)	69
Number of water molecules	93
Mean B value for water molecules (Å²)	45
Clashscore	2.58
MolProbity score	1.16
Rotamer outliers (%)	0.21
Ramachandran outliers (%)	0.00
Ramachandran favored (%)	97.41

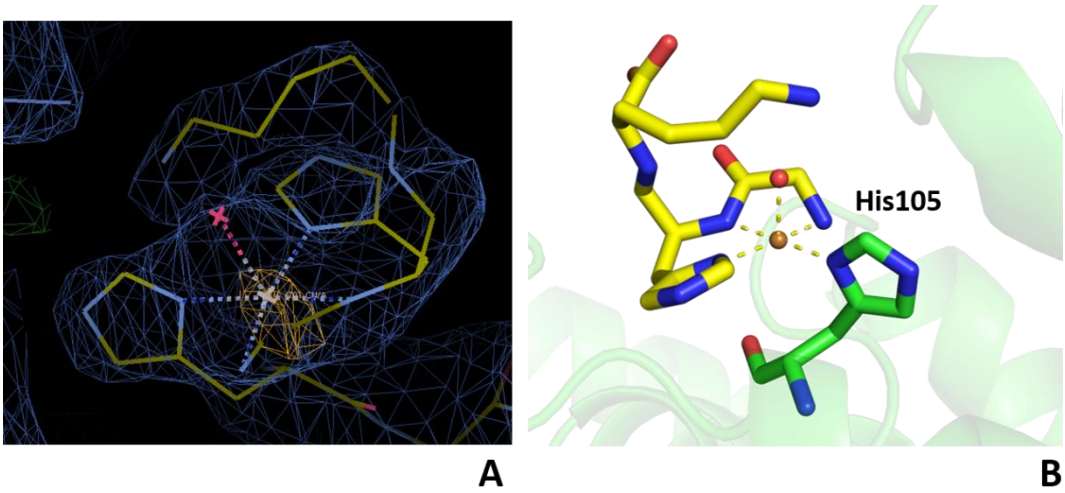

Figure 3.43. A) Electron density observed for GHK(Cu) complex bound to ESA. 2mFo–DFc electron density map (RMSD 1.0) presented in blue; anomalous difference map is presented in yellow (RMSD 3.0). Carbon atoms are presented in yellow, nitrogen atoms in blue, copper ion in white, and water molecule in pink. B) GHK(Cu) (yellow carbon atoms) and His105 (green carbon atoms) are shown in stick representation. The copper ion is shown in brown and the water molecule in pink. The electron density can be inspected interactively at https://molstack.bioreproducibility.org/project/view/lL3gsKTCsHpP5RD8tV3y/.

3.5. Metabolite binding by serum albumin

3.5.1. Structures of ESA complexes with glucose

Two structures of ESA-glucose complexes were determined at 2.28 Å (ESA-glucose 1) and 2.70 Å (ESA-glucose 2) resolution (**Table 3.18**). Both structures were obtained from the same conditions (both crystals grew in the same crystallization drop), and the soaking was performed in the very similar manner (amount of the added powder, incubation time) but revealed glucose binding to different sites (**Table 3.18**, **Figure 3.44**). Perhaps, crystals had different morphology and size, which affected the process of soaking. Also, the unit cell parameters are slightly different for these crystals. Albumin co-crystallization with glucose and crystallization of glycated albumin (albumin was incubated with glucose for several days prior to the crystallization) were not successful, likely due to the heterogeneity of the formed products. The observed electron density indicated glucose binding to drug sites 1, 2, 6, 7, and 9 in the ESA-glucose 1 structure, and to drug sites 3, 7, and 9 in the ESA-glucose 2 structure. The electron density (regular and omit maps) for both structures can be inspected at https://molstack.bioreproducibility.org/collection/view/wvoKH9OfW3wPywf3Zuwn/. In the structures collected for albumin crystals obtained from the same crystallization condition but not soaked with glucose, the analogous binding sites remain unoccupied, except for drug site 1. Drug site 1 was reported to bind glucose in HSA (PDB ID: 4IW2).[66]

The electron density observed for glucose in the reported structures suggests that some sugar molecules are present in the linear form and other in the cyclic form (**Figure**

3.44). This observation agrees with the previous report suggesting that albumin catalyzes the ring-opening of glucose.[66] Glucose molecules bound to albumin not only occupy the binding sites but also can covalently bind to side-chains of arginines and lysines (see 1.1.2). In the drug site 3, a glucose molecule was observed to bind covalently to Lys185 and likely form a Schiff base (**Figure 3.45**). However, the glycation of albumin happens spontaneously, may affect multiple residues, and the observed electron density can be a result of various glycation related modifications of Lys185 in ESA molecules in the crystal.

Table 3.18. Data collection, structure refinement, and structure quality statistics for the ESA-glucose structures. Values in parentheses are for the highest resolution shell. Ramachandran plot statistics are calculated by MolProbity.

Name	ESA-glucose 1	ESA-glucose 2
PDB ID	-	-
Diffraction images DOI	-	-
Data collection statistics		
Crystallization conditions	0.2 M lithium sulfate, 1.8 M ammonium sulfate, 0.1 M Tris buffer pH 7.4	
SA source	ESA isolated from horse blood (Equitech-Bio #ESA62)	
SA concentration	34 mg/mL	
Additives	Glucose powder was added directly to the crystallization drops containing crystals for 48 h before harvesting	
Resolution (Å)	50.00-2.28 (2.32-2.28)	50.00-2.70 (2.75-2.70)
Beamline	19-ID	19-ID
Wavelength (Å)	0.979	0.979
Space group	$P6_1$	$P6_1$
Unit-cell dimensions (Å)	a=b=94.8 c=142.2	a=b=94.4 c=142.6
Protein chains in the ASU	1	1
Completeness (%)	100.0 (99.9)	100.0 (100.0)
Number of unique reflections	33439 (1685)	19761 (971)
Redundancy	10.0 (7.7)	9.1 (7.9)
<I>/<σ(I)>	27.2 (1.)	20.6 (1.4)
CC ½	(0.50)	(0.55)
R_{merge}	0.103 (2.336)	0.167 (2.975)
Refinement statistics		
R_{work}/R_{free}	0.179/0.236	0.195/0.241
Bond lengths RMSD (Å)	0.004	0.002
Bond angles RMSD (°)	1.2	1.2
Mean B value (Å²)	44	55
Mean B value for sugar molecules (Å²)	56	81
Number of protein atoms	4551	4523
Mean B value for protein (Å²)	44	55
Number of water molecules	223	130
Mean B value for water molecules (Å²)	38	40
Clashscore	2.31	2.68
MolProbity score	1.10	1.12
Rotamer outliers (%)	1.01	1.03
Ramachandran outliers (%)	0.00	0.00
Ramachandran favored (%)	97.58	97.75

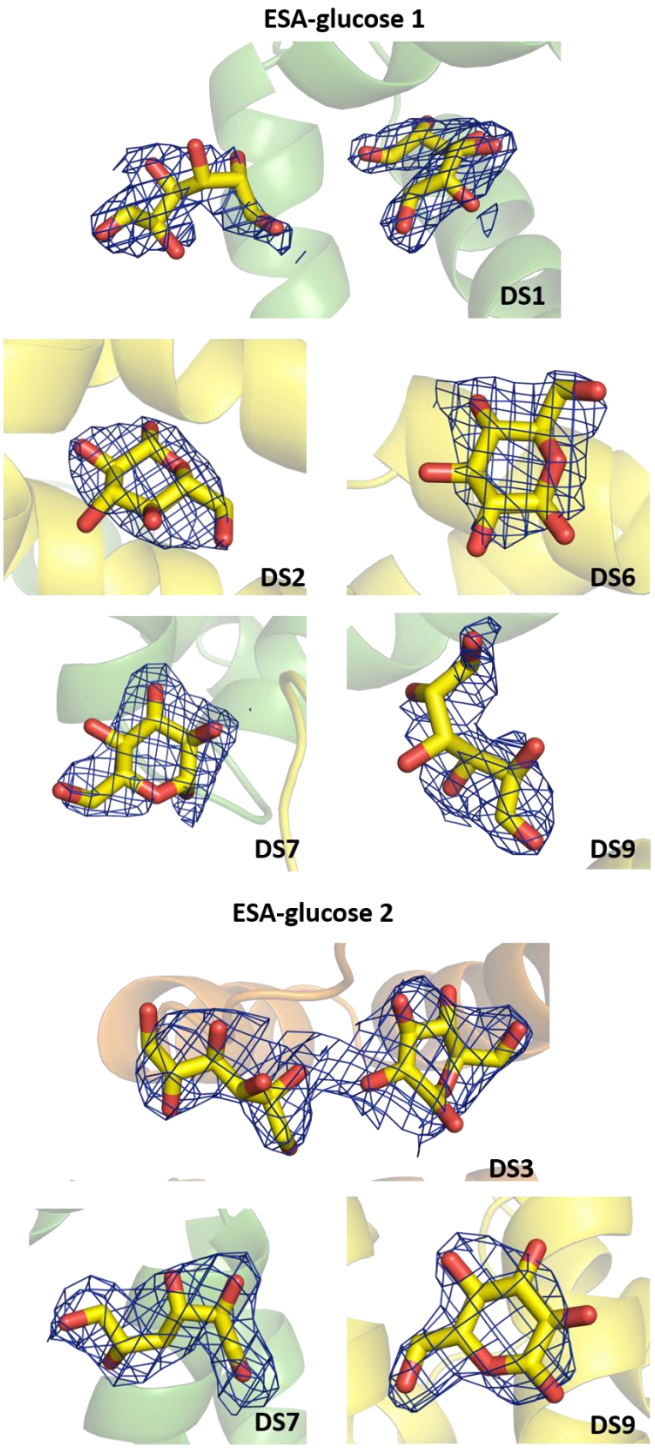

Figure 3.44. Glucose binding sites in ESA with 2mFo–DFc electron density map (RMSD 1.0) presented in blue. Glucose molecules are shown in stick representation with oxygen atoms in red and carbon atoms in yellow. DS stands for a drug site.

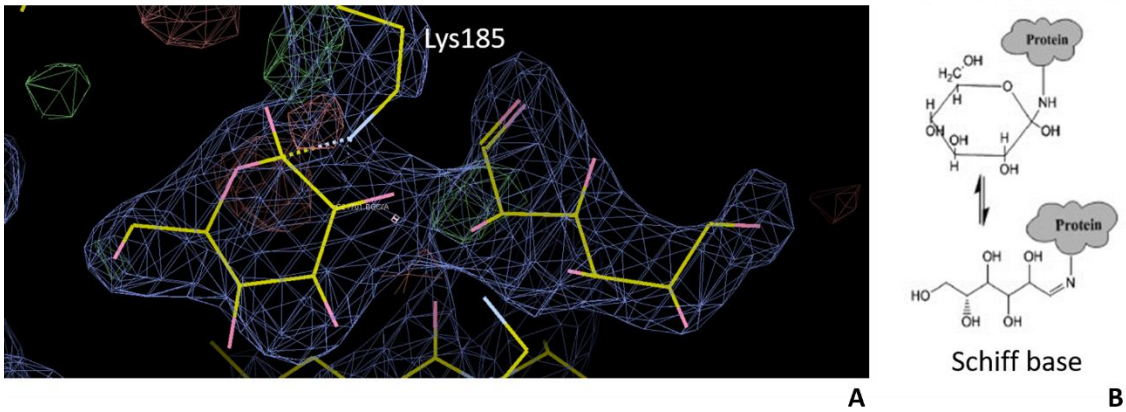

Figure 3.45. A) Sugar molecules bound to drug site 3. The observed electron density suggests that the glucose molecule can be covalently bound to Lys185 (likely Schiff base). B) Structure of one of the early stage glycation products proposed by Anguizola et al.[58]

3.5.2. Structure of HSA complex with myristic acid

HSA complexed with myristic acid crystallized in the *C*2 space group with one protein copy in the asymmetric unit. The structure was determined at 1.95 Å resolution (**Table 3.19**). Well-ordered electron density indicates binding of seven molecules of myristic acid to multiple sites (**Figure 3.46**, **Figure 3.47**) that were previously characterized as drug and fatty acid binding sites: drug site 1 (FA7), drug site 2 (FA3 and FA4), drug site 3 (FA1), drug site 7 (FA6), drug site 8 (FA5), drug site 10 (FA2). Fatty acids overlap with locations previously reported to bind drugs and potentially prevent their binding (**Figure 3.48**). The HSA complex with myristic acid determined in this study structure has a fold essentially identical to the previously reported albumin complexes with fatty acids (e.g., PDB IDs: 1BJ5, 6HSC) despite containing a higher number of bound molecules of fatty acids. The electron density for the reported structure can be inspected at

https://molstack.bioreproducibility.org/project/view/txbkOPoPleefZXknjFLq/. The model is complete except for the first residue, due to the lack of electron density.

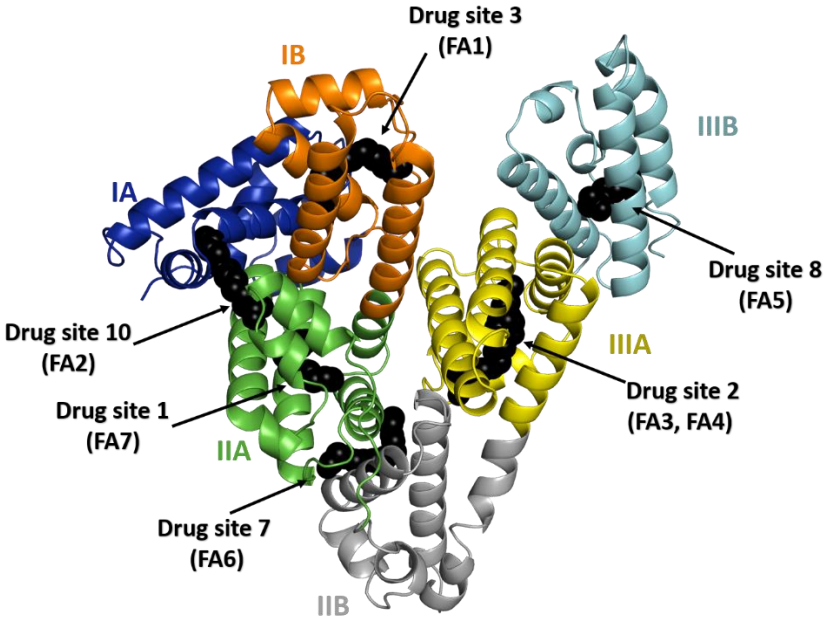

Figure 3.46. The overall structure of the HSA complex with myristic acid. Albumin subdomains are shown each in a different color. Roman numerals (I, II, III) are associated with domains and letters (e. g., IB) with subdomains. Fatty acid molecules are shown with atoms in black spheres.

Table 3.19. Data collection, structure refinement, and structure quality statistics for the HSA-myristic acid structure. Values in parentheses are for the highest resolution shell. Ramachandran plot statistics are calculated by MolProbity.

Name	HSA-myristic acid
PDB ID	-
Diffraction images DOI	-
Data collection statistics	
Crystallization conditions	50 mM potassium phosphate buffer at pH 7.0 and 24% PEG 3350
SA source	HSA isolated from human blood (Sigma-Aldrich #A8763)
SA concentration	100 mg/mL
Additives	Protein was incubated with 5 mM myristic acid (dissolved in 100% ethanol) for 48 h at 37 °C prior to crystallization
Resolution (Å)	50.00-1.95 (1.98-1.95)
Beamline	19-ID
Wavelength (Å)	0.979
Space group	*C*2
Unit-cell dimensions (Å)	a=186.5 b=38.5 c=96.0
Protein chains in the ASU	1
Completeness (%)	98.4 (98.2)
Number of unique reflections	48071 (2357)
Redundancy	5.5 (4.2)
$\langle I \rangle / \langle \sigma(I) \rangle$	17.2 (1.2)
CC ½	(0.57)
R_{merge}	0.086 (1.380)
Refinement statistics	
R_{work}/R_{free}	0.210/0.229
Bond lengths RMSD (Å)	0.002
Bond angles RMSD (°)	1.1
Mean B value (Å²)	30
Mean B value for fatty acids (Å²)	40
Number of protein atoms	4609
Mean B value for protein (Å²)	29
Number of water molecules	341
Mean B value for water molecules (Å²)	35
Clashscore	0.96
MolProbity score	0.84
Rotamer outliers (%)	0.80
Ramachandran outliers (%)	0.00
Ramachandran favored (%)	97.76

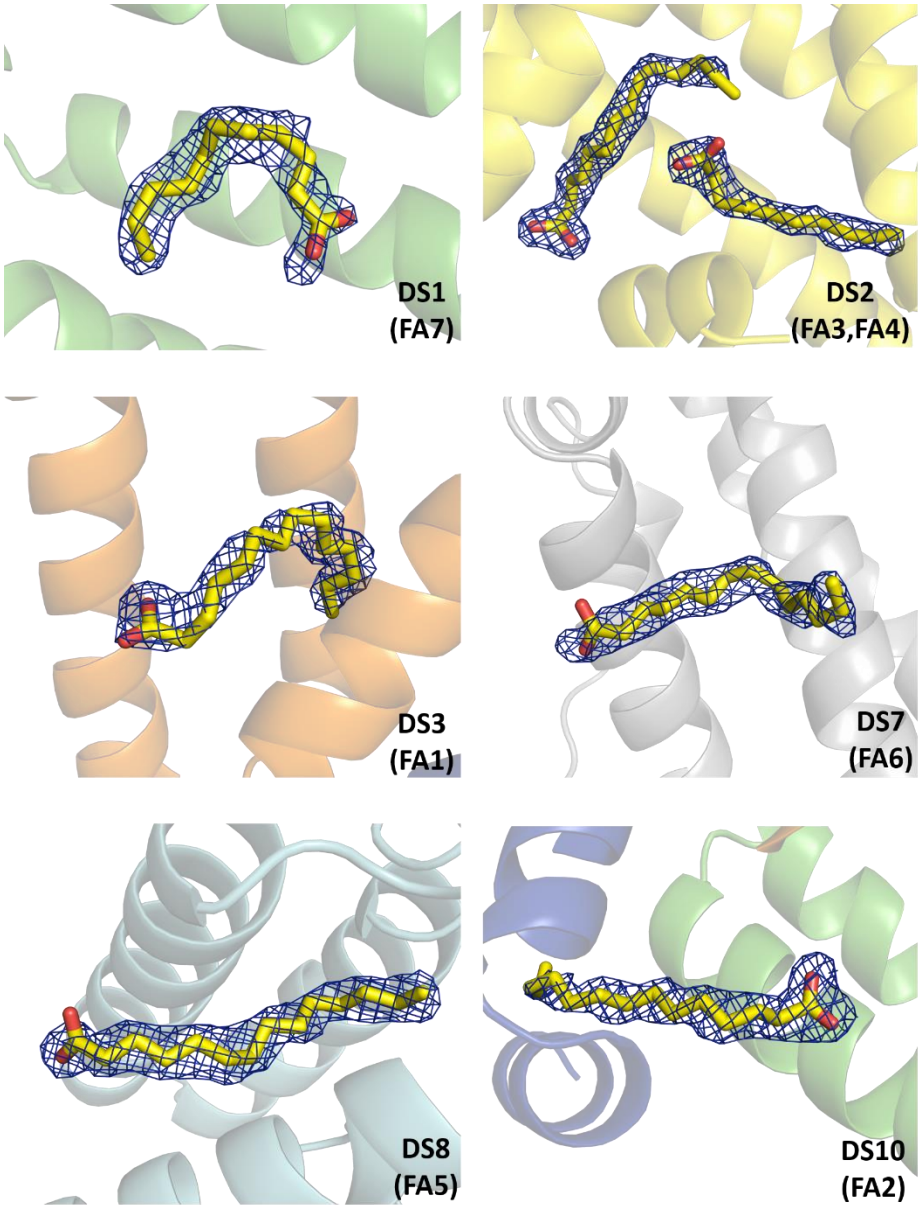

Figure 3.47. Myristic acid binding sites in HSA with 2mFo–DFc electron density map (RMSD 1.0) presented in blue. Myristic acid molecules are shown in stick representation with oxygen atoms in red and carbon atoms in yellow. DS stands for a drug site; FA stands for fatty acid binding site.

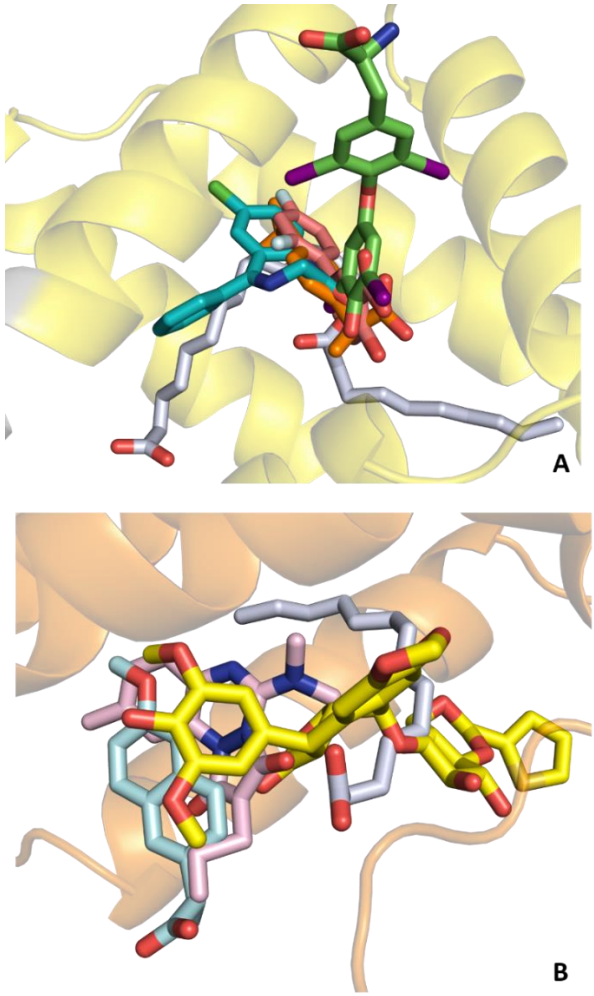

Figure 3.48. Superposition of the HSA-myristic acid complex with the albumin complexes with the selected FDA-approved drugs known to bind to drug sites 2 and 3. Fatty acids and drugs are shown in stick representation with oxygen atoms in red, nitrogen atoms in blue, chloride in pale green, fluoride in white, and iodine in violet. Molecules of myristic acid are shown with carbon atoms in gray. A) Drug site 2: diazepam (cyan; PDB ID: 2BXF), ibuprofen (orange; PDB ID: orange), diflunisal (pink; PDB ID: 2BXE). B) Drug site 3: azapropazone (pink; PDB ID: 2BXI), naproxen (light blue; PDB ID: 2VDB), teniposide (yellow; PDB ID: 4L9Q).

3.6. Structural analysis of the fatty acid effect on SA drug-binding properties

The PDB contains a high number of structures of SA-drug complexes. However, albumin complexes with only five drugs (warfarin, thyroxine, azapropazone, phenylbutazone, and oxyphenbutazone) were determined in both conditions with and without fatty acids. The analysis of these complexes shows that the binding of warfarin (PDB ID: 2BXD, 1H9Z, and 1HA2),[81,121] azapropazone (PDB ID: 2BX8, 2BXI),[81] and phenylbutazone (PDB ID: 2BXC, 2BXP)[81] is not affected by the presence of fatty acid. These drugs bind to the same sites regardless of the presence of fatty acids. The other two drugs, thyroxine, and oxyphenbutazone bind to albumin differently in the absence and in the presence of fatty acids.

Thyroxine has been shown to bind to drug sites 1, 2, and 8 of HSA in the absence of the fatty acid (PDB ID: 1HK1).[87] In the HSA-thyroxine structure determined in the presence of the fatty acids, these sites are occupying by fatty acids that prevent the binding of thyroxine (PDB ID: 1HK4). However, fatty acids affect the conformation of albumin, which is now 'wider' and created a new thyroxine-binding site that overlaps with drug site 9 (**Figure 3.49**). It has also been reported that unmodified albumin binds thyroxine stronger than albumin complexed with myristic acid.[87]

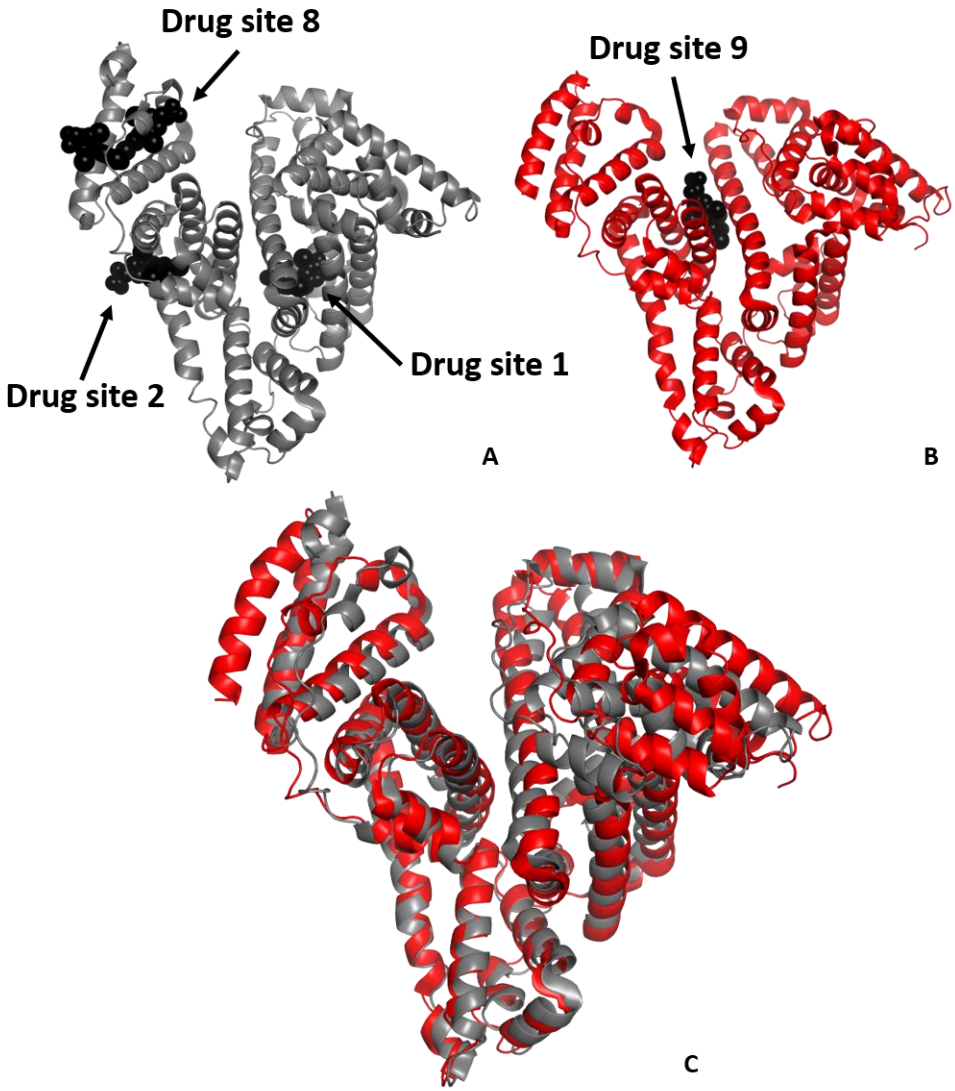

Figure 3.49. The presence of fatty acids affects thyroxine binding to albumin. A) HSA complex with thyroxine (PDB ID: 1HK1). B) HSA complex with thyroxine and myristic acid (PDB ID: 1HK4). C) Superposition of HSA-thyroxine complexes determined in the presence (PDB ID: 1HK4) and absence (PDB ID: 1HK1) of fatty acids. RMSD calculated between the aligned Cα atoms: 2.7 Å.

Oxyphenbutazone has also been shown to bind to albumin differently in the presence of fatty acids. In the absence of fatty acids, oxyphenbutazone binds only to drug site 1 (PDB ID: 2BXB), while in their presence, it also binds to drug site 6 (PDB ID: 2BXBO; see **Figure 3.50**). The presence of a fatty acid molecule (myristic acid) in drug site 1 causes the re-orientation of the oxyphenbutazone molecule (**Figure 3.51**). In the drug site 6, myristic acid interacts with the oxyphenbutazone molecule. It suggests that the presence of a fatty acid molecule at this site is required to stabilize the drug molecule.

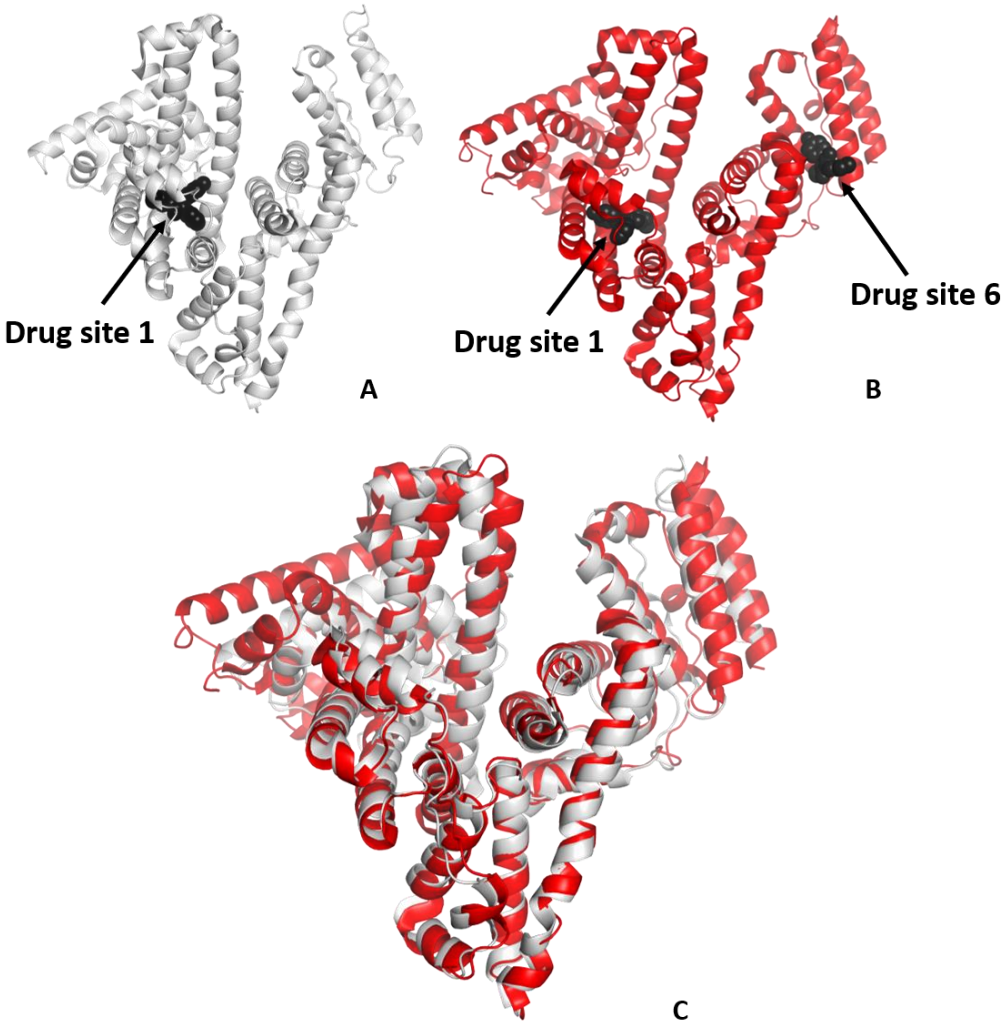

Figure 3.50. The presence of fatty acids affects oxyphenbutazone binding to albumin. A) HSA complex with oxyphenbutazone (PDB ID: 2BXB). B) HSA complex with oxyphenbutazone and myristic acid (PDB ID: 2BXO). C) Superposition of HSA-oxyphenbutazone complexes determined in the presence (PDB ID: 2BXO) and absence (PDB ID: 2BXB) of fatty acids. RMSD calculated between the aligned Cα atoms: 2.7 Å.

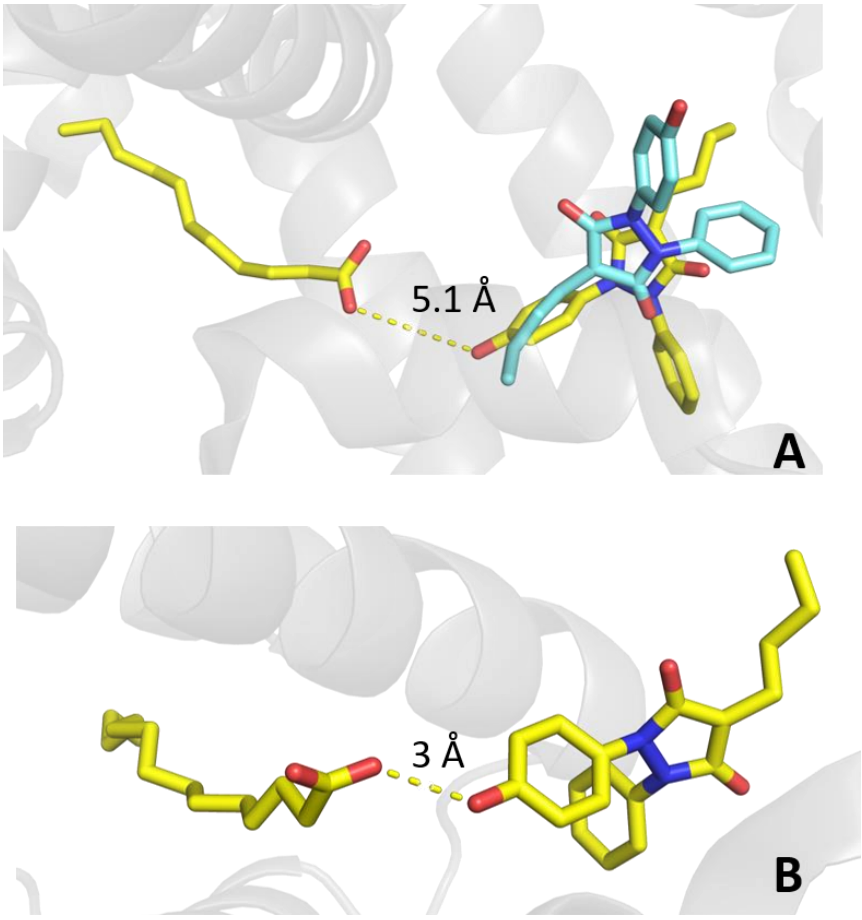

Figure 3.51. A) Drug site 1: superposition of HSA-oxyphenbutazone complexes obtained in the presence (carbon atoms in yellow; PDB ID: 2BXO) and absence (carbon atoms in cyan; PDB ID: 2BXB) of fatty acids. The presence of a fatty acid molecule in the binding site causes the re-orientation of oxyphenbutazone. B) Drug site 6: interactions between fatty acid and oxyphenbutazone molecules.

4. Discussion

4.1. Summary of albumin drug-binding sites

In this study, I report SA complexes with the following FDA-approved drugs: ibuprofen, ketoprofen, etodolac, nabumetone, 6-MNA, testosterone, progesterone, dexamethasone, hydrocortisone, warfarin, tolbutamide, haloperidol, and ampicillin. In addition, I report structures that revealed binding sites of the JMS-053 compound, GHK(Cu), glucose, and fatty acids. The binding of these FDA-approved drugs has previously been investigated through non-structural methods, such as equilibrium dialysis, and showed that they significantly bind to plasma proteins, mainly to SA, typically with micromolar affinities.[239–243] Binding studies generally show a good correlation between drug binding by SA from human plasma and SA from other species (such as dog, rat, or mouse[69]) but do not provide conclusive information about the residues involved in binding. The lack of binding site identification prevents understanding how different small molecules compete for binding to SA, how small molecules are transported *in vivo*, and how SA-facilitated drug transport differs between species.

Prior to this study, crystal structures of only 29 FDA-approved drugs in complexes with SA had been determined (**Table 1.1**), which represents only a small fraction of the hundreds of pharmaceuticals that bind to SA.[14,69,77] The structures reported in this study extended this list to 38 FDA-approved drugs and revealed that albumin has at least ten drug-binding sites (**Table 4.1**), which are described in this study using an expanded

nomenclature of sites that is based on the site numbers used previously by other scientists.[79] Seven of these sites were reported to bind at least five FDA-approved drugs.

The presence of multiple SA binding sites provides the flexibility that permits drugs, their metabolites, and close analogs to utilize different binding sites, as is the case of nabumetone, its metabolite 6-MNA, and nabumetone's close structural analog naproxen. Based on the crystal structures, nabumetone binds to ESA at drug sites 2 and 6, naproxen binds to ESA at drug sites 2 and 7 (PDB ID: 4OT2[131]), and 6-MNA binds to all three of these drug sites (2, 6, and 7). The differences in binding sites among these three structurally related molecules may be explained by steric considerations and the presence of specific functional groups. Naproxen contains a branch, whereas nabumetone and 6-MNA are not branched; this may explain why naproxen does not bind to ESA at drug site 6. Naproxen and 6-MNA binding at drug site 7 may be explained by the presence of a carboxyl group in naproxen and 6-MNA. They form salt bridges with Lys350's side-chain in drug site 7, whereas nabumetone's ketone group cannot form such interactions. However, the differences in observed binding preferences could also be the result of different crystallization conditions and methods (naproxen was co-crystallized with ESA at pH 4.6; nabumetone complex was obtained by soaking crystals that grew at pH 7.4). Naproxen has also been co-crystallized with HSA (PDB ID: 2VDB[130]), BSA (PDB ID: 4OR0[131]), and LSA (PDB ID: 4PO0[131]). In SAs from all of these species, naproxen binds to drug sites 2 and 7 in a mode similar to ESA and binds to drug site 3 in HSA. However, the crystal structure of HSA in complex with naproxen was obtained in the presence of the GA module (the protein G-related albumin-binding module) and fatty acids, which may affect

the availability of SA drug-binding sites. Additionally, naproxen has been observed to bind to drug site 1 in BSA.

The observed species-specific binding of these closely related drugs is probably related to the differences described above, but it is also possible that some of the variations result from differences in crystallization conditions. For example, crystallization condition dependent binding of ibuprofen was observed for ESA (see 3.1.1.5). Though the presence of electron density corresponding to a drug is the best evidence that a drug can bind to a particular binding site, the absence of electron density does not rule out the possibility that a drug could bind to that site under different conditions or a higher drug concentration. Furthermore, the concentration of a ligand used for crystal soaking or protein co-crystallization must often be much higher than its physiological range to see electron density in the determined structure. For instance, the final concentration of etodolac used for soaking in this study was 10 mM, while its plasma concentration in patients is between 0.05 and 0.1 mM.[244] Although the concentrations of drugs used for soaking are much higher than those found in the blood under normal dosages, a direct comparison between crystallization and blood concentrations is not straightforward because crystallization conditions are drastically different from physiological conditions. Additionally, a key point toward understanding why drugs may not bind to the sites to which they are expected to bind is the presence of endogenous metabolites (e.g., sugars, fatty acids). These molecules may compete with drugs for binding to SA.

Table 4.1. Summary of SA drug-binding sites and FDA-approved drugs that were reported to bind in these sites based on crystal structures of the respective complexes. Drugs whose complexes with SA are presented in this study are in bold. PDB IDs for structures of HSA, ESA, BSA, and LSA complexes with drugs available in the PDB are shown in parentheses. Alternative names for binding sites are also indicated in parentheses in headings. Tolbutamide binding to drug site 6 is not listed in the table because it was observed due to the protein crystal contacts and likely will not occur in physiological conditions.

Drug site 1 (Sudlow site I, FA7)	**Drug site 2 (Sudlow Site II, FA3, FA4)**	**Drug site 3 (FA1)**
Amantadine (HSA: 3UIV[123])	Aripiprazole (HSA: 6A7P[122])	**Ampicillin** (ESA: **see 3.3.1.4**)
Aspirin / salicylic acid (HSA: 3B9M,[124] 2I30,[126] 2I2Z[126])	Diazepam (HSA: 2BXF[81])	Azapropazone (HSA: 2BXI,[81] 2BX8[81])
Azapropazone (HSA: 2BXI,[81] 2BX8,[81] 2BXK[81])	Diclofenac (ESA: 4ZBQ;[128] OSA: 6HN0; CSA: 6HN1)	Bicalutamide (HSA: 4LA0[80])
Diclofenac (HSA: 4Z69[127])	Diflunisal (HSA: 2BXE[81])	Diclofenac (HSA: 4Z69,[127] OSA: 6HN0; CSA: 6HN1)
Diflunisal (HSA: 2BXE[81])	**Haloperidol** (ESA: **see 3.3.1.3**)	**Etodolac** (ESA: **5V0V**[228])
Etodolac (ESA: **5V0V**[228])	Halothane (HSA: 1E7B[118])	Fusidic acid (HSA: 2VUF[120])
Halothane (HSA: 1E7C[118])	**Ibuprofen** (HSA: 2BXG;[81] ESA: **6U4X**,[228] 6OCI[115])	Idarubicin (HSA: 4LB2[80])
Indomethacin (HSA: 2BXK,[81] 2BXM,[81] 2BXQ[81])	**Ketoprofen** (LSA: 6OCK;[115] HSA: **7JWN**)	Indomethacin (HSA: 2BXM,[81] 2BXQ[81])
Iodipamine (HSA: 2BXN[81])	**Nabumetone / 6-MNA** (ESA: **6CI6**,[228] **6U5A**[228])	**Ketoprofen** (HSA: **7JWN**)
Ketoprofen (BSA: 6QS9[129])	Naproxen (ESA: 4ZBR,[128] 5DBY;[128] 4OT2;[131] BSA: 4OR0;[131] LSA: 4PO0[131])	Lidocaine (HSA: 3JQZ[119])
Naproxen (BSA: 4OR0[131])	Phenylbutyric acid (HSA: 5YOQ[125])	Naproxen (HSA: 2VDB[130])
Oxyphenbutazone (HSA: 2BXB,[81] 2BXO[81])	Propofol (HSA: 1E7A[118])	Salicylic acid (HSA: 3B9M,[124] 2I30[126])
Phenylbutazone (HSA: 2BXC,[81] 2BXP,[81] 2BXQ[81])	Suprofen (ESA: 6OCJ[115]; LSA: 6OCL[115])	Teniposide (HSA: 4L9Q[80])
Thyroxine (HSA: 1HK1,[87] 1HK2,[87] 1HK3[87])	Thyroxine (HSA: 1HK1,[87] 1HK2,[87] 1HK3[87])	Zidovudine (HSA: 3B9L[124])
Warfarin (HSA: 2BXD,[81] 1H9Z,[121] 1HA2[121])	**Tolbutamide** (ESA: **see 3.3.1.2**)	
Zidovudine (HSA: 3B9L,[124] 3B9M[124])	**Warfarin** (ESA: **see 3.3.1.1**)	

Drug site 4	Drug site 5	Drug site 6	Drug site 7 (FA6)	Drug site 8 (FA5)	Drug site 9 (Cleft, FA8, FA9)	Drug site 10 (FA2)
Cetirizine (ESA: 5DQF[79])	Etoposide (HSA: 4LB9[80])	Diclofenac (ESA: 4ZBQ,[128] 4ZBR,[128] 5DBY[128]; OSA: 6HN0; CSA: 6HN1)	**Ampicillin** (ESA: **see 3.3.1.4**)	Fusidic acid (HSA: 2VUF[120])	Diclofenac (OSA: 6HN0)	Halothane (HSA: 1E7C[118])
Diclofenac (OSA: 6HN0; CSA: 6HN1)		**Ketoprofen** (ESA: **6U4R**;[228] LSA: 6OCK[115])	Cetirizine (ESA: 5DQF[79])	Propofol (HSA: 1E7A[118])	Iodipamine (HSA: 2BXN[81])	**Ketoprofen** (ESA: **6U4R**[228])
Ibuprofen (ESA: **6U4X**[228])		**Nabumetone / 6-MNA** (ESA: **6CI6**,[228] **6U5A**[228])	**Dexamethasone** (ESA: **see 3.2.1.4**)	Thyroxine (HSA: 1HK1,[87] 1HK2,[87]1HK3[87])	**Ketoprofen** (HSA: **7JWN**)	**Tolbutamide** (ESA: **see 3.3.1.2**)
Ketoprofen (ESA: **6U4R**[228])		Naproxen (LSA: 4PO0[131])	Diclofenac (HSA: 4Z69;[127] OSA: 6HN0; CSA: 6HN1)		Thyroxine (HSA: 1HK4,[87] 1HK5[87])	
Progesterone (ESA: **see 3.2.2**)		Oxyphenbutazone (HSA: 2BXO[81])	Diflunisal (HSA: 2BXE[81])		**Tolbutamide** (ESA: **see 3.3.1.2**)	
Testosterone (ESA: **6MDQ**[105])			**Etodolac** (ESA: **5V0V**[228])			
Tolbutamide (ESA: **see 3.3.1.2**)			Halothane (HSA: 1E7B,[118] 1E7C[118])			
			Hydrocortisone (ESA: **see 3.2.1.3**)			
			Ibuprofen (HSA: 2BXG[81]; ESA: 6OCI[115])			
			6-MNA (ESA: **6U5A**[228])			
			Naproxen (ESA: 4ZBR;[128] 4OT2;[131] BSA: 4OR0;[131] LSA: 4PO0[131])			
			Testosterone (ESA: **6MDQ**[105])			

4.2. Drug co-administration

Information about the location of a drug's binding site may be a key element to understanding phenomena associated with drug co-administration and avoiding adverse reactions due to drug-drug displacement. It is especially important for drugs whose margins of safety are small (such as warfarin) to avoid toxicity, which may be caused by drug displacement leading to increases in the free fraction of the drug.[89] The increase in the free fraction of the displaced drug may also result in its decreased half-life.[85,89] So far, based on all available crystal structures, we can distinguish ten SA drug-binding sites, which can bind multiple drugs and other small molecules (**Table 4.1**). Nine of these sites were shown to bind at least three different drugs, and most of them overlap with some of the nine fatty acid binding sites. Drug sites 1 and 2 (Sudlow sites I and II) have the highest number of drugs reported to bind to them (16 drugs to each site), including warfarin and several NSAIDs; interactions between warfarin and NSAIDs during co-administration may lead to gastrointestinal bleeding.[245] Phenylbutazone, an NSAID that was shown to bind to drug site 1,[81] is known to cause increases in the free fraction of etodolac by roughly 80%,[244] which yields a narrow safety margin and can lead to toxic effects like adverse gastrointestinal and hepatic reactions. The mechanism of interactions between etodolac and phenylbutazone is not known, but the structural analysis of their complexes with SA (phenylbutazone PDB ID: 2BXC, 2BXP, 2BXQ; etodolac PDB ID: 5V0V) indicates that they share a common binding site (drug site 1), which may result in drug-drug displacement (**Figure 4.1**). Another possible interaction between co-administered drugs is their co-binding. For instance, it was shown that indomethacin may interact with

phenylbutazone or azapropazone, and the pair of drugs bind together to drug site 1 in HSA (**Figure 4.2**).[81] When these drugs were complexed with albumin separately, they bound to different sites. However, it has not been studied how co-administration of these drugs affects their free fraction in the blood plasma.

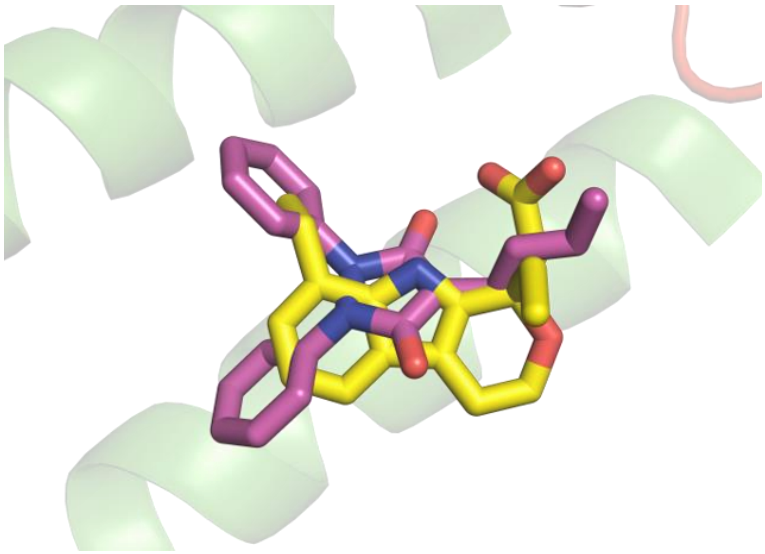

Figure 4.1. Superposition of ESA-etodolac (carbon atoms shown in yellow; PDB ID: 5V0V) and HSA-phenylbutazone (carbon atoms shown in magenta; PDB ID: 2BXC) complexes. Both drugs were reported to bind to drug site 1. Nitrogen atoms are shown in blue, and oxygen atoms in red.

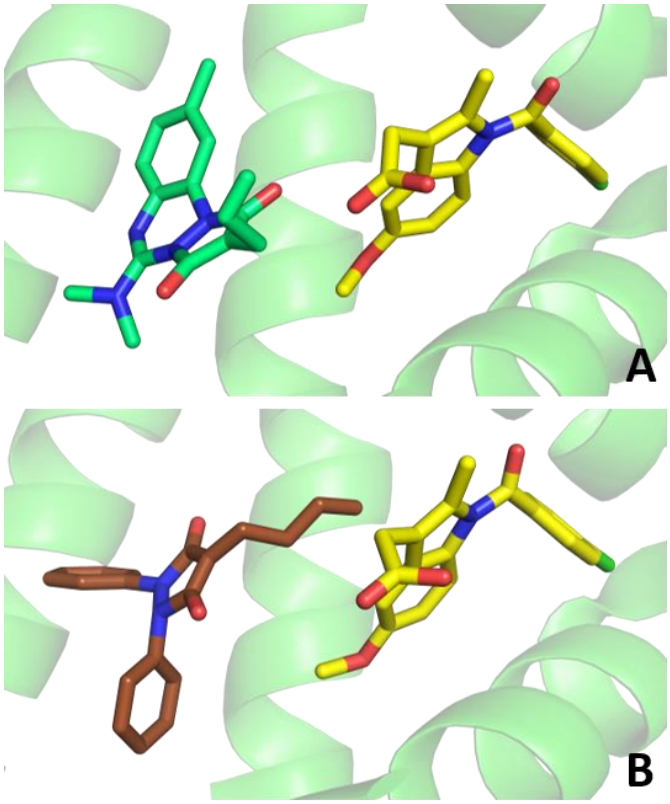

Figure 4.2. A) Co-binding of azapropazone and indomethacin to drug site 1 in the HSA. (PDB ID: 2BXK). B) Co-binding of phenylbutazone and indomethacin to drug site 1 in the HSA (2BXQ). Indomethacin is shown with carbon atoms in yellow, azapropazone with carbon atoms in cyan, and phenylbutazone with carbon atoms in brown. Nitrogen atoms are shown in blue, oxygen atoms in red, and chloride atom in green.

As a protein with crucial therapeutic implications, SA is at the frontier of uncharted knowledge yet to be uncovered. Specifically, obtaining more information about the location of drug-binding sites, which includes the amino acid residues involved in the binding of each particular drug, will be useful for the elucidation of phenomena observed in patients taking multiple drugs and patients with metabolic disorders. The analysis of all known SA drug-binding sites and their potential modifications suggest that some patients may need higher or lower drug doses to achieve the desired therapeutic effect or avoid unexpected toxicity. The characterization of binding sites for the drugs presented in this thesis is but a starting point for further studies of commonly used drugs that have narrow therapeutic ranges, such as digoxin (a cardiovascular medication), theophylline (a bronchodilator), and acenocumarol (an anticoagulant), which are 25%, 40%, and 99%, respectively, bound to plasma proteins (mainly to SA).[246–248] The knowledge that we can obtain for such drugs will have tremendous implications in personalized medical treatments that require comprehensive knowledge of a number of organ systems, and a foundation for these treatments can be achieved through detailed structural studies of how these and other commonly prescribed drugs bind to SA.

4.3. Can common metabolites affect drug binding to serum albumin?

The structures determined in this study revealed multiple sites where glucose can bind to albumin. Even if albumin was not incubated with glucose intentionally, and the protein interacted with sugars only in the blood (ESA used in this study was isolated and purified from horse blood), positive electron density suggests sugar binding to drug site 1 (ESA complexes with ibuprofen, progesterone, hydrocortisone, warfarin, tolbutamide, haloperidol) and drug site 4 (ESA complex with hydrocortisone). Previously, drug site 1 was reported to bind glucose and fructose in HSA.[66] The structures obtained from soaking ESA crystals with glucose indicated glucose binding to drug sites 1, 2, 3, 6, 7, and 9. Glucose was observed to bind to these sites in the linear or cyclic form, and also forms covalent bonds with Lys185 and Lys221. Multiple lysines and arginines involved directly in drug binding or comprising drug-binding sites are known to undergo glycation (**Figure 1.2**). The presence of sugar molecules in the drug-binding sites or their alterations by glycation-related modifications may affect drug transport in different ways. Sugars may compete with drugs for binding to albumin or block access to the drug sites (especially glycation products), but they may also stabilize drugs bound to albumin by acting as hydrogen bond donors or acceptors. These results suggest that high blood sugar levels alter the properties of all known albumin drug-binding sites. However, binding of only a small number of FDA-approved drugs to glycated albumin has been studied.[64,249,250] For instance, cetirizine has been reported to exhibit stronger binding to glycated albumin than to the non-glycated form.[64] Because of SA's glycation, cetirizine administration in diabetic patients may need to be distinct from the standard dose in order to achieve the

same curative effect.[64] Due to the overlap of cetirizine and testosterone binding sites and the similarities of the ligand–residue interactions, it is possible that the relationship between low testosterone levels and insulin resistance in men with type 2 diabetes[251] may be related to the glycation of residues comprising drug sites 4 and 7.

Fatty acids are also known to affect SA's drug-binding properties. They may compete with drugs for binding to SA (**Figure 3.48**), interact with drugs bound to SA (**Figure 3.14**), or affect the conformation of SA.[96,252] The analysis of SA-drug complexes available in the PDB shows that for some drugs, SA utilizes different sets of binding sites in the absence and in the presence of fatty acids (see 3.6).[87] It can be a result of the availability of drug-binding sites in SA (seven of the drug sites overlap with previously characterized fatty acid binding sites) or conformational changes of SA that alter the size of drug-binding sites. The effect of fatty acids on drug interactions with HSA has been studied for selected drugs using chromatographic methods (ultrafiltration and high-performance affinity chromatography), which showed that the presence of fatty acids weakens drug binding to SA and increases free drug concentration.[249] Similarly, the presence of citrate (average citrate concentration in human plasma is about 100–150 μM)[233] has been shown in this study to weaken interactions between SA and testosterone (see 3.2.1.1.2). The albumin concentration in the blood (600 μM)[2] is much higher than the typical concentration of a drug but lower than glucose (3.9-5.5 mM in fasting healthy patients)[54] or fatty acids (typically, 0.5-2 moles of fatty acids are bound per mole of HSA).[93] Together, these results clearly show that the effect of metabolites on drug transport by serum albumin should not be neglected, and further studies should be conducted to

evaluate adjusting drug dosing regimens for patients suffering from diabetes or those having high fatty acid levels.

These results also suggest that SA's binding affinities to drugs measured *in vitro* in the absence of metabolites may be far from those measured in truly physiological conditions. However, binding studies of hydrophobic compounds, such as steroids or other drugs used in this study, are challenging even in the absence of other molecules mimicking physiological conditions because compounds of this nature are poorly soluble in water and often require the use of organic solvents. Due to this limitation, the TFQ (see 3.2.1.1.1) and ITC (data not shown) experiments did not provide reliable results allowing characterization of albumin interactions with drugs described in this study. Also, BLI experiments were unsuccessful because the sensitivity of the device was too low to detect SA interactions with drugs (data not shown). Fortunately, UAE was employed to characterize SA interactions with testosterone. UAE experiments do not require high concentrations of ligands; this aspect of the experimental design allowed us to use aqueous phosphate buffers without the addition of DMSO to solubilize testosterone. DMSO is known to destabilize proteins (presence of 20% of DMSO results in partial unfolding of SA),[231] and zonal elution studies performed in the presence of 20% DMSO showed that testosterone's binding affinity for HSA decreases by 54% when compared to the conditions without the organic solvent. The application of UAE for drug binding studies to glycated SA or SA complexed with fatty acids has been previously described in the literature,[249] and this technique could be used in the future to validate or broaden hypothesis based on the crystal structures presented in this study.

4.4. Albumin stereoselectivity

Opposite enantiomers of some drugs may have preferences for different binding sites on SA. It has been previously reported that HSA often binds one of the drug's enantiomers with significantly higher affinity than the opposite enantiomer.[243] Racemic mixtures of the (*R*)- and (*S*)-enantiomers of those drugs that are marketed as racemates were used in this study for the soaking of native SA crystals (ibuprofen, ketoprofen, and etodolac) or cocrystallization (warfarin, ketoprofen). In the ESA-warfarin complex, well-ordered electron density clearly indicated binding of (*R*)-warfarin to drug site 2. However, previous structural reports showed that both enantiomers of warfarin can bind to drug site 1 in HSA.[81,121] While modeling the racemic NSAIDs into the electron density observed in the ESA structures, the choice of which enantiomer was not immediately obvious in many cases. Both enantiomers of these drugs could initially be modeled in some of the binding pockets, but I tried to resolve the ambiguities by considering the fit to the $2mF_O$-DF_C and mF_O-DF_C omit maps, B-factors of the drugs and drug-binding residues, and interactions with neighboring amino acid residues. I decided to model the (*S*)-enantiomer of ibuprofen at drug sites 2 and 4, (*S*)-ketoprofen at drug sites 4, 6, and 10, (*S*)-etodolac at drug sites 1 and 7, and (*R*)-etodolac at drug sites 3 and 7. However, based on the established criteria, I cannot exclude the possibility of some (*R*)-ibuprofen binding at drug site 4. Likewise, some (*R*)-etodolac may be bound at the drug site 7 subsite, where I modeled (*S*)-etodolac. It is highly probable that the electron density observed for drugs at those sites is a result of binding both enantiomers with different affinities. These observations seem to confirm the hypothesis that drug sites on SA do not have structural

features that allow them to exclusively bind (*S*)- or (*R*)-enantiomers of drugs but that their stereoselectivity instead depends on the structure of the particular drug and experimental conditions.[115]

Previously, predictions about the location of NSAID binding sites were made based on non-structural studies of drugs' enantiomers binding to SA. For instance, both etodolac enantiomers were thought to bind to drug site 2, and only (*R*)-etodolac was thought to bind to drug site 1.[239] The structural results presented here clearly contradict this hypothesis. To further probe the binding of those drugs' enantiomers to SA, structures of SA with each enantiomer should be determined to discern the location of (*R*)- and (*S*)-enantiomer binding sites without interference on one on another. This will allow comparisons between these structures and that of ESA with the racemic mixture to understand the stereoselectivity of NSAID binding to SA in greater detail, which could further our understanding of how different enantiomers of drugs exhibit different effects in circulation.

5. Future perspectives

New structures of albumin complexes with drugs and metabolites, together with results of binding studies contribute to a better understanding of small molecule transport in the blood. However, most of these studies were performed only for albumin from one species (typically human or horse). It would be valuable to study the binding of the most commonly used drugs not only to HSA but also to SA from model organisms like mice or rats. Studying drug binding to SA across species would help us better understand the molecular determinants of binding and allow us to evaluate the usefulness of different model organisms. It could be done using structural methods (X-ray crystallography) to explore how small changes in the SA sequence affect the binding of drugs at the molecular level, but also using equilibrium dialysis, UAE, or other suitable techniques to characterize the binding affinity of SA from different species to drugs in close to physiological conditions. These studied could also be extended to include the most common mutations of HSA to investigate whether they affect drug transport by SA.

To further address the question “Can common metabolites affect drug binding to serum albumin?” and evaluate results obtained *in vitro*, the mice model could be employed. In this experiment, transport of drugs which blood transport is expected to be affected by high levels of fatty acids or glucose (e.g., drugs known to bind to drug site 1 and 2) would be tested in healthy mice and in mice suffering from diabetes or obesity by monitoring free drug concentration and its plasma half-life. I believe the results of these experiments could contribute to our understanding of drug transport in patients suffering

from metabolic disorders and have implications in personalized medical treatments for those patients. For instance, the information about the effect of various factors on free drug levels in the blood could be aggregated in a publicly available database. In a step towards personalized medicine, this database would serve as a web-based resource that allows researchers and physicians to evaluate the potential effects of patients' natural HSA mutations, drug co-administration, and abnormal levels of common metabolites on drug pharmacokinetics and aid physicians with drug prescription dosage based on the characteristics of a particular patient.

6. References

(1) Peters, T. J. T. *All About Albumin: Biochemistry, Genetics, and Medical Applications*, 1st ed.; Academic Press: San Diego, CA, USA, 1995.

(2) Rifai, N. *Tietz Textbook of Clinical Chemistry and Molecular Diagnostics*, 6th ed.; Saunders: St. Louis, MO, USA, 2018.

(3) Evans, T. W. Review Article: Albumin as a Drug-Biological Effects of Albumin Unrelated to Oncotic Pressure. *Aliment. Pharmacol. Ther.* **2002**, *16* (s5), 6–11.

(4) Caraceni, P.; Tufoni, M.; Bonavita, M. E. Clinical Use of Albumin. *Blood Transfus.* **2013**, *11 Suppl 4*, s18-25.

(5) Brennan, S. O.; Carrell, R. W. A Circulating Variant of Human Proalbumin. *Nature* **1978**, *274* (5674), 908–909.

(6) Chojkier, M. Inhibition of Albumin Synthesis in Chronic Diseases. *J. Clin. Gastroenterol.* **2005**, *39* (Supplement 2), S143–S146.

(7) Thalacker-Mercer, A. E.; Campbell, W. W. Dietary Protein Intake Affects Albumin Fractional Synthesis Rate in Younger and Older Adults Equally. *Nutr. Rev.* **2008**, *66* (2), 91–95.

(8) Fanali, G.; Di Masi, A.; Trezza, V.; Marino, M.; Fasano, M.; Ascenzi, P. Human Serum Albumin: From Bench to Bedside. *Mol. Aspects Med.* **2012**, *33* (3), 209–290.

(9) Suzuki, S.; Hashizume, N.; Kanzaki, Y.; Maruyama, T.; Kozuka, A.; Yahikozawa, K. Prognostic Significance of Serum Albumin in Patients with Stable Coronary Artery Disease Treated by Percutaneous Coronary Intervention. *PLoS One* **2019**, *14* (7), e0219044.

(10) Aziz, M.; Fatima, R.; Lee-Smith, W.; Assaly, R. The Association of Low Serum Albumin Level with Severe COVID-19: A Systematic Review and Meta-Analysis. *Crit. Care* **2020**, *24* (1), 255.

(11) Huang, J.; Cheng, A.; Kumar, R.; Fang, Y.; Chen, G.; Zhu, Y.; Lin, S. Hypoalbuminemia Predicts the Outcome of COVID-19 Independent of Age and Co-morbidity. *J. Med. Virol.* **2020**, jmv.26003.

(12) Shabalin, I. G.; Czub, M. P.; Majorek, K. A.; Brzezinski, D.; Grabowski, M.; Cooper, D. R.; Panasiuk, M.; Chruszcz, M.; Minor, W. Molecular Determinants of Vascular Transport of Dexamethasone in COVID-19 Therapy. *IUCrJ* **2020**, *7* (6).

(13) Trainor, G. L. The Importance of Plasma Protein Binding in Drug Discovery. *Expert Opin. Drug Discov.* **2007**, *2* (1), 51–64.

(14) Lombardo, F.; Berellini, G.; Obach, R. S. Trend Analysis of a Database of Intravenous Pharmacokinetic Parameters in Humans for 1352 Drug Compounds. *Drug Metab. Dispos.* **2018**, *46* (11), 1466–1477.

(15) Bohnert, T.; Gan, L.-S. Plasma Protein Binding: From Discovery to Development. *J. Pharm. Sci.* **2013**, *102* (9), 2953–2994.

(16) Merlot, A. M.; Kalinowski, D. S.; Richardson, D. R. Unraveling the Mysteries of Serum Albumin-More than Just a Serum Protein. *Front. Physiol.* **2014**, *5*, 299.

(17) Sitar, M. E.; Aydin, S.; Çakatay, U. Human Serum Albumin and Its Relation with Oxidative Stress. *Clin. Lab.* **2013**, *59* (9–10), 945–952.

(18) Margarson, M. P.; Soni, N. Serum Albumin: Touchstone or Totem? *Anaesthesia* **1998**, *53* (8), 789–803.

(19) McMillan, D. C.; Watson, W. S.; O'Gorman, P.; Preston, T.; Scott, H. R.; McArdle, C. S. Albumin Concentrations Are Primarily Determined by the Body Cell Mass and the Systemic Inflammatory Response in Cancer Patients with Weight Loss. *Nutr. Cancer* **2001**, *39* (2), 210–213.

(20) Handing, K. B.; Shabalin, I. G.; Kassaar, O.; Khazaipoul, S.; Blindauer, C. A.; Stewart, A. J.; Chruszcz, M.; Minor, W. Circulatory Zinc Transport Is Controlled by Distinct Interdomain Sites on Mammalian Albumins. *Chem. Sci.* **2016**, *7* (11), 6635–6648.

(21) Merlot, A. M.; Kalinowski, D. S.; Kovacevic, Z.; Jansson, P. J.; Lane, D. J. R.; Huang, M. L.-H.; Sahni, S.; Richardson, D. R. Making a Case for Albumin – a Highly Promising Drug-Delivery System. *Future Med. Chem.* **2015**, *7* (5), 553–556.

(22) Nation, R. L.; Theuretzbacher, U.; Tsuji, B. T.; International Society of Anti-Infective Pharmacology (ISAP). Concentration-Dependent Plasma Protein Binding: Expect the Unexpected. *Eur. J. Pharm. Sci.* **2018**, *122*, 341–346.

(23) Cohn, E. J.; Luetscher, J. A.; Oncley, J. L.; Armstrong, S. H.; Davis, B. D. Preparation and Properties of Serum and Plasma Proteins. III. Size and Charge of Proteins Separating upon Equilibration across Membranes with Ethanol—Water Mixtures of Controlled PH, Ionic Strength and Temperature. *J. Am. Chem. Soc.* **1940**, *62* (12), 3396–3400.

(24) Patek, A. J.; Mankin, H.; Colcher, H.; Lowell, A.; Earle, D. P. The Effects of Intravenous Injection of Concentrated Human Serum Albumin upon Blood Plasma, Ascites and Renal Functions in Three Patients with Cirrhosis of the Liver. *J. Clin. Invest.* **1948**, *27* (1), 135–144.

(25) Armstrong, S. H. Mechanisms of Action of Serum Albumin Therapy in Internal Medicine. *Am. J. Med.* **1948**, *4* (3), 390–397.

(26) Faloon, W. W.; Eckhardt, R. D.; Murphy, T. L.; Cooper, A. M.; Davidson, C. S. An

Evaluation of Human Serum Albumin in the Treatment of Cirrhosis of the Liver. *J. Clin. Invest.* **1949**, *28* (4), 583–594.

(27) Erstad, B. L. Viral Infectivity of Albumin and Plasma Protein Fraction. *Pharmacotherapy* **1996**, *16* (6), 996–1001.

(28) Latta, M.; Knapp, M.; Sarmientos, P.; Bréfort, G.; Becquart, J.; Guerrier, L.; Jung, G.; Mayaux, J.-F. Synthesis and Purification of Mature Human Serum Albumin from E. Coli. *Nat. Biotechnol.* **1987**, *5* (12), 1309–1314.

(29) Kobayashi, K.; Kuwae, S.; Ohya, T.; Ohda, T.; Ohyama, M.; Ohi, H.; Tomomitsu, K.; Ohmura, T. High-Level Expression of Recombinant Human Serum Albumin from the Methylotrophic Yeast Pichia Pastoris with Minimal Protease Production and Activation. *J. Biosci. Bioeng.* **2000**, *89* (1), 55–61.

(30) He, Y.; Ning, T.; Xie, T.; Qiu, Q.; Zhang, L.; Sun, Y.; Jiang, D.; Fu, K.; Yin, F.; Zhang, W.; Shen, L.; Wang, H.; Li, J.; Lin, Q.; Sun, Y.; Li, H.; Zhu, Y.; Yang, D. Large-Scale Production of Functional Human Serum Albumin from Transgenic Rice Seeds. *Proc. Natl. Acad. Sci. U. S. A.* **2011**, *108* (47), 19078–19083.

(31) Echelard, Y.; Williams, J. L.; Destrempes, M. M.; Koster, J. A.; Overton, S. A.; Pollock, D. P.; Rapiejko, K. T.; Behboodi, E.; Masiello, N. C.; Gavin, W. G.; Pommer, J.; Van Patten, S. M.; Faber, D. C.; Cibelli, J. B.; Meade, H. M. Production of Recombinant Albumin by a Herd of Cloned Transgenic Cattle. *Transgenic Res.* **2009**, *18* (3), 361–376.

(32) Wiedmann, R. T.; Reisinger, K. S.; Hartzel, J.; Malacaman, E.; Senders, S. D.; Giacoletti, K. E. D.; Shaw, E.; Kuter, B. J.; Schödel, F.; Musey, L. K. M-M-R(®)II Manufactured Using Recombinant Human Albumin (RHA) and M-M-R(®)II Manufactured Using Human Serum Albumin (HSA) Exhibit Similar Safety and Immunogenicity Profiles When Administered as a 2-Dose Regimen to Healthy Children. *Vaccine* **2015**, *33* (18), 2132–2140.

(33) Kimura, T.; Shinohara, R.; Böttcher, C.; Komatsu, T. Core–Shell Clusters of Human Haemoglobin A and Human Serum Albumin: Artificial O 2 -Carriers Having Various O 2 -Affinities. *J. Mater. Chem. B* **2015**, *3* (30), 6157–6164.

(34) Haruki, R.; Kimura, T.; Iwasaki, H.; Yamada, K.; Kamiyama, I.; Kohno, M.; Taguchi, K.; Nagao, S.; Maruyama, T.; Otagiri, M.; Komatsu, T. Safety Evaluation of Hemoglobin-Albumin Cluster “HemoAct” as a Red Blood Cell Substitute. *Sci. Rep.* **2015**, *5* (1), 12778.

(35) Hypoallergenic albumin, Albagen, https://www.albuminbio.com/our-shop/recombinant-human-serum-albumin/albumin-recombinant-human-ultra-pure/ [accessed 10.01.2020].

(36) Hypoallergenic albumin, Sigma-Aldrich, https://www.sigmaaldrich.com/catalog/product/sigma/a7736?lang=en&region=

US [accessed 10.01.2020].

(37) Seige, M.; Kreymann, B.; Jeschke, B.; Schweigart, U.; Kopp, K. F.; Classen, M. Long-Term Treatment of Patients with Acute Exacerbation of Chronic Liver Failure by Albumin Dialysis. *Transplant. Proc. 31* (1–2), 1371–1375.

(38) Stange, J.; Ramlow, W.; Mitzner, S.; Schmidt, R.; Klinkmann, H. Dialysis against a Recycled Albumin Solution Enables the Removal of Albumin-Bound Toxins. *Artif. Organs* **1993**, *17* (9), 809–813.

(39) Mitzner, S.; Klammt, S.; Stange, J.; Schmidt, R. Albumin Regeneration in Liver Support-Comparison of Different Methods. *Ther. Apher. Dial.* **2006**, *10* (2), 108–117.

(40) Lorey, F. W.; Ahlfors, C. E.; Smith, D. G.; Neel, J. V. Bilirubin Binding by Variant Albumins in Yanomama Indians. *Am. J. Hum. Genet.* **1984**, *36* (5), 1112–1120.

(41) Kragh-Hansen, U.; Minchiotti, L.; Brennan, S. O.; Sugita, O. Hormone Binding to Natural Mutants of Human Serum Albumin. *Eur. J. Biochem.* **1990**, *193* (1), 169–174.

(42) Kragh-Hansen, U.; Brennan, S. O.; Galliano, M.; Sugita, O. Binding of Warfarin, Salicylate, and Diazepam to Genetic Variants of Human Serum Albumin with Known Mutations. *Mol. Pharmacol.* **1990**, *37* (2), 238–242.

(43) Genetic variants of serum albumin, https://albumin.org/genetic-variants-of-human-serum-albumin/ [accessed 05.17.2019].

(44) Kragh-Hansen, U.; Minchiotti, L.; Galliano, M.; Peters, T. Human Serum Albumin Isoforms: Genetic and Molecular Aspects and Functional Consequences. *Biochim. Biophys. Acta - Gen. Subj.* **2013**, *1830* (12), 5405–5417.

(45) Variation viewer, https://www.ncbi.nlm.nih.gov/variation/view/ [acceessed 05.29.2020].

(46) Osaki, Y.; Hayashi, Y.; Nakagawa, Y.; Yoshida, K.; Ozaki, H.; Fukazawa, H. Familial Dysalbuminemic Hyperthyroxinemia in a Japanese Man Caused by a Point Albumin Gene Mutation (R218P). *Japanese Clin. Med.* **2016**, *7*, 9–13.

(47) Sunthornthepvarakul, T.; Angkeow, P.; Weiss, R. E.; Hayashi, Y.; Refetoff, S. An Identical Missense Mutation in the Albumin Gene Results in Familial Dysalbuminemic Hyperthyroxinemia in 8 Unrelated Families. *Biochem. Biophys. Res. Commun.* **1994**, *202* (2), 781–787.

(48) Kragh-Hansen, U.; Galliano, M.; Minchiotti, L. Clinical, Genetic, and Protein Structural Aspects of Familial Dysalbuminemic Hyperthyroxinemia and Hypertriiodothyroninemia. *Front. Endocrinol. (Lausanne).* **2017**, *8*, 297.

(49) Cho, Y. Y.; Song, J. S.; Park, H. D.; Kim, Y. N.; Kim, H. I.; Kim, T. H.; Chung, J. H.; Ki, C. S.; Kim, S. W. First Report of Familial Dysalbuminemic Hyperthyroxinemia With

an ALB Variant. *Ann. Lab. Med.* **2017**, *37* (1), 63–65.

(50) Ryan, J. B.; Brennan, S. O.; Potter, H.; Wolmarans, L.; Florkowski, C. M.; George, P. M. Familial Dysalbuminaemic Hyperthyroxinaemia: A Rapid and Novel Mass Spectrometry Approach to Diagnosis. *Ann. Clin. Biochem.* **2016**, *53* (4), 504–507.

(51) Minchiotti, L.; Galliano, M.; Iadarola, P.; Zepponi, E.; Ferri, G. The Molecular Defect of Albumin Castel Di Sangro: 536 Lys----Glu. *Biochim. Biophys. Acta* **1990**, *1039* (2), 204–208.

(52) Minchiotti, L.; Kragh-Hansen, U.; Nielsen, H.; Hardy, E.; Mercier, A. Y.; Galliano, M. Structural Characterization, Stability and Fatty Acid-Binding Properties of Two French Genetic Variants of Human Serum Albumin. *Biochim. Biophys. Acta* **1999**, *1431* (1), 223–231.

(53) Nielsen, H.; Kragh-Hansen, U.; Minchiotti, L.; Galliano, M.; Brennan, S. O.; Tárnoky, A. L.; Franco, M. H.; Salzano, F. M.; Sugita, O. Effect of Genetic Variation on the Fatty Acid-Binding Properties of Human Serum Albumin and Proalbumin. *Biochim. Biophys. Acta* **1997**, *1342* (2), 191–204.

(54) American Diabetes Association Website, https://www.diabetes.org/diabetes/medication-management/blood-glucose-testing-and-control/checking-your-blood-glucose [accessed 05.08.2020].

(55) CDC 2015-2016 National Health and Nutrition Examination Survey, https://wwwn.cdc.gov/nchs/nhanes/ContinuousNhanes/Default.aspx?BeginYear=2015 [accessed 05.20.2020].

(56) Shaklai, N.; Garlick, R. L.; Bunn, H. F. Nonenzymatic Glycosylation of Human Serum Albumin Alters Its Conformation and Function. *J. Biol. Chem.* **1984**, *259* (6), 3812–3817.

(57) Roohk, H. V.; Zaidi, A. R. A Review of Glycated Albumin as an Intermediate Glycation Index for Controlling Diabetes. *J. Diabetes Sci. Technol.* **2008**, *2* (6), 1114–1121.

(58) Anguizola, J.; Matsuda, R.; Barnaby, O. S.; Hoy, K. S.; Wa, C.; DeBolt, E.; Koke, M.; Hage, D. S. Review: Glycation of Human Serum Albumin. *Clin. Chim. Acta* **2013**, *425*, 64–76.

(59) Nakajou, K.; Watanabe, H.; Kragh-Hansen, U.; Maruyama, T.; Otagiri, M. The Effect of Glycation on the Structure, Function and Biological Fate of Human Serum Albumin as Revealed by Recombinant Mutants. *Biochim. Biophys. Acta* **2003**, *1623* (2–3), 88–97.

(60) Lee, P.; Wu, X. Review: Modifications of Human Serum Albumin and Their Binding Effect. *Curr. Pharm. Des.* **2015**, *21* (14), 1862–1865.

(61) Kuo, H.-C.; Liang, C.-D.; Wang, C.-L.; Yu, H.-R.; Hwang, K.-P.; Yang, K. D. Serum

Albumin Level Predicts Initial Intravenous Immunoglobulin Treatment Failure in Kawasaki Disease. *Acta Paediatr.* **2010**, *99* (10), 1578–1583.

(62) Yoshizawa, M.; Hayashi, H.; Tashiro, Y.; Sakawa, S.; Moriwaki, H.; Akimoto, T.; Doi, O.; Kimura, M.; Kawarasaki, Y.; Inoue, K.; Itoh, K. Effect of VKORC1-1639 G>A Polymorphism, Body Weight, Age, and Serum Albumin Alterations on Warfarin Response in Japanese Patients. *Thromb. Res.* **2009**, *124* (2), 161–166.

(63) Singha Roy, A.; Ghosh, P.; Dasgupta, S. Glycation of Human Serum Albumin Alters Its Binding Efficacy towards the Dietary Polyphenols: A Comparative Approach. *J. Biomol. Struct. Dyn.* **2016**, *34* (9), 1911–1918.

(64) Liu, X.; Du, Y.; Sun, W.; Kou, J.; Yu, B. Study on the Interaction of Levocetirizine Dihydrochloride with Human Serum Albumin by Molecular Spectroscopy. *Spectrochim. Acta. A. Mol. Biomol. Spectrosc.* **2009**, *74* (5), 1189–1196.

(65) Baraka-Vidot, J.; Guerin-Dubourg, A.; Bourdon, E.; Rondeau, P. Impaired Drug-Binding Capacities of in Vitro and in Vivo Glycated Albumin. *Biochimie* **2012**, *94* (9), 1960–1967.

(66) Wang, Y.; Yu, H.; Shi, X.; Luo, Z.; Lin, D.; Huang, M. Structural Mechanism of Ring-Opening Reaction of Glucose by Human Serum Albumin. *J. Biol. Chem.* **2013**, *288* (22), 15980–15987.

(67) Matsuda, R.; Kye, S.-H.; Anguizola, J.; Hage, D. S. Studies of Drug Interactions with Glycated Human Serum Albumin by High-Performance Affinity Chromatography. *Rev. Anal. Chem.* **2014**, *33* (2).

(68) Majorek, K. A.; Porebski, P. J.; Dayal, A.; Zimmerman, M. D.; Jablonska, K.; Stewart, A. J.; Chruszcz, M.; Minor, W. Structural and Immunologic Characterization of Bovine, Horse, and Rabbit Serum Albumins. *Mol. Immunol.* **2012**, *52* (3–4), 174–182.

(69) Colclough, N.; Ruston, L.; Wood, J. M.; MacFaul, P. A. Species Differences in Drug Plasma Protein Binding. *Med. Chem. Commun.* **2014**, *5* (7), 963–967.

(70) Yamasaki, K.; Enokida, T.; Taguchi, K.; Miyamura, S.; Kawai, A.; Miyamoto, S.; Maruyama, T.; Seo, H.; Otagiri, M. Species Differences in the Binding of Sodium 4-Phenylbutyrate to Serum Albumin. *J. Pharm. Sci.* **2017**, *106* (9), 2860–2867.

(71) Puigdemont, A.; Arboix, M.; Gaspari, F.; Bortolotti, A.; Bonati, M. In-Vitro Plasma Protein Binding of Propafenone and Protein Profile in Eight Mammalian Species. *Res. Commun. Chem. Pathol. Pharmacol.* **1989**, *64* (3), 435–440.

(72) Acharya, M. R.; Sparreboom, A.; Sausville, E. A.; Conley, B. A.; Doroshow, J. H.; Venitz, J.; Figg, W. D. Interspecies Differences in Plasma Protein Binding of MS-275, a Novel Histone Deacetylase Inhibitor. *Cancer Chemother. Pharmacol.* **2006**, *57* (3), 275–281.

(73) Zeitlinger, M. A.; Derendorf, H.; Mouton, J. W.; Cars, O.; Craig, W. A.; Andes, D.; Theuretzbacher, U. Protein Binding: Do We Ever Learn? *Antimicrob. Agents Chemother.* **2011**, *55* (7), 3067–3074.

(74) Sudlow, G.; Birkett, D. J.; Wade, D. N. The Characterization of Two Specific Drug Binding Sites on Human Serum Albumin. *Mol. Pharmacol.* **1975**, *11* (6), 824–832.

(75) Sudlow, G.; Birkett, D. J.; Wade, D. N. Further Characterization of Specific Drug Binding Sites on Human Serum Albumin. *Mol. Pharmacol.* **1976**, *12* (6), 1052–1061.

(76) Yamasaki, K.; Chuang, V. T. G.; Maruyama, T.; Otagiri, M. Albumin-Drug Interaction and Its Clinical Implication. *Biochim. Biophys. Acta* **2013**, *1830* (12), 5435–5443.

(77) Lexa, K. W.; Dolghih, E.; Jacobson, M. P. A Structure-Based Model for Predicting Serum Albumin Binding. *PLoS One* **2014**, *9* (4), e93323.

(78) Bohnert, T.; Gan, L.-S.; Howard, M. L.; Hill, J. J.; Galluppi, G. R.; McLean, M. A. Plasma Protein Binding in Drug Discovery and Development. *Comb. Chem. High Throughput Screen.* **2010**, *13* (9), 170–187.

(79) Handing, K. B.; Shabalin, I. G.; Szlachta, K.; Majorek, K. A.; Minor, W. Crystal Structure of Equine Serum Albumin in Complex with Cetirizine Reveals a Novel Drug Binding Site. *Mol. Immunol.* **2016**, *71*, 143–151.

(80) Wang, Z.; Ho, J. X.; Ruble, J. R.; Rose, J.; Rüker, F.; Ellenburg, M.; Murphy, R.; Click, J.; Soistman, E.; Wilkerson, L.; Carter, D. C. Structural Studies of Several Clinically Important Oncology Drugs in Complex with Human Serum Albumin. *Biochim. Biophys. Acta* **2013**, *1830* (12), 5356–5374.

(81) Ghuman, J.; Zunszain, P. A.; Petitpas, I.; Bhattacharya, A. A.; Otagiri, M.; Curry, S. Structural Basis of the Drug-Binding Specificity of Human Serum Albumin. *J. Mol. Biol.* **2005**, *353* (1), 38–52.

(82) Kratz, F.; Elsadek, B. Clinical Impact of Serum Proteins on Drug Delivery. *J. Control. Release* **2012**, *161* (2), 429–445.

(83) Hervé, F.; Urien, S.; Albengres, E.; Duché, J. C.; Tillement, J. P. Drug Binding in Plasma. A Summary of Recent Trends in the Study of Drug and Hormone Binding. *Clin. Pharmacokinet.* **1994**, *26* (1), 44–58.

(84) Liu, X.; Wright, M.; Hop, C. E. C. A. Rational Use of Plasma Protein and Tissue Binding Data in Drug Design. *J. Med. Chem.* **2014**, *57* (20), 8238–8248.

(85) Sułkowska, A.; Bojko, B.; Równicka, J.; Sułkowski, W. Competition of Drugs to Serum Albumin in Combination Therapy. *Biopolymers* **2004**, *74* (3), 256–262.

(86) Chuang, V. T. G.; Otagiri, M. How Do Fatty Acids Cause Allosteric Binding of Drugs to Human Serum Albumin? *Pharm. Res.* **2002**, *19* (10), 1458–1464.

(87) Petitpas, I.; Petersen, C. E.; Ha, C.; Bhattacharya, A. A.; Zunszain, P. A.; Ghuman, J.; Bhagavan, N. V; Curry, S. Structural Basis of Albumin-Thyroxine Interactions and Familial Dysalbuminemic Hyperthyroxinemia. *Proc. Natl. Acad. Sci. U. S. A.* **2003**, *100* (11), 6440–6445.

(88) Barnett, J. P.; Blindauer, C. A.; Kassaar, O.; Khazaipoul, S.; Martin, E. M.; Sadler, P. J.; Stewart, A. J. Allosteric Modulation of Zinc Speciation by Fatty Acids. *Biochim. Biophys. Acta* **2013**, *1830* (12), 5456–5464.

(89) McElnay, J. C.; D'Arcy, P. F. Protein Binding Displacement Interactions and Their Clinical Importance. *Drugs* **1983**, *25* (5), 495–513.

(90) Davidson, B. L.; Verheijen, S.; Lensing, A. W. A.; Gebel, M.; Brighton, T. A.; Lyons, R. M.; Rehm, J.; Prins, M. H. Bleeding Risk of Patients with Acute Venous Thromboembolism Taking Nonsteroidal Anti-Inflammatory Drugs or Aspirin. *JAMA Intern. Med.* **2014**, *174* (6), 947–953.

(91) Sellers, E. M.; Koch-Weser, J. Kinetics and Clinical Importance of Displacement of Warfarin from Albumin by Acidic Drugs. *Ann. N. Y. Acad. Sci.* **1971**, *179*, 213–225.

(92) Nigam, S. K.; Wu, W.; Bush, K. T.; Hoenig, M. P.; Blantz, R. C.; Bhatnagar, V. Handling of Drugs, Metabolites, and Uremic Toxins by Kidney Proximal Tubule Drug Transporters. *Clin. J. Am. Soc. Nephrol.* **2015**, *10* (11), 2039–2049.

(93) Cistola, D. P.; Small, D. M. Fatty Acid Distribution in Systems Modeling the Normal and Diabetic Human Circulation. A 13C Nuclear Magnetic Resonance Study. *J. Clin. Invest.* **1991**, *87* (4), 1431–1441.

(94) Haeri, H. H.; Schunk, B.; Tomaszewski, J.; Schimm, H.; Gelos, M. J.; Hinderberger, D. Fatty Acid Binding to Human Serum Albumin in Blood Serum Characterized by EPR Spectroscopy. *ChemistryOpen* **2019**, *8* (5), 650–656.

(95) Sueyasu, M.; Fujito, K.; Shuto, H.; Mizokoshi, T.; Kataoka, Y.; Oishi, R. Protein Binding and the Metabolism of Thiamylal Enantiomers in Vitro. *Anesth. Analg.* **2000**, *91* (3), 736–740.

(96) Curry, S.; Mandelkow, H.; Brick, P.; Franks, N. Crystal Structure of Human Serum Albumin Complexed with Fatty Acid Reveals an Asymmetric Distribution of Binding Sites. *Nat. Struct. Biol.* **1998**, *5* (9), 827–835.

(97) Karush, F.; Sonenberg, M. Interaction of Homologous Alkyl Sulfates with Bovine Serum Albumin. *J. Am. Chem. Soc.* **1949**, *71* (4), 1369–1376.

(98) Guide to Equilibrium Dialysis, Harvard Apparatus, https://www.harvardapparatus.com/media/harvard/pdf/Guide to Equilibrium Dialysis.pdf [accessed 09.05.2020].

(99) Sterling, K.; Rosen, P.; Tabachnick, M. Equilibrium Dialysis Studies of the Binding of Thyroxine by Human Serum Albumin. *J. Clin. Invest.* **1962**, *41* (5), 1021–1030.

(100) Viaene, L.; Annaert, P.; de Loor, H.; Poesen, R.; Evenepoel, P.; Meijers, B. Albumin Is the Main Plasma Binding Protein for Indoxyl Sulfate and p -Cresyl Sulfate. *Biopharm. Drug Dispos.* **2013**, *34* (3), 165–175.

(101) Wilting, J.; 'T Hart, B. J.; De Gier, J. J.; Hart, B. J.; De Gier, J. J. The Role of Albumin Conformation in the Binding of Diazepam to Human Serum Albumin. *Biochim. Biophys. Acta - Protein Struct.* **1980**, *626* (2), 291–298.

(102) Vermeulen, A.; Verdonck, L. Studies on the Binding of Testosterone to Human Plasma. *Steroids* **1968**, *11* (5), 609–635.

(103) Metsu, D.; Lanot, T.; Fraissinet, F.; Concordet, D.; Gayrard, V.; Averseng, M.; Ressault, A.; Martin-Blondel, G.; Levade, T.; Février, F.; Chatelut, E.; Delobel, P.; Gandia, P. Comparing Ultrafiltration and Equilibrium Dialysis to Measure Unbound Plasma Dolutegravir Concentrations Based on a Design of Experiment Approach. *Sci. Rep.* **2020**, *10* (1), 12265.

(104) Yang, B.; Zheng, X.; Hage, D. S. Binding Studies Based on Ultrafast Affinity Extraction and Single- or Two-Column Systems: Interactions of Second- and Third-Generation Sulfonylurea Drugs with Normal or Glycated Human Serum Albumin. *J. Chromatogr. B* **2018**, *1102–1103*, 8–16.

(105) Czub, M. P.; Venkataramany, B. S.; Majorek, K. A.; Handing, K. B.; Porebski, P. J.; Beeram, S. R.; Suh, K.; Woolfork, A. G.; Hage, D. S.; Shabalin, I. G.; Minor, W. Testosterone Meets Albumin - the Molecular Mechanism of Sex Hormone Transport by Serum Albumins. *Chem. Sci.* **2019**, *10* (6), 1607–1618.

(106) Zheng, X.; Matsuda, R.; Hage, D. S. Analysis of Free Drug Fractions by Ultrafast Affinity Extraction: Interactions of Sulfonylurea Drugs with Normal or Glycated Human Serum Albumin. *J. Chromatogr. A* **2014**.

(107) Tao, P.; Li, Z.; Woolfork, A. G.; Hage, D. S. Characterization of Tolazamide Binding with Glycated and Normal Human Serum Albumin by Using High-Performance Affinity Chromatography. *J. Pharm. Biomed. Anal.* **2019**, *166*, 273–280.

(108) Rich, R. L.; Day, Y. S. N.; Morton, T. A.; Myszka, D. G. High-Resolution and High-Throughput Protocols for Measuring Drug/Human Serum Albumin Interactions Using BIACORE. *Anal. Biochem.* **2001**, *296* (2), 197–207.

(109) Markey, F. Principles of Surface Plasmon Resonance. In *Real-Time Analysis of Biomolecular Interactions*; Springer Japan: Tokyo, 2000; pp 13–22.

(110) Shah, N. B.; Duncan, T. M. Bio-Layer Interferometry for Measuring Kinetics of Protein-Protein Interactions and Allosteric Ligand Effects. *J. Vis. Exp.* **2014**, No. 84.

(111) Wani, T. A.; Bakheit, A. H.; Abounassif, M. A.; Zargar, S. Study of Interactions of an Anticancer Drug Neratinib With Bovine Serum Albumin: Spectroscopic and Molecular Docking Approach. *Front. Chem.* **2018**, *6*, 47.

(112) Protein Fluorescence. In *Principles of Fluorescence Spectroscopy*; Springer US: Boston, MA, 2006; pp 529–575.

(113) Mansoor, S. E.; Dewitt, M. A.; Farrens, D. L. Distance Mapping in Proteins Using Fluorescence Spectroscopy: The Tryptophan-Induced Quenching (TrIQ) Method. *Biochemistry* **2010**, *49* (45), 9722–9731.

(114) Hevener, K. E.; Pesavento, R.; Ren, J.; Lee, H.; Ratia, K.; Johnson, M. E. Hit-to-Lead: Hit Validation and Assessment; 2018; pp 265–309.

(115) Zielinski, K.; Sekula, B.; Bujacz, A.; Szymczak, I. Structural Investigations of Stereoselective Profen Binding by Equine and Leporine Serum Albumins. *Chirality* **2020**, *32* (3), 334–344.

(116) Afrin, S.; Rahman, Y.; Tabish, M. Elucidating the Interaction of Ticlopidine with Serum Albumin and Its Role in Bilirubin Displacement in Vitro. *J. Biomol. Struct. Dyn.* **2019**, *37* (4), 863–876.

(117) Ràfols, C.; Zarza, S.; Bosch, E. Molecular Interactions between Some Non-Steroidal Anti-Inflammatory Drugs (NSAID's) and Bovine (BSA) or Human (HSA) Serum Albumin Estimated by Means of Isothermal Titration Calorimetry (ITC) and Frontal Analysis Capillary Electrophoresis (FA/CE). *Talanta* **2014**, *130*, 241–250.

(118) Bhattacharya, A. A.; Curry, S.; Franks, N. P. Binding of the General Anesthetics Propofol and Halothane to Human Serum Albumin: High Resolution Crystal Structures. *J. Biol. Chem.* **2000**, *275* (49), 38731–38738.

(119) Hein, K. L.; Kragh-Hansen, U.; Morth, J. P.; Jeppesen, M. D.; Otzen, D.; Møller, J. V; Nissen, P. Crystallographic Analysis Reveals a Unique Lidocaine Binding Site on Human Serum Albumin. *J. Struct. Biol.* **2010**, *171* (3), 353–360.

(120) Zunszain, P. A.; Ghuman, J.; McDonagh, A. F.; Curry, S. Crystallographic Analysis of Human Serum Albumin Complexed with 4Z,15E-Bilirubin-IXalpha. *J. Mol. Biol.* **2008**, *381* (2), 394–406.

(121) Petitpas, I.; Bhattacharya, A. A.; Twine, S.; East, M.; Curry, S. Crystal Structure Analysis of Warfarin Binding to Human Serum Albumin: Anatomy of Drug Site I. *J. Biol. Chem.* **2001**, *276* (25), 22804–22809.

(122) Sakurama, K.; Kawai, A.; Tuan Giam Chuang, V.; Kanamori, Y.; Osa, M.; Taguchi, K.; Seo, H.; Maruyama, T.; Imoto, S.; Yamasaki, K.; Otagiri, M. Analysis of the Binding of Aripiprazole to Human Serum Albumin: The Importance of a Chloro-Group in the Chemical Structure. *ACS omega* **2018**, *3* (10), 13790–13797.

(123) Yang, F.; Lee, P.; Ma, Z.; Ma, L.; Yang, G.; Wu, X.; Liang, H. Regulation of Amantadine Hydrochloride Binding with IIA Subdomain of Human Serum Albumin by Fatty Acid Chains. *J. Pharm. Sci.* **2013**, *102* (1), 84–92.

(124) Zhu, L.; Yang, F.; Chen, L.; Meehan, E. J.; Huang, M. A New Drug Binding Subsite

on Human Serum Albumin and Drug-Drug Interaction Studied by X-Ray Crystallography. *J. Struct. Biol.* **2008**, *162* (1), 40–49.

(125) Kawai, A.; Yamasaki, K.; Enokida, T.; Miyamoto, S.; Otagiri, M. Crystal Structure Analysis of Human Serum Albumin Complexed with Sodium 4-Phenylbutyrate. *Biochem. Biophys. reports* **2018**, *13*, 78–82.

(126) Yang, F.; Bian, C.; Zhu, L.; Zhao, G.; Huang, Z.; Huang, M. Effect of Human Serum Albumin on Drug Metabolism: Structural Evidence of Esterase Activity of Human Serum Albumin. *J. Struct. Biol.* **2007**, *157* (2), 348–355.

(127) Zhang, Y.; Lee, P.; Liang, S.; Zhou, Z.; Wu, X.; Yang, F.; Liang, H. Structural Basis of Non-Steroidal Anti-Inflammatory Drug Diclofenac Binding to Human Serum Albumin. *Chem. Biol. Drug Des.* **2015**, *86* (5), 1178–1184.

(128) Sekula, B.; Bujacz, A. Structural Insights into the Competitive Binding of Diclofenac and Naproxen by Equine Serum Albumin. *J. Med. Chem.* **2016**, *59* (1), 82–89.

(129) Castagna, R.; Donini, S.; Colnago, P.; Serafini, A.; Parisini, E.; Bertarelli, C. Biohybrid Electrospun Membrane for the Filtration of Ketoprofen Drug from Water. *ACS omega* **2019**, *4* (8), 13270–13278.

(130) Lejon, S.; Cramer, J. F.; Nordberg, P. Structural Basis for the Binding of Naproxen to Human Serum Albumin in the Presence of Fatty Acids and the GA Module. *Acta Crystallogr. Sect. F. Struct. Biol. Cryst. Commun.* **2008**, *64* (Pt 2), 64–69.

(131) Bujacz, A.; Zielinski, K.; Sekula, B. Structural Studies of Bovine, Equine, and Leporine Serum Albumin Complexes with Naproxen. *Proteins* **2014**, *82* (9), 2199–2208.

(132) Wenskowsky, L.; Wagner, M.; Reusch, J.; Schreuder, H.; Matter, H.; Opatz, T.; Petry, S. M. Resolving Binding Events on the Multifunctional Human Serum Albumin. *ChemMedChem* **2020**, *15* (9), 738–743.

(133) Drugs.Com: Prednisone and Other Corticosteroids Entry, Www.Drugs.Com/Mca/Prednisone-and-Other-Corticosteroids [Accessed 08.26.20].

(134) Rooyackers, O. E.; Nair, K. S. Hormonal Regulation of Human Muscle Protein Metabolism. *Annu. Rev. Nutr.* **1997**, *17* (1), 457–485.

(135) Melmed, S.; Polonsky, K. S.; Larsen, P. R.; Kronenberg, H. M. *Williams Textbook of Endocrinology*, 13th ed.; Elsevier: Los Angeles, CA, USA, 2016.

(136) Taraborrelli, S. Physiology, Production and Action of Progesterone. *Acta Obstet. Gynecol. Scand.* **2015**, *94*, 8–16.

(137) Carmina, E.; Stanczyk, F. Z.; Lobo, R. A. Laboratory Assessment. In *Yen & Jaffe's Reproductive Endocrinology*; Elsevier, 2014; pp 822-850.e3.

(138) Drugbank: progesterone entry, https://www.drugbank.ca/drugs/DB00396 [accessed 08.24.2020].

(139) Yuanjing, C.; Li, K.; Pu, H.; Wu, T. Corticosteroids for Pneumonia. In *Cochrane Database of Systematic Reviews*; Wu, T., Ed.; John Wiley & Sons, Ltd: Chichester, UK, 2009.

(140) DrugBank, dexamethasone entry: https://www.drugbank.ca/drugs/DB01234 [accessed 06.24.2020].

(141) RECOVERY Collaborative Group; Horby, P.; Lim, W. S.; Emberson, J. R.; Mafham, M.; Bell, J. L.; Linsell, L.; Staplin, N.; Brightling, C.; Ustianowski, A.; Elmahi, E.; Prudon, B.; Green, C.; Felton, T.; Chadwick, D.; Rege, K.; Fegan, C.; Chappell, L. C.; Faust, S. N.; Jaki, T.; Jeffery, K.; Montgomery, A.; Rowan, K.; Juszczak, E.; Baillie, J. K.; Haynes, R.; Landray, M. J. Dexamethasone in Hospitalized Patients with Covid-19 - Preliminary Report. *N. Engl. J. Med.* **2020**, NEJMoa2021436.

(142) Drugs.com: hydrocortisone entry, https://www.drugs.com/monograph/hydrocortisone.html [accessed 08.24.2020].

(143) Oakley, R. H.; Cidlowski, J. A. The Biology of the Glucocorticoid Receptor: New Signaling Mechanisms in Health and Disease. *J. Allergy Clin. Immunol.* **2013**, *132* (5), 1033–1044.

(144) Conaghan, P. G. A Turbulent Decade for NSAIDs: Update on Current Concepts of Classification, Epidemiology, Comparative Efficacy, and Toxicity. *Rheumatol. Int.* **2012**, *32* (6), 1491–1502.

(145) Zhou, Y.; Boudreau, D. M.; Freedman, A. N. Trends in the Use of Aspirin and Nonsteroidal Anti-Inflammatory Drugs in the General U.S. Population. *Pharmacoepidemiol. Drug Saf.* **2014**, *23* (1), 43–50.

(146) Singh, G. Gastrointestinal Complications of Prescription and Over-the-Counter Nonsteroidal Anti-Inflammatory Drugs: A View from the ARAMIS Database. Arthritis, Rheumatism, and Aging Medical Information System. *Am. J. Ther.* **2000**, *7* (2), 115–121.

(147) Argoff, C. NSAIDs or Opioids, Damned If You Do, Damned If You Don't?: Evidence-Based Selections to Optimize Therapeutic Goals and Minimize Harms. *Pain Med.* **2013**, *14 Suppl 1*, S40-2.

(148) Beretta, C.; Garavaglia, G.; Cavalli, M. COX-1 and COX-2 Inhibition in Horse Blood by Phenylbutazone, Flunixin, Carprofen and Meloxicam: An in Vitro Analysis. *Pharmacol. Res.* **2005**, *52* (4), 302–306.

(149) Landoni, M. F.; Lees, P. Pharmacokinetics and Pharmacodynamics of Ketoprofen Enantiomers in the Horse. *J. Vet. Pharmacol. Ther.* **1996**, *19* (6), 466–474.

(150) Lascelles, B. D. X.; McFarland, J. M.; Swann, H. Guidelines for Safe and Effective

Use of NSAIDs in Dogs. *Vet. Ther.* **2005**, *6* (3), 237–251.

(151) Ricciotti, E.; FitzGerald, G. A. Prostaglandins and Inflammation. *Arterioscler. Thromb. Vasc. Biol.* **2011**, *31* (5), 986–1000.

(152) Sugimoto, Y.; Yamasaki, A.; Segi, E.; Tsuboi, K.; Aze, Y.; Nishimura, T.; Oida, H.; Yoshida, N.; Tanaka, T.; Katsuyama, M.; Hasumoto, K.; Murata, T.; Hirata, M.; Ushikubi, F.; Negishi, M.; Ichikawa, A.; Narumiya, S. Failure of Parturition in Mice Lacking the Prostaglandin F Receptor. *Science* **1997**, *277* (5326), 681–683.

(153) Hayball, P. J. Chirality and Nonsteroidal Anti-Inflammatory Drugs. *Drugs* **1996**, *52 Suppl 5*, 47–58.

(154) Evans, A. M. Comparative Pharmacology of S(+)-Ibuprofen and (RS)-Ibuprofen. *Clin. Rheumatol.* **2001**, *20 Suppl 1*, S9-14.

(155) Neupert, W.; Brugger, R.; Euchenhofer, C.; Brune, K.; Geisslinger, G. Effects of Ibuprofen Enantiomers and Its Coenzyme A Thioesters on Human Prostaglandin Endoperoxide Synthases. *Br. J. Pharmacol.* **1997**, *122* (3), 487–492.

(156) Ghezzi, P.; Melillo, G.; Meazza, C.; Sacco, S.; Pellegrini, L.; Asti, C.; Porzio, S.; Marullo, A.; Sabbatini, V.; Caselli, G.; Bertini, R. Differential Contribution of R and S Isomers in Ketoprofen Anti-Inflammatory Activity: Role of Cytokine Modulation. *J. Pharmacol. Exp. Ther.* **1998**, *287* (3), 969–974.

(157) Kolluri, S. K.; Corr, M.; James, S. Y.; Bernasconi, M.; Lu, D.; Liu, W.; Cottam, H. B.; Leoni, L. M.; Carson, D. A.; Zhang, X. The R-Enantiomer of the Nonsteroidal Antiinflammatory Drug Etodolac Binds Retinoid X Receptor and Induces Tumor-Selective Apoptosis. *Proc. Natl. Acad. Sci. U. S. A.* **2005**, *102* (7), 2525–2530.

(158) Inoue, N.; Nogawa, M.; Ito, S.; Tajima, K.; Kume, S.; Kyoi, T. The Enantiomers of Etodolac, a Racemic Anti-Inflammatory Agent, Play Different Roles in Efficacy and Gastrointestinal Safety. *Biol. Pharm. Bull.* **2011**, *34* (5), 655–659.

(159) Verbeeck, R. K.; Blackburn, J. L.; Loewen, G. R. Clinical Pharmacokinetics of Non-Steroidal Anti-Inflammatory Drugs. *Clin. Pharmacokinet.* **1983**, *8* (4), 297–331.

(160) Drugbank: warfarin entry, https://www.drugbank.ca/drugs/DB00682, [accessed 08.24.2020].

(161) Hou, J.; Zheng, J.; Shamsi, S. A. Separation and Determination of Warfarin Enantiomers in Human Plasma Using a Novel Polymeric Surfactant for Micellar Electrokinetic Chromatography-Mass Spectrometry. *J. Chromatogr. A* **2007**, *1159* (1–2), 208–216.

(162) Kuruvilla, M.; Gurk-Turner, C. A Review of Warfarin Dosing and Monitoring. *Proc. (Bayl. Univ. Med. Cent).* **2001**, *14* (3), 305–306.

(163) Teklay, G.; Shiferaw, N.; Legesse, B.; Bekele, M. L. Drug-Drug Interactions and Risk of Bleeding among Inpatients on Warfarin Therapy: A Prospective Observational

Study. *Thromb. J.* **2014**, *12*, 20.

(164) Drugs.com: tolbutamide entry, https://www.drugs.com/pro/tolbutamide.html [accessed 08.25.20].

(165) Drugbank: tolbutamide entry, https://www.drugbank.ca/drugs/DB01124 [acccessed 08.25.20].

(166) Thiessen, J. J.; Sellers, E. M.; Denbeigh, P.; Dolman, L. Plasma Protein Binding of Diazepam and Tolbutamide in Chronic Alcoholics. *J. Clin. Pharmacol.* **1976**, *16* (7), 345–351.

(167) Joseph, K. S.; Anguizola, J.; Hage, D. S. Binding of Tolbutamide to Glycated Human Serum Albumin. *J. Pharm. Biomed. Anal.* **2011**, *54* (2), 426–432.

(168) Joseph, K. S.; Hage, D. S. Characterization of the Binding of Sulfonylurea Drugs to HSA by High-Performance Affinity Chromatography. *J. Chromatogr. B. Analyt. Technol. Biomed. Life Sci.* **2010**, *878* (19), 1590–1598.

(169) Yoo, M. J.; Hage, D. S. Use of Peak Decay Analysis and Affinity Microcolumns Containing Silica Monoliths for Rapid Determination of Drug-Protein Dissociation Rates. *J. Chromatogr. A* **2011**, *1218* (15), 2072–2078.

(170) Dold, M.; Samara, M. T.; Li, C.; Tardy, M.; Leucht, S. Haloperidol versus First-Generation Antipsychotics for the Treatment of Schizophrenia and Other Psychotic Disorders. *Cochrane database Syst. Rev.* **2015**, *1*, CD009831.

(171) Drugs.com: haloperidol entry, https://www.drugs.com/monograph/haloperidol.html [accessed 08.25.20].

(172) Drugbank: haloperidol entry, https://www.drugbank.ca/drugs/DB00502 [accessed 08.25.20].

(173) Boks, M. P. M. Epigenetic Effects of Currently Used Psychotropic Drugs. In *Epigenetics in Psychiatry*; Elsevier, 2014; pp 481–496.

(174) Hughes, I.; Jellett, L.; Ilett, K. The Influence of Various Factors in the in Vitro Distribution of Haloperidol in Human Blood. *Br. J. Clin. Pharmacol.* **1976**, *3* (2), 285–288.

(175) Berić, J. D.; Stojanović, S. D.; Mrkalić, E. M.; Matović, Z. D.; Milovanović, D. R.; Sovrlić, M. M.; Jelić, R. M. Interaction of Haloperidol with Human Serum Albumin and Effect of Metal Ions on the Binding. *Monatshefte für Chemie - Chem. Mon.* **2018**, *149* (12), 2359–2368.

(176) Drugs.com: ampicillin entry, https://www.drugs.com/mtm/ampicillin.html [accessed 08.26.20].

(177) Drugbank: Ampicillin Entry, Https://Www.Drugbank.ca/Drugs/DB00415 [Accessed 08.26.20].

(178) Rolinson, G. N.; Sutherland, R. The Binding of Antibiotics to Serum Proteins. *Br. J. Pharmacol. Chemother.* **1965**, *25* (3), 638–650.

(179) Hutchins, J. E.; Tyczkowska, K.; Aronson, A. L. Determination of Ampicillin in Serum by Using Simple Ultrafiltration Technique and Liquid Chromatographic Analysis. *J. Assoc. Off. Anal. Chem.* **1986**, *69* (5), 757–759.

(180) Wong, G.; Briscoe, S.; Adnan, S.; McWhinney, B.; Ungerer, J.; Lipman, J.; Roberts, J. A. Protein Binding of β-Lactam Antibiotics in Critically Ill Patients: Can We Successfully Predict Unbound Concentrations? *Antimicrob. Agents Chemother.* **2013**, *57* (12), 6165–6170.

(181) Bundgaard, H.; Hansen, J. Reaction of Ampicillin with Serum Albumin to Produce Penicilloyl-Protein Conjugates and a Piperazinedione. *J. Pharm. Pharmacol.* **1982**, *34* (5), 304–309.

(182) Lazo, J. S.; Blanco, I. K.; Tasker, N. R.; Rastelli, E. J.; Burnett, J. C.; Garrott, S. R.; Hart, D. J.; McCloud, R. L.; Hsu, K.-L.; Wipf, P.; Sharlow, E. R. Next-Generation Cell-Active Inhibitors of the Undrugged Oncogenic PTP4A3 Phosphatase. *J. Pharmacol. Exp. Ther.* **2019**, *371* (3), 652–662.

(183) McQueeney, K. E.; Salamoun, J. M.; Burnett, J. C.; Barabutis, N.; Pekic, P.; Lewandowski, S. L.; Llaneza, D. C.; Cornelison, R.; Bai, Y.; Zhang, Z.-Y.; Catravas, J. D.; Landen, C. N.; Wipf, P.; Lazo, J. S.; Sharlow, E. R. Targeting Ovarian Cancer and Endothelium with an Allosteric PTP4A3 Phosphatase Inhibitor. *Oncotarget* **2018**, *9* (9), 8223–8240.

(184) Tasker, N. R.; Rastelli, E. J.; Burnett, J. C.; Sharlow, E. R.; Lazo, J. S.; Wipf, P. Tapping the Therapeutic Potential of Protein Tyrosine Phosphatase 4A with Small Molecule Inhibitors. *Bioorg. Med. Chem. Lett.* **2019**, *29* (16), 2008–2015.

(185) Wei, M.; Haney, M. G.; Rivas, D. R.; Blackburn, J. S. Protein Tyrosine Phosphatase 4A3 (PTP4A3/PRL-3) Drives Migration and Progression of T-Cell Acute Lymphoblastic Leukemia in Vitro and in Vivo. *Oncogenesis* **2020**, *9* (1), 6.

(186) Czub, M. P.; Boulton, A. M.; Rastelli, E. J.; Tasker, N. R.; Maskrey, T. S.; Blanco, I. K.; McQueeney, K. E.; Bushweller, J. H.; Minor, W.; Wipf, P.; Sharlow, E. R.; Lazo, J. S. Structure of the Complex of an Iminopyridinedione PTP4A3 Phosphatase Inhibitor with Human Serum Albumin. *Mol. Pharmacol.* **2020**, MOLPHARM-AR-2020-000131.

(187) Drugbank: prezatide entry, https://www.drugbank.ca/drugs/DB11296 [accessed 08.27.20].

(188) Pickart, L.; Margolina, A. Regenerative and Protective Actions of the GHK-Cu Peptide in the Light of the New Gene Data. *Int. J. Mol. Sci.* **2018**, *19* (7).

(189) Pickart, L.; Vasquez-Soltero, J. M.; Margolina, A. GHK Peptide as a Natural Modulator of Multiple Cellular Pathways in Skin Regeneration. *Biomed Res. Int.*

2015, *2015*, 648108.

(190) Pickart, L. The Human Tri-Peptide GHK and Tissue Remodeling. *J. Biomater. Sci. Polym. Ed.* **2008**, *19* (8), 969–988.

(191) Salamoun, J. M.; McQueeney, K. E.; Patil, K.; Geib, S. J.; Sharlow, E. R.; Lazo, J. S.; Wipf, P. Photooxygenation of an Amino-Thienopyridone Yields a More Potent PTP4A3 Inhibitor. *Org. Biomol. Chem.* **2016**, *14* (27), 6398–6402.

(192) Grabowski, M.; Cymborowski, M.; Porebski, P. J.; Osinski, T.; Shabalin, I. G.; Cooper, D. R.; Minor, W. The Integrated Resource for Reproducibility in Macromolecular Crystallography: Experiences of the First Four Years. *Struct. Dyn.* **2019**, *6* (6), 064301.

(193) Otwinowski, Z.; Minor, W. Processing of X-Ray Diffraction Data Collected in Oscillation Mode. *Methods Enzymol.* **1997**, *276*, 307–326.

(194) Minor, W.; Cymborowski, M.; Otwinowski, Z.; Chruszcz, M. HKL-3000: The Integration of Data Reduction and Structure Solution-from Diffraction Images to an Initial Model in Minutes. *Acta Crystallogr. D. Biol. Crystallogr.* **2006**, *62* (Pt 8), 859–866.

(195) Borek, D.; Cymborowski, M.; Machius, M.; Minor, W.; Otwinowski, Z. Diffraction Data Analysis in the Presence of Radiation Damage. *Acta Crystallogr. D. Biol. Crystallogr.* **2010**, *66* (Pt 4), 426–436.

(196) Luo, Z.; Rajashankar, K.; Dauter, Z. Weak Data Do Not Make a Free Lunch, Only a Cheap Meal. *Acta Crystallogr. D. Biol. Crystallogr.* **2014**, *70* (Pt 2), 253–260.

(197) Porebski, P. J.; Cymborowski, M.; Pasenkiewicz-Gierula, M.; Minor, W. Fitmunk: Improving Protein Structures by Accurate, Automatic Modeling of Side-Chain Conformations. *Acta Crystallogr. Sect. D, Struct. Biol.* **2016**, *72* (Pt 2), 266–280.

(198) Vagin, A.; Teplyakov, A. Molecular Replacement with MOLREP. *Acta Crystallogr. D. Biol. Crystallogr.* **2010**, *66* (Pt 1), 22–25.

(199) Murshudov, G. N.; Skubák, P.; Lebedev, A. A.; Pannu, N. S.; Steiner, R. A.; Nicholls, R. A.; Winn, M. D.; Long, F.; Vagin, A. A. REFMAC5 for the Refinement of Macromolecular Crystal Structures. *Acta Crystallogr. D. Biol. Crystallogr.* **2011**, *67* (Pt 4), 355–367.

(200) Winn, M. D.; Ballard, C. C.; Cowtan, K. D.; Dodson, E. J.; Emsley, P.; Evans, P. R.; Keegan, R. M.; Krissinel, E. B.; Leslie, A. G. W.; McCoy, A.; McNicholas, S. J.; Murshudov, G. N.; Pannu, N. S.; Potterton, E. A.; Powell, H. R.; Read, R. J.; Vagin, A.; Wilson, K. S. Overview of the CCP4 Suite and Current Developments. *Acta Crystallogr. D. Biol. Crystallogr.* **2011**, *67* (4), 235–242.

(201) Emsley, P.; Cowtan, K. Coot: Model-Building Tools for Molecular Graphics. *Acta Crystallogr. Sect. D Biol. Crystallogr.* **2004**, *60* (12 I), 2126–2132.

(202) Emsley, P.; Lohkamp, B.; Scott, W. G.; Cowtan, K. Features and Development of Coot. *Acta Crystallogr. D. Biol. Crystallogr.* **2010**, *66* (Pt 4), 486–501.

(203) Shabalin, I. G.; Porebski, P. J.; Minor, W. Refining the Macromolecular Model - Achieving the Best Agreement with the Data from X-Ray Diffraction Experiment. *Crystallogr. Rev.* **2018**, *24* (4), 236–262.

(204) Kumar, A.; Chiu, H. J.; Axelrod, H. L.; Morse, A.; Elsliger, M. A.; Wilson, I. A.; Deacon, A. Ligands in PSI Structures. *Acta Crystallogr. Sect. F. Struct. Biol. Cryst. Commun.* **2010**, *66* (Pt 10), 1309–1316.

(205) Kowiel, M.; Jaskolski, M.; Dauter, Z. ACHESYM: An Algorithm and Server for Standardized Placement of Macromolecular Models in the Unit Cell. *Acta Crystallogr. D. Biol. Crystallogr.* **2014**, *70* (Pt 12), 3290–3298.

(206) Painter, J.; Merritt, E. A. Optimal Description of a Protein Structure in Terms of Multiple Groups Undergoing TLS Motion. *Acta Crystallogr. Sect. D Biol. Crystallogr.* **2006**, *62* (4), 439–450.

(207) Merritt, E. A. To B or Not to B: A Question of Resolution? *Acta Crystallogr. D. Biol. Crystallogr.* **2012**, *68* (Pt 4), 468–477.

(208) Majorek, K. A.; Zimmerman, M. D.; Grabowski, M.; Shabalin, I. G.; Zheng, H.; Minor, W. Assessment of Crystallographic Structure Quality and Protein–Ligand Complex Structure Validation. In *Structural Biology in Drug Discovery*; Wiley, 2020; pp 253–275.

(209) Web Grade Server, http://grade.globalphasing.org/ [accessed 08.09.2020].

(210) Long, F.; Nicholls, R. A.; Emsley, P.; Graæulis, S.; Merkys, A.; Vaitkus, A.; Murshudov, G. N. AceDRG: A Stereochemical Description Generator for Ligands. *Acta Crystallogr. Sect. D, Struct. Biol.* **2017**, *73* (Pt 2), 112–122.

(211) Chen, V. B.; Arendall, W. B.; Headd, J. J.; Keedy, D. A.; Immormino, R. M.; Kapral, G. J.; Murray, L. W.; Richardson, J. S.; Richardson, D. C. MolProbity: All-Atom Structure Validation for Macromolecular Crystallography. *Acta Crystallogr. D. Biol. Crystallogr.* **2010**, *66* (Pt 1), 12–21.

(212) Gore, S.; Sanz García, E.; Hendrickx, P. M. S.; Gutmanas, A.; Westbrook, J. D.; Yang, H.; Feng, Z.; Baskaran, K.; Berrisford, J. M.; Hudson, B. P.; Ikegawa, Y.; Kobayashi, N.; Lawson, C. L.; Mading, S.; Mak, L.; Mukhopadhyay, A.; Oldfield, T. J.; Patwardhan, A.; Peisach, E.; Sahni, G.; Sekharan, M. R.; Sen, S.; Shao, C.; Smart, O. S.; Ulrich, E. L.; Yamashita, R.; Quesada, M.; Young, J. Y.; Nakamura, H.; Markley, J. L.; Berman, H. M.; Burley, S. K.; Velankar, S.; Kleywegt, G. J. Validation of Structures in the Protein Data Bank. *Structure* **2017**, *25* (12), 1916–1927.

(213) Zimmerman, M. D.; Grabowski, M.; Domagalski, M. J.; Maclean, E. M.; Chruszcz, M.; Minor, W. Data Management in the Modern Structural Biology and Biomedical Research Environment. *Methods Mol. Biol.* **2014**, *1140*, 1–25.

(214) Cooper, D. R.; Grabowski, M.; Zimmerman, M. D.; Porebski, P. J.; Shabalin, I. G.; Woinska, M.; Domagalski, M. J.; Zheng, H.; Sroka, P.; Cymborowski, M.; Czub, M. P.; Niedzialkowska, E.; Venkataramany, B. S.; Osinski, T.; Fratczak, Z.; Bajor, J.; Gonera, J.; MacLean, E.; Wojciechowska, K.; Wajerowicz, W.; Chruszcz, M.; Minor, W. State-of-the-Art Data Management: Improving the Reproducibility, Consistency, and Traceability of Structural Biology and In Vitro Biochemical Experiments. In *Structural Genomics: General Applications, Methods in Molecular Biology*; Yiu, Yu Wai Chen, C.-P. B., Ed.; Springer, 2020.

(215) Porebski, P. J.; Sroka, P.; Zheng, H.; Cooper, D. R.; Minor, W. Molstack-Interactive Visualization Tool for Presentation, Interpretation, and Validation of Macromolecules and Electron Density Maps. *Protein Sci.* **2018**, *27* (1), 86–94.

(216) Porebski, P. J.; Bokota, G.; Venkataramany, B. S.; Minor, W. Molstack: A Platform for Interactive Presentations of Electron Density and Cryo-EM Maps and Their Interpretations. *Protein Sci.* **2020**, *29* (1), 120–127.

(217) Grabowski, M.; Langner, K. M.; Cymborowski, M.; Porebski, P. J.; Sroka, P.; Zheng, H.; Cooper, D. R.; Zimmerman, M. D.; Elsliger, M. A.; Burley, S. K.; Minor, W. A Public Database of Macromolecular Diffraction Experiments. *Acta Crystallogr. Sect. D, Struct. Biol.* **2016**, *72* (Pt 11), 1181–1193.

(218) Grabowski, M.; Cymborowski, M.; Porebski, P. J.; Osinski, T.; Shabalin, I. G.; Cooper, D. R.; Minor, W. The Integrated Resource for Reproducibility in Macromolecular Crystallography: Experiences of the First Four Years. *Struct. Dyn. (Melville, N.Y.)* **2019**, *6* (6), 064301.

(219) van de Weert, M.; Stella, L. Fluorescence Quenching and Ligand Binding: A Critical Discussion of a Popular Methodology. *J. Mol. Struct.* **2011**, *998* (1–3), 144–150.

(220) Ehrenberg, M.; Cronvall, E.; Rigler, R. Fluorescence of Proteins Interacting with Nucleic Acids. Correction for Light Absorption. *FEBS Lett.* **1971**, *18* (2), 199–203.

(221) Zheng, X.; Bi, C.; Brooks, M.; Hage, D. S. Analysis of Hormone-Protein Binding in Solution by Ultrafast Affinity Extraction: Interactions of Testosterone with Human Serum Albumin and Sex Hormone Binding Globulin. *Anal. Chem.* **2015**, *87* (22), 11187–11194.

(222) Mallik, R.; Yoo, M. J.; Briscoe, C. J.; Hage, D. S. Analysis of Drug-Protein Binding by Ultrafast Affinity Chromatography Using Immobilized Human Serum Albumin. *J. Chromatogr. A* **2010**, *1217* (17), 2796–2803.

(223) Zheng, X.; Li, Z.; Podariu, M. I.; Hage, D. S. Determination of Rate Constants and Equilibrium Constants for Solution-Phase Drug-Protein Interactions by Ultrafast Affinity Extraction. *Anal. Chem.* **2014**, *86* (13), 6454–6460.

(224) Holm, L.; Laakso, L. M. Dali Server Update. *Nucleic Acids Res.* **2016**, *44* (W1), W351-5.

(225) UniProt Consortium, T. UniProt: The Universal Protein Knowledgebase. *Nucleic Acids Res.* **2018**, *46* (5), 2699–2699.

(226) Zheng, H.; Cooper, D. R.; Porebski, P. J.; Shabalin, I. G.; Handing, K. B.; Minor, W. CheckMyMetal: A Macromolecular Metal-Binding Validation Tool. *Acta Crystallogr. Sect. D, Struct. Biol.* **2017**, *73* (Pt 3), 223–233.

(227) Rice, P.; Longden, I.; Bleasby, A. EMBOSS: The European Molecular Biology Open Software Suite. *Trends Genet.* **2000**, *16* (6), 276–277.

(228) Czub, M. P.; Handing, K. B.; Venkataramany, B. S.; Cooper, D. R.; Shabalin, I. G.; Minor, W. Albumin-Based Transport of Nonsteroidal Anti-Inflammatory Drugs in Mammalian Blood Plasma. *J. Med. Chem.* **2020**, *63* (13), 6847–6862.

(229) Holm, L.; Rosenström, P. Dali Server: Conservation Mapping in 3D. *Nucleic Acids Res.* **2010**, *38* (Web Server issue), W545-9.

(230) Bertolini, J.; Goss, N.; Curling, J. *Production of Plasma Proteins for Therapeutic Use*; Bertolini, J., Goss, N., Curling, J., Eds.; John Wiley & Sons, Inc.: Hoboken, NJ, USA, 2013.

(231) Batista, A. N. L.; Batista, J. M.; Ashton, L.; Bolzani, V. S.; Furlan, M.; Blanch, E. W. Investigation of DMSO-Induced Conformational Transitions in Human Serum Albumin Using Two-Dimensional Raman Optical Activity Spectroscopy. *Chirality* **2014**, *26* (9), 497–501.

(232) Pearlman, W. H.; Crépy, O. Steroid-Protein Interaction with Particular Reference to Testosterone Binding by Human Serum. *J. Biol. Chem.* **1967**, *242* (2), 182–189.

(233) Costello, L. C.; Franklin, R. B. Plasma Citrate Homeostasis: How It Is Regulated; and Its Physiological and Clinical Implications. An Important, but Neglected, Relationship in Medicine. *HSOA J. Hum. Endocrinol.* **2016**, *1* (1), 1–19.

(234) Curry, S. Beyond Expansion: Structural Studies on the Transport Roles of Human Serum Albumin. *Vox Sang.* **2002**, *83 Suppl 1*, 315–319.

(235) Naldi, M.; Baldassarre, M.; Nati, M.; Laggetta, M.; Giannone, F. A.; Domenicali, M.; Bernardi, M.; Caraceni, P.; Bertucci, C. Mass Spectrometric Characterization of Human Serum Albumin Dimer: A New Potential Biomarker in Chronic Liver Diseases. *J. Pharm. Biomed. Anal.* **2015**, *112*, 169–175.

(236) Sigma-Aldrich: Ampicillin Product Information, https://www.sigmaaldrich.com/content/dam/sigma-aldrich/docs/Sigma/Product_Information_Sheet/a0166pis.pdf [accessed 09.09.20].

(237) Simard, J. R.; Zunszain, P. A.; Hamilton, J. A.; Curry, S. Location of High and Low Affinity Fatty Acid Binding Sites on Human Serum Albumin Revealed by NMR Drug-Competition Analysis. *J. Mol. Biol.* **2006**, *361* (2), 336–351.

(238) Hureau, C.; Eury, H.; Guillot, R.; Bijani, C.; Sayen, S.; Solari, P.-L.; Guillon, E.; Faller, P.; Dorlet, P. X-Ray and Solution Structures of CuIIGHK and CuIIDAHK Complexes: Influence on Their Redox Properties. *Chem. - A Eur. J.* **2011**, *17* (36), 10151–10160.

(239) Mignot, I.; Presle, N.; Lapicque, F.; Monot, C.; Dropsy, R.; Netter, P. Albumin Binding Sites for Etodolac Enantiomers. *Chirality* **1996**, *8* (3), 271–280.

(240) Whitlam, J. B.; Crooks, M. J.; Brown, K. F.; Pedersen, P. V. Binding of Nonsteroidal Anti-Inflammatory Agents to Proteins--I. Ibuprofen-Serum Albumin Interaction. *Biochem. Pharmacol.* **1979**, *28* (5), 675–678.

(241) Rahman, M. H.; Yamasaki, K.; Shin, Y. H.; Lin, C. C.; Otagiri, M. Characterization of High Affinity Binding Sites of Non-Steroidal Anti-Inflammatory Drugs with Respect to Site-Specific Probes on Human Serum Albumin. *Biol. Pharm. Bull.* **1993**, *16* (11), 1169–1174.

(242) Ogata, K.; Takamura, N.; Tokunaga, J.; Ikeda, T.; Setoguchi, N.; Tanda, K.; Yamasaki, T.; Nishio, T.; Kawai, K. A Novel Injection Strategy of Flurbiprofen Axetil by Inhibiting Protein Binding with 6-Methoxy-2-Naphthylacetic Acid. *Eur. J. Drug Metab. Pharmacokinet.* **2016**, *41* (2), 179–186.

(243) Shen, Q.; Wang, L.; Zhou, H.; Jiang, H.; Yu, L.; Zeng, S. Stereoselective Binding of Chiral Drugs to Plasma Proteins. *Acta Pharmacol. Sin.* **2013**, *34* (8), 998–1006.

(244) Lodine Patient Information Leaflet, https://www.accessdata.fda.gov/drugsatfda_docs/label/2006/018922s022,020584s009lbl.pdf [accessed 07.09.2019].

(245) Chan, T. Y. Adverse Interactions Between Warfarin and Nonsteroidal Antiinflammatory Drugs: Mechanisms, Clinical Significance, and Avoidance. *Ann. Pharmacother.* **1995**, *29* (12), 1274–1283.

(246) DrugBank: digoxin entry, https://www.drugbank.ca/drugs/DB00390#reference-L6775 [accessed 07.19.2020].

(247) DrugBank: theophylline entry, https://www.drugbank.ca/drugs/DB00277 [accessed 07.09.2020].

(248) DrugBank: acenocumarol entry, https://www.drugbank.ca/drugs/DB01418 [accessed 07.19.2020].

(249) Anguizola, J. A.; Basiaga, S. B. G.; Hage, D. S. Effects of Fatty Acids and Glycation on Drug Interactions with Human Serum Albumin. *Curr. Metabolomics* **2013**, *1* (3), 241–252.

(250) Joseph, K. S.; Anguizola, J.; Jackson, A. J.; Hage, D. S. Chromatographic Analysis of Acetohexamide Binding to Glycated Human Serum Albumin. *J. Chromatogr. B. Analyt. Technol. Biomed. Life Sci.* **2010**, *878* (28), 2775–2781.

(251) Grossmann, M.; Thomas, M. C.; Panagiotopoulos, S.; Sharpe, K.; MacIsaac, R. J.; Clarke, S.; Zajac, J. D.; Jerums, G. Low Testosterone Levels Are Common and Associated with Insulin Resistance in Men with Diabetes. *J. Clin. Endocrinol. Metab.* **2008**, *93* (5), 1834–1840.

(252) Bhattacharya, A. A.; Grüne, T.; Curry, S. Crystallographic Analysis Reveals Common Modes of Binding of Medium and Long-Chain Fatty Acids to Human Serum Albumin. *J. Mol. Biol.* **2000**, *303* (5), 721–732.